Application of pharmaceutical quality approaches and the development of process analytical technologies to improve pharmaceutical product and process understanding

Thesis presented by

Ana Luiza Pinto Queiroz, BSc Chemical Engineering

for the degree of

Doctor of Philosophy

University College Cork

School of Pharmacy

Head of School: Prof. Stephen Byrne

Supervisors: Dr. Abina Crean, Dr. Sonja Vucen

2020

To,

My beloved parents

Rosa Maria Pinto Queiroz and Geraldo de Oliveira Queiroz, and my grandmother Francisca Rosa Seabra

In memory of Nicola Q.V.

TABLE OF CONTENTS

DECLARATION

This thesis is submitted to the National University of Ireland, University College Cork by Ana Luiza Pinto Queiroz for examination in the degree of Doctor of Philosophy (Pharmacy – Pharmaceutics). This thesis has not been submitted for any other purpose or degree offered by this or any other university. The material presented in this thesis is entirely the author's own original work, except where duly noted and acknowledged. This thesis was authored by Ana Luiza Pinto Queiroz with supervision and editorial advice from my PhD supervisors, Dr. Abina Crean and Dr. Sonja Vucen.

Dynamic Vapour Sorption experiments were performed with assistance from Dr. Waleed Faisal and Dr. Fatma Farag, School of Pharmacy, UCC. Dissolution experiments using traditional apparatus were performed with the assistance of Roisin Keane and Ailbhe Kearney, School of Pharmacy, UCC. Raman imaging was performed by Dr. Hazel Garvie-Cook at Renishaw, UK. Small scale co-crystal screening using multi-well plate was performed by Marisa Rodrigues at the School of Pharmacy, University of Porto, Portugal.

Signature:  **Date** 29/09/2020

ACKNOWLEDGEMENTS

I would like to thank my supervisors Dr. Abina Crean and Dr. Sonja Vucen for all the support and guidance. They believed in me from the beginning; they provided me with all necessary financial support, intellectual independence, and great regard at all times. They gave me all the tools to develop hard and soft skills, then combine them to innovate in my research field and become progressively more resilient and confident in my work. I would like to thank Dr. Mafalda Sarraguça for supervising me during my Erasmus exchange in Portugal, and my colleagues and all the staff in the School of Pharmacy of the University of Porto. In particular, Marisa Rodrigues and Thaise Martins.

I want to thank all the staff in the School of Pharmacy of the University College Cork. In particular, the technical staff of the School; Dr. Michael Cronin, Dr. Ken Devine, and Dr. Tom O'Mahony. I also would like to thank Mr. Dave Waldron, senior technical officer at the School of Food and Nutritional Sciences. They trained me in most of the techniques and assisted me at all times in a very friendly way. I would like to thank the administrative staff of the School of Pharmacy Ms. Noreen Moynihan, Ms. Kathleen Murphy, and Ms. Aisha Murphy who have also ensured that the paperwork has flowed smoothly throughout my research.

I would like to give a special thanks to my colleagues in the School of Pharmacy of the University College Cork that were a source of support, help, and friendship, Dr. Caroline Blacksheilds, Ziad Sartawi, Annachiara Dozzo, Dr. Raghu Peddapatla, Dr. Monique Mendonca, Ayse Kont, Emily Knox, Eze Buchi, Dr. Carol McCarthy, Dr. Tania Hidalgo, Dr. Aoife Mc Gillicuddy, Brian Kerins, Harriet Bennett-Lenane, Dr. Jacinta

Walsh, Khaled H. El Kassass, Marzia Pendino, Dr. Laura Henze, Dr. Niklas Köhl, Olivia Schmidt, Dr. Valeria Gervasi, Mirela Kovač, and Fernanda Favarin.

I would also like to thank the SSPC and SFI for the funding I received that allowed me to pursue this study. I have been lucky to collaborate with and learn from several different researchers while compiling the work of this thesis. To Professor Anne Marie Healy (Trinity College Dublin) for insights and providing access to pieces of equipment, to Dr. Jayprakash Yadav (Trinity College Dublin) for going forward on the research presented in Chapter 2, Dr. Kevin Moroney (University of Limerick) for brainstorms on modelling, to Dr. Manuel Kurl, Dr. Barbara Schaller and Dr. Renuka Devi Krishnaraj for training and advice on the use of Raman spectroscopy, Dr. Barbara Wood for collaborating on the research presented in Chapter 5, Dr. Marry Ellen Crowley for insights on Chapter 2, Dr. Hazel Garvie-Cook for insights on Raman imaging and performance of Raman imaging experiments, Dr. Waleed Faisal and Dr. Fatma Farag for collaborating in different aspects of this work. I would like to acknowledge the excipient manufacturers FMC, JRS and Asahi Kasei for providing me with the MCC samples studied in Chapter 2 of this thesis.

I would like to thank immensely my parents Rosa Maria Pinto Queiroz and Geraldo de Oliveira Queiroz for their unconditional love, support, and encouragement in every day of my life, especially throughout the course of my PhD. They always stood by me, even when they did not understand or agreed with my choices. I also would like to thank my brothers Rafael and Roger for inspiring me to be a strong and independent woman.

I would like to thank my dear friends Mrs Caitriona Devine and Dr. Ken Devine for motivated me to pursue a PhD at the University College Cork. I have no words to describe how this opportunity has changed my life, I can only thank them very much for pointing me the direction that initiated such a fulfilling and exciting career in the pharmaceutical sector.

Last, but not least, I would like to thank very much my housemates Clare McSweeney, Michael Keane, and Barry Cronin, and my friends Dhayanne Vianna, Mariana Paixão, Bryan McGrath, Airton Esmerio, Pedro Bettio, Patricia Moraes, Cedric Merilon, Marystela Lopes, Natalhia Machado, and Dave Sheedy for their care, encouragement, and support.

LIST OF FIGURES

LIST OF TABLES

PUBLICATIONS AND PRESENTATIONS ASSOCIATED WITH THIS THESIS

Peer reviewed publications

- Queiroz, A.L.P., Faisal, W., Devine, K., Garvie-Cook, H., Vucen, S. and Crean, A.M., 2019. The application of percolation threshold theory to predict compaction behaviour of pharmaceutical powder blends. Powder Technology, 354, pp.188-198. https://doi.org/10.1016/j.powtec.2019.05.027
- Queiroz, A.L.P., Wood, B., Faisal, W., Farag, F., Garvie-Cook, H., Glennon, B., Vucen, S. and Crean, A.M., 2020. Application of percolation threshold to disintegration and dissolution of ibuprofen tablets with different microcrystalline cellulose grades. International Journal of Pharmaceutics, 598, pp 119838. https://doi.org/10.1016/j.ijpharm.2020.119838
- Queiroz, A.L., Rodrigues, M., Zeglinski J., Crean, A.M., Sarraguça, M.C., and Vucen, S., 2021 Determination of co-crystal phase purity by mid infrared spectroscopy and multiple curve resolution. International Journal of Pharmaceutics. https://doi.org/10.1016/j.ijpharm.2021.120246
- Queiroz, A.L.P., Farag, F., Faisal, W., Kerins, B.M., Yadav, J., Healy, A.M., Crowley, M.E., Vucen, S. and Crean, A.M., 2021. Determination of crystallinity variability in commercial batches of microcrystalline cellulose using Raman spectroscopy. Cellulose.

Inventorship

Queiroz, A.L.P., Vucen, S. and Crean, A.M., 2019. The invention of the online crystallinity calculator MCCrystal developed in Chapter 2 was formally disclosed and it is an intellectual property of the University College Cork. MCCrystal is available at

the SSPC the Science Foundation Ireland Research Centre for Pharmaceuticals website, https://sspc.ie/mccrystal/.

Conference publications - Oral presentations

- Queiroz, A.L.P., Crean, A.M., 2018. Understanding the Compression Behavior of Blends: The Application of Percolation Threshold Theory and Multivariate Analysis. 2018 AIChE Annual Meeting, October 30th, at David L. Lawrence Convention Center, Pittsburgh, USA.
- Queiroz, A.L.P., 2018. The Application of Percolation Threshold Theory to Predict the Compaction Behaviour of Pharmaceutical Powder Blends. SSPC Technical meeting December 6th, at Trinity College Dublin, Dublin, Ireland.
- Queiroz, A.L.P., Crean, A.M., 2018. Identification of Critical Excipient Characteristics for Robust Drug Product Production and Performance. SSPC Scientific Advisory Board Meeting, May 31st, at University College Cork, Cork, Ireland.

Conference publications – Poster presentations

- Queiroz, A.L.P., Faisal, W., & Crean A.M., 2019. Understanding blends compression behaviour: The application of percolation threshold theory and multivariate analysis. SSPC 6 Year Review, September 17th, at University of Limerick, Limerick, Ireland.
- Queiroz, A.L.P., Faisal, W., & Crean A.M., 2019. Application of the percolation threshold model in the design of robust direct compression tablet

formulations. School of Pharmacy Research Day, May 23rd, at the University College Cork, Cork, Ireland.

- Faisal, W., Queiroz, A.L.P., & Crean, A.M., 2018. Ibuprofen/microcrystalline cellulose percolation threshold impact on tablet dissolution process. American Association of Pharmaceutical Scientists, AAPS meeting, November 7th, at Walter E. Washington Convention Center, Washington, D.C., USA.
- Queiroz, A.L.P., Faisal, W., & Crean A.M., 2018. Designing robust tablet formulations for continuous tableting process applying Percolation Threshold model. EuPAT 9: Ninth pan-European QbD & PAT Science, May 14th, at The Science and Industry Museum, Manchester, UK.
- Faisal, W., Queiroz, A.L.P., & Crean, A.M., 2018. The impact of microcrystalline cellulose variability on ibuprofen dissolution from direct compression tablets. EuPAT 9: Ninth pan-European QbD & PAT Science, May 14th, at The Science and Industry Museum, Manchester, UK.
- A.L.P. Queiroz, Faisal, W., & Crean A.M., 2017. Application of the percolation threshold model in the design of robust direct compression tablet formulations. SSPC International Site Review with SFI, November 9th, University of Limerick, Limerick, Ireland.

ABSTRACT

The pharmaceutical industry is undergoing a paradigm change with the advancement towards the Fourth Industrial Revolution. The manufacturing framework is moving from batch to continuous, which has been accompanied by the necessity of the implementation of process analytical technologies (PAT) for continuous process monitoring and control. There has also been a need to develop advanced quality approaches such as Quality by Design (QbD) and Quality by Control (QbC). Within these quality approaches, modelling has been used to expand knowledge related to raw material attributes and transformations that happen during the process, and to monitor and control process parameters. Besides the development of models for process and product transformations understanding and monitoring, predictive models have been an important advancement to reduce experimental cost during formulation development and process design. There are challenges that need to be addressed in order to complete the implementation of continuous process and advanced quality approaches in that pharmaceutical sector. It is necessary to extend the full mechanistic knowledge of processes, to develop data analysis and computer simulation, to expand the number of equipment and models to scale up solutions, and to upskill personnel to work with the technologies required.

The general aim of this thesis was to increase understanding of pharmaceutical materials and processes by the development of PAT and models for quantitative characterization and prediction of drug substance and drug product critical properties. To achieve this aim, several specific objectives were established focused on different aspects of oral dosage form manufacture.

Initially, a PAT was developed to rapidly characterize microcrystalline cellulose (MCC) percentage crystallinity index. MCC crystallinity was determined from Raman spectral data. Then, MCC moisture sorption and moisture monolayer were determined from isotherms obtained using dynamic vapor sorption (DVS). A correlation between both attributes was investigated. However, it was not possible to confirm the relationship between the monolayer moisture sorption and the percentage crystallinity. A total of 30 commercial batches of MCC were used to design and validate the MCC crystallinity model. Furthermore, a web application, McCrystal, was designed to disseminate the model. Available at https://sspc.ie/mccrystal/.

Secondly, a PAT was developed to determine the endpoint and monitor form changes during slurry co-crystallization. This PAT tool involved the application of in situ Raman spectroscopy combined with principal component analysis (PCA). An additional PAT tool was developed using Mid Infrared spectroscopy (MIRS) combined with multivariate curve resolution (MCR) in order to quantitatively evaluate phase purity of co-crystals produced by slow evaporation and slurry co-crystallization. The models developed were applied to different combinations of active pharmaceutical ingredients (APIs) and coformers, and were able to determine the co-crystallization endpoint for all systems where the solvents exhibited a weak Raman signal. Moreover, the phase purity for all co-crystals systems investigated was determined.

The third challenge addressed by this study relates to particle-particle interactions in powder blends to predict the general behaviour of the blend when it is directly compressed into pharmaceutical tablets. Percolation threshold model was used to

determine a critical drug load, above which the powder blend behaves similarly to the drug substance. As a result, the formulation may show undesirable properties above the threshold, which can lead to non-compliance or process difficulties. The application of PCA to determine the critical drug loading was investigated. The predicted values of critical drug loading were confirmed by changes in powder flowability, tablet weight variation, and Raman spectroscopic analysis of drug distribution. PCA was not able to precisely predict the threshold, however, it aided in clarifying differences between the blends containing different ibuprofen loadings and different MCC grades.

Expanding on the impact of critical drug loading on tablet critical quality attributes, the final objective was to investigate the impact of critical drug loads, determined from compaction data, on disintegration and dissolution performance. The application of novel process analytical technologies, in-process video microscopy (PVM) and focused-beam reflectance measurement (FBRM), to study tablet disintegration was also proposed and investigated in-depth. FBRM and PVM provided important information of tablet disintegration behaviour that cannot be captured by the traditional disintegration testing. The critical drug load predicted from compaction data was also relevant for disintegration and dissolution behaviour. Above the threshold drug loading, disintegration and drug release rates were decreased. A PCA model developed from Raman spectra acquired from tablet surfaces further supported the finding that blends manufactured with different grades of MCC differed more significantly above the critical drug load.

The work presented in this thesis is a contribution to solid dosage formulation design, co-crystallization understanding, tableting process scale up and scale down, and data handling. The models and PAT developed can be used to predict formulation performance, determine process parameters based on raw material critical attributes, determine process endpoint, and thoroughly assess final product critical quality attributes.

Keywords: *Pharmaceutical Technology, Quality by Design (QbD), Process Analytical Technology (PAT), Co-crystal, Tablet, Critical Material Attribute, Critical Quality Attribute.*

ABBREVIATIONS

a	Eigenvectors
Ace	Acetone
ACN	Acetonitrile
ALS	Alternating Least Squares
API	Active Pharmaceutical Ingredient
BET	Brunauer, Emmett and Teller
CE	Circle equivalent
CF	Chloroform
CFD	Computational fluid dynamics
CMA	Critical material attribute
CPP	Critical process parameter
CPS	Cyber-Physical Systems
CQA	Critical quality attribute
D	Tablet diameter
D10	Diameter at which 10% of a sample's mass is comprised of smaller particles
D50	Diameter at which 50% of a sample's mass is comprised of smaller particles (median particle size)
D90	Diameter at which 90% of a sample's mass is comprised of smaller particles
DCM	Dichloromethane
DEM	Discrete element methods
DoE	Design of Experiments
DSC	Differential scanning calorimeter
DVS	Dynamic vapour sorption
EMA	European Medicines Agency
EtOAc	Ethyl acetate
EtOH	Ethanol
FDA	Food and drug administration
FTIR	Fourier transform infrared spectroscopy
GAB	Guggenheim, Anderson, de Boer
G_{mix}	Gibbs free energy of mixing
H	Tablet hardness

HB	Hydrogen bonding to intermolecular interaction of API and coformer
H_{ex}	Excess enthalpy
HR	Hauser ratio
HTZ	Hydrochlorothiazide
I	Spectral intensity
I	Generic identity matrix
ICH	International Conference for Harmonisation
loT	Internet of Things
m	Mass
MCC	Microcrystalline Cellulose
MCR	Multivariate curve resolution
MeOH	Methanol
MIR	Mid-infrared spectroscopy
MVA	Multivariate analysis
n	Number of rows in a generic matrix
NCT	Nicotinamide
NIR	Near-infrared spectroscopy
P	Generic matrix of loadings
p	Number of columns in a generic matrix
PAT	Process Analytical Technology
PC	Principal Component
PCA	Principal Component Analysis
Ph	European Pharmacopeia
PLS	Partial least squares
PXRD	Powder X-ray diffraction
q	Percolation threshold generic exponent
QbC	Quality by control
QbD	Quality by design
QbT	Quality by testing
QTPP	Quality target product profile
r	Pearson correlation coefficient
RH	Relative humidity
RMSEC	Root Mean Squared Error of Calibration
RMSEP	Root Mean Square Error of Prediction

S	Covariance matrix
SEM	Scanning electron microscopy
SNV	Standard Normal Variate
T	Generic matrix of scores, tablet thickness
T_f	Percolation threshold coefficient for tablets tensile strength
TGA	Thermogravimetric analysis
W	Weight of moisture absorbed onto the surface of a solid per weight of the dry solid
% CI	Percentage crystallinity index
% w/w	Mass fraction
$\bar{x}$	Arithmetic mean
µm	Micron/micrometer
X	Generic matrix of independent variables
X_c	Mass fraction, critical drug loading in the percolation threshold theory
Y	Generic matrix of dependent variables
ε	Porosity
λ	Eigenvalues
ρ	Relative density/occupation probability
ρ_{bulk}	Powder bulk density
ρ_c	Percolation threshold
ρ_{tablet}	Tablet density
ρ_{tapped}	Powder tapped density
ρ_{true}	Powder true density
P_{yield}	Yield pressure
σ	Standard deviation, compaction pressure
σ_T	Tablet tensile strength

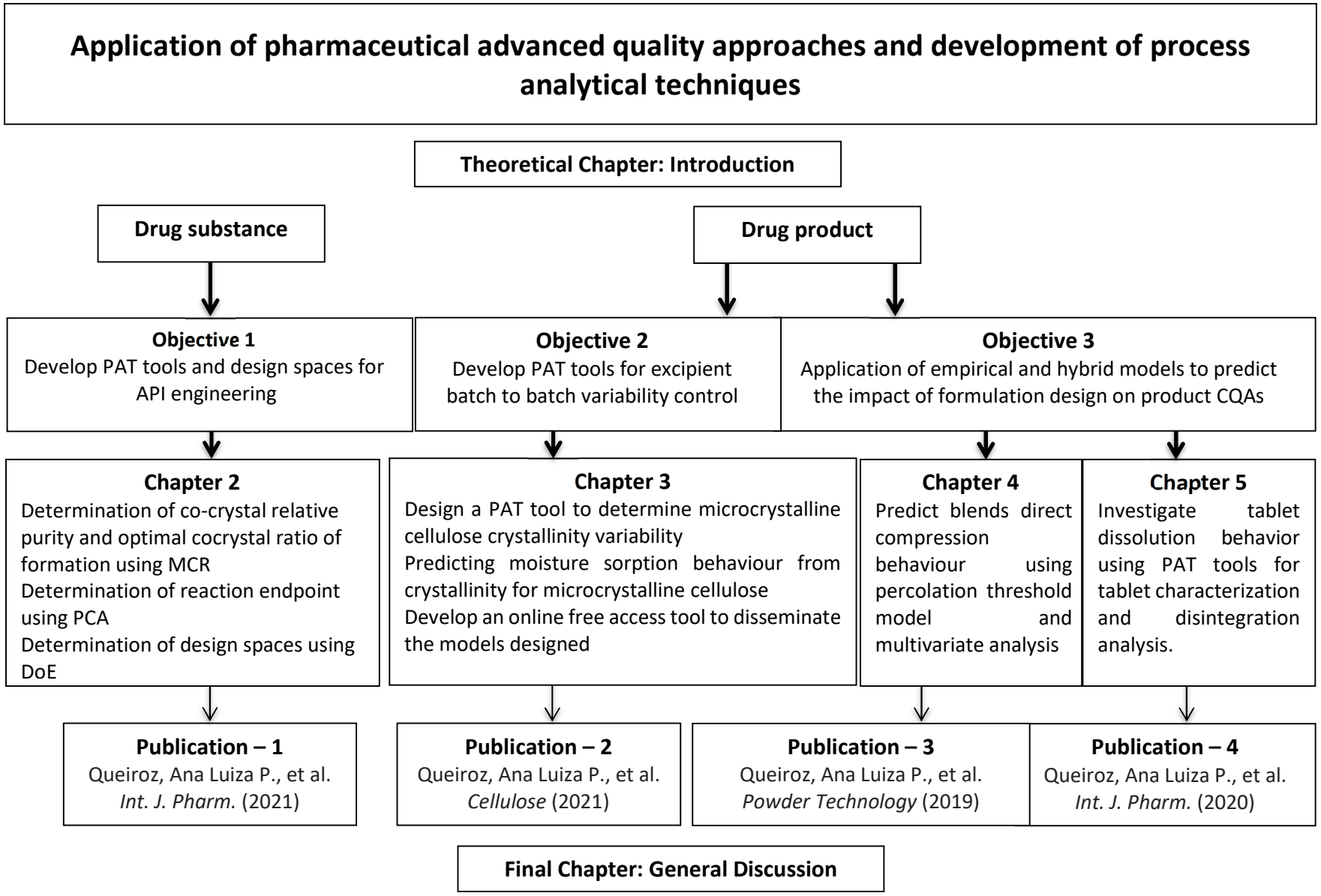
Application of pharmaceutical advanced quality approaches and development of process analytical techniques
Theoretical Chapter: Introduction
Drug substance
Drug product
Objective 1
Develop PAT tools and design spaces for API engineering
Objective 2
Develop PAT tools for excipient batch to batch variability control
Objective 3
Application of empirical and hybrid models to predict the impact of formulation design on product CQAs
Chapter 2
Determination of co-crystal relative purity and optimal cocrystal ratio of formation using MCR
Determination of reaction endpoint using PCA
Determination of design spaces using DoE
Chapter 3
Design a PAT tool to determine microcrystalline cellulose crystallinity variability
Predicting moisture sorption behaviour from crystallinity for microcrystalline cellulose
Develop an online free access tool to disseminate the models designed
Chapter 4
Predict blends direct compression behaviour using percolation threshold model and multivariate analysis
Chapter 5
Investigate tablet dissolution behavior using PAT tools for tablet characterization and disintegration analysis.
Publication – 1
Queiroz, Ana Luiza P., et al. Int. J. Pharm. (2021)
Publication – 2
Queiroz, Ana Luiza P., et al. Cellulose (2021)
Publication – 3
Queiroz, Ana Luiza P., et al. Powder Technology (2019)
Publication – 4
Queiroz, Ana Luiza P., et al. Int. J. Pharm. (2020)
Final Chapter: General Discussion

Chapter 1 - General Introduction

1.1 Background

The Fourth Industrial Revolution, Industry 4.0, has been changing the dynamic of industrial production. According to Lasi et al (Lasi et al., 2014), the future of manufacturing systems will be technology-pushed and application-pulled. The physical world would be integrated with the virtual space by technologies such as Internet of Things (IoT) (Gubbi et al., 2013), Cyber-Physical Systems (CPS) (Lee et al., 2015), and semantic machine-to-machine communication (Da Xu et al., 2018). Smart factories will be progressively more equipped with sensors and autonomous systems so that physical parameters will be digitally recorded and processed. In relation to automation and control, this means that computational models that contain statistical analysis can be used to interpret if processes are trending to achieve quality targets. If the production is not within designed spaces, signals can be automatically sent back to the process so that the necessary adjustments are implemented in every unit operation required. Thus, smart factories are characterized by increased efficiency, science-based approaches and continuous process verification and optimization. Thorough process understanding and big data analysis are seen as key to the transition towards smart factories (Da Xu et al., 2018; Spes and Levin, 2018).

Pharmaceutical and biopharmaceutical manufacturers have been traditionally operating in batch processes that were controlled by rigid frameworks. In this approach, quality is ensured by testing the raw materials, the process parameters and the final product characteristics (Rantanen and Khinast, 2015). When defective products are detected, batches can be easily separated for disposal or reprocessing

(Crowley and Crean, 2015). This enabled batch production and a quality by testing (QbT) system to remain in place for many decades. Even though, this combination is known to be limited (Rantanen and Khinast, 2015; Rathore and Winkle, 2009). Product wastage is the main problem encountered in this approach, being reported to be as much as 50% of the product manufactured in some cases (Rathore and Winkle, 2009). Process understanding is not a priority under batch manufacturing and QbT. As a result, most of the data generated during the process is only used for compliance (Manzano and Langer, 2018). Delays in technological advances in the pharmaceutical and biopharmaceutical industries, has been attributed to this traditional approach and the regulatory agencies rigorous oversight of the sector. Both factors have contributed to the delay and cost of developing, implementing and validating new technologies within the sector (Rathore and Winkle, 2009).

In recent years regulatory agencies acknowledged the advantages of encouraging innovative technological solutions and fundamental scientific work to guide pharmaceutical development (Rantanen and Khinast, 2015). Regulatory agencies have adopted guidelines for the implementation of well-established chemical engineering knowledge to pharmaceutical and biopharmaceutical manufacturing (International Council for Harmonisation, 2014, 2008, 2005a, 2005b). The published guidelines aim to increase safety and quality of medications, reduce manufacturing costs and implement more structured pharmaceutical development and manufacturing approaches (Rantanen and Khinast, 2015).

Highlights of those guidelines include (*i*) migration from batch to continuous manufacturing, (*ii*) implementation of process analytical technologies (PAT)

combined with predictive models, and (*iii*) implementation of advanced quality approaches, namely quality by design (QbD) (Yu et al., 2014) and quality by control (QbC) (Su et al., 2019). Those three subjects are linked to each other. QbD principles are encouraged for both batch and continuous manufacturing processes (Potter, 2009). However, continuous manufacturing has many advantages (see section 1.3) and is being supported by regulatory agencies. To enable the transition from batch to continuous processes, the application of QbD concepts and PAT is essential. Moreover, a new quality approach, QbC has been developed to address specific quality challenges of continuous manufacturing.

Continuous manufacturing, advanced quality approaches and predictive modelling appear to be the basis of the advances towards Pharma 4.0 (De Matas et al., 2016; Steinwandter et al., 2019; Su et al., 2019). Thus, the focus of this thesis was the underlying science and the main techniques involved in QbD and QbC approaches with emphasis on control tools that could be applied to continuous manufacturing. PAT tools as well as formulation and process knowledge developed in this thesis addressed some of these challenges.

1.2 Advanced quality approaches

1.2.1 Overview

A high-quality drug product was defined as being reliably available, not contaminated and to consistently deliver all characteristics stated in the label and clinical performance (Woodcock, 2004). A drug product is the final result of an extensive work that includes development, manufacture, and registration stages

(Steinwandter et al., 2019). Hence, in an optimal scenario, quality should be built in the entire drug product life cycle rather than in the final product only.

In a control strategy point of view, the traditional quality by testing approach (Level 3, Figure 1.1) is now considered obsolete and has been replaced by QbD. QbD has been encouraged by regulatory agencies for both batch and continuous processes (Yu et al., 2014). This means that control strategy is moving from Level 3 to Levels 2 and 1, towards real-time control strategies upon flexible processes. Besides QbD, a new approach, known as QbC, has being developed (Nunes de Barros et al., 2017; Sommeregger et al., 2017; Su et al., 2019; Szilágyi et al., 2019). The concept of QbC emerged from the developments around the Level 1 control strategy proposed by Yu et al. (Su et al., 2019). Thus, QbC as a framework is intended for application to continuous manufacturing and aims to optimize the Level 1 of control strategy.

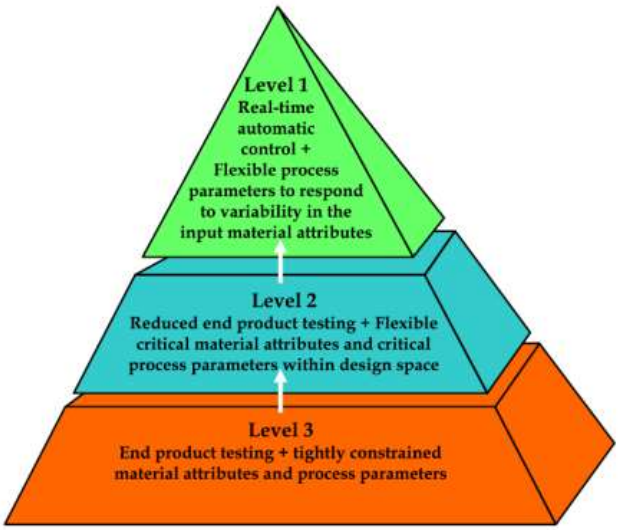

Figure 1.1. Control strategy options (Yu et al., 2014).

QbD and QbC entail widespread scientific understanding, especially extensive product and process knowledge (De Matas et al., 2016; Su et al., 2019). This is one important milestone to enable the features of Pharma 4.0 (Steinwandter et al.,

2019). Product and process understanding has been defined as key factors to enable high-quality drug products manufacturing and excellence in clinical performance. Sun et al. indicated that the pathway to achieve pharma smart manufacturing is to invest in continuous processes ruled by quality approaches that emphasize predictive understanding and integrated active process control (Figure 1.2) (Su et al., 2019). QbD, QbC, and continuous manufacturing will be discussed in detail in the following sections.

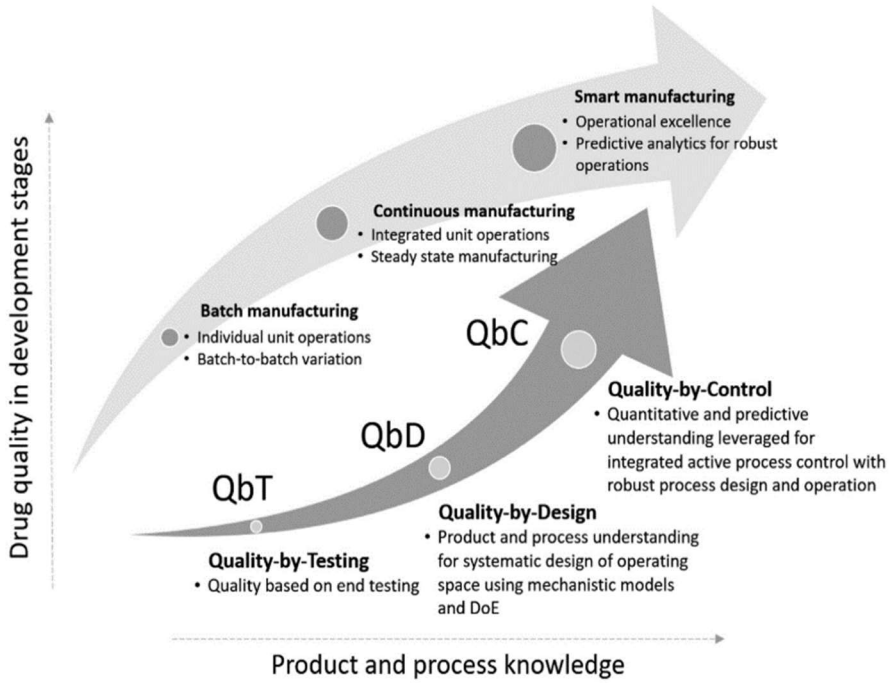

Figure 1.2. Progression of pharmaceutical quality approaches (Su et al., 2019).

1.2.2 QbD approach to pharmaceutical development

Quality by design was developed in 1992 (Juran, 1992). The main concept proposed was that most quality problems of a product were due to the way that the product was designed. The objectives of QbD include the achievement of meaningful product quality specifications, improvement of process capability, reduction of product variability and defects, and increase in product development and manufacturing

efficiency (Yu et al., 2014). QbD was developed further by the pharmaceutical industry and published by the International Council for Harmonization of Technical Requirements for Pharmaceuticals for Human Use as a series of guidelines: Q8 (R2) Pharmaceutical Development, Q9 Quality Risk Management, Q10 Pharmaceutical Quality System, Q11 Development and Manufacture of Drug Substance, and Q12 Lifecycle Management (International Council for Harmonisation, 2014, 2008, 2005a, 2005b).

Pharmaceutical QbD is defined as "a systematic approach to development that begins with predefined objectives and emphasizes product and process understanding and process control, based on sound science and quality risk management" (International Council for Harmonisation, 2005a). Hence, quality is ensured when QbD elements are applied to guide the systematic understanding and control of the formulation and the manufacturing variables (Yu, 2008). The main elements of QbD are:

- Quality Target Product Profile (QTPP): detailed information about the final product characteristics.
- Critical Quality Attributes (CQA): physical, chemical, biological, or microbiological property or characteristic of the excipients, the drug substance, intermediates and drug product that should be within an appropriate limit, range, or distribution to ensure the desired product quality (CQAs for other delivery systems are out of the scope of this thesis).
- Risk Assessment: used to identify which process parameters and material attributes influence product CQAs.

- Design Space: multidimensional relationship between the process inputs (material attributes and process parameters) and the critical quality attributes.
- Control Strategy: a set of controls that ensure process performance and product quality. Controls can include parameters and attributes related to drug substance and drug product materials and components, facility and equipment operating conditions, in-process controls, finished product specifications, the associated methods, and frequency of monitoring and control. The development of these controls requires rich formulation, product and process understanding (International Council for Harmonisation, 2008).

1.2.3 QbC approach to pharmaceutical development

The main concept of QbC is that high-quality products are obtained when the process is effectively controlled, especially when it is applied to continuous manufacturing (Nunes de Barros et al., 2017; Sommeregger et al., 2017; Su et al., 2019; Szilágyi et al., 2019). QbC is defined as "the design and operation of a robust manufacturing system that is achieved through an active process control system designed in accordance with hierarchical process automation principles, based on a high degree of quantitative and predictive product and process understanding" (Su et al., 2019). This approach includes many QbD elements, such as CQAs and critical process parameters (CPPs). However, QbD does not provide guidance on systematic quantitative procedures for the design of the suitable control architecture and methodology. Hence, QbC was developed to address this issue by providing a

framework to the implementation of efficient real-time process control, especially in continuous manufacturing (Su et al., 2019)

The proposed framework (Figure 1.3) aims to facilitate the integration of hardware and software for control strategy implementation, especially to continuous manufacturing. D1 and D2 refer to an extensive raw material characterization and product design, respectively. D3 requires specific knowledge of the manufacturing process to produce the designed product. Subsequently the manufacturing process or pilot plant (P2) is configured with the corresponding control platform and PAT sensors (P1). A model library (S1) will be recorded and accessed by flowsheet simulation software (S2). This is an important advantage of QbC regarding storage and processing of the model of control strategy, as QbD does not provide guidelines for that. Simulations performed on S2 will allow continuous verification of the models by means of sensitivity analysis and system identification (C1). Subsequently, a control design and analysis (C2) will be performed. When the steady state operation is identified on C1, the control design and analytics constructs a state-space model, which is a set of differential and algebraic equations that represents the system. The models designed are then verified by C3, C4, and C5. This three-step verification will be performed in loop until the designed models meet real time release requirements (Su et al., 2017).

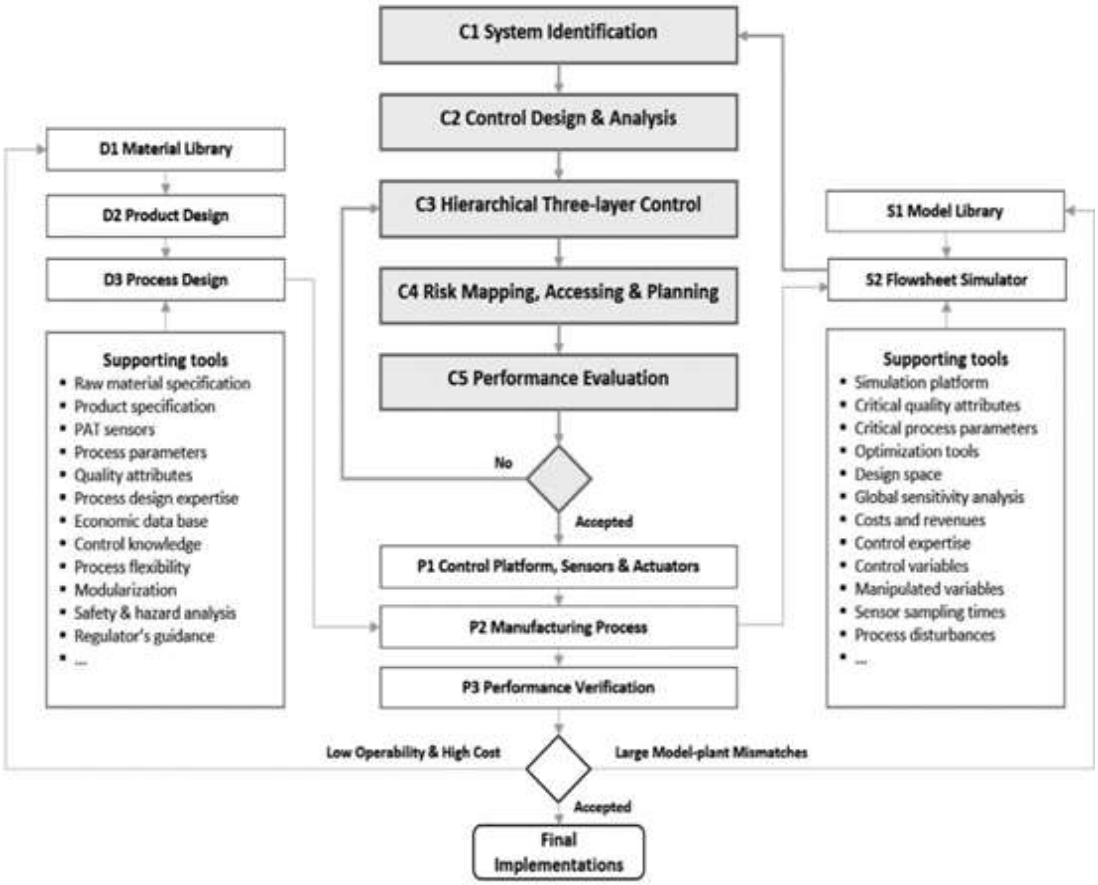

Figure 1.3. Quality by control framework (Su et al., 2017).

Advancements in PAT tools and mechanistic understanding of processes are part of QbC framework. Thus, the objectives of this thesis aim to contribute to the development of QbC in the design of model-based process quality assurance in pharmaceutical process operations.

1.3 Continuous manufacturing

A proposed definition of a continuous manufacturing is “an industry with processes that are integrated, based on a systems approach, having model-based control, and making use of flow” (Badman and Trout, 2014). Continuous manufacturing has been indirectly discussed in previously published quality guidelines (International Council for Harmonisation, 2014, 2008, 2005a, 2005b). However, the International

Conference on Harmonization (ICH) has endorsed a new guideline (ICH Q13) to provide a basis for the implementation of continuous manufacturing, which is expected to be finalised in 2021 (International Council for Harmonisation, 2018). ICH Q13 aims to address technical and scientific requirements necessary to fulfill regulatory expectations regarding continuous manufacturing.

Companies have been investing in continuous manufacturing and, as a result, a number of drug substances have been approved by FDA to be produced by continuous manufacturing, such as Orkambi (lumacaftor/ivacaftor) from Vertex in 2015, Prezista (darunavir) from Janssen in 2016, Verzenio (abemaciclib) from Lilly and Symdeko (glasdegib) from Pfizer in 2018 (Su et al., 2019). The benefits of operating in a continuous manufacturing have been widely discussed and include the following (Badman and Trout, 2014; Crowley and Crean, 2015; S. L. Lee et al., 2015; Mascia et al., 2013; Nasr et al., 2017; Rogers and Jensen, 2019):

- Reduction in manufacturing costs. Continuous manufacturing requires smaller equipment and infrastructure and allows reduction of unit operations. Continuous manufacturing can also enable end-to-end production. In other words, drug substance and drug product, that are currently often separately located, can be produced in the same facilities.
- Increase in reliability and safety. For example, hazardous intermediates can be converted during production, in isolated systems.
- Improved flexibility. For example, the amount of product manufactured can be changed by running the process for shorter or longer periods of time.

- Novel pathways that enable the production of Active Pharmaceutical Ingredients (APIs) or final drug products that are not otherwise accessible.
- Built in quality throughout the process and reduced product time to market.

The challenges to implement continuous manufacturing have also been discussed. It is important to note that continuous manufacturing is already common in other industry segments e.g., petrochemical and bulk chemical industries (Darby and Nikolaou, 2012; Lee et al., 2015). However, to enable continuous manufacturing in the pharma industry it is necessary to expand the full mechanistic knowledge of processes, develop modeling and computer simulations, expand the number of equipment to scale up solutions from bench to pilot and industrial scales. It is also necessary to develop advanced control strategies, such as QbD, and implement PAT for real-time control. Furthermore, addressing difficulties such as processing dry solids and solid-laden fluids, and multi-unit-operation connectivity would also be required (Baxendale et al., 2015; Mascia et al., 2013). Another challenge to implement continuous manufacturing is to ensure that there are personnel skilled to work with the technologies required (Badman and Trout, 2014; De Matas et al., 2016). The skill set essential for continuous manufacturing includes chemical engineering, physical chemistry, flow chemistry, chemistry–process interface, and process-data science interface skills (Baxendale et al., 2015; Steinwandter et al., 2019).

The focus of this thesis was drug product manufacture. Solid oral dosage forms are is the most common dosage form for drug administration due to their its high degree of drug stability and dosage accuracy. Among solid dosage forms, tablets are the

most prevalent. Tablets can be manufactured by different processes, including wet granulation, dry granulation and direct compression. However, direct compression is the most direct route of manufacturing (Figure 1.4). Pharmaceutical companies have announced investments in research and development around small molecules to adjust APIs for continuous manufacturing of tablets using direct compression processes (Hausner, 2018; Nunes de Barros et al., 2017; Su et al., 2019). The smaller number of unit operations involved in this process facilitates the migration from batch to continuous manufacturing, the application of advanced quality control strategies, and usage of robust PAT and models for manufacturing control (Gohel and Jogani, 2005). In this thesis, models for prediction and process understanding that can be applied to continuous manufacturing related to tablet direct compression were investigated.

Step	Direct compression	Dry granulation	Wet granulation
1	Mixing/blending of API and adjuvants	Mixing/blending of API and adjuvants	Mixing/blending of API and adjuvants
2	Compression	Compression into slugs	Preparation of binder solution
3		Size reduction of slug and sieving	Massing of binder solution of step 2 with powder mixture of step 1
4		Mixing of granules with pharmaceutical aid/s	Wet screening of damp mass
5		Compression	Drying of wet granules
6			Resifting of dried granules and blending with pharmaceutical aid/s
7			Compression

Figure 1.4. Direct compression, dry granulation and wet granulation tableting process (Gohel and Jogani, 2005).

1.4 Process analytical technology

A Process Analytical Technology is "a system for designing, analyzing, and controlling manufacturing through timely measurements i.e., during processing, of critical quality and performance attributes of raw and in-process materials and processes, with the goal of ensuring final product quality" (European Medicines Agency, n.d.; US FDA, 2004). PAT is used to improve understanding and control manufacturing processes and it is a broad field that includes process analysis, chemical engineering, chemometrics, knowledge and risk management, and process automation and control (Bakeev, 2010). Thus, PAT is a tool to enable continuous manufacturing and represent an important aspect of QbD and QbC (Page et al., 2015).

As per the definition published from the joint report of US FDA and EMA, PAT is not only used in process control strategy. The implementation of PAT results in a high degree of process understanding. PAT is used at different stages of manufacturing process which includes process development studies, before process, in process, after process and QbD (Pomerantsev and Rodionova, 2012). PAT used before a process to control raw material properties is an important part of PAT since properties of input material may tune process parameters. After process PAT refers to real-time release testing to confirm if the product has satisfactory quality. In QbD, PAT works to help build quality into the product throughout the entire lifecycle. In this case, QbD tools are used to define the design space and to reveal the sources of process variability. PAT is then placed to control the process within the defined design space (Pomerantsev and Rodionova, 2012).

PAT technologies are reliant on mathematical and statistical models that are designed to interpret the signals generated by PAT instruments. Near infrared (NIR) (Reich, 2005), Raman spectroscopy (De Beer et al., 2011), and middle infrared (MIR) (Van Eerdenbrugh and Taylor, 2011) are the most commonly used PAT instruments (Figure 1.5) (Bakeev, 2010). Among numerous chemometric techniques used in PAT, multivariate data analysis represents the most applied model in PAT (Figure 1.6) (Esbensen and Swarbrick, 2019; Pomerantsev and Rodionova, 2012). The PAT models used in this thesis will be discussed in detail in the next sections.

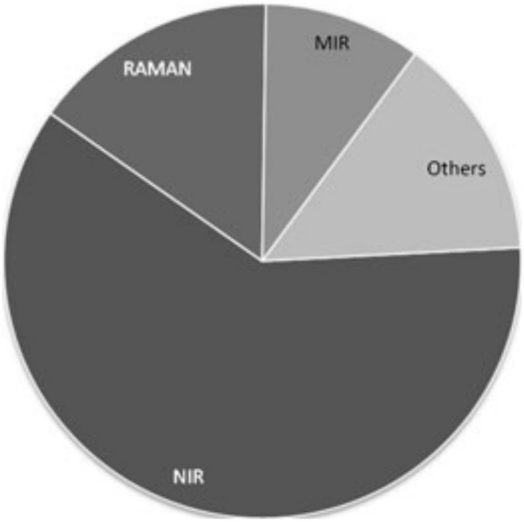

Figure 1.5. Spectroscopic techniques used in PAT applications (Pomerantsev and Rodionova, 2012).

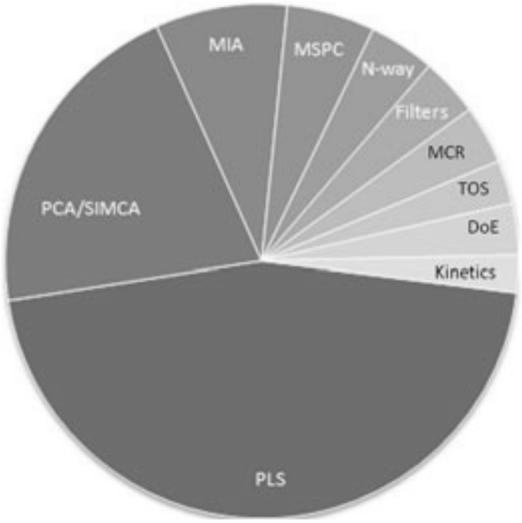

Figure.1.6. Chemometric models used for PAT applications. Multivariate image analysis (MIA), multivariate statistical process control (MSPC), multiway (N-way), multivariate curve resolution (MCR), theory of sampling (TOS), design of experiments (DoE), partial least squares (PLS), and principal component analysis/soft independent modelling of class analogy (PCA/SIMCA) (Pomerantsev and Rodionova, 2012).

1.5 Data analysis and models of control

Mathematical models are ways to describe a system using mathematical language (Kourti et al., 2014). Modelling and big data analysis are key for pharmaceutical technological advancements. They appear in all quality approaches, represent a

fundamental part of PAT, and are the basis for the 4th industrial revolution (Sin et al., 2009; Steinwandter et al., 2019; Yu et al., 2014). However, mathematical modelling is still in development in the pharmaceutical industry. There is an enormous amount of data being generated by sensors placed on processes. However, most of the data generated is still only used for compliance (Manzano and Langer, 2018). This gap is explained by the complexity of designing practical applications integrating big data from heterogeneous sources and the lack of skilled personnel to perform this work (Da Xu et al., 2018).

Quantitative models are generally classified as mechanistic, empirical or hybrid. The information required and the overall understanding to derive the models decreases from the mechanistic to empirical approaches (Figure 1.7) (Chatterjee et al., 2017).

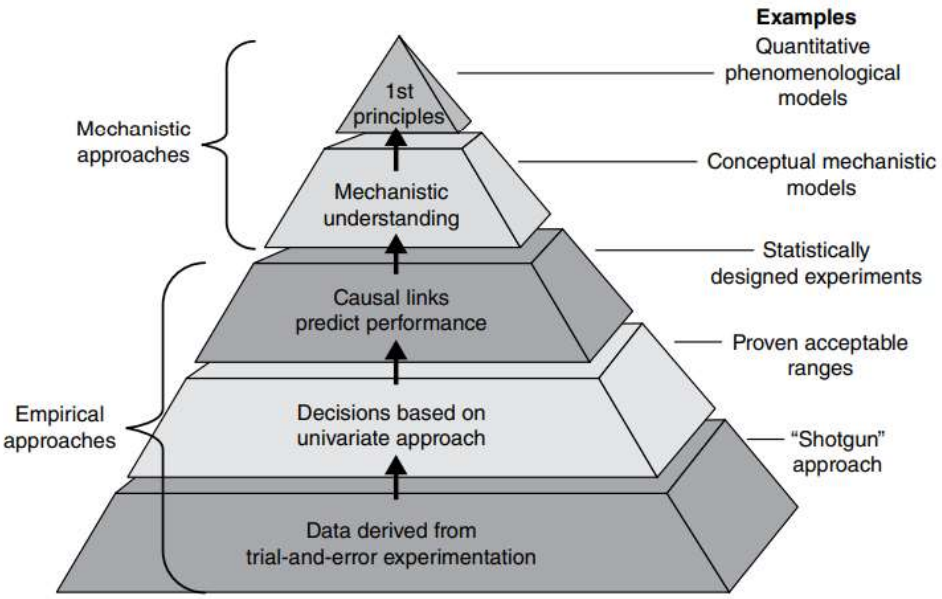

Figure 1.7. Knowledge of process required in different model classes (Chatterjee et al., 2017).

Empirical models are built based on data acquired from a process and not as much from an understanding of that process. Most of these models have a retrospective

character because they are based on historical data, and they are usually used to identify relationships between input and output variables (Djuris and Djuric, 2017). Multivariate empirical analysis such as Design of Experiments (DoE), and chemometric models such as Multivariate Curve Resolution (MCR), Partial least squares (PLS) and Principal Component Analysis (PCA) are examples of empirical models. The application of this class of model is extremely valuable for complex process understanding and control when representative data is available for design and validation. However, it has a limited application to new experimental or operational setups. In other words, an empirical driven model is only valid in the design space used to build the model. This problem can be solved by the addition of data collected in the new operational setup to the original model (Esbensen and Swarbrick, 2019). This class of models is typically used within PAT.

Mechanistic models are based on physical/chemical laws e.g., conservation of energy, fluid flow, and mass balance. Thus, discrete element methods (DEM) (Ketterhagen et al., 2009), finite element methods (FEM) (Reddy, 1989), and computational fluid dynamics (CFD) (Anderson et al., 1995) simulations are examples of this class of models (Djuris and Djuric, 2017). Empirical models are derived from a high-level process understanding, and thus provide a very transparent representation of the underlying phenomenon (Chatterjee et al., 2017). Developing mechanistic models can be very complicated and encounter many difficulties. Besides the development of equations, it is necessary to associate parameters that represent the system accurately. Pharmaceutical in-line analytical measurement and data recording systems have yet to be greatly improved (Djuris and Djuric, 2017).

Hybrid models are the result of a combination between mechanistic and empirical models. They are usually applied to scale-up and to estimate properties such as compression and compaction parameters (Djuris and Djuric, 2017). Heckel, Kawakita, and Shapiro equations, and the Percolation Threshold model are examples of hybrid models.

1.6 Mathematical models investigated in this thesis

1.6.1 Principal component Analysis

Principal component Analysis (PCA) (Pearson, 1901) is a statistical model used to reduce the number of variables, independent or correlated in a data matrix. The vast number of variables of the original data matrix is transformed into a new set of variables named principal components (PCs) that are ranked so that the first few PCs explains the most of the variability in the data (Joliffe and Morgan, 1992; Jolliffe, 1982; Pearson, 1901). In other words, a small number of PCs is used to explain a large variability in the data. The optimal number of PCs depends on the objectives of the work. It is important to observe that even PCs that show low amounts of variability information may offer predictive value (Jolliffe, 1982). PCs are linear combinations of the original variables geometrically defined as orthogonal directions that maximize the variance of the data. Therefore, PCs do not hold a physical meaning.

Besides the principal components, a PCA model also returns scores (T) and loadings (P) of a data matrix X (Equation 1.1). The variability not explained by the PCs is given as the error E. The data matrix is organized so that the observations e.g., time points or batches, are distributed in the n rows and the variables in the p columns.

$$X_{n,p} = \begin{matrix} x_{11} & x_{12} & \cdots & x_{1p} \\ x_{21} & x_{22} & \cdots & x_{2p} \\ \vdots & \vdots & \ddots & \vdots \\ x_{n1} & x_{n2} & \cdots & x_{np} \end{matrix}$$

$$X = TP^T + E \qquad \text{(Equation 1.1)}$$

The scores are new values assumed by the observations (samples or time points) in the new geometric space determined by the principal components i.e., by the new set of variables with reduced dimensionality ($k < p$). The scores are used to identify similarities among the observations. Loadings explain which variables are responsible for the similarity or dissimilarity among the observations identified in the scores plot. Scores and loadings should be analyzed together because they provide complementary information.

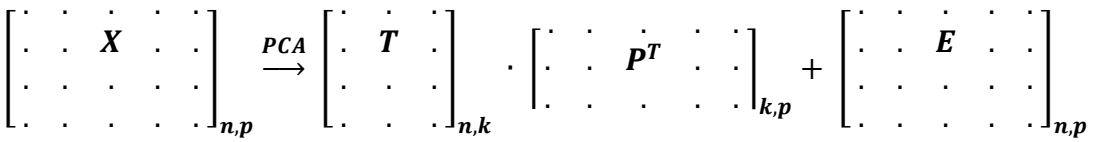

Figure 1.8. Matrix interpretation of principal component analysis.

PCA can be performed by eigenvalue decomposition as described in the following steps (Rencher, 2003):

Step 1: Determine the mean ($\bar{x}$) and the standard deviation (σ) of each variable. Equation 1.2 shows calculation of the mean and Equation 1.3 shows the calculation of the standard deviation of the jth variable.

$$\bar{x}_j = \frac{1}{n}\sum_{i=1}^{n} x_{ij} \qquad \text{(Equation 1.2)}$$

$$\sigma_j = \sqrt{\frac{1}{n}\sum_{i=1}^{n}\left(x_{ij} - \bar{x_j}\right)^2} \qquad \text{(Equation 1.3)}$$

Step 2: Standardize the variables when the variables are not in the same scale. Equation 1.4 manipulates the variables, so they have a mean of zero and standard deviation of one-unit variance. The following steps considered $x_{ij,standardized}$ equal to x_{ij}.

$$x_{ij,standardized} = \frac{x_{ij} - \bar{x_j}}{\sigma_j} \qquad \text{(Equation 1.4)}$$

Step 3: Mean-centre the data. Shift of the data so the centre point is the centre of the swarm of point by making $x_{ij,centered} = x_{ij} - \bar{x_j}$

Step 4: Calculate the covariance matrix (S) (Equation 1.5). The covariance matrix explains how the variables are related to each other. This results in a symmetric and non-negative matrix and the eigenvectors of S are orthogonal and the eigenvalues non-negative.

$$S = \frac{1}{n-1}X^T X = \begin{bmatrix} {s_1}^2 & c_{12} & \cdots & c_{1p} \\ c_{21} & s_2^2 & \cdots & c_1^2 \\ \vdots & \vdots & \ddots & \vdots \\ c_{p1} & c_{p2} & \cdots & s_p^2 \end{bmatrix} \qquad \text{(Equation 1.5)}$$

Where the diagonal (${s_i}^2$) elements are the sample variances for each variable (Equation 1.6) and the off-diogonal elements (c_{ik}) are the sample covariances between pairs of variacles i and k (Equation 1.7).

$$s_i^2 = \frac{1}{n-1}\sum_{j=1}^{n}(x_{ij} - \bar{x}_i)^2 \qquad \text{(Equation 1.6)}$$

$$c_{ik} = \frac{1}{n-1}\sum_{j=1}^{n}(x_{ij} - \bar{x}_j)(x_{kj} - \bar{x}_k) \qquad \text{(Equation 1.7)}$$

Step 5: Determine the eigenvalues (λ_i) (Equation 1.8) and eigenvectors (a_i , *i* = 1, 2, …, p) (Equation 1.9). There exists one eigenvalue for each eigenvector. Thus, each eigenvalue is the variance explained by the corresponding eigenvector. Geometrically, the eigenvectors are the directions of the axes of the most variance, therefore, they are the principal components. All the eigenvectors of a matrix are orthogonal to each other, which agrees with the definition of principal components. In Equation 1.8, I is an identity matrix i.e., the diagonal elements are equal to one and the off-diagonal elements are equal to zero. In Equation 1.9 a_i represent the principal components (a_i , i = 1, 2, …, p).

$$\det(S - \lambda_i I) = 0 \qquad \text{(Equation 1.8)}$$

$$(S - \lambda_i)a_i = 0 \qquad \text{(Equation 1.9)}$$

Eigenvectors can only be calculated for square matrices. Given a nxn matrix there are n eigenvectors. If the eigenvector is multiplied by a scalar, the eigenvector will have the length changed but the direction will remain the same. All the eigenvectors of a matrix are orthogonal to each other.

Step 6: Convert the eigenvectors (a_i) to unit vectors ($\hat{a}_i$) i.e., all the eigenvectors will have magnitude of 1. This is done using Equation 1.10 where $\|a_i\|$ is the magnitude of the eigenvector a_i. This conversion does not change eigenvector direction, it only

gives the simpler form of the eigenvector in order to avoid multiple solutions. In Equation 10, $\hat{a}_i$ is the unit vector.

$$\hat{a}_i = \frac{a_i}{\|a_i\|} \qquad \text{(Equation 1.10)}$$

Step 7: Rank the eigenvalues (λi) from highest to lowest in order to rank the principal components in order of significance.

Step 8: Choose the number of PCs and create the feature vector A i.e., a matrix containing the principal components (eigenvectors).

Step 9: Compute the scores matrix (T) i.e., recast the data along the principal components axes using dot product (Equation 1.11), where X is the standardized, and mean centred data matrix, and A is a matrix containing all the principal components chosen in the previous step in column mode. This is the actual dimensionality reduction step. The score matrix defines the location of the orthogonal projection of the original observations in the latent subspace (Tauler et al., 2009).

$$T = X \cdot A \qquad \text{(Equation 1.11)}$$

Step 10: The loading matrix is composed by eigenvectors corresponding to the largest eigenvalues of the covariance matrix of the data set. The loading vectors define the directions of highest variability of the new latent subspace (Tauler et al., 2009) and the loadings can be described as the directional coefficients that compose each PC i.e., loadings are the elements of an eigenvector (Esbensen and Swarbrick, 2019).

Practical issues of PCA are as follows:

- Principal components do not hold physical meaning.

- PCA is too expensive for applications with extremely big data (e. g. extensive web data).
- PCA is based on linearity, thus it does not work well for a data set that has a manifold structure.
- PCA projects the data to a lower dimension data set. Therefore, if the dataset has outliers or special cases of interest, this information would be lost.
- PCA does not recognize class labels, therefore when the classes are known, an additional step is necessary in order to highlight the different classes e.g., name the scores by the class to which they belong. Alternatively, if the classes are not previously known, clustering algorithms can be applied to the PCA scores in order to determine groups that are statistically significantly different from each other.
- PCA is an unsupervised algorithm, thus, the direction of maximal variance is not necessarily the one that makes the best separation of classes. The analyst has to choose carefully the PCs that best describe the phenomenon studied.
- Loadings plot helps the analyst to verify the reasons for the separation obtained from the model (i.e. observed in the PCA scores plot), however the results must be also supported by physicochemical knowledge.

1.6.2 Partial least squares regression

Partial least squares regression (PLS) is a multivariate regression model used to correlate information in one data matrix of independent variables (X) to the information in a matrix of dependent variables (Y) (de Jong, 1993). Similarly to PCA, PLS regression captures the maximum variance within X. However, PLS also captures

the maximum variance in Y, and calculates the maximum correlation between X and Y. As a result, in the future, if only X is known, Y can be predicted.

Considering X a mean-centered *n x m* matrix and Y a mean-centered *n x p* matrix, PLS is derived from a covariance matrix of X and Y, S(X,Y), determined by Equation 1.12. The correlation between X and Y is determined by equation 1.13 (Ng, 2013).

$$\mathrm{S}\,(\mathrm{X},\mathrm{Y}) = \frac{1}{\mathrm{n}-1}\mathrm{X}^{\mathrm{T}}\mathrm{Y} \qquad \text{(Equation 1.12)}$$

$$corr(X,Y) = \sqrt{var(X)\cdot cov(X,Y)\cdot\sqrt{var(Y)}} \qquad \text{(Equation 1.13)}$$

There are different algorithms from which PLS can be determined. In this study, an orthogonalized PLSR algorithm for one Y-variable from the software the Unscrambler (CAMO Analytics, 2011) was used.

1.6.3 Multivariate Curve Resolution

Multivariate Curve Resolution (MCR) (Lawton and Sylvestre, 1971; Martens, 1979) is a group of algorithms developed to implement constraints on loadings and scores so that they have an exact physical interpretation and explain the variance in the data (De Juan and Tauler, 2006; Mendieta et al., 1998). MCR decomposes the data matrix (X) into a matrix of the variation among the observations, named concentration profiles (C), a transpose variance matrix associated with the variation among the variables, named spectra profiles (S^T), and a matrix of residuals not explained by the model (E) (Equation 1.14). As a result, the spectra fingerprint of the single components of a mixture are extracted. The model fit is given by the percentage lack

of fit (%LOF) (Equation 1.15), where x_{ij} is an element of X and e_{ij} is the respective residual. Ideally, %LOF should be close to zero.

$$X=CS^T+E \quad \text{(Equation 1.14)}$$

$$\%\ LOF = 100 \cdot \sqrt{\frac{\sum_{ij} {e_{ij}}^2}{\sum_{ij} {x_{ij}}^2}} \quad \text{(Equation 1.15)}$$

Juan, Jaumot and Tauler, 2014 listed and compared the main MCR algorithms available and discussed the benefits of the algorithm Multivariate Curve Resolution-Alternating Least Squares (MCR-ALS) (De Juan et al., 2014). MCR-ALS is an iterative algorithm that performs alternating optimization in each iterative cycle. The algorithm is based as follows (Esbensen and Swarbrick, 2019; Tauler, 1995):

Step 1: Determine the number of compounds in the data matrix e.g., using PCA or previous knowledge about the system.

Step 2: Determine the initial estimate. The initial estimate can be a pure spectra of some of the compounds that is known, any other information that is available, or the initial estimate can be mathematically determined by local rank map methodologies (Booth, 2005; De Juan et al., 2014). The local rank algorithms screen the profiles in order to identify “windows” i.e., regions from which chemical information can be obtained such as selective information regions, zero-concentration regions, and regions of (A-1) components. The algorithm will correctly determine the initial guess if the following theorems are true (Manne, 1995):

I. The concentration profile of a compound can be determined if all the interfering compounds that are identified inside of the concentration window the given compound can be also identified outside that window.

II. The spectrum profile of a compound can be determined if there is a sub window where no other component information is present.

Step 3: Use the initial estimate S^T to calculate C (or C to calculate S^T) under the applicable constraints.

Step 4: Recalculate S^T using C determined in step 3 (using Equation 1.12, with data matrix=X).

Step 5: Apply Equation 1.12 i.e., multiply C and S^T from steps 3 and 4 in order to calculate the estimated data matrix X.

Step 6: Repeat steps 3, 4, and 5 until convergence i.e., until the fit between two consecutive iterations fall below a previously determined threshold or until a previously determined number of iterations are reached.

The ALS optimization is performed in each cycle for spectra and for concentration profiles estimations, therefore, a sensible initial guess is required in order to shorten the iteration process and guide the convergence to an accurate solution (Mendieta et al., 1998). The set of constraints is what avoids ambiguities inherent to curve resolution due to the fact that different C and S^T type matrixes can represent the data set with the same quality of fit. However, they show different profiles with different shape (rotational ambiguity, mathematically given by Equation 1.16, where T is the T

PCA matrix of scores) or different magnitude (intensity ambiguity) (Esbensen and Swarbrick, 2019).

$$X = CS^T = X(TT^{-1})S^T = (CT)(T^{-1}S^T) = C'S'^T \qquad \text{(Equation 1.16)}$$

The constraints applied to MCR model for optimization can be divided into (1) mathematical conditions, (2) natural constraints, and (3) process constraints (Figure 1.9).

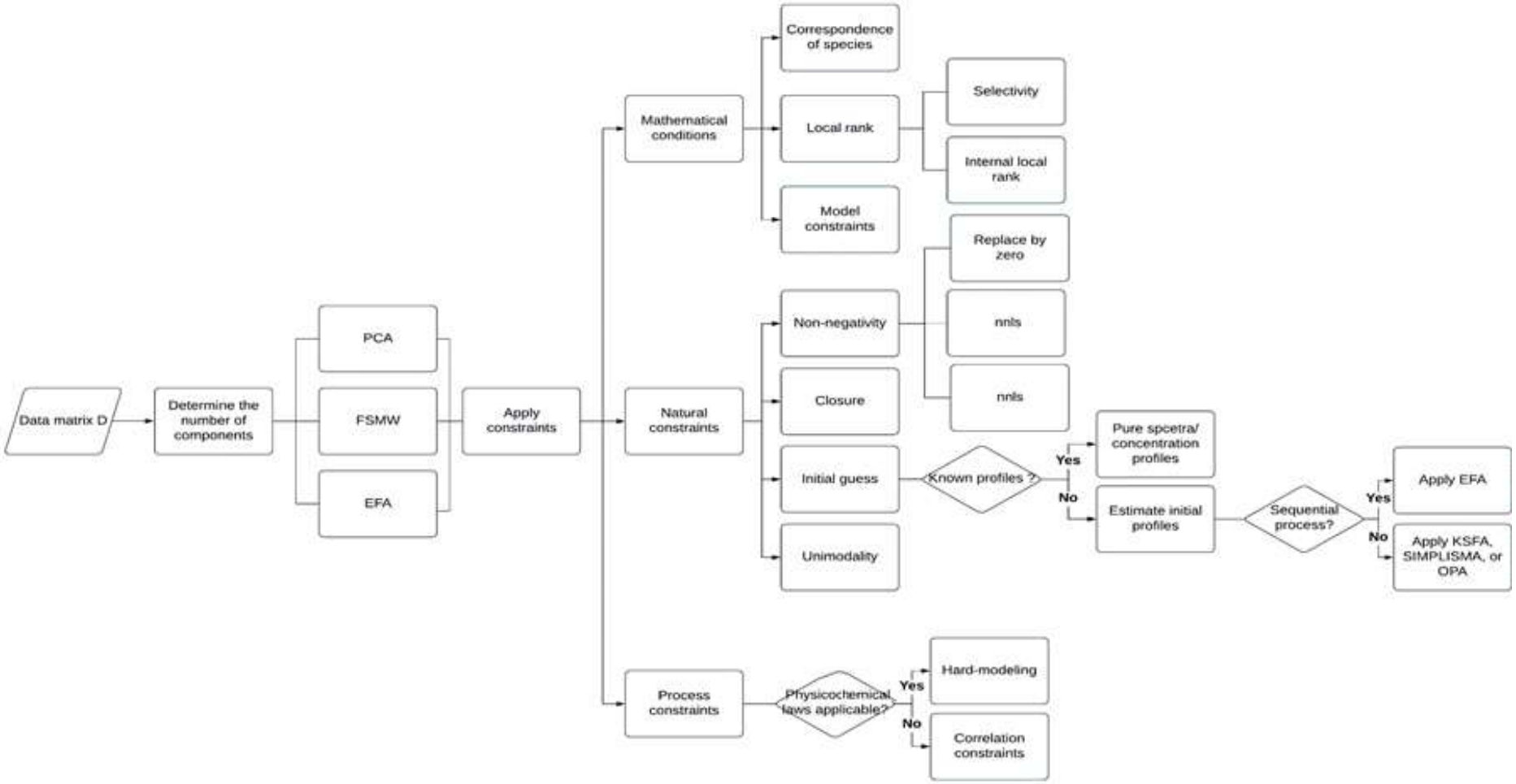

Figure 1.9. Multivariate Curve Resolution workflow.

Mathematical conditions

1- Correspondence of species: useful when data matrices from several different samples are modelled together. Correspondence of species is used to determine the presence or absence of components in the analysed samples and it is also used to reduce ambiguity.
2- Local rank: it is usually applied to concentration profiles in order to avoid ambiguity. This constraint identifies zones of the profile (windows) where there is absence of components. The windows can be determined by local rank analysis methods e.g., EFA. When only one component is observed in a certain window of the profile the selectivity constraint can be applied i.e., there is only one component and therefore it is possible to select the spectra of that region as the initial guess of a pure component. When some components are observed in a zone of the profile, an internal local rank can be applied.
3- Model constraints: proper for multiset data matrices. It can be understood as the applications of conditions of trilinearity, multilinearity, or factor interaction.

Natural constraints

1- Non-negativity: suitable for all concentration profiles and can be used for spectra that do not show values in the negative region. Thus, it cannot be applied to derivative spectra. It forces the profiles to be formed by null or positive values. Non-negative least-squares or fast non-negative least-squares.

2- Closure: it is appropriate when the mass balance conditions are true.

3- Known pure spectral concentration profiles: it forces the spectrum of a component to be equal to a certain known predefined shape.

4- Unimodality: employed when there is the presence of a single peak or a consistent increasing or consistent decreasing profile. It is not applicable when different batches are being compared as screening studies.

Process constraints

1- Hard modelling: constrain concentration profiles by setting physicochemical parameters.

2- Correlation constraint: it is used to predict concentrations in unknown samples when internal univariate calibration models are available.

1.6.4 Heckel model

Heckel model is commonly used for interpretation of the relationship between relative density and applied pressure (Ilkka and Paronen, 1993). It describes the densification of the powder density under pressure as a first-order kinetics process (Patel et al., 2006). According to its differential form (Equation 1.17), the higher the porosity (ε), which is directly related to the density, the more the porosity decreases due to the application of pressure (σ).

$$-\frac{d\varepsilon}{d\sigma} = k \cdot \varepsilon \qquad \text{(Equation 1.17)}$$

The relation between relative density and porosity is known as $\rho = 1 - \varepsilon$ (Leuenberger and Leu, 1992). Rewriting Equation 1.17 for relative density and integrating, the following linear correlation is obtained:

$$\mathrm{Ln}\left(\frac{1}{1-\rho}\right) = \mathrm{K}\cdot\sigma + \mathrm{A} \qquad \text{(Equation 1.18)}$$

where ρ is the tablet relative density, σ is the compaction pressure, A is a constant that represents the degree of packing that can be achieved by rearrangement of particles i.e., before considerable inter-particle bonding take place, and K is a constant related to the ability of the powder to undergo plastic deformation.

1.6.5 Percolation threshold

Percolation threshold theory can be used in pharmaceutical formulation design to determine a concentration range where the property analysed undergoes a sudden change, which can be observed as an edge of failure of formulation processability or CQAs. From this theory it is possible to predict the blends that would present suboptimal properties and thereby determine an optimum drug concentration range to achieve blends designs that are robust with respect to those properties. Percolation threshold theory is mathematically described by the power law of Equation 1.19.

$$X = k_1 \cdot (\rho - \rho_c)^q \qquad \text{(Equation 1.19)}$$

where X is one property observed e.g., tablet strength, drug release, compactibility or electrical conductibility (Fuertes et al., 2006; Gonçalves-Araújo et al., 2008; Guyon et al., 1987; Hwang et al., 2017). The constant k_1 is a proportionality constant or scaling factor, ρ is the occupation probability, ρ_c represents the percolation threshold and *q* is a critical exponent, also known as percolation coefficient.

Since the interest of this thesis is to work with tensile strength, the power law of percolation threshold (Equation 1.19) can be rewritten as Equation 1.20.

$$\sigma_T^{\frac{1}{T_f}} = k_1^{\frac{1}{T_f}} \cdot [\rho - \rho_c(AB)] \quad \text{(Equation 1.20)}$$

Where σ_T is the tensile strength (Equation 1.21), T_f is the percolation coefficient when is calculated for tensile strength, $\rho_c(AB)$ is the percolation threshold, and ρ is the tablet relative density (Equation 1.22).

Tensile strength can be calculated using Equation 1.25.

$$\sigma_T = \frac{2 \cdot H}{\pi \cdot D \cdot T} \quad \text{(Equation 1.21)}$$

In which *T* is thickness, *D* is diameter, and *H* is hardness.

$$\rho = \frac{\rho_{tablet}}{\rho_{true}} \quad \text{(Equation 1.22)}$$

Tablet density,ρ_{tablet}, is obtained dividing tablet weight by tablet volume and ρ_{true} can be measured using a gas displacement pycnometer.

Thus, Equation 1.20 can be applied by performing the linear fit $\sigma_T^{\frac{1}{T_f}} = a \cdot \rho + b$, in which tensile strength (σ_T) and tablet relative density (ρ) are values obtained empirically, T_f can be found in the literature or determined using a modified Heckel Model, and $\rho_c(AB) = -b/a$.

1.6.5.1 Determination of the percolation coefficient using modified Heckel Model

Heckel equation is valid only when ε «ε_c i.e., at high pressures, not in the vicinity of bulk porosity (Kuentz and Leuenberger, 1999). Critical porosity (ε_c) is the maximum

porosity of a powder bed. There is no rigid structure existing aboveε_c. If $\varepsilon \geq \varepsilon_c$there is a fluid with particles moving without resistance. On the other hand, percolation threshold applies for lower pressure, under which there is a rearrangement of the particles inside the die. In order to modify Heckel equation so that it can be used for $\varepsilon < \varepsilon_c$ or $\rho > \rho_c$ i.e., under low pressures, a new parameter, X_p (Equation 1.23), was introduced so that Equation 1.24 is obtained (Kuentz and Leuenberger, 1999). In Equation 1.24, ε is porosity, σ pressure, and q is the generic percolation threshold coefficient.

$$\mathrm{X_p} = \frac{\mathrm{c}}{(\varepsilon_\mathrm{c} - \varepsilon)^\mathrm{q}} \qquad \text{(Equation 1.23)}$$

$$-\frac{d\varepsilon}{d\sigma} \cdot \frac{1}{\varepsilon} = \frac{k_2}{(\varepsilon_c - \varepsilon)^q} \qquad \text{(Equation 1.24)}$$

Rewriting the last equation for relative density (ρ, $\rho = 1 - \varepsilon$) and performing the integration, Equation 1.25 is obtained. This mathematical transformation was described in details by (Kuentz and Leuenberger, 1999).

$$\sigma = \frac{1}{c}\left[\rho_c - \rho - (1 - \rho_c) \cdot Ln\left(\frac{1 - \rho}{1 - \rho_c}\right)\right] \qquad \text{(Equation 1.25)}$$

Equation 1.25 was simplified using Taylor expansion (Kuentz and Leuenberger, 2000). As a result, Equation 1.26 was obtained. This equation is only valid in the vicinity of the percolation threshold, ρ_c.

$$\sigma = \frac{1}{2k_3}\left(\frac{(\rho - \rho_c)^2}{1 - \rho_c}\right) \qquad \text{(Equation 1.26)}$$

Isolating $(\rho - \rho_c)$ in Equations 1.20 and 1.26 and then matching them, the Equation 1.27 is obtained.

$$\sigma_T = k_4 \cdot P^{\frac{T_f}{2}} \qquad \text{(Equation 1.27)}$$

Thus, the percolation coefficient T_f can be determined by the exponential fit of Equation 1.27, where k_4 is a constant, P is the experimental compaction pressure, and σ_T is the tensile strength of tablets compacted at each compaction pressure.

1.6.5.2 Percolation threshold and critical mass fraction

Modelling percolation depends on the dimensionality of the cluster and the system. A tablet is a 3-D system and, in order to best fit the percolation theory, it is considered as a binary system, even though the blend has more than two substances (Leuenberger and Ineichen, 1997). In this case, there are three percolation thresholds: $\rho_c(B)$ the percolation threshold of the API, and $\rho_c(A)$ the percolation threshold of the excipient and $\rho_{c,AB}$ the total percolation threshold. Moreover, the tableting process can be divided into two stages to simplify.

The first stage is when the blend is made by creating weak-bond percolation which corresponds to the vicinity of the relative density ($\rho_{C\approx}\rho_r$) (Leuenberger and Leu, 1992; Sharma et al., 2014). The pressure in this phase is low and the porosity is just smaller than the critical porosity (Kuentz et al., 1999). When this simplification is made, many properties can be described by a straight line. The second stage occurs when the compaction happens forcing the blend to undergo deformation and/or fracture. This phase happens under higher pressure and the compaction process can be considered as a two-dimensional process due to a uniaxial compression where the stress is transmitted from particle to particle (Sharma et al., 2014). This stage is more complex to calculate. Fortunately, for some properties it is possible to consider the

entire process happening as the first stage, so that the property can be approximated by a straight line. This approach works for tensile strength (σ_T) for microcrystalline cellulose compacts (Kuentz and Leuenberger, 2000).

Tensile strength can be explained with a law of percolation theory for a blend in which one component dominates the overall strength of the tablet (Kuentz and Leuenberger, 2000). For each ρ defined empirically, there is a corresponding σ_T calculated. Therefore a straight line equation ($y = a.x + b$) is observed (${\sigma_T}^{1/T_f}$, $x = \rho$, $-K\rho_c = b$ and $K = a$).

$${\sigma_T}^{1/T_f} = a \cdot \rho + b \qquad \text{(Equation 1.28)}$$

The percolation threshold is calculated where ${\sigma_T}^{1/T_f} = 0$ i.e., Equation 1.29.

$$\rho_C(AB) = \frac{-b}{a} \qquad \text{(Equation 1.29)}$$

The values of the percolation threshold of each blend, ρ_c(AB), are then used to obtain two other percolation threshold values $\rho_C(A)$ and $\rho_C(B)$ (Equation 1.30). While $\rho_C(B)$ represents the minimum relative density, or solid fraction, above which there is a change in tensile strength behavior, $\rho_C(A)$ is related to the dilution capacity of substance A. Thus, $\rho_C(A)$ provides the fraction of substance B that could be loaded into the blend with substance A in such a way that substance A still leads the overall properties of the blend.

$$\rho_c(AB) = X_A \cdot \rho_c(A) + (1 - X_A) \cdot \rho_c(B) \qquad \text{(Equation 1.30)}$$

A dilution capacity model was applied in order to express the $\rho_C(A)$ in terms of mass fraction (X_c), Equation 1.31 (Kuentz and Leuenberger, 2000). This conversion was performed as dilution capacity which is a useful parameter to consider when designing a pharmaceutical tablet formulation.

$$X_c = -\frac{\varphi}{2} \pm \sqrt{\frac{\varphi^2}{2} - \emptyset} \qquad \text{(Equation 1.31)}$$

In which φ and ϕ are parameters dependent of the true density of substances A and B respectively and calculated using Equations 1.32 and 1.33, respectively.

$$\emptyset = \frac{\rho_{true}(A)}{\rho_{true}(A) + \rho_{true}(B)} \qquad \text{(Equation 1.32)}$$

$$\varphi = \frac{-2 \cdot \rho_c(A) \cdot \rho_{true}(A) - \rho_{true}(B)}{\rho_c(A) \cdot [\rho_{true}(A) + \rho_{true}(B)]} \qquad \text{(Equation 1.33)}$$

1.7 Background to aspects of pharmaceutical development investigated in this thesis

1.7.1 Raw material CQAs variability

ICH Q11 highlights the importance of linking material attributes and process parameters to CQAs as part of the QbD approach (International Council for Harmonisation, 2012). Raw material attributes has been considered by many authors as a potential source of process variability and an important aspect of pharmaceutical manufacturing to be investigated within the QbD framework (Burke and Zylberberg, 2019; Kushner IV, 2013; Kushner et al., 2011; Mockus et al., 2015; Stauffer et al.,

2019, 2018; Thoorens et al., 2014). The effects of raw material variability on a process is also important based on the QbC approach.

In this thesis, microcrystalline cellulose (MCC) (Figure 1.10) was used as a case study excipient for the development of models to quantitatively determine raw material variability and its impact on processes. MCC is one of the most commonly used excipients in solid dosage pharmaceutical formulations (Thoorens et al., 2014). MCC is inert to most pharmaceutical formulations, has high compactability and some lubricant functionality, and therefore it is widely used as bulking agent for tablet and capsules formulations (Rowe et al., 2009; Thoorens et al., 2015, 2014). MCC also acts as an effective tablet disintegrant (Järvinen et al., 2013). Besides being used in pharmaceutical formulations as binder and filler, MCC is used in other industries as fat replacement and stabilizer in food products, as rheology control agent in cosmetics, and as composite in biodegradable polymers and wooden products (Gibis et al., 2015; Terinte et al., 2011; Thoorens et al., 2014; Vonbehren et al., 2010; Yang et al., 2018).

MCC is obtained by acid hydrolysis of wood or cotton cellulose followed by rinsing and drying (Sun, 2008). Microcrystalline cellulose is a semi-crystalline material with inherent variable crystallinity due to raw material source and variable processing conditions (O'Regan, 2018). Due to its natural origin, batches of microcrystalline cellulose can show significant variability in properties such as crystallinity, moisture content, surface area, porous structure and molecular mass (El-Sakhawy and Hassan, 2007). The different drying processes used to produce MCC are also causes of variability in physicochemical properties of MCC (Sinha et al., 2018). When MCC is

used as a component of solid dosage formulation, batch variability can affect the final product CQAs e.g., tablet hardness and dissolution rates (Thoorens et al., 2014).

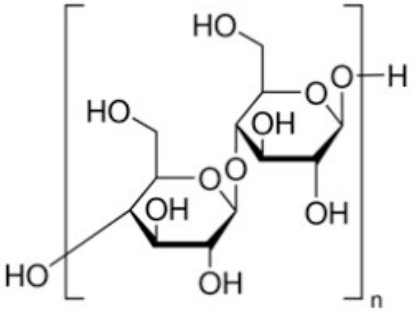

Figure.1.10. Chemical structure of microcrystalline cellulose.

1.7.2 Active pharmaceutical ingredient engineering

More than 35% of frequently prescribed APIs are classified as poorly water soluble according to the Biopharmaceutics Classification System (International Council for Harmonisation, 2019) (Wu and Benet, 2005). A poorly water soluble drug substance is not well absorbed after oral administration, which results in reduced drug bioavailability and efficacy (Vasconcelos et al., 2007). In the aspect of manufacturing, many APIs are not suitable for direct compression with many others not being suitable in high-dose formulations (Leane et al., 2018; Patel et al., 2006; Sun et al., 2017). API engineering approaches have an important role to play in order to address these and other issues that prevent APIs being commercialised or require drug products manufactured through high-cost processes. Examples of API engineering are solvation, hydration, salting, polymorphism, and co-crystallization (Vishweshwar et al., 2006).

Co-crystallization is a crystal engineering approach that has been used to improve API solid state properties (Vishweshwar et al., 2006). Co-crystallization emerged in

recent years and has been widely investigated to enable drug substances to be manufactured for oral administration with high-level bioavailability (Goud et al., 2012; Qiao et al., 2011; Remenar et al., 2003; Rodrigues et al., 2018a; Shan et al., 2014; Silva Filho et al., 2018; Trask et al., 2005). The European Medicine Agency defined co-crystals as "homogenous (single phase) crystalline structures made up of two or more components in a definite stoichiometric ratio where the arrangement in the crystal lattice is not based on ionic bonds (as with salts)" (European Medicines Agency, 2015). Co-crystal can be formed by an API and a coformer, by a co-crystal and a nutraceutical molecule, or by two APIs (Rodrigues, 2019). A coformer is a pharmaceutical substance that meets safety and quality standards (European Medicines Agency, 2015). A nutraceutical molecule is a substance that is part of a food and shows medical or health benefits (Schultheiss et al., 2010).

The development of new co-crystals is an area in significant development. Entresto® and Odomzo® from Novartis, and Steglatro®, Segluromet® and Steglujan® from Merk are among the marketed products containing co-crystals (Rodrigues, 2019). In this thesis, PAT tools and models that yield product and process understanding and process control during co-crystal formation were investigated.

1.7.3 Tablet manufacturing

Solid oral administration is the preferable route of drug delivery due to high stability, small bulk, accurate dosage and easy production (Patel et al., 2006; Rathbone et al., 2003; Vasconcelos et al., 2007). Tablet manufacturing through granulation involves blending the API with excipients to form denser and larger particles. The larger particles produced show improved tableting performance (Mangal and Kleinebudde,

2018). There are different granulation operations such as high shear and fluidized bed, which are employed in wet granulation processes. There are also dry granulation processes, such as roller compaction. Roller compaction is considered the most suitable granulation process when granulation must be performed in continuous manufacturing (Betz et al., 2003). When tablets are produced by direct compression the powder blend does not need to be pre-processed. That is why tablet direct compression has been researched for the implementation of continuous manufacturing and advanced quality approaches (Engisch and Muzzio, 2014; Hausner, 2018; Järvinen et al., 2013).

Direct compression is the simplest tablet manufacturing system. In this process, powder blends of API and excipients are directly compacted into tablets (Figure 1.11) (Gohel and Jogani, 2005). This process has the total operation units reduced, which decrease production costs and time to market (Mangal and Kleinebudde, 2018).

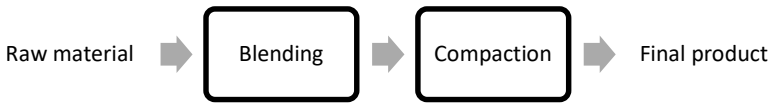

Figure 1.11. Flowchart of a direct compression process.

In this context, compaction is the unit operation in which pressure is applied to a powder bed so that a coherent compact is formed (Patel et al., 2006). This is a critical unit operation because it determines physical and mechanical properties of tablets, such as hardness, friability and density. Those properties are discussed in the next section.

Powder blends containing high-dose, poorly compressible APIs may exhibit compaction problems such as capping, lamination, sticking and picking (Patel et al., 2006). Those problems are expected to increase as the API dosage is increased (Teng et al., 2009). Percolation threshold is a hybrid model that has been investigated to predict the levels of high-dose poorly compressible drug in solid dosage formulations that can be direct compacted with optimal process performance and product quality (Leane et al., 2018, 2015; Leu and Leuenberger, 1993) (See section 1.6.1).

Risk assessment, as part of the control strategy, requires the identification of potentially risky effects of critical material attributes (CMAs) and process variables on product CQAs. Yu, L. X. et al. listed input materials, process parameters and quality attributes that are typically relevant to tableting (Table 1.1) (Yu, 2008). From those, content and uniformity of mass, strength (hardness/friability), disintegration and dissolution are generally considered tablet physicochemical CQAs (FDA, 2015, 2012; International Council for Harmonisation, 1999). Case studies were designed in this thesis to investigate the effects of input material (excipient and formulation) attributes listed by Yu L.X. et al. on the CQA attributes outlined above.

Table 1.1. Input materials, process parameters and quality attributes that are typically relevant to tableting. Adapted from (Yu, 2008)

Input material attributes	**Quality attributes**
Particle/granule size and distribution	Tablet appearance
Fines/oversize	Tablet weight
Particle/granule shape	Weight uniformity
Cohesive/adhesive properties	Hardness/tablet breaking force/tensile strength
Electrostatic properties	Thickness/dimensions
Hardness/plasticity	Tablet porosity/density/solid fraction
Bulk/tapped/true density	Friability
Viscoelasticity	Tablet defects
Brittleness	Moisture content
Elasticity	Disintegration
Solid form/polymorph	Dissolution
Moisture	

1.8 Aims and objectives

The overall goal of this thesis is to increase understanding of pharmaceutical materials attributes and processes performance. For that intensive characterization of CMAs, interactions between API and excipient, and CQAs were investigated. PATs are designed for quantitative characterization and for predicting drug substance and drug product critical properties in order to support the overall goals of this thesis.

Different aspects of pharmaceutical manufacturing were used as case studies and the following objectives were established and split into the following chapters:

Chapter 2

- To develop a PAT technique to quantify variability in MCC crystallinity batch to batch.
- To develop a PAT tool to predict MCC moisture sorption based on the output of the PAT technique to determine MCC crystallinity.

Chapter 3

- To develop PAT tools for co-crystallization process control.
- To develop PAT tools to quantitatively evaluate co-crystal purity.

Chapter 4

- To predict blend direct compression behavior using percolation threshold model and multivariate analysis.

Chapter 5

- To investigate tablet dissolution behavior through the application of PAT tools for tablet characterization and disintegration analysis.

Chapter 2 - Investigating variability in microcrystalline cellulose using Raman spectroscopy

Revised from publication in: *Cellulose (2021)*

2.1 Abstract

Microcrystalline cellulose (MCC) is a semi-crystalline material with inherent variable crystallinity due to raw material source and variable manufacturing conditions. MCC crystallinity variability can result in downstream process variability. The aim of this study was to develop models to determine MCC crystallinity index (%CI) from Raman spectra of 30 commercial batches using Raman probes with spot sizes of 100 µm (MR probe) and 6 mm (PhAT probe). MCC moisture sorption is critical for several industrial processes. Thus, the relationship between %CI and moisture content for those MCC batches was also investigated. A principal component analysis model separated Raman spectra of the same samples captured using the different probes. The differences were attributed to the larger sampling area and depth of the PhAT probe. The %CI was determined using a univariate model based on the ratio of the peaks at 380 and 1096 cm^{-1}. The univariate model was adjusted for each probe. The %CI was also predicted from spectral data from each probe using partial least squares regression models, where Raman spectra and univariate %CI were the dependent and independent variables, respectively. A web application, MCCrystal, containing all the models developed was developed and is available at https://sspc.ie/mccrystal/. A correction between %CI and moisture sorption behaviour could not be established.

2.2 Introduction

Microcrystalline cellulose is widely used and has diverse applications across different industry sectors. MCC is used as a binder and filler in pharmaceutical formulations, a fat replacement and stabilizer in food products, a rheology control agent in cosmetics, and as a component of biodegradable polymers and wooden products (Gibis et al., 2015; Terinte et al., 2011; Thoorens et al., 2014; Vonbehren et al., 2010; Yang et al., 2018). The most common source of MCC is wood. Cellulose chains are present in wood pulp in the form of packed layers that are held together by lignin, and strong hydrogen bonds (Thoorens et al., 2014). MCC is obtained by purification of wood pulp using mineral acid solution i.e., acid hydrolysis, followed by rinsing and drying. The presence of hydroxyl groups in the product of this purification process and the relatively large surface to volume ratio of micro fibrils give rise to MCC's hygroscopic character (Sun, 2008).

MCC has an atypical semi-crystalline structure and its attributes can vary between suppliers and batches. Batch to batch variability can be caused by different factors, such as wood source (hard or soft wood), climate differences from region to region, harvesting time, the process of pulp delignification, hydrolysis reaction time, and the process of drying (O'Regan, 2018). The term crystallinity index (%CI) refers to the percentage by weight occupied by the crystallites (Foster et al., 2018). During depolymerization (hydrolysis) the acid preferentially attacks the amorphous regions of the pulp (Landín et al., 1993) and increases percentage crystallinity.

MCC crystallinity has been reported to influence its behaviour during processing. Tabletability was investigated with differences observed between batches with

substantial differences in crystallinity. Suzuki and Nakagami used a rod mill to reduce crystallinity of a MCC batch from an initial %CI of 65%. A reduction in tabletability was observed for batches with a %CI below 12%, and an increase in dissolution rate was observed for acetaminophen tablets produced with MCC that had a %CI less than 26% (Suzuki and Nakagami, 1999). The crystallinity of MCC has also been shown to influence water sorption (Amidon and Houghton, 1995; Bolhuis and Chowhan, 1996; Nokhodchi, 2005). Increased water sorption was observed with decreased MCC crystallinity, as moisture sorption occurs predominantly in amorphous regions which are more hydrophilic than the crystalline regions (Mihranyan et al., 2004; Segal et al., 1959; Suzuki and Nakagami, 1999).

A range of techniques has been utilised to determine MCC crystallinity. Diffraction techniques are most widely reported, employing the Segal peak height method (Segal et al., 1959), peak decomposition or deconvolution (Lanson 1997; Park et al. 2010; Ahvenainen et al. 2016, Yao et al. 2020), and Rietveld refinement based methods (Madsen et al. 2011; Ling et al. 2019). Other spectroscopic techniques proposed include Fourier transform infrared (Liu and Kim 2015), solid state NMR (Atalla and Vanderhart 1984; Harris et al. 2012; Wickholm et al. 1998), and Sum frequency generation (Ling et al. 2019). Raman spectroscopy, the focus of this study, has been investigated to determine cellulose crystallinity. An initial Raman approach for quantifying MCC crystallinity employed relatively weak bands at 1462 and 1481 cm^{-1} (CH_2 bending modes) in conjunction with spectral deconvolution (Schenzel et al., 2005). Two further methods were proposed employing bands at 380 and 93 cm^{-1} (Agarwal et al., 2018, 2010). The 93 cm^{-1} method

is advantageous compared to the 380 cm^{-1} method as it differentiates crystalline and organized cellulose and an aggregated form which is not crystalline. However, the 93 cm^{-1} method requires an FT-Raman instrument with 1064 nm excitation to avoid Rayleigh scattering that masks the sample Raman scattering at 93 cm^{-1}.

The quantification of cellulose crystallinity using Raman spectroscopic analysis has primarily employed Raman instruments with laser spot sizes between 50 µm and 1 mm and limited depth of penetration (Agarwal et al., 2018, 2010; Foster et al., 2018). The irradiation area of such instrumental setups results in a limited area being sampled. Therefore, analysis requires the acquisition of multiple spectra across a number of locations to obtain a representative profile of the sample. Reduced depth of penetration also results in spectra that focus on surface spectral features. To date Raman probes with larger laser spot sizes and depth penetration, designed for non-contact analysis of solids, have not been applied to the quantification of cellulose crystallinity. It was hypothesised the larger sample volume irradiated using these probes would reduce the requirement for multiple spectra acquisition and surface mapping. Contact probes are usually used for suspensions/solutions and the probe window of a contact probe is in contact with the suspension. Non-contact probes are usually used for solid samples and the probe window needs to be placed at the minimum distance specified by the equipment supplier.

The objective of this study was to demonstrate the capability of Raman spectra acquired using non-contact Raman probes to predict the %CI of commercial MCC batches. Raman spectra acquired for 30 commercial MCC batches, using two probes with spot sizes of 100 µm (MR probe) and 6 mm (PhAT probe), were used to develop

models to determine %CI. The relationship between MCC %CI and moisture sorption behaviour was also investigated.

2.3 Materials

Thirty batches of microcrystalline cellulose were studied. Samples comprised MCC manufactured by 3 different suppliers; 25 batches from Dupont Nutrition & Biosciences, 4 batches from JRS Pharma, and 1 batch from Asahi Kasei Corporation. All MCC grades analysed compiled with USP/NF, Ph.Eur and JP pharmacopeia. Wood pulp was confirmed as the botanical source for 29 of the 30 batches analysed, for one batch the botanical source could not be confirmed.

2.4 Methods

2.4.1 Milling standards to produced reference amorphous

Milling was performed in order to obtain amorphous reference spectra. Prior to milling, the samples were kept in the oven at 40 °C for 24 hours. To produce amorphous reference materials for each batch 1 g of MCC was milled at 25 Hz in an oscillatory ball mill, Mixer Mill MM400 (Retsch GmbH, Germany), in order to decrease the crystallinity (Mattonai et al., 2018). All samples were milled for 90 min to replicate the methodology of previous studies (Agarwal et al., 2010). A break of 15 minutes was performed after every 30 min of milling operation. Samples of 7 batches were confirmed to be amorphous after 90 min milling by powder X-Ray diffraction (PXRD). These batches included MCC batches

from each supplier and each grade. PXRD diffractograms of these batches before and after ball milling are included Fig. S2-S8 in the supplemental material.

2.4.2 Powder X-ray diffraction

Powder X-Ray Diffraction (PXRD) analysis was performed using a Stoe Stadi MP diffractometer operating in transmission mode, with a tube voltage of 40 kV and current of 40 mA, using Cu Kα1 monochromated radiation (1.5406 Å) and a gas-filled PSD detector. MCC powder samples were held between acetate foils and the diffraction was recorded over 5 to 45° 2θ in steps of 2° 2θ at 90 sec/step.

2.4.3 Preparation of pellets for Raman spectroscopy

Cylindrical, flat, 13 mm diameter, 250 mg pellets were produced using an Atlas 15T Manual Hydraulic Press (Specac Ltd, Orpington, UK). Three tonnes force were applied for a duration of 30 seconds. Two pellets were produced for each batch; one from the powder as received and one from the corresponding ball milled sample.

2.4.4 Raman spectroscopy

Raman spectra for each pellet were acquired using two different probes. The first was a MR probe connected to a RamanRxn™ instrument (Kaiser Optical Systems Inc., Ann Arbor, USA), with nominal laser beam diameter at a focal position of 100 µm. The exposure time set was 60 s, using a laser power of 785 mW, over the range 200-1500 cm^{-1}, and analysis was performed in triplicate. The second was a PhAT probe connected to a $RamanRxn_2PhAT^{TM}$ instrument (Kaiser Optical Systems Inc., Ann Arbor, USA), with nominal laser beam diameter at a focal position of 6 mm. The exposure time was set to 15 s, using a laser power of 785 mW, over the range 200-

1500 cm^{-1}, and analysis was performed in duplicate. Moreover, while the MR probe is primarily a surface technique, the PhAT probe has a collection zone depth of around 2 mm.

In addition to the sample Raman fingerprint, the spectra obtained contained a background contribution that may be caused by fluorescence or thermal fluctuations on the Charge Coupled Device (CCD detector) (Bocklitz et al., 2011; Gautam et al., 2015). The fluorescence background was removed by pre-processing. The spectra underwent a baseline subtraction of an interpolated linear fit between the anchor points fixed on the X axis: 1500, 1200, 952, 857, 743, 632, 550, 260, and 200 cm^{-1} (Figure 2.1). The intensity differences observed between the spectra were removed by standard normal variate (SNV). This normalization consisted of subtracting each spectrum from the mean and dividing the result by the spectrum standard deviation.

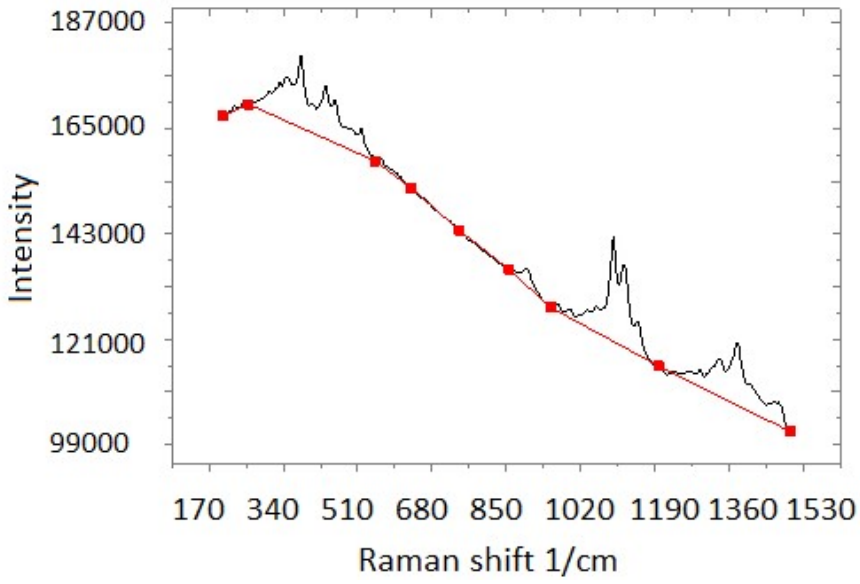

Figure2.1. Representation of the interpolation between the 9 anchor points defined. The baseline was obtained by subtracting the line interpolated between the 9 points (red) from the spectra (black), and it was performed individually for each spectrum.

2.4.5 Univariate determination of crystallinity index

Crystallinity index was calculated according to the method proposed by Agarwal et al., which is based on the ratio between the intensity of the peaks at 380 cm^{-1} and 1096 cm^{-1} deconvoluted from a reference amorphous spectrum (referred to henceforth as the "380-method") (Equation 2.1) (Agarwal et al., 2010). Deconvolution is required because cellulose Raman spectra are composed of the amorphous and crystalline spectra superimposed (Agarwal et al., 2010). Deconvolution in this study refers to the extraction of the amorphous and the crystalline spectral contributions from the actual measured spectrum. The ratio of these peaks was compared to other peaks ratios and showed efficiency and great sensitivity to cellulose crystallinity changes (Agarwal et al., 2018, 2010).

$$\%CI = \frac{\left(I_{380} - I_{380\_am} \Big/ I_{1096} - I_{1096\_am}\right) - 0.0286}{0.0065} \qquad \text{(Equation 2.1)}$$

I_{380} and I_{380_am} are the intensities at the Raman shift 380 cm^{-1} of the commercial batch as received and its corresponding amorphous sample, respectively. I_{1096} and I_{1096_am} are the intensities at the Raman shift 1096 cm^{-1} of the commercial batch as received and its amorphous corresponding sample, respectively.

The spectra of corresponding amorphous samples were obtained by ball milling a sample of the batch (section 2.4.1), pressing the powder into a pellet (section 2.4.2), and acquiring spectra of the pellet. Following the method previously reported by Agarwal et al (Agarwal et al., 2010), each Raman spectrum was pre-processed and peak normalized by equalizing the intensity values at Raman shifts above 857 cm^{-1} to the intensity at 857 cm^{-1} (Agarwal et al., 2010). The resulting spectrum was

considered to represent the amorphous contribution to the Raman spectra of the sample as received (Agarwal et al., 2010). Thus, in Equation 2.1, I_{380_am} and I_{1096_am} are equal to the intensity of the peaks at 380 cm^{-1} and 857 cm^{-1} in the spectrum of the milled sample, respectively.

2.4.6 Correction of 380-method due to Raman instrument-dependence

The 380-method (Equation 2.1) was developed using the Raman instrument RFS-100 (Bruker Inc.) (Agarwal et al., 2010). Crystallinity values determined by the 380-method show instrument-dependence and therefore a set of calibration samples have to be prepared and analysed on each instrument employed (Foster et al., 2018). A calibration study was therefore performed to correct this methodology for the Raman instruments used in the current study i.e., the MR and the PhAT probes connected to a RamanRxn™ and a RamanRxn$_2$PhAT^{TM}), respectively. A single MCC batch was randomly chosen to create the calibration set. The crystallinity of this batch, referred to as "control", was determined by PXRD (Equation 2.2) in triplicate.

$$\%CI_{control} = \frac{(I_{22.6} - I_{18.7})}{I_{22.6}} \qquad \text{(Equation 2.2)}$$

The $\%CI_{control}$ is the PXRD crystallinity index, I_{200} is the intensity at 22.6° 2 theta representing the crystalline peak, and $I_{18.7}$ is the baseline intensity at 18.7° 2 theta corresponding to the amorphous scatter (Segal et al., 1959). PXRD diffractograms were measured in transmission mode using a D8 ADVANCE (Bruker AXS Inc., GmbH, Germany) using Cu Kα (λ = 1.5406 Å) radiation. The samples were analysed over the 2 theta range 3.5 to 45 in steps of 0.5 ° at 1.7 sec per step. A representative diffractogram is shown in Figure 2.2.

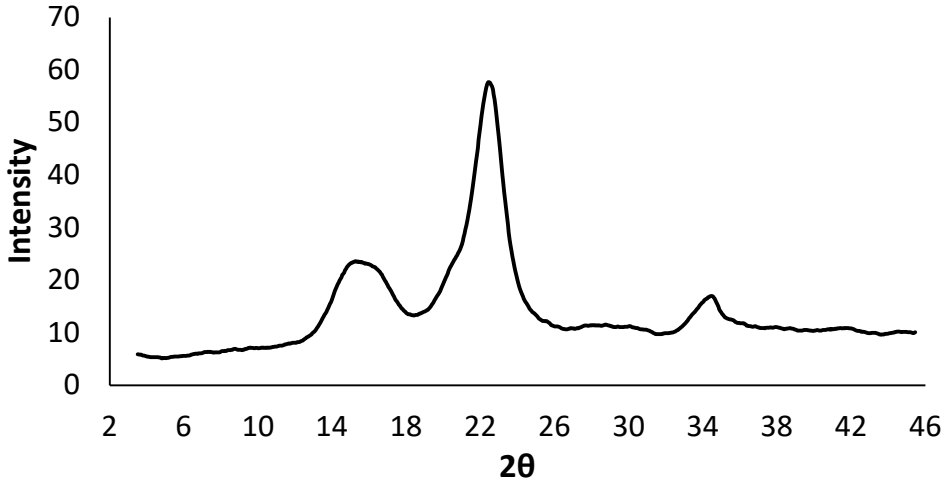

Figure 2.2. Representative PXRD diffractogram of microcrystalline cellulose.

Binary mixtures of control (MCC as received, prior to ball milling) and amorphous (MCC ball milled) were prepared at a total mass of 0.50 ± 0.03 g. The blends analysed contained 83%, 72%, 58%, 44%, 33%, and 22% w/w of control sample. The 100% control and the 100% amorphous samples were also used in the calibration. The theoretical crystallinity index ($\%CI_T$) of each blend prepared was calculated from $\%CI_{control}$, correcting for amorphous content using Equation 2.3.

$$\%CI_T = \frac{\%CI_{control} \cdot m_{control}}{m_{blend}} \quad \text{(Equation 2.3)}$$

where $m_{control}$ is the mass in gram of the control and m_{blend} is the total mass of the blend (grams of control plus amorphous MCC).

The values of the theoretical crystallinity indexes determined by PXRD (Equation 3) were plotted against the peak ratio of the Raman wavenumbers 380/1096 cm^{-1} after amorphous contribution subtraction. A linear regression between the theoretical % CI and the ratio 380/1096 cm^{-1} was obtained for each instrument and the linear

equation obtained was used to determine the % CI by the 380-method for all other batches.

2.4.7 Principal Component Analysis

Principal component analysis (PCA) was performed in order to identify differences between the Raman spectra obtained for the 30 commercial batches of MCC investigated. Unscrambler® X 11.0 software (CAMO software, Norway) was used to perform the analysis on the treated (baseline corrected and normalized) Raman spectra. The algorithm NIPALS and cross validation were performed with 29 segments determined so that spectra of the same batch acquired using both probes were kept within the same segment to avoid overfitting. A total of 145 spectra were used to build the PCA model. These spectra were acquired for the 30 different batches using two different probes.

2.4.8 Partial least squares Regression

Two partial least squares regression models were built using Unscrambler® X 11.0 software (CAMO software, Norway) aimed at predicting the crystallinity index from Raman spectral analysis of the 30 commercial MCC batches. One model was built using the treated (baseline corrected and SNV) Raman spectra acquired using the MR probe and another model using the treated spectra acquired using the PhAT probe. The intensity of the treated Raman spectra between 1500-250 cm^{-1} were used as X variables. For both models, the Y variable was the % CI determined by the 380-method. The algorithm Kernel was used. A total of 24 batches were used to calibrate

the model and 6 batches were used to validate the model. The number of spectra used were 85 and 60 for MR probe and PhAT probe models, respectively.

2.4.9 Determination moisture monolayer

A commonly used approach to quantify moisture content in hydrated polymers is % loss on drying. However, strongly associated water molecules are not accurately quantified by this technique (Agrawal et al., 2004) and ambient humidity influences the moisture content quantified by % loss on drying. Therefore, dynamic vapour sorption (DVS) was applied to provide a more in-depth analysis of moisture sorption behaviour of MCC across a range of relative humidity.

A Dynamic Vapour Sorption, DVS Intrinsic® (Surface Measurement Systems, London, UK) system was used to quantify the equilibrium moisture sorption of all MCC samples. Samples were analysed over relative humidity range of 0-90 % RH with a 10 % relative humidity (RH) stepwise humidity change for both sorption and desorption cycles (n=2). The sample weight was maintained between 10-15 mg. All samples were analysed at 25 C, with 5 s data collection intervals and a total flow rate of 200 sccm (standard cubic centimetre per minute). The actual humidity values were controlled to ± 0.5 % of the target RH and the mass change in samples was recorded every minute. Initially a drying step was completed at 0% RH for six hours. Equilibrium moisture sorption was deemed to have been achieved when the total mass change was < 0.002 %/min for greater than 10 min. When the equilibrium condition was met, the RH was automatically increased/decreased by 10 % RH until a sorption/desorption cycle of 0-90-0 % RH was completed.

Moisture monolayer value was determined using the Guggenheim, Anderson and de Boer (GAB) sorption isotherm (Blahovec and Yanniotis, 2008; Timmermann, 2003). The GAB equation (Equation 2.4) was converted to a second-order polynomial equation (Equation 2.5). The monolayer moisture sorption value was calculated by fitting the isotherm sorption values obtained for each batch to Equation 2.5 using R studio software (Agrawal et al., 2004)

$$W = \frac{W_m \cdot C_g \cdot K(P/P_0)}{[1 - K(P/P_0)][1 - K(P/P_0) + C_g \cdot K(P/P_0)} \quad \text{(Equation 2.4)}$$

$$\frac{P/P_0}{W} = \alpha \left(\frac{P}{P_0}\right)^2 + \beta(P/P_0) + \gamma \quad \text{(Equation 2.5)}$$

where W is the weight of moisture per weight of dry solid absorbed by the MCC sample at a particular relative pressure (P/P_o), W_m is the weight of vapour per weight of dry solid assumed to be associated with all primary binding sites, and C_g and K are constants related to free energy of sorption. The constants α, β and γ values in Equation 2.5 are determined from quadratic regression analysis and used to calculate W_m using the following equation (Equations 2.6).

$$W_m = \frac{1}{\sqrt{\beta^2 - 4\alpha\gamma}} \quad \text{(Equation 2.6)}$$

2.4.10 Correlation of DVS moisture monolayer and crystallinity index

A Pearson correlation (Benesty et al., 2009) between moisture monolayer and % CI for each batch was performed in order to investigate if the layer of water tightly bound to the MCC structure (moisture monolayer obtained by fitting the GAB equation to DVS isotherms) can be predicted from the crystallinity index determined

using the 380 method. Two linear equations were built; one fitting to the moisture monolayer and % CI determined using the MR probe, and a second fitting to the moisture monolayer and the %CI determined using the PhAT probe. PLS models were also investigated. The intensity of the treated Raman spectra between 1500-250 cm^{-1} were used as X variables. For both models, the Y variable was the moisture monolayer determined by GAB equation applied to the DVS isotherms. The algorithm Kernel was used. A total of 24 batches were used to calibrate the model and 6 batches were used to validate the model. The number of spectra used were 85 and 60 for MR probe and PhAT probe, respectively.

2.4.11 Shiny web application

A web application, MCCrystal, was built using 'shiny' (Chang et al., 2019) version 1.4.0 in R (R Core Team, 2019) using the development environment RStudio (RStudio Team, 2019). This application was built to facilitate the dissemination of the models developed in this study. The web application framework for R was developed in tab set panels using the package 'shinydashboard' (Chang and Borges Ribeiro, 2018) version 0.7.1. The package 'RcppArmadillo' (Eddelbuettel and Sanderson, 2014) version 0.9.800.3.0 was used to manipulate matrices, graphics were built using the package 'ggplot2' (Wickham, 2016) version 3.2.1, the spectra were normalized using the package 'prospectr' (Stevens and Ramirez-Lopez, 2013) version 0.1.3, and manipulated using the package 'spectrolab' (Meireles et al., 2018) version 0.0.8. Spectra baseline correction i.e., linear interpolation between predetermined points, was performed using the package 'spftir' (Pozo Valenzuela and Rodriguez-Llamazares, 2016) version 0.1.0. Principal component analysis was performed using

'pracma' (Borchers, 2019) version 2.2.9. Partial least squares regression was performed using the package 'PLS' version 2.7.2 (Mevik and Wehrens, 2015). The package 'basicTrendline' (Mei and Yu, 2018) version 2.0.3 was used to plot the trendline between %CI determined by the univariate model (380-model) and the PLS model. MCCrystal can be accessed at https://sspc.ie/mccrystal/.

2.5 Results

2.5.1 Raman spectra fluorescence background removal

Prior to designing models to predict MCC %CI from Raman spectra, it was necessary to remove spectral interference. Fluorescence background, baseline shifts and intensity differences were observed (Figure 2.3). The baseline subtraction method developed eliminated the fluorescence background and SNV eliminated intensity differences observed between the spectra. All spectra used in this study were baselined and SNV normalized accordingly.

A

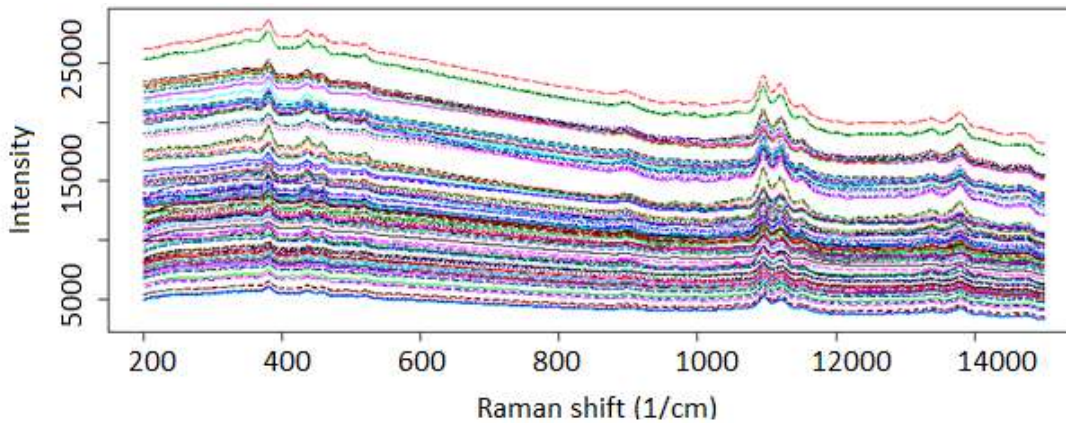

B

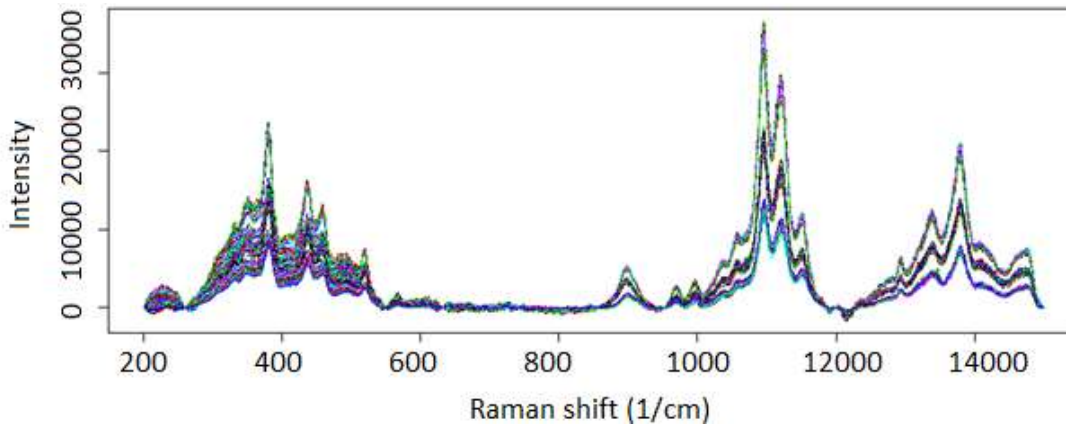

C

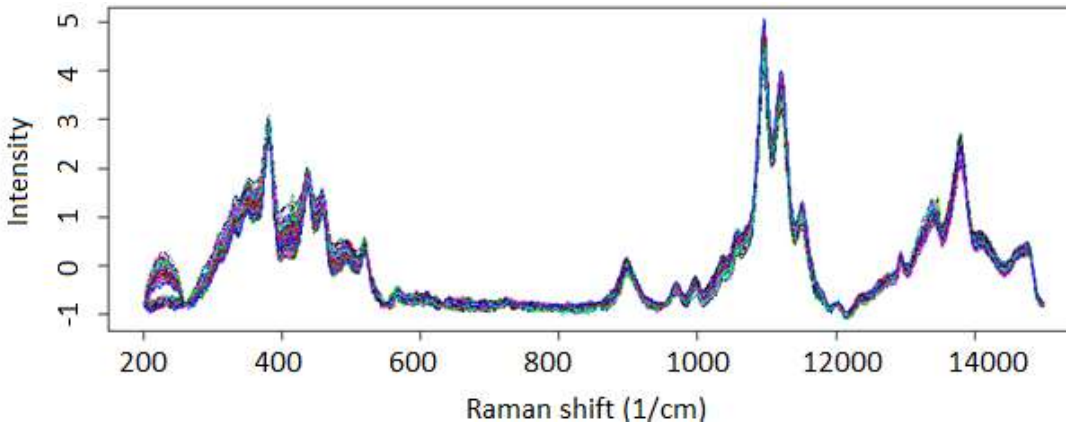

Figure 2.3. Spectra acquired by the PhAT probe (A) raw spectra exhibiting the fluorescence background and intensity shifts, (B) spectra following baseline transformation, and (C) spectra following SNV and baseline transformation.

2.5.2 Principal component analysis

A PCA model was used to explore spectral differences due to the probe set-up used. For this purpose, the model was built from treated spectra (baseline and SNV) acquired using both MR and PhAT probes. The scores plot (Figure 2.4a) shows a clear separation of the samples into two groups based on the spectra acquired using either the MR probe or the PhAT probe. The Raman shifts that lie within the upper and lower bounds of the correlation loadings plot are the regions where the variability was modelled by that principal component (Figure 2.4b and 2.4c). Variability in the regions containing the peaks at 380 and 1096 cm^{-1} are captured by the PCA model. Spectral comparisons showed that the peak intensity at 1096 cm^{-1} is higher and at 380 cm^{-1} is lower for the PhAT probe in comparison to the MR probe. Figure 2.5 provides representative spectra for a single batch highlighting that differences in intensities were observed for spectra acquired using the different probes, and these differences could not be removed by baseline correction or SNV. This is a strong indication that the %CI determined using spectral data from a MR probe cannot be compared to the crystallinity index determined using spectra data from a PhAT probe.

A

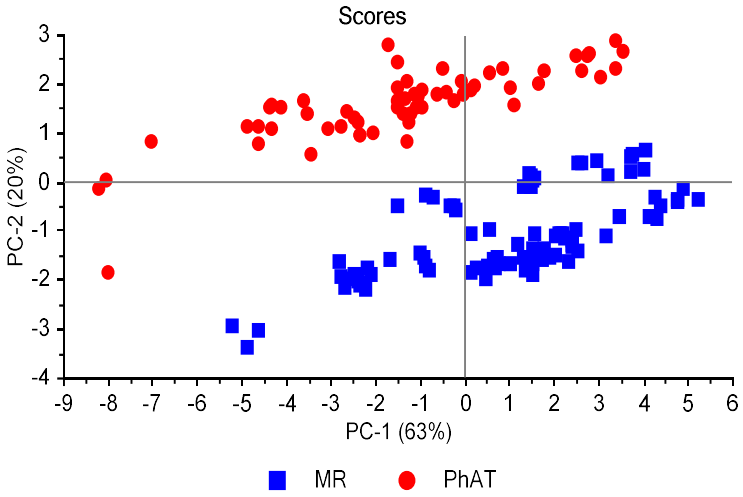

B

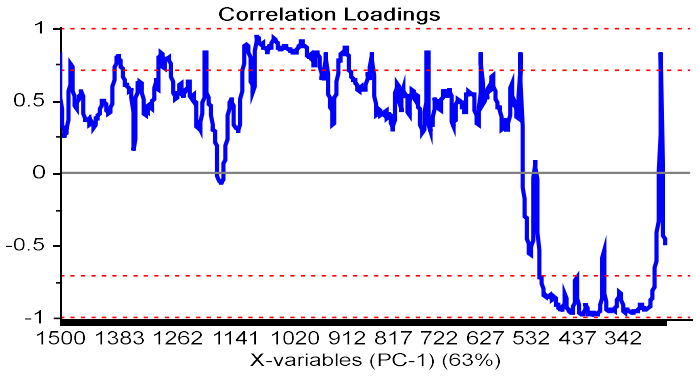

C

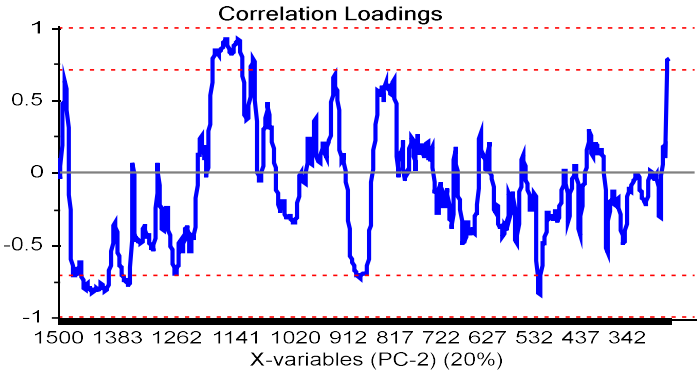

Figure 2.4. (A) PCA scores plot, (B) correlation loadings of the first principal component and (C) correlation loadings of the second principal component of the model built using spectra of 30 MCC batches acquired with MR (n= 85 spectra) and PhAT (n= 60 spectra) probes.

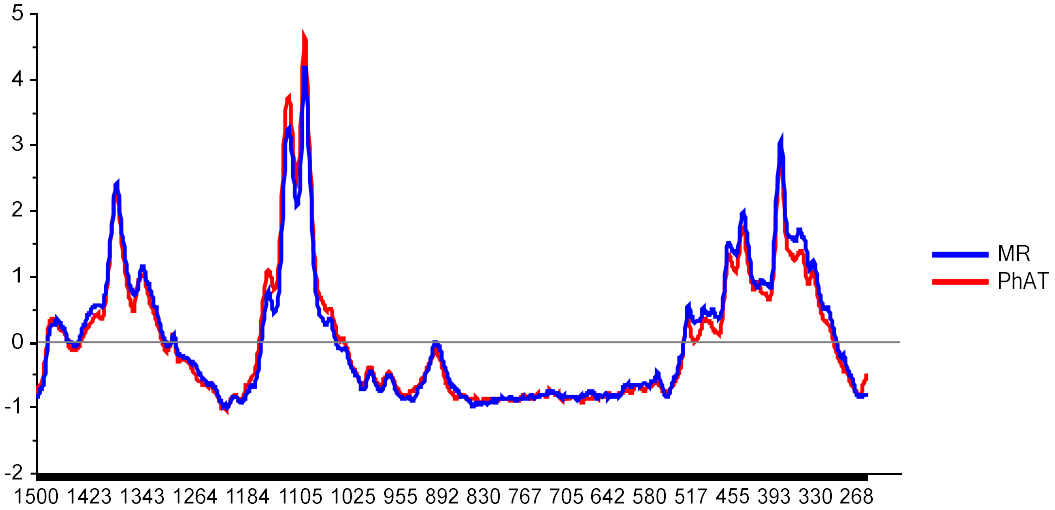

Figure 2.5. Spectra acquired using MR and PhAT probes after baseline correction and SNV normalization for a sample of single batch.

2.5.3 Development of specific 380-method equations for MR and PhAT Raman instruments

Linear regression plots of theoretical crystallinity index determined from PXRD ($\%CI_T$) and the ratio between the Raman intensities at 380 and 1096 cm^{-1} showed correlation for spectra acquired using both the MR and PhAT probes. Pearson's r values of 0.960 and 0.986 for the MR probe and PhAT probe, respectively were obtained (Figure 2.6). Differences in the linear relationship can be explained by the capacity of each probe to capture the intrinsic crystallinity heterogeneity of MCC samples. A PhAT probe averages a larger area (12.57 mm^2) in comparison to a MR probe (7.85 x 10^{-3} mm^2). Thus, the PhAT probe was able to capture a more representative measurement of the sample. This may explain why the PhAT probe showed a marginally better correlation to the theoretical crystallinity index, $\%CI_T$. Replicate spectra acquired by the PhAT probe also provided more consistent peak ratio values for the same sample. Figure 2.6 contains replicates (n=3 for MR probe

and n=2 for PhAT probe) and it was clear that the replicate PhAT probe measurement deviated less than the MR probe measurements.

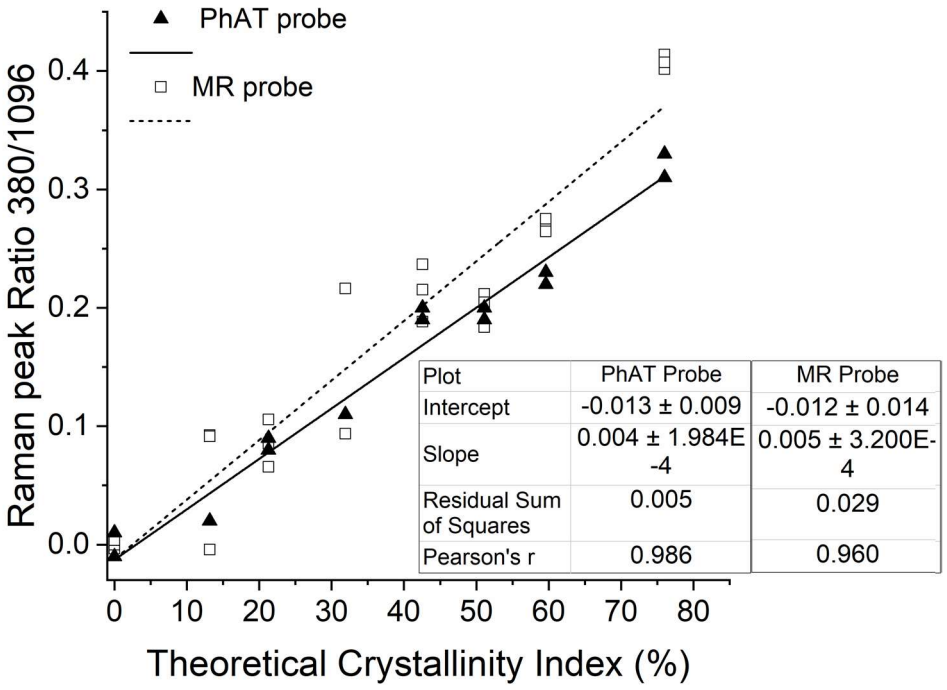

Figure 2.6. Correlation between the ratio of the Raman intensities at 380 and 1096 cm^{-1}, and the theoretical crystallinity index determined using PXRD. Pre-treated spectra obtained for blends using MR and PhAT probes were used.

Based on the correlations shown in Figure 2.6, specific 380-method equations were proposed for MR and PhAT instrumental systems, Equations 2.7 and 2.8, respectively.

$$\%CI_{MRprobe} = \frac{\left(I_{380} - I_{380_{am}} \Big/ I_{1096} - I_{1096\_am}\right) + 0.0124}{0.0050} \qquad \text{(Equation 2.7)}$$

$$\%CI_{PhATprobe} = \frac{\left(I_{380} - I_{380\_am} \Big/ I_{1096} - I_{1096\_am}\right) + 0.0128}{0.0043} \qquad \text{(Equation 2.8)}$$

2.5.4 Determination of MCC crystallinity indices for commercial batches

The %CI for a set of 30 commercial batches was determined using the corrected 380-method (Equations 2.7 and 2.8) applied to spectral data acquired using the MR and

PhAT probes, respectively. Amorphous spectra were obtained for each MCC batch with both probes. From the processed amorphous spectra from each batch obtained using the MR probe (n=70) and PhAT probe (n=55), an averaged amorphous spectrum was generated for both probes. The averaged intensities and standard deviations for the peaks of interest for the MR probe averaged amorphous spectrum were I_{380_am} (0.627 ± 0.246) and I_{1096_am} (-0.886 ± 0.042) and for the PhAT probe averaged amorphous spectrum were I_{380_am} (1.194 ± 0.277) and I_{1096_am}(-0.907 ± 0.022). These averaged amorphous spectra were used in the determination of %CI for each batch. The % CI values obtained for all MCC batches investigated are shown in Figure 2.7.

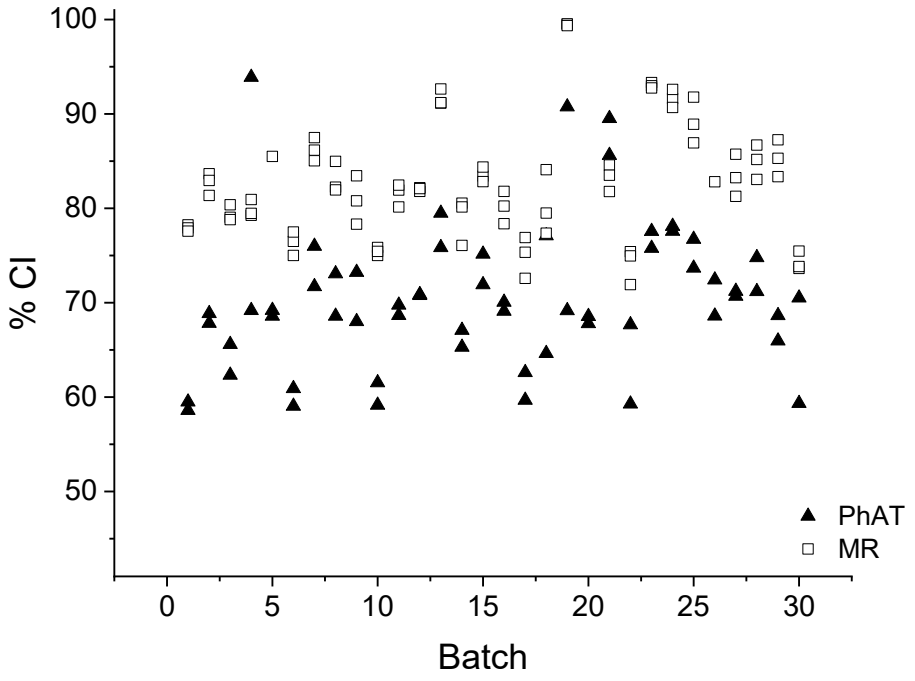

Figure 2.7. Crystallinity index (%CI) determined for commercial batches using spectra obtained for pellets and different probes (MR probe n = 3, and PhAT probe n = 2, using Equation 2.7 and 2.8, respectively).

2.5.5 Partial least squares regression models

A PLS model was built as an alternative to the 380-method in order to avoid having to undertake milling and spectra deconvolution steps. Agarwal et al. also used a PLS model to determine %CI (Agarwal et al., 2010). However, the present study involved a greater number of MCC batches and reflects the variability across commercial batches, while the study published by Agarwal et al. included several blends of commercial batches as received and their reference milled sample, at different mass fractions.

Statistically significant PLS models were determined for both probes (Table 2.1, Figures 2.8 and 2.9). The optimal number of factors for both models was considered to be three, which represented 97.82 % of variance for the MR probe data and 98.57 % of the variance for PhAT probe data. The variability captured by the first factor of both models included the Raman shifts known to be correlated to MCC crystallinity (and used to calculate MCC crystallinity by the 380-method), which was not surprising because the independent variable used to build the model was the %CI from the 380-method. This can be seen in the correlation loadings where the Raman shifts that fall within the upper or lower outer lines are the Raman shifts used by that factor to build the model (Figures 2.8 B-D, and 2.9 B-D).

Table 2.1. Summary statistics of the Partial least squares Regression models. N is the Number of factors, RMSEC is the Root Mean Square Error of Calibration, RMSEP is the Root Mean Square Error of Prediction.

Statistical descriptors	**MR probe**			**PhAT probe**		
Number of calibration samples	67			48		
Number of validation samples	18			12		
Optimal number of factors	3			3		
N	1	2	3	1	2	3
RMSEC	1.928	1.101	0.922	1.683	1.459	0.896
RMSEP	1.594	1.093	1.052	1.779	1.917	1.319
Explained variance (Calibration) (%)	90.47	96.89	97.82	94.97	96.22	98.57
Explained variance (validation) (%)	91.66	96.08	96.37	95.02	64.22	97.26
Bias	-0.760	-0.277	0.396	-0.271	0.138	0.431

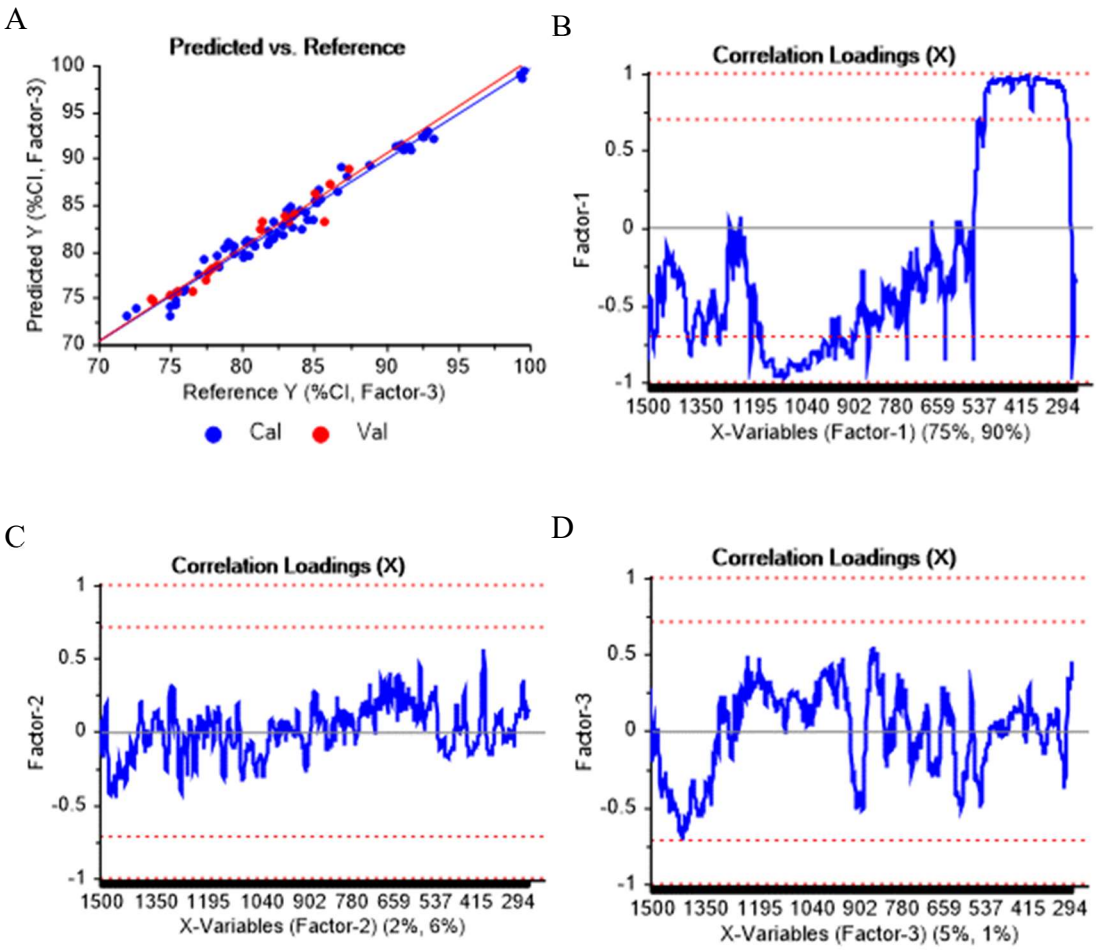

Figure 2.8. (A) Values of crystallinity index (%CI) predicted by the Partial least squares Regression model vs Reference values for the MR probe and considering three factors, and (B, C, and D) correlation loadings of factors 1, 2, and 3, respectively, obtained from the model designed using baselined and normalized spectra. The further the correlation loading is from the zero, the stronger the Raman shift contributed to explain the variability encountered by the factor. In blue are the calibration and in red the validation sets.

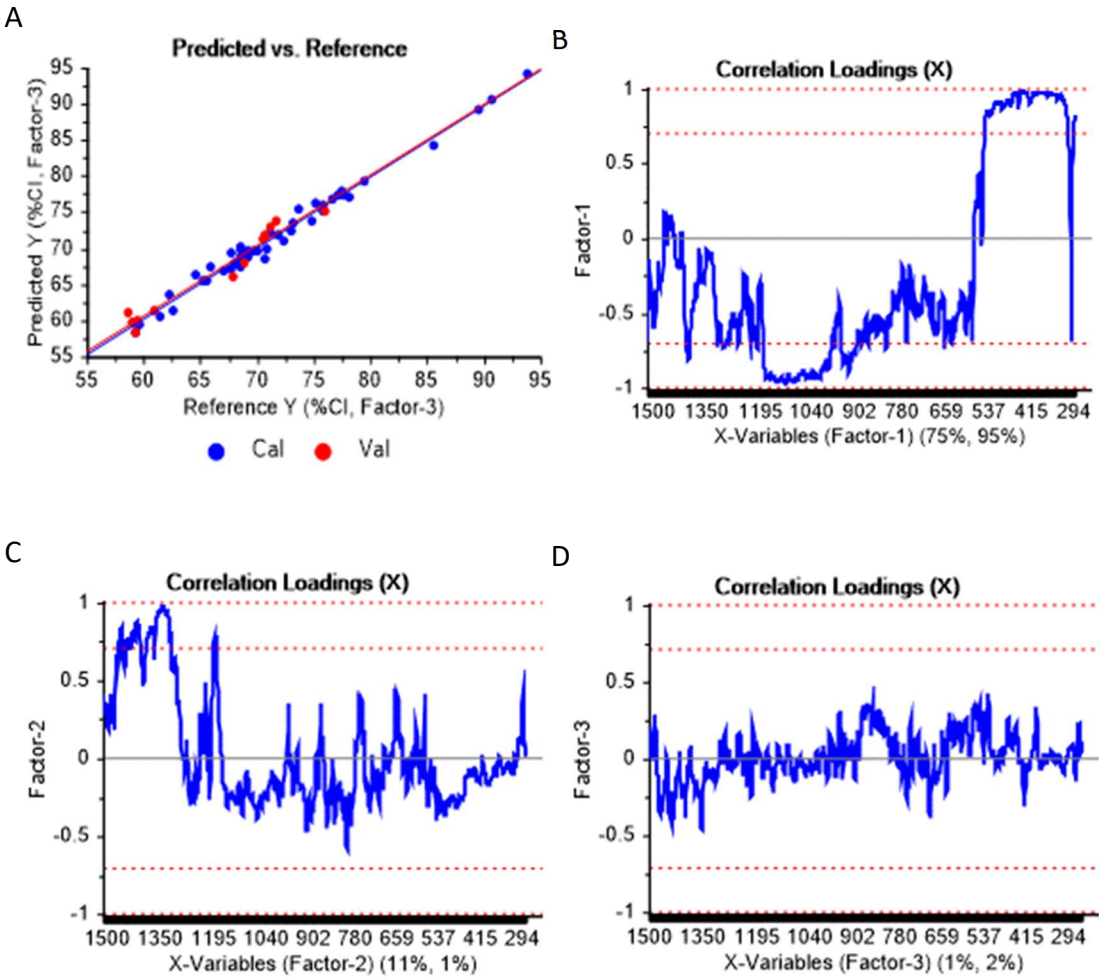

Figure 2.9. (A) Values of crystallinity index (%CI) predicted by the Partial least squares Regression model vs Reference values for the PhAT probe and considering three factors, and (B, C, and D) correlation loadings of factors 1, 2, and 3, respectively, obtained from the model designed using baselined and normalized spectra. The further the correlation loading is from the zero, the stronger the Raman shift contributed to explain the variability encountered by the factor. In blue are the calibration and in red the validation sets.

The scores plot of the PLS models was used to investigate spectral differences between batches of different average particle size and grades. However, the model was not able to separate the batches by average particle size nor grade i.e., the PLS model was not able to identify patterns in the Raman spectra to cluster the batches in groups of the same average particle size nor groups of the same grade (Figure 2.10).

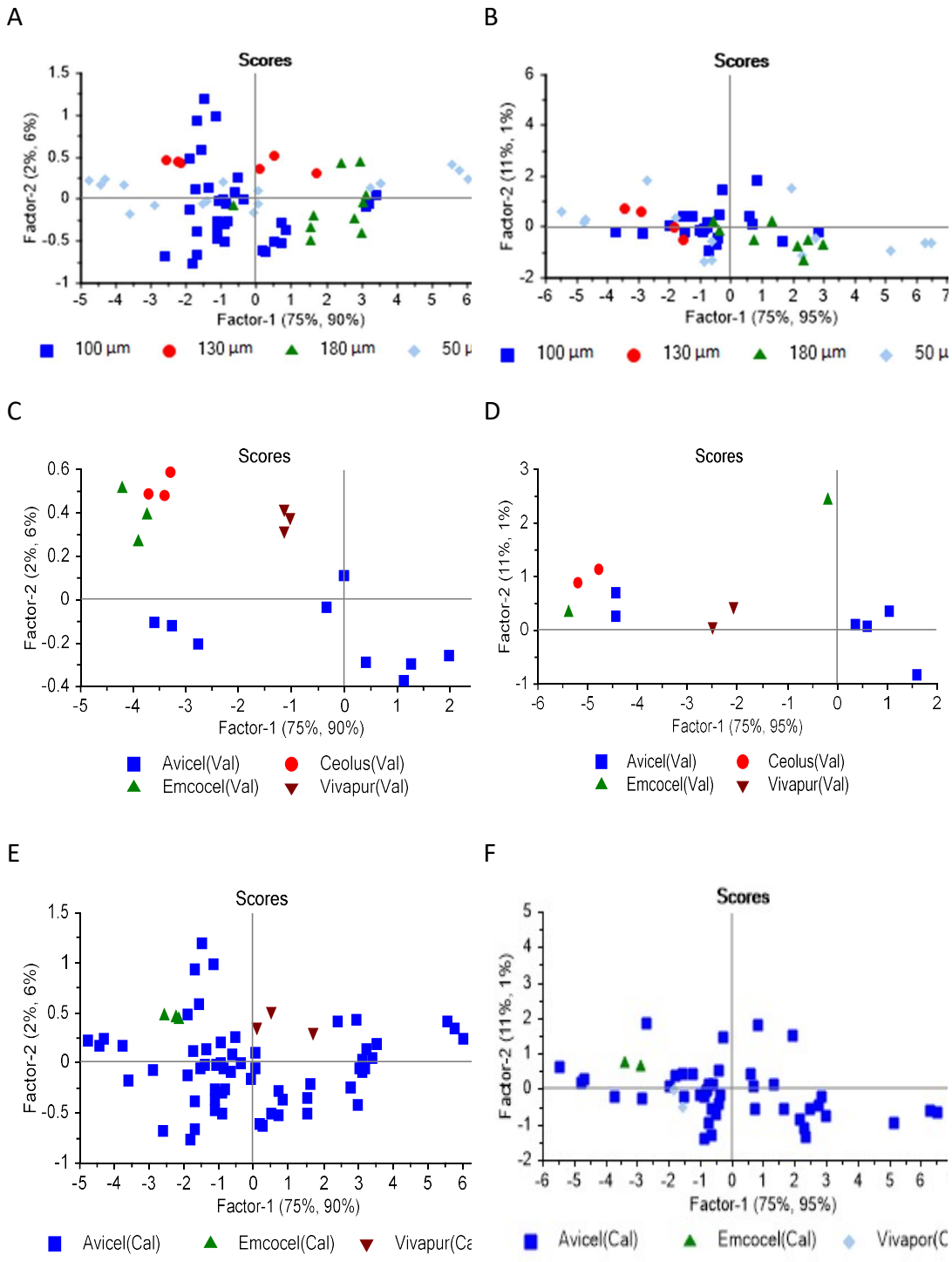

Figure 2.10. Scores plots of factors one and two highlighted by (A and B) average particle size for the calibration set, (C and D) manufacturer for the validation set, (E and F) manufacturer for the calibration set for the MR and PhAT probes, respectively.

2.5.6 Relationship between %CI and monolayer moisture content

Finally, a correlation between MCC sample crystallinity index and moisture monolayer values of all 30 batches was investigated. The set of samples used in this study was not sufficient to build a predictive linear regression model. Pearson's correlation coefficients of -0.459 and -0.476 were obtained using the PhAT probe and MR probe, respectively (Figure 2.11). PLS models (Raman spectra as independent variable, moisture monolayer as dependent variable) and correlation models (between %CI and the moisture absorbed at different relative humidity, determined using DVS) were also investigated, and they showed similarly poor correlations between %CI and moisture sorption. Among the batches analysed, two batches showed greater %CI and lower moisture monolayer in comparison to the other batches (~1.5 and 1.7 mM/g). These samples contributed to an increase in the correlation coefficient value.

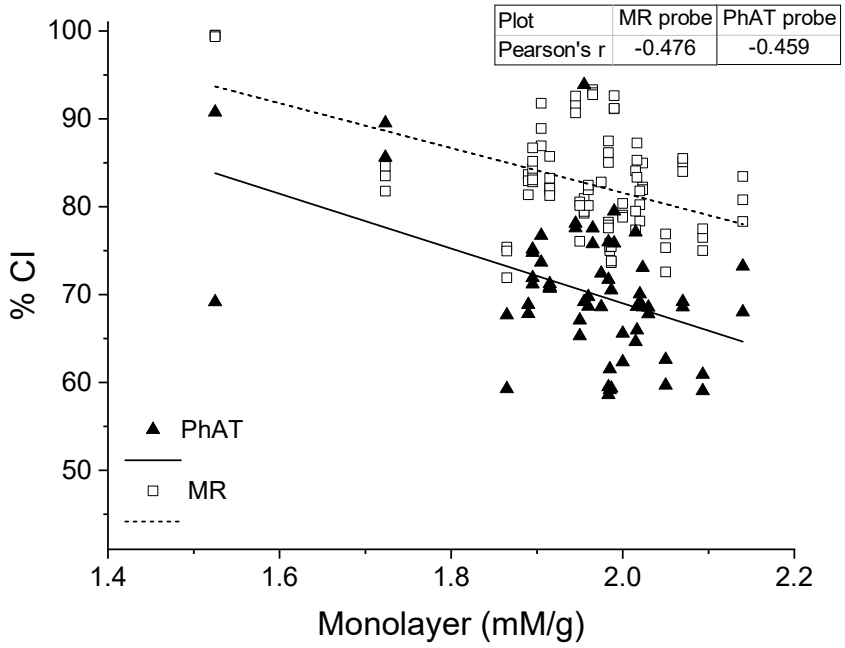

Figure 2.11. Correlation between crystallinity index (%CI) determined from Raman spectra acquired using a PhAT and a MR probe.

2.6 Discussion

It is challenging to determine the properties of microcrystalline cellulose compared to other materials. MCC shows great variability due to its natural source i.e., wood pulp, and the different processes from which the commercial grades are produced, especially different drying processes. As a result, there is a lack of standards and references and most techniques give relative results (Foster et al., 2018). In this study the application of two models to determine the crystallinity index of MCC commercial batches was investigated. Both models showed predictive power.

The crystallinity of MCC was firstly determined using the 380-method proposed by Agarwal et al. (Agarwal et al., 2010). A calibration curve was developed and used to correct the model for each instrument employed in this study (MR and PhAT probes, Kaiser Optical Systems Inc., USA). This modification was previously performed for a different instrument (Foster et al., 2018). Reference amorphous spectra for each batch were produced and an averaged spectrum (n=30 batches) was determined for each probe. As a result, the production of a reference amorphous material and spectral subtraction for new batches are no longer required for future analysis. The time for analysis was shortened and milling and PXRD analysis steps (required to confirm that the sample is indeed amorphous) can be eliminated from the analytical procedure.

Crystallinity of MCC was also determined by partial least squares regression models. The crystallinity values used in this regression analysis were those determined using the established 380-method. The ability of the models to predict crystallinity from Raman spectra were 97.82 % for MR and 98.57 % for PhAT probes and the predicted

values for the test set showed a small prediction error (RSMEP equal to 1.0522 and 1.3189 for MR and PhAT probe, respectively). The correlation loadings showed that the main wavenumbers used to build the model were 380, 437, 458, 521, 1,096, 1,120, 1,330, 1,340, 1,380, and 1,475 cm^{-1}. Those wavenumbers were correlated to a change in cellulose crystallinity due to contributions from OH rocking and bending, CH and CH_2 bending, CO and COC stretching, CH wagging, and anhydroglucose ring stretching, twisting, and torsion modes (Agarwal et al., 2010). The models built may be used to rapidly determine crystallinity for future MCC batches without the necessity to produce an amorphous reference spectrum. A PLS model had been previously used to predict crystallinity (Agarwal, 2019; Agarwal et al., 2010), however, the model was built with only ten samples (a control, 4 mixtures, 3 samples milled during different times and 2 commercial MCC grades). The present study investigated thirty MCC commercial batches including ones with different particle sizes (from 50 to 180 µm average particle size) and MCC grades. Thus, the present study confirmed the finding of the previous study reported by Agarwal et al. and enriched the validation of the models by investigating the variability encountered in commercial grades of MCC.

In this study Raman probes that can scan large surface areas and give an averaged spectrum in a short time were used (1 min for MR probe and 15 sec for PhAT probe). Previous studies used Raman spectra of microscopic surface areas (Agarwal, 2019; Agarwal et al., 2010; Foster et al., 2018). The PhAT probe used in the present study acquires spectra from an area of 12.57 mm^2 and the MR probe from an area of 7.85 x 10^{-3} mm^2. A PhAT probe also has a depth of analysis of approximately 2 mm. Thus,

less replicates are necessary to achieve a representative sample when a PhAT probe is used. As a result, Raman spectrum containing more averaged information of the overall semi-crystalline structure of MCC samples is obtained. Comparing the PhAT and the MR probes, the larger coverage area of the PhAT probe resulted in better fits for both the 380-method and PLS models. This was quantified by Pearson's coefficients obtained from the calibration of the 380-method (Figure 6, Pearson's-r of 0.986 and 0.960 for PhAT and MR probes, respectively) and the PLS model (correlation of 0.986 and 0.978 for PhAT and MR probes, respectively). LaPlant and Zhang also observed that in comparison to the MR probe, the PhAT probe gave more consistent and representative results in a study of polymorphic content in a drug product (LaPlant and Zhang, 2005). In the current study, variability observed between duplicate values determined using the PhAT probe was greater than when using the MR probe, for a number of the commercial samples. A possible explanation may be due to spectra being acquired on the same surface of the pellet (top surface) for the MR probe, while for the PhAT probe one spectrum was acquired on the top surface and another was acquired on the bottom surface of the pellet. The difference in %CI due to the differences in the positions from which the Raman spectra were may be due to the characteristic of uniaxial compression, which does not hold a homogeneous stress distribution in the interior of the pellet (Takeuchi et al., 2004).

It is important to also emphasis the limitations of quantifying the %CI of cellulose materials, including MCC, using the Raman spectroscopy. Key limitations include the lack of 100% crystalline or amorphous cellulose standards or references and the need to adjust model parameters for each

instrumental set-up by calibration against diffraction data. Therefore, the %CI determined by Raman analysis is dependent on the diffraction analysis methodology. In this study, a simplistic approach was undertaken which mimicked that of Agarwal et al. 2010. The %CI of calibration set samples were determined using the Segal peak height method and theoretical %CI values were determined based on the %CI of a single MCC batch. It is proposed that an improvement to this approach should include a wider calibration set of samples in the calibration study to improve model robustness. It is also important to extend the diffraction methodologies employed to measure %CI of the calibration sample set. Advancement from the Segal peak height method during calibration, towards more advanced methods such as decomposition or deconvolution of peak area during calibration (Lanson 1997; Park et al. 2010; Ahvenainen et al. 2016, Yao et al. 2020), and Rietveld refinement based methods (Madsen et al. 2011; Ling et al. 2019) could further improve the models proposed in this study. The respective strengths and limitations of more commonly diffraction method discussed by French 2020, as are standards for conducting crystallographic work to study cellulose crystallinity (French 2020).

It was not possible to establish a relationship between MCC moisture monolayer and calculated crystallinity. Moisture monolayer was determined from DVS moisture sorption isotherms and used to build a regression model with crystallinity determined by the univariate 380-method. Moisture monolayer was also used as a response variable in a PLS model in order to investigate if moisture monolayer could be predicted from Raman spectra. Neither of the models, univariate or multivariate,

showed a relationship between the moisture monolayer and crystallinity (or Raman wavenumbers related to changes in cellulose crystallinity). The relationship between moisture sorption and crystallinity observed by other authors (Awa et al., 2015; Mihranyan et al., 2004) was not conclusively confirmed for the set of commercial grades analysed in this study (correlation coefficients of -0.459 and -0.476 were obtained using moisture monolayer and the %CI determined using Raman spectra collected using a PhAT probe and MR probe, respectively). This may be due to the range of crystallinity values within the set of samples studied which did not result in a large variability in the moisture monolayer values measured. The finding of this study indicates that moisture sorption of MCC commercial grades may depend not only on crystallinity, but also on other structural factors such as surface area and pore volume, as suggested by Mihranyan et al. (Mihranyan et al., 2004).

A R Shiny web application was designed (*i*) to perform baseline correction and SNV normalization, (*ii*) to predict MCC crystallinity using the 380-method for the MR and the PhAT probes, (*iii*) to predict MCC crystallinity from PLS models, and (*iv*) to perform PCA from Raman spectra within the range of 1500 to 250 cm^{-1}. This application was developed based on the knowledge generated in this study. Thus, baseline correction, SVN normalization, and the PCA model can be applied to Raman spectra of microcrystalline cellulose obtained using different Raman instruments. However, the prediction of the crystallinity index can only be undertaken if a MR or a PhAT probe was used to acquire the Raman spectra. Even if those Raman instruments are used, results should be evaluated with caution since different units of a same instrument design might require instrument-specific correction of the model.

2.7 Conclusions

Crystallinity index was determined for 30 commercial batches of microcrystalline cellulose using two different models i.e., 380-method and PLS regression. Both models showed adequate predictive power. However, the development of the PLS model takes substantially less time for analysis because it eliminates the need for milling and deconvolution of the spectra of the milled sample into amorphous and crystalline contributions before the actual %CI determination. For these models a general reference amorphous Raman spectrum was proposed for each instrument. Spectral comparison and principal component analysis showed that values of crystallinity index were relative to the instrument used to acquire the Raman spectra. Also, larger laser spot sizes give more reproducible and representative information on the overall crystallinity of the sample. The crystallinity index values obtained with either model depend on the XRD methodology and calibration sample set employed during calibration. The methodology presented can be further advanced by employing a broader sample set and more advanced XRD methodologies to measure microcrystalline cellulose crystallinity during calibration of the model. A web application, MCCrystal, was developed which facilitates the use of the predictive models developed in this study to measure MCC crystallinity. It was not possible to establish a regression model to predict moisture monolayer from crystalline indices determined from the Raman spectra, indicating that in addition to crystallinity, other structural properties such as pore volume and surface area need to be considered in predicting MCC moisture monolayer.

Chapter 3 - Application of Multivariate Curve Resolution to determine co-crystal phase purity by mid infrared spectroscopy

Revised from publication in: *International Journal of Pharmaceutics* (2021)

https://doi.org/10.1016/j.ijpharm.2021.120246

3.1 Abstract

Multivariate Curve Resolution (MCR) was used to determine the phase purity of pharmaceutical co-crystals from mid infrared spectra. An in-silico coformer screening was used to choose one of ten potential coformers. This analysis used quantum chemistry simulation to predict which coformers are thermodynamically inclined to form co-crystals with the model drug, hydrochlorothiazide. The coformer chosen was nicotinamide. An experimental solvent screening by ultrasound assisted slurry co-crystallization was performed to evaluate the capacity of the MCR method to determine phase purity. Afterwards, slurry and slow evaporation co-crystallizations were performed at 10, 25, and 40 °C using 7 solvent systems, and two levels of agitation for the evaporation co-crystallization (on and off). MIR analysis of the products of these co-crystallisations were used to develop an MCR model to determine co-crystal phase purity. Loadings related to component 1 of the MCR model correlated with the MIR spectra of a reference co-crystal. MIR, PXRD and DSC were used to assess the reference co-crystal form and phase purity. Experimental design (DoE) was used to investigate the effect of solvents, temperature, and agitation on the purity of co-crystals produced by slurry and evaporation. Principal component analysis of on-line Raman spectra captured the co-crystal formation process and allowed to determine slurry co-crystallization endpoint. The MCR phase purity model developed from MIR spectra was employed to determine co-crystal phase purities of products. DoE revealed that evaporation co-crystallization with agitating at 65 rpm formed co-crystals with greater phase purity. The optimal temperature varied with the solvent used.

3.2 Introduction

Co-crystallization is a crystal engineering approach that has been used to enhance mechanical and physicochemical properties and chemical stability of drugs (Rodrigues et al., 2018a; Sun, 2013). According to the European Medicines Agency (EMA), pharmaceutical co-crystals are “homogenous (single phase) crystalline structures made up of two or more components in a definite stoichiometric ratio where the arrangement in the crystal lattice is not based on ionic bonds (as with salts)”. The components of a co-crystal may, nevertheless, be neutral as well as ionized (European Medicines Agency, 2015). Also, co-crystals differ from solvates because all the molecules in co-crystals are solid at ambient temperature, while in the solvates at least one component is liquid at ambient temperature. There are also co-crystals solvates in which the solvent is trapped in the crystal lattice during co-crystallization (Sarraguça et al., 2015). During crystal engineering development, modelling tools such as quantum chemistry simulation have been used to predict the propensity of co-crystal formation, preferably to those other crystal structures (Loschen and Klamt, 2015). The crystal structure of the predicted product is then confirmed experimentally using analytical techniques such as X-ray powder diffraction (XRD) and vibrational spectroscopy (Datta and Grant, 2004).

The nature of the interaction and the molecular structure of API and coformer are different from that observed for the starting material (Ross et al., 2016). Therefore, the most relevant advantage of co-crystallization to the pharmaceutical industry is that critical material attributes such as flowability, compressibility, compactability, and solubility can be designed to improve drug processability and bioavailability.

Also, co-crystallization processes can be designed to be scalable and can be performed in continuous manufacturing plants within a quality by design framework (Rodrigues et al., 2018a). Rodrigues et al. described and compared several co-crystallization methods reported to date, such as isothermal slurry, slow evaporation, spray drying, neat grinding, freeze drying, and hot melt extrusion. Solvent-based methods are the most common co-crystallization approaches deployed at laboratory scale and they are also reportedly used in industrial scale in continuous manufacturing (Zhao et al., 2014). This can be explained by the fact that solvent-based procedures are relatively simple, as are the apparatus required to perform them.

Solid-state analysis must be employed in order to be able to determine co-crystal phase purity, since most solvents, including water can destroy the non-covalent bonds in co-crystals (Chi et al., 2013). Instead, a variety of combined solid-state techniques are used, with particular emphasis on crystallographic and vibrational spectroscopy methods (Emami et al., 2018). Vibrational spectroscopic techniques are the most commonly used for in-line and on-line process monitoring because they are rapid, non-destructive and the spectroscopic techniques can be built into the manufacturing process by means of immersion probes, flow-through cells, and quartz windows (Pomerantsev and Rodionova, 2012). Spectroscopic techniques can assess differences between crystalline forms, crystalline form transformations, differences between amorphous and crystalline forms and between anhydrous and hydrate forms (Erxleben, 2016). Thus, vibrational spectroscopic techniques are of great interest when it comes to the development of process analytical technology for co-crystal phase purity control. In this paper, phase purity relates to the lack of solid

phases other than a specific co-crystal e.g., co-crystal (pseudo)polymorphs or starting materials and/or their (pseudo)polymorphs. The spectroscopic techniques most used for industrial process control and product characterization applications are near-infrared spectroscopy (NIR), Raman spectroscopy and mid-infrared spectroscopy (MIR) (Pomerantsev and Rodionova, 2012). The application of those techniques to co-crystal production has also been investigated. Table 3.1 shows studies in which vibrational spectroscopic techniques were applied to monitor and control co-crystallization processes (in-line and online) and to characterize co-crystals (offline).

Table 3.1 Application of vibrational spectroscopic techniques to co-crystallization process monitoring and co-crystal characterization. NIR = near-infrared spectroscopy and MIR = mid-infrared spectroscopy.

Technique	References		
	On-line	**In-line**	**Offline**
NIR	(Silva et al., 2017)	(Kelly et al., 2012; Markl et al., 2013; Sarraguça et al., 2016)	(Gagniere et al., 2012; Kelly et al., 2012; Sarraguça and Lopes, 2009; Silva et al., 2017)
MIR	(Ishihara et al., 2019)	(Gagniere et al., 2012)	(Alshahateet, 2010; Mittapalli et al., 2019; Zhao et al., 2014)
Raman	(Inoue et al., 2017; Otaki et al., 2018; Sheng et al., 2016; Tanaka et al., 2019)	(Kojima et al., 2010; Lee et al., 2014; Soares and Carneiro, 2017, 2013)	(Aher et al., 2010; Markl et al., 2013; Powell et al., 2015)
NIR, Raman and MIR	-	-	(Goud et al., 2012; Rodrigues et al., 2018b)
NIR and Raman	-	(Islam et al., 2015)	(Allesø et al., 2008)
NIR and MIR	(Sarraguça et al., 2014)	-	(Sarraguça et al., 2014)
MIR and Raman	(Powell et al., 2016)	(Bian et al., 2013; Du et al., 2017)	(Barmpalexis et al., 2018; Basavoju et al., 2006; Childs and Hardcastle, 2007; Du et al., 2017; Emami et al., 2018; Powell et al., 2016)

Multivariate analysis methods such as principal component analysis (Pearson, 1901) can be used to investigate co-crystal phase purity from a reference co-crystal spectrum (Rodrigues et al., 2018b). However, during the co-crystal development, products of sufficient purity may not be available to obtain a high-quality reference spectrum. Multivariate Curve Resolution (MCR) (Lawton and Sylvestre, 1971; Martens, 1979) is a group of algorithms developed to implement constraints on

loadings and scores obtained from a matrix decomposition. That means that loadings have an exact physical interpretation i.e., spectra of different components of a mixture. The scores also assume a physical meaning, the concentration of the component in the mixture. The loadings also explain the variance in the data (De Juan and Tauler, 2006; Mendieta et al., 1998). Thus, MCR can potentially be used to extract the spectrum corresponding to co-crystal present in a mixture.

De Juan et al. listed and compared the main MCR algorithms available and discussed the benefits of the algorithm Multivariate Curve Resolution-Alternating Least Squares (MCR-ALS) (De Juan et al., 2014). MCR-ALS is an iterative algorithm that performs alternating optimization by applying constraints in each iterative cycle. The constraints applied to MCR model for optimization can be divided into (*i*) mathematical conditions, (*ii*) natural constraints, and (*iii*) process constraints. De Juan et al. provides a detailed explanation of these constraints (De Juan et al., 2014). There is a small number of publications in which MCR and MCR-ALS were applied to co-crystallization. Co-crystal concentration estimation (Mazivila et al., 2019; Mazivila and Olivieri, 2018), co-crystal formation (Inoue et al., 2017; Ishihara et al., 2019; Soares and Carneiro, 2013), and polymorphism (Lukin et al., 2017; Soares and Carneiro, 2017) were investigated for different co-crystals. However, co-crystal phase purity was only investigated applying MCR-ALS to PXRD and Raman spectral data. Substances that present weak Raman signals are usually analysed using MIR (Abbas et al., 2012). Fluorescence is frequently observed during acquisition of Raman scattering. Since fluoresce has much stronger intensity, the Raman signal can be masked. This problem can be diminished with increase in the laser wavelength or using Coherent Anti-stokes Raman Scattering (CARS) (Alula et al., 2018; Paudel et al.,

2015; Rodrigues et al., 2020). Alternatively, MIRS can be used. Determination of co-crystal phase purity applying MCR to MIR spectral data has not been investigated to date without a reference spectrum.

The overall aim of this study was to use MCR-ALS to determine co-crystals phase purity using MIR spectra, and apply the methodology developed to establish a co-crystallization process design space. For that end, hydrochlorothiazide (HTZ) was used as model drug. The co-crystallization of this API has been well studied by Rodrigues et al. (Rodrigues et al., 2019, 2018b). Hydrochlorothiazide is a poorly water-soluble drug substance chemically classified as a thiazide, a diuretic class mainly used in the treatment of hypertension and is a good candidate to produce co-crystals with improved solubility. An in-silico study was performed to determine the best coformer for the experimental co-crystallization. Afterwards, the ability of MCR to determine co-crystal phase purity model was investigated by applying the model to MIR data from a screening slurry co-crystallization.

3.3 Materials and methods

3.3.1 In-silico coformer screening

Quantum chemistry simulations were performed to select one coformer to be investigated experimentally, and to generate thermodynamic understanding of the co-crystal formation. Propensity for co-crystallisation of an API molecule with 10 potential coformers was estimated using fluid phase thermodynamic modelling accessible in the COSMOthermX computational platform, version 19.0.1 (COSMOlogic GmbH & Co. KG Imbacher, Germany). COSMOS-RS thermodynamics used in this contribution is based on the statistical physics of interacting molecular

surface segments. The polar and hydrogen bond interaction energies are quantified based on the surface screening charge densities, which result from a quantum chemical continuum solvation calculation (Abramov et al., 2012).

COSMO-RS (COnductor like Screening MOdel for Real Solvents) was employed to predict propensity for co-crystal formation assuming that more negative the excess enthalpy (which reflects stronger intermolecular interactions between the active pharmaceutical ingredient (API) and the coformer), the higher the probability of forming a co-crystal. The model considers a fluid phase only, thus a long-range order and specific packing within a crystal phase is not considered here (Sinnecker et al., 2006).

The API molecule investigated was hydrochlorothiazide and the coformers were mannitol, caffeine, para-aminobenzoic acid, malic acid, arginine, tromethamine, adenine, citric acid, tryptophan, and nicotinamide. To prepare input structures for the coformer screening, molecular geometry of the API and all the considered coformers were optimized using quantum chemistry TURBOMOLE software (COSMOlogic GmbH & Co. KG Imbacher, Germany). All the compounds were modelled as neutral molecules, so no extra charge or charge separation was considered. For that, the Density Functional Theory level BP-TZVPD-FINE was used. This level uses a Becke–Perdew (BP) functional (Becke, 1988) and a triple-z valence polarized basis set (TZVP) (Schäfer et al., 1994) with a fine grid marching tetrahedron cavity (FINE) and delivers the best quality results. However, it demands the most computational power (Paduszyński, 2017). The optimised geometries, along with the charge density maps of the API and the coformer molecules were then used to

predict propensity for co-crystal formation with the proposed coformers in the ratios 1:1 and 1:2.

3.3.2 Materials

Hydrochlorothiazide (HTZ) ≥ 99.0% and nicotinamide (NCT) ≥ 99.5% were obtained from Sigma-Aldrich, USA. The analytical grades of the following solvents were used in this study: chloroform (CF) (Sigma-Aldrich, Portugal), methanol (MeOH) and acetone (Ace) (VWR Chemicals, France), acetonitrile (ACN) (Fisher Scientific, UK), 2-propanol (iPro) and and Ethyl acetate (EtOAc) (Sigma-Aldrich, USA), and ethanol (EtOH) (Chem-Lab, Belgium).

3.3.3 Methods

3.3.3.1 Experimental solvent screening

Solvent and ratio screenings was performed to produce co-crystals with varying phase purities. This analysis produced data for the development of models to predict phase purity and optimal ratio of co-crystal formation. The API:coformer ratios investigated were 1:1 and 1:2. Co-crystallization was performed by ultrasound assisted slurry co-crystallization in a well plate. Five different solvents were used in the screening study: methanol, ethanol, acetone, 2-propanol, and acetonitrile.

3.3.3.2 Reference co-crystal preparation

One gram of hydrochlorothiazide and the equivalent amount of coformer (stoichiometric ratio of 1:1) were weighted. The powder blend was then dissolved in 50 ml of acetone at 40 °C. Solvent was left to evaporate at 25 °C using a water bath

with a thermostat (microprocessor control MPC, Huber Kältemaschinenbau AG, Germany) without agitation. The reference co-crystal was characterized by X-ray diffraction and differential scanning calorimetry.

3.3.3.3 Laboratory-scale co-crystallizations

3.3.3.3.1.1 Experimental design

Full factorial design of experiments was performed to determine the design space of the laboratory-scale co-crystallization. The specific aim of this analysis was to investigate how the co-crystal phase purity was affected by different solvent choices, temperature and, for evaporation co-crystallization, the presence or absence of agitation. The three factors of the model were agitation (2 levels), solvent (7 levels), and temperature (3 levels) (Table 3.2). A reduced fifth model was fit to the designed experiments using the phase purity obtained from the MCR model as response. The results of the experimental trials were analyzed using Analysis of Variance (ANOVA). Design-Expert® DOE Software (Stat-Ease Inc., Minneapolis, USA) was used to perform the DoE.

Table 3.2. Experimental design factors for the determination of the co-crystallizations design space. EtOH = ethanol, MeOH = methanol, ACN = acetonitrile CF = chloroform, Ace = acetone, DCM = dichloromethane, EtOAc = ethyl acetate. *For evaporation co-crystallization only

Factor 1	**Factor 2**	**Factor 3**
Temperature (°C)	Solvent System	Agitation (rpm)*
10; 25; 40	EtOH; MeOH; ACN; CF:Ace 1:1; DCM:Ace 1:1; EtOAc:Ace 4:1; DCM:Ace 1:1	0; 65

3.3.3.3.1.2 Solvent evaporation co-crystallization

Approximately 300 mg of HTZ with the corresponding stoichiometric ratio in mass of coformer was added to 100 mL beakers followed by the addition of 50 mL of solvent. The systems were agitated until reaching complete dissolution on a stirrer table (RSLAB-5C 10-chanel analogical stirrer table with heating option) at room temperature.

The flasks were then transferred to water bath (Huber K15 Bath with MPC Controller, Heating/Cooling recirculating Unit) with temperature controlled with or without agitation (see Table 3.2) to allow solvent evaporation. The powder obtained was kept on a hot plate at 30 °C for 3 hours prior characterization in order to ensure total solvent release.

3.3.3.3.1.3 Co-crystallization in slurry

3.3.3.3.1.4 Determination of slurry co-crystallization endpoint

The endpoint of the co-crystallization in slurry was determined by a PCA model of Raman spectra obtained during online monitoring. Approximately 600 mg HTZ and the corresponding amount of coformer (ratio 1:1) were added to a glass flask followed by the addition of 20 mL of solvent (MeOH, EtOH, Ace, EtOAc, DCM, ACN or CF) and a magnetic stirrer. The flask was sealed and placed on a stirrer table (RSLAB-5C 10-chanel analogical stirrer table with heating option) where the system was kept under agitation at 120 rpm for five days. Raman spectroscopy was used to monitor the co-crystallization process online. Co-crystallization endpoint was considered the

time point at which the scores of the first principal component of PCA achieved steady state.

3.3.3.3.1.5 Slurry co-crystallization

Approximately 300 mg of HTZ and the corresponding amount of coformer (ratio 1:1) were added to a 100 mL Erlenmeyer flask followed by the addition of 10 mL of solvent and a magnetic stirrer. The flask was sealed and transferred to the water bath (Huber K15 Bath with MPC Controller, Heating/Cooling recirculating Unit) with temperature control, and with or without agitation (Table 3.2) for 120 hours. The flasks were then unsealed and left in a fume hood at room temperature to allow solvent evaporation. The powder obtained was kept on a hot plate at 30 °C for 3 hours prior to characterization in order to ensure total solvent release.

In a slurry co-crystallization, the slurry is normally filtered at the end point in order to isolate the solids. However, the goal of these experiments was to produce co-crystals with different purities in comparison to evaporation co-crystallization. Hence, at the end of the slurry co-crystallization, filtration was not performed, and solvent was evaporated at room temperature.

3.3.3.4 Characterization techniques

3.3.3.4.1.1 Mid infrared spectroscopy

The co-crystals produced were characterized by mid infrared spectroscopy (MIR). Spectra (n=5) were acquired using a Frontier Spectrometer (PerkinElmer, UK) equipped with an attenuated total reflectance (ATR) accessory (PerkinElmer, UK). The co-crystal samples were placed directly on the crystal of the ATR accessory and

each spectrum was the resultant of 32 accumulations at a resolution of 4 cm^{-1} over the range 4000-600 cm^{-1}. The background spectrum was acquired for the crystal following cleaning.

3.3.3.4.1.2 Raman spectroscopy

For online monitoring a Raman spectrometer equipped with a probe (i-Raman® Plus BWS415-785H, BW Tek, USA) was used. Raman spectra were acquired every 20 min, with exposure time of 20 seconds, 2 accumulations, and laser power of 785 mW at 100% over the range 300-1800 cm^{-1}. The probe was placed perpendicular to the flask containing the sample. The flask and the end of the probe were inserted in a bespoke black box of polylactic acid constructed in-house to avoid external light interference. The system was kept under agitation at 120 rpm and at the temperature of 40 °C on a stirrer table (RSLAB-5C 10-chanel analogical stirrer table with heating option).

3.3.3.4.1.3 X-ray diffraction

X-ray diffraction patterns and DSC thermograms were collected for the isolated pure reference co-crystals for phase purity characterization. Powder X-ray analysis was performed in reflection mode using a benchtop X-ray diffraction (XRD) instrument Rigaku Miniflex II (Rigaku, Tokyo, Japan) equipped with a Cu Kα X-ray source and Haskris cooling unit (Grove Village, IL, USA). The samples were front-loaded by gently pressing using a glass slide on a zero-background silicon sample holder. The PXRD patterns were recorded for a 2θ ranging from 3 to 40 degrees with a step-size of 0.05 degrees per second.

The experimental X-ray diffractogram collected was compared with the simulated theoretical diffractogram generated from a Crystallographic Information File (CIF) of hydrochlorothiazide-nicotinamide co-crystal (CCDC ref. code PIRXUL) using Mercury software v. 3.10.3.

3.3.3.4.1.4 Differential scanning calorimetry

A TA Instruments DSC Q1000 differential scanning calorimeter and thermal analysis controller (TA Instruments, New Castle, DE, USA) was used to determine the enthalpy and the melting point of the reference co-crystal. Approximately 2–3 mg of co-crystal was heated at a heating rate of 10 °C/min from 25 to 275 °C. Nitrogen was used to purge the system at 50 ml/min.

3.3.3.5 Data Analysis

3.3.3.5.1.1 Principal Component analysis

PCA was performed as an exploratory technique in the screening experiments and to analyze the Raman spectra from the online monitoring. The raw spectra were pre-treated by mean centering and Standard Normal Variate (SNV). PCA was performed using the algorithm Nonlinear Iterative Partial least squares (NIPALS). Internal cross-validation was performed by categorical variable (solvent type), so that every segment had one solvent missing. The optimal number of components was determined by the minimal number of components that resulted in a minimal residual variance.

PCA was performed using the software Matlab 8.3 (MathWorks, Natick, USA) and the PLS Toolbox version 7.5 (Eigenvector research Inc., Wenatchee, USA).

3.3.3.5.1.2 Multivariate Curve Resolution

MCR decomposes the data matrix (X) i.e., the table containing one MIR spectra per line, into a matrix of the variation among the spectra, named concentration profiles (C), a transpose variance matrix associated with the variation among the variables, named spectra profiles (S^T), and a matrix of residuals not explained by the model (E) (Equation 1). As a result, it is possible to extract the spectra fingerprint of each single component of a mixture.

$$X = C \cdot S^T + E \qquad \text{(Equation 3.1)}$$

MCR-ALS applies constraints to optimize MCR results. PCA was used to determine the number of components and the spectra were pre-processed by Standard Normal Variate (SNV). A constraint of non-negativity was applied to the concentration profiles using fasternnls algorithm(Lawson and Hanson, 1995). No spectral estimation was used.

MCR loadings obtained were compared to the spectra of a reference co-crystal and to spectra of the reference starting materials. The aim of this analysis was to identify which components loading represented the co-crystal information and which components loading represented unreacted individual components information. In other words, it was necessary to investigate if the model expressed the co-crystal information as loadings of component 1 or of component 2. For that, Pearson correlation analysis (Ntschi and Bolboac, 2006) was performed between the spectrum obtained from the MCR i.e., MCR loadings, and the average spectrum of a reference co-crystal (n=5), using Origin data analysis and graphing software

(OriginLab, USA). Spectral analysis was also performed to support the statistical analysis.

Equation 3.2 was used to calculate percentage phase purity (% phase purity). $MCR_{conc,x}$ is concentration (obtained by MCR) of the component that holds the co-crystal information, and $\mathrm{MCR}_{conc,com} + \mathrm{MCR}_{conc,comp}$ is the sum of the concentrations (obtained by MCR) of the 2 first components. The component that holds the co-crystal information was the component which the loadings had the greatest Pearson correlation coefficient with the spectra of a reference co-crystal.

$$\%\ \text{phase purity} = \frac{100 \cdot \mathrm{MCR}_{conc,x}}{\mathrm{MCR}_{conc,comp1} + \mathrm{MCR}_{conc,comp2}} \qquad \text{(Equation 3.2)}$$

Values of phase purity obtained with ratios 1:1 and 1:2 were compared to determine which ratio produces the co-crystal with higher purity. The optimum ratio for co-crystal formation should show greater phase purity. Another indication for the optimum ratio for phase purity is the component explained variance. The optimum ratio should show the greatest percentage variance explained by the component that holds the co-crystal information.

MCR-ALS was performed using the software Matlab 8.3 (MathWorks, Natick, USA) and the PLS Toolbox version 7.5 (Eigenvector research Inc., Wenatchee, USA).

3.4 Results

3.4.1 In-silico coformer screening

In order to aid selection of a model co-crystal system for this study, the propensity for co-crystallisation of hydrochlorothiazide was assessed computationally

considering 10 different coformers at two API:coformer molar ratios: 1:1 and 1: 2 (Table 3.3). Excess enthalpies (H_{ex}), Gibbs free energies of mixing (G_{mix}) and contributions from hydrogen bonding to intermolecular interaction of API and coformer (HB) were computed using fluid phase thermodynamic modelling framework implemented in COSMO-RS. The model assumes that the interactions in the crystal are similar to those in a virtual supercooled liquid. Thus, the strength of the interactions in the co-crystal, as compared with the pure reactants, can be estimated via the mixing enthalpy (or equivalently the excess enthalpy) of the API-coformer with given stoichiometry; Gibbs free energy of mixing and the contribution of H-bonding to the mixing energy are other descriptors of the mixing efficiency. It is generally assumed that the higher (more negative) values of H_{ex}, G_{mix}, and *HB,* the stronger the interaction between API and coformer, and higher propensity for forming co-crystal. The computed values of $H_{ex,}$ G_{mix}, and *HB* are relatively higher for the compounds possessing carboxyl groups (COOH), such as malic acid, citric acid, and tryptophan, suggesting that the mixing between API and coformer is not thermodynamically preferred. On the other hand, the negative values of H_{ex}, G_{mix}, and *HB* were computed for caffeine, arginine, tromethamine, adenine, nicotinamide, and mannitol indicating stronger API-solvent interaction, and suggesting overall higher propensity for co-crystallisation. The computations also suggest that for those coformers the 1:1 molar ratio is preferred (more negative values) over the 1:2 ratio.

Table 3.3. Propensity for solvate formation computed with COSMO-RS fluid phase thermodynamics modelling at 1:1 and 1:2 API to coformer molar ratio. Hex, Gmix, and HB given in (kcal/mol).

Coformer	Ratio 1:1			Ratio 1:2		
	Hex	Gmix	HB	Hex	Gmix	HB
Caffeine	-1.514	-0.723	-1.363	-1.349	-0.64	-1.237
Arginine	-1.009	-0.796	-0.856	-0.989	-0.756	-0.849
Tromethamine	-0.717	-0.471	-0.69	-0.669	-0.425	-0.661
Adenine	-0.635	-0.62	-0.57	-0.614	-0.572	-0.557
Nicotinamide	-0.435	-0.564	-0.426	-0.411	-0.503	-0.422
Mannitol	-0.168	-0.206	-0.186	-0.138	-0.189	-0.163
Para-aminobenzoic acid	0.148	-0.311	0.025	0.137	-0.232	0.063
Malic acid	0.148	-0.26	0.077	0.139	-0.281	0.021
Citric acid	0.22	-0.236	0.143	0.201	-0.216	0.123
Tryptophan	0.273	-0.151	0.069	0.249	-0.139	0.058

Comparing the results from the experimental screening (Rodrigues et al., 2020; Rodrigues et al., 2018b) with the in-silico results some differences can be discussed. From the experimental screening the coformers caffeine, adenine and tryptophan did not form a cocrystal, and the cocrystallization with arginine was inconclusive. Additionally, except for the cocrystal with nicotinamide, all the cocrystals obtained were in the ratio of 1:2. The difference between the in-silo studies and the experimental screening can be due to the approximations made in the in-silico studies, or by experimental factors. It is well known that different co-crystallization methods, different solvents, and experimental conditions such as temperature can affect the co-crystallization output. However, since the main objective of the work was to use multiple curve resolution to determine co-crystal phase purity, we

decided to use the coformer in which the experimental results were in accordance with the in-silico studies. Therefore, nicotinamide was the coformer chosen to be further investigated in this study due to its relatively high negative values of mixing enthalpy/energy computed for the co-crystal of nicotinamide and hydrochlorothiazide. Also, the reference co-crystal HTZ-NCT had already been successfully produced and extensively characterized (Rodrigues et al., 2019). Therefore, the models produced in this study can be validated with the knowledge about this co-crystal already available in the literature. The chemical structure of HTZ and the coformer investigated in this study along with the structure of the 1:1 co-crystal synthon are shown in (Figure 3.1).

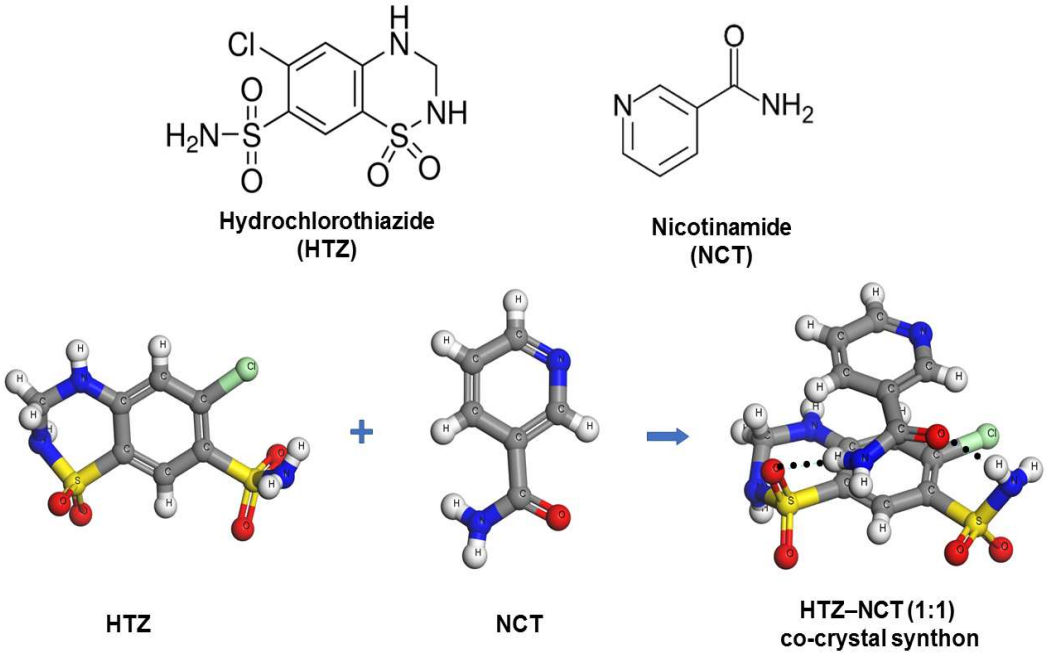

Figure 3.1. Chemical structure of hydrochlorothiazide and nicotinamide – top, and 3D representation of the co-crystallisation reagents and the final co-crystal synthon present in the crystal lattice of the HTZ-NCT 1:1 co-crystal – bottom. H-bonds (NH···O=S and NH···O=C) between the coformer and the API molecule shown as black dots.

3.4.2 Reference co-crystal characterization

Phase purity of the reference co-crystal obtained was confirmed by comparing the XRD pattern of the prepared co-crystal with the simulated XRD derived from single crystal data (Figure 3.2). The small intensity differences between the experimental and the theoretical diffractograms, and the noise observed in the experimental diffractogram can be related to the nature of the sample (powder vs. single crystal) and the XRD instrument resolution. However, all peaks predicted in the theoretical diffractogram were observed in the experimental diffractogram. The differential scanning calorimetry endotherm obtained (Figure 3.3) was comparable to the endotherm published for this co-crystal (onset x of 173.65 °C and temperature peak at 174.55 °C) , an additional small endotherm was observed in the present study and by Sanphui and Rajput (Sanphui and Rajput, 2014). This was attributed to a small amount of non-co-crystallized material present in the final product. However, none of the other characterization techniques showed any presence of unreacted components. Therefore, this additional broad endothermic peak can also be due to co-crystal degradation.

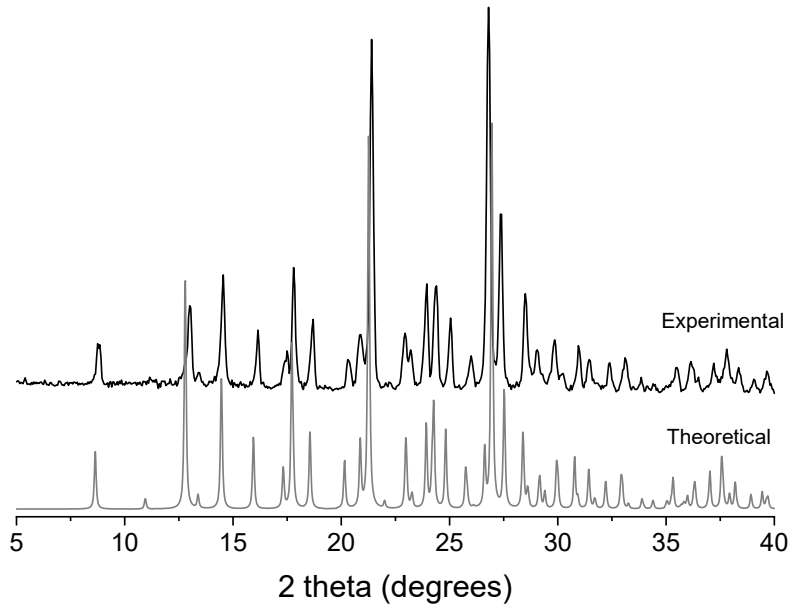

Figure 3.2. PXRD diffractograms of the prepared co-crystal (experimental) and the simulated XRD derived from single crystal data (theoretical) for the co-crystal of hydrochlorothiazide and nicotinamide, stoichiometric ratio 1:1.

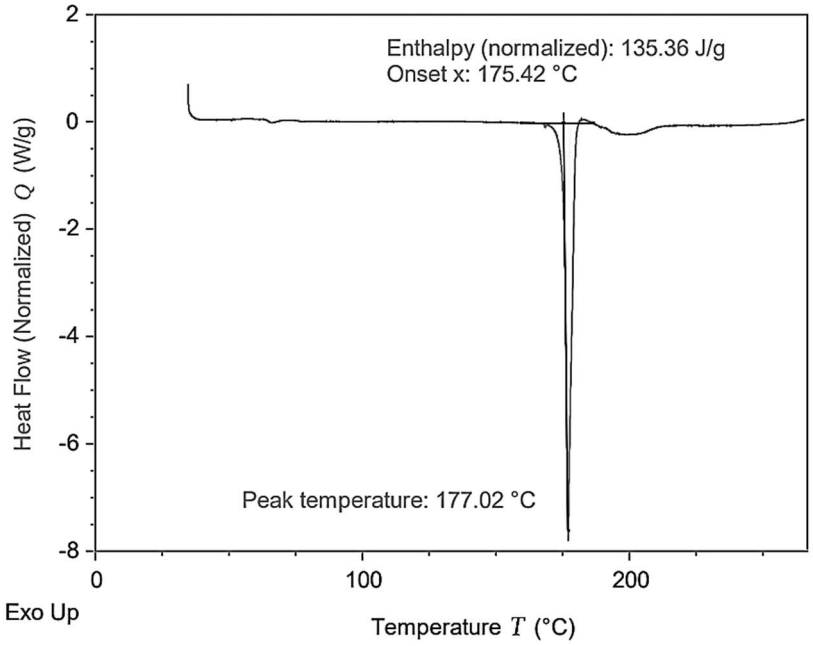

Figure 3.3. Differential scanning calorimetry endotherms of HTZ 1:1 NCT reference co-crystal.

3.4.3 Experimental screening experiments

The spectra of all products of the experimental solvent screening were used to calculate the MCR models. An MCR model was produced for each ratio, using MIR

spectra of the co-crystals produced to predict phase purity. The total percentage variance explained by 2 components were 99.82% for the model of ratio 1:1 and 99.89% for the model of ratio 1:2.

Pearson correlation was used to compare the spectra of hydrochlorothiazide, nicotinamide and co-crystal ratio 1:1 with the loadings of each component, for each model. MCR loadings of HTZ:NCT 1:1 showed that component 1 had the strongest correlation and carried most of the reference co-crystal spectral information (Table 3.4). Component 2 also showed a significant correlation coefficient with the spectra of the reference co-crystal. Phase purity of co-crystals obtained using this ratio was high for all solvents, except for MeOH. The phase purity of samples used to build the model may have resulted in component 2 also holding co-crystal information. For the ratio 1:2, loadings of component 1 showed co-crystal information, while component 2 showed a greater correlation to NCT. This shows that the co-crystal was formed in the ratio 1:1, hence, there was excess of NCT which was captured by the component 2.

Table 3.4. Pearson correlation coefficient for MCR model loadings correlated with the MIR spectra of the reference co-crystal produced at the ratio of HTZ:NCT 1:1 and reactants (HTZ and NCT). The closer the coefficient is to 1 the stronger the correlation.

Model component (% variance explained)	**HTZ:NCT 1:1 Co-crystal**	**HTZ**	**NCT**
HTZ:NCT 1:1 Comp. 1 (78.80%)	0.9994	0.8963	0.7351
HTZ:NCT 1:1 Comp. 2 (21.02%)	0.9560	0.8734	0.8187
HTZ:NCT 1:2 Comp. 1 (80.56%)	0.9992	0.9019	0.7286
HTZ:NCT 1:2 Comp. 2 (19.33%)	0.8995	0.7766	0.9497

Spectral analysis confirmed the MCR models results. MIR spectral analysis showed that component 2 of HTZ:NCT 1:1 ratio was somewhat similar to those observed in the co-crystal spectra, however it showed a different peak in the region of 3429-3389 cm^{-1}, and significant differences in intensity in the regions of 1800-1600 cm^{-1}, 1500-1350, 1295-1175 cm^{-1}, and 1139-1060 cm^{-1} (Figure 3.4). Component 2 of HTZ:NCT 1:2 ratio was also similar to NCT spectra, however, it showed peaks (3462-3422 cm^{-1}) and patterns (1551-1489 cm^{-1}, and 1350-100 cm^{-1}) somewhat similar to the observed in the co-crystal spectra (Figure 3.5). This may indicate that the co-crystal was formed, however there is unreacted NCT. The above differences highlight that these MCR loadings for component 2 may carry some co-crystal information, but they also contain information related to one the reactants indicating some phase impurity. MCR loadings that carry the greatest co-crystal information (component 1 of each ratio) showed good semblance to the reference co-crystal MIR spectrum; presence of different peaks or significant intensity differences were not observed.

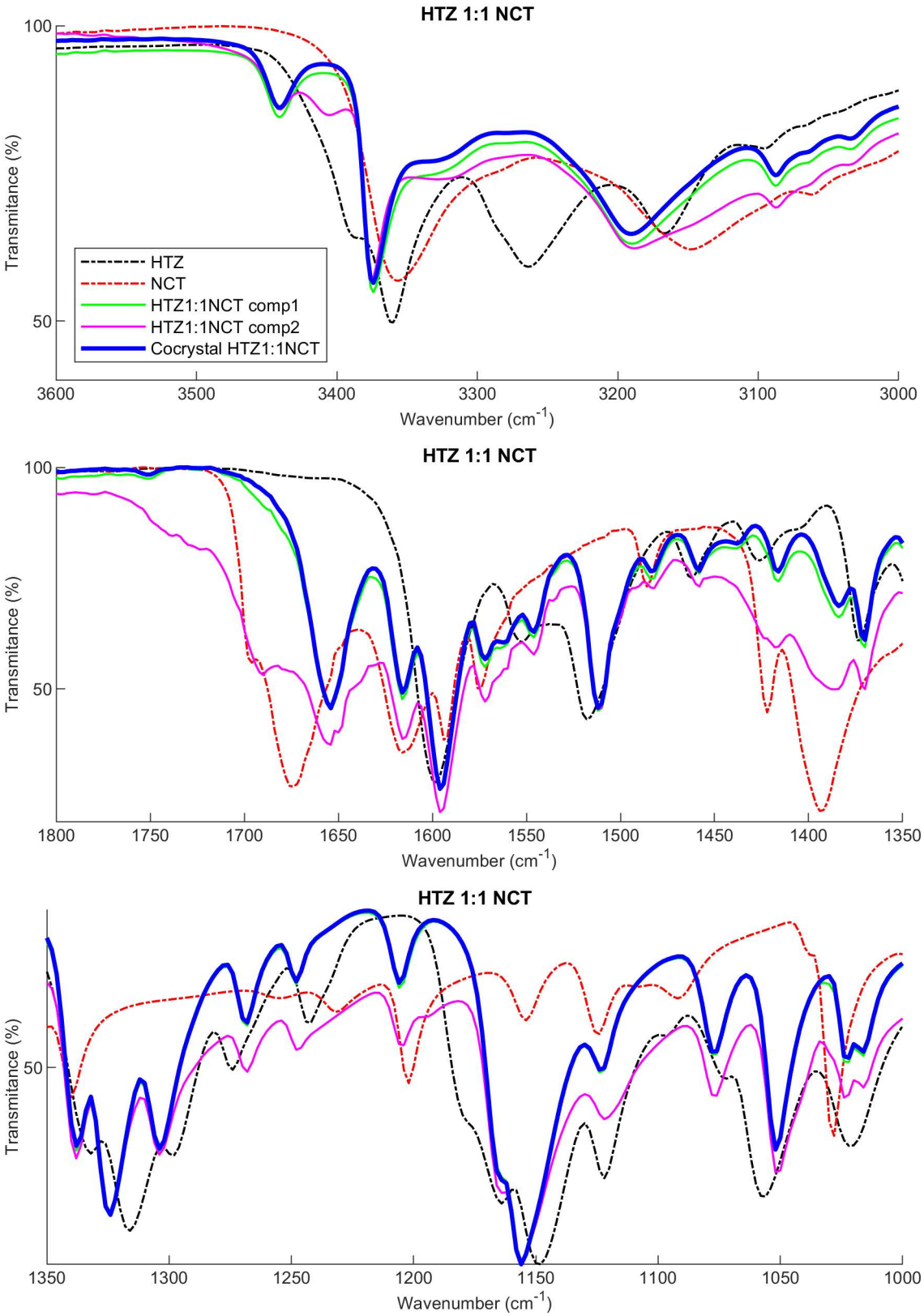

Figure 3.4. MIR spectrum of the HTZ:NCT 1:1 reference co-crystal (average n=5), MCR loading plots from the samples produced with the stoichiometric ratio of HTZ:NCT 1:1, NCT MIR spectrum (average n=5), and HTZ MIR spectrum (average n=5).

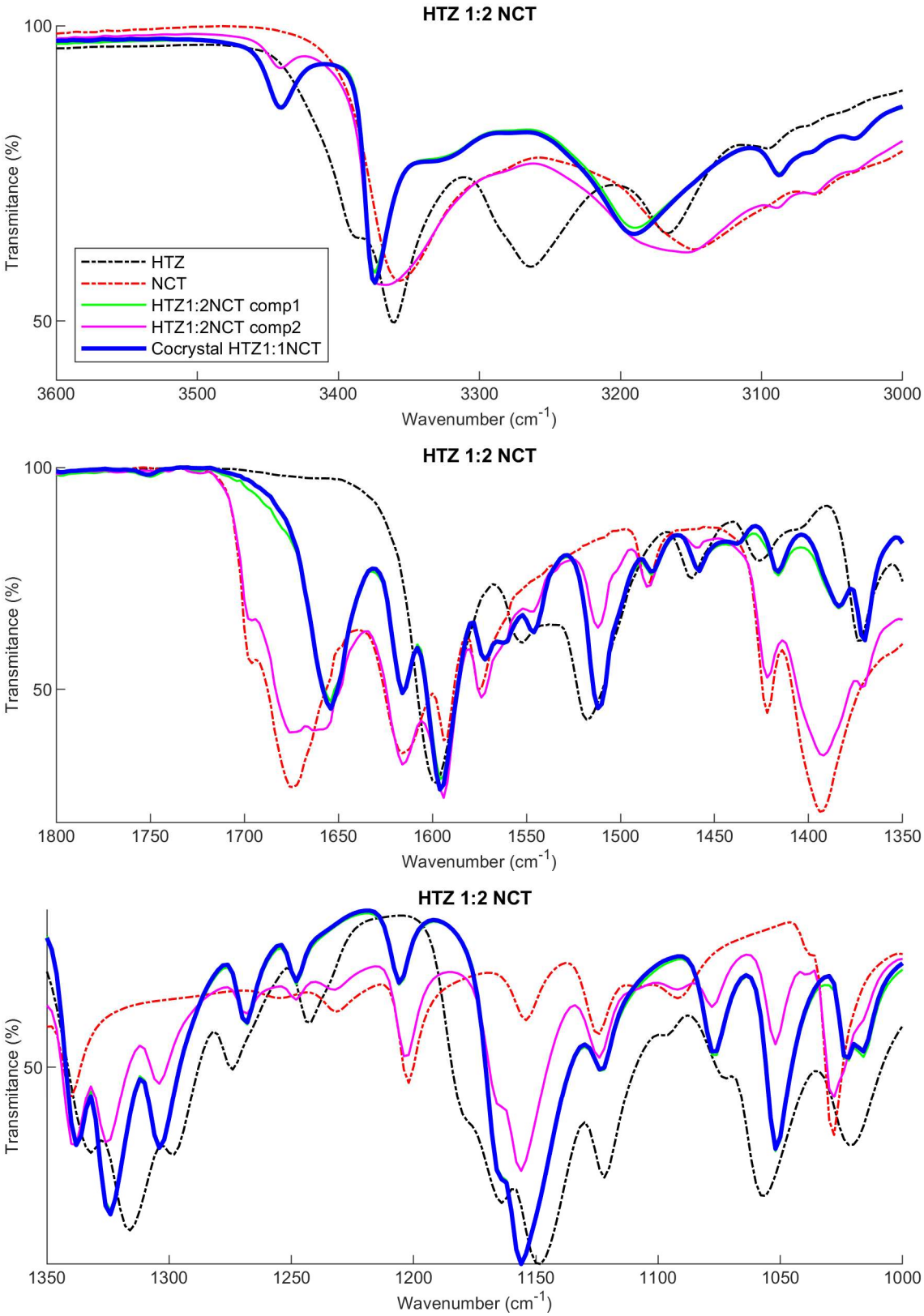

Figure 3.5. MIR spectrum of the HTZ:NCT 1:1 reference co-crystal (average n=5), MCR loading plots from the samples produced with the stoichiometric ratio of HTZ:NCT 1:2, NCT MIR spectrum (average n=5), and HTZ MIR spectrum (average n=5).

MCR scores of component 1 for co-crystal systems, prepared at both ratios in a range of solvents, were used in Equation 3.2 to determine phase purity. Greater phase purity was obtained using the ratio of HTZ:NCT 1:1, except when ACN and MeOH was used as solvent (Figure 3.6). The percentage variance explained by the component that represents the co-crystal information was similar to both ratios, around 80%. However, greater purity was reached using the ratio 1:1.

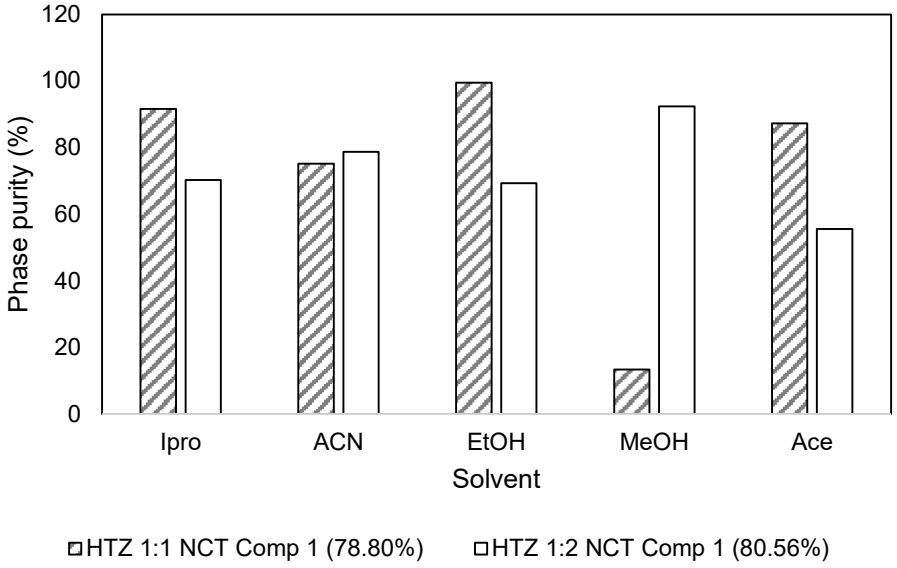

Figure 3.6. Percentage phase purity calculated using Equation 2 for screening samples produced with the stoichiometric ratio of HTZ:NCT 1:1 and HTZ:NCT 1:2. IPro = 2-propanol, ACN = acetonitrile, EtOH = ethanol, MeOH = methanol, Ace = acetone.

3.4.4 Laboratory scale co-crystallization

Prior laboratory scale co-crystallization of NCT:HTZ 1:1 co-crystals, it was necessary to determine the slurry co-crystallization time. Slurry experiments were performed and monitored by Raman spectroscopy. PCA of Raman spectra acquired was used to determine the co-crystallization endpoint for all solvents investigated. The results showed that for complete co-crystal formation the endpoint was dependent on the solvent used (Table 3.5). The PCA model was able to identify the transition of

intermediate forms to co-crystal formation. That was observed for the CF solvent system, in which an intermediate may have been formed at 40 h and transformed into the co-crystal 10 hours later (Figure 3.7a). After the co-crystal formation, further transformations were not observed up to 120 h for all the solvents investigated. Thus, slurry co-crystallization time used for the scale up experiments was 120 h to standardize the time across the different solvents and ensure completion of co-crystal formation. The abrupt shifts observed may be due to the formation of bonds as the co-crystal is formed, since those bonds have strong Raman shifts.

Table 3.5. Endpoint of NCT:HTZ 1:1 co-crystal formation for different solvents used in slurry co-crystallization at room temperature. Endpoint was determined by PCA of Raman spectra acquired online. EtOH = ethanol, MeOH = methanol, Ace = acetone, EtOAc = ethyl acetate, DCM = dichloromethane, CF = chloroform, and ACN = acetonitrile. *Solvent showed overwhelming Raman signal; therefore, no spectral differences were captured during the time analyzed and it was not possible to monitor the process using Raman spectroscopy

Solvents	**Endpoint (h)**
EtOH	*
MeOH	110
Ace	*
EtOAc	3
DCM	65
CF	45
ACN	60

A

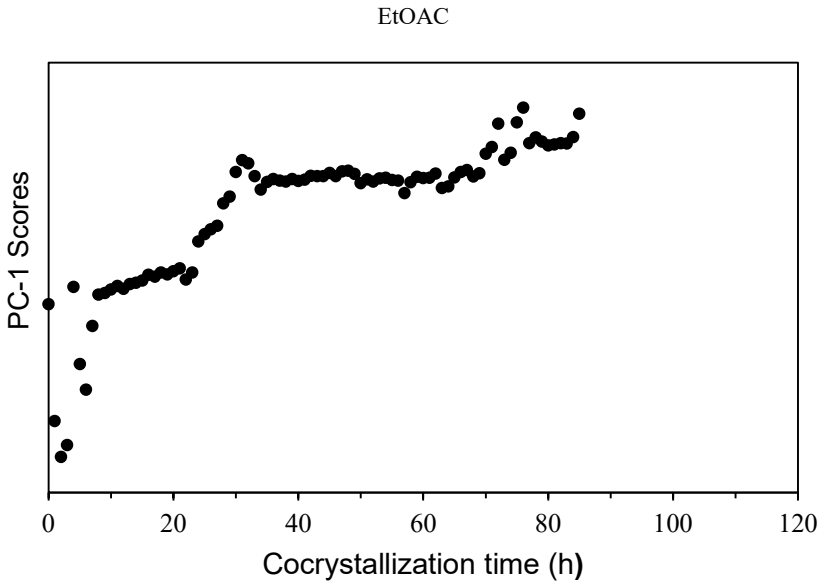

B

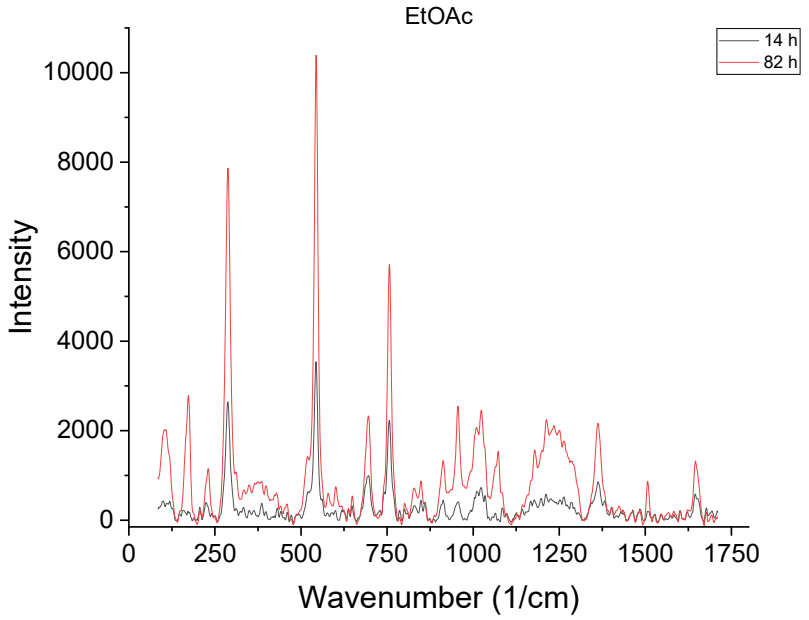

Figure 3.7. (A) Online multivariate Raman tracker of slurry co-crystallization from ethyl acetate, at room temperature, and (B) Raman spectra acquired after 14h and 82h.

A

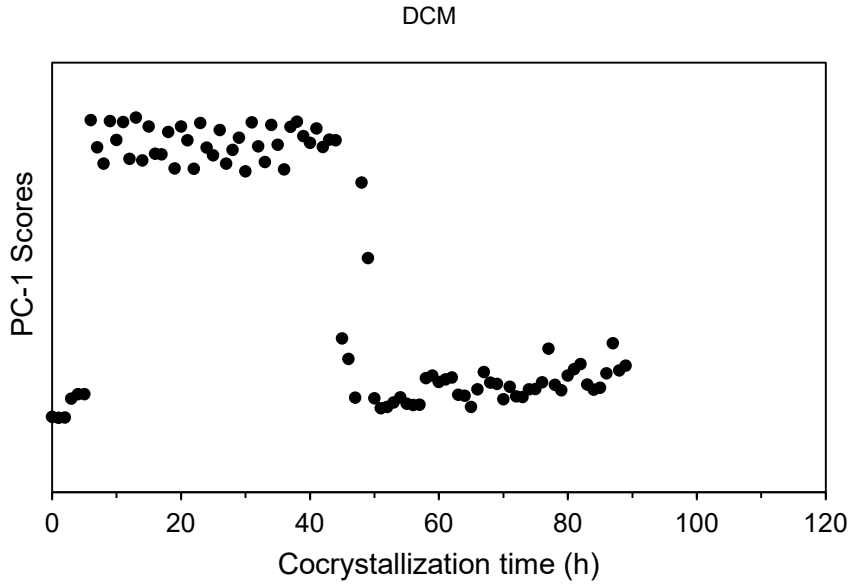

B

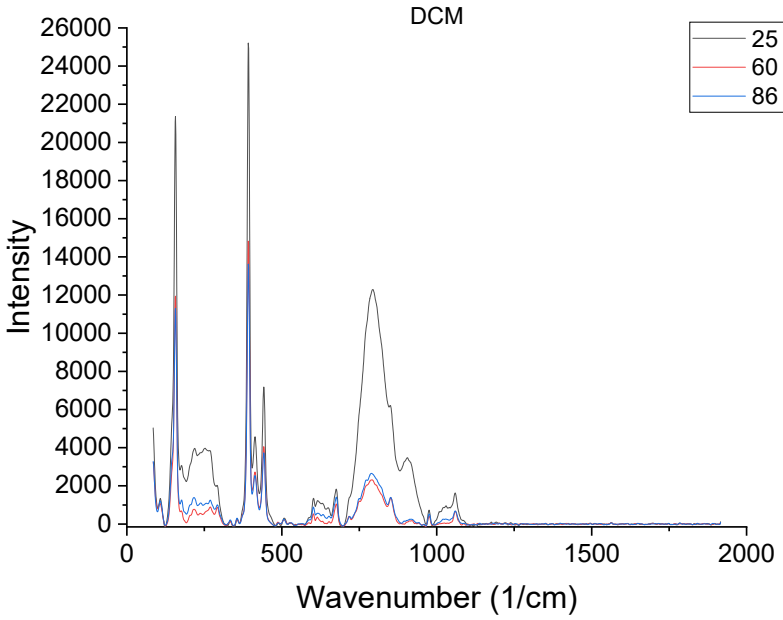

Figure 3.8. (A) Online multivariate Raman tracker of slurry co-crystallization from dichloromethane, at room temperature, and (B) Raman spectra acquired after 25 h, 60 h and 86 h.

A

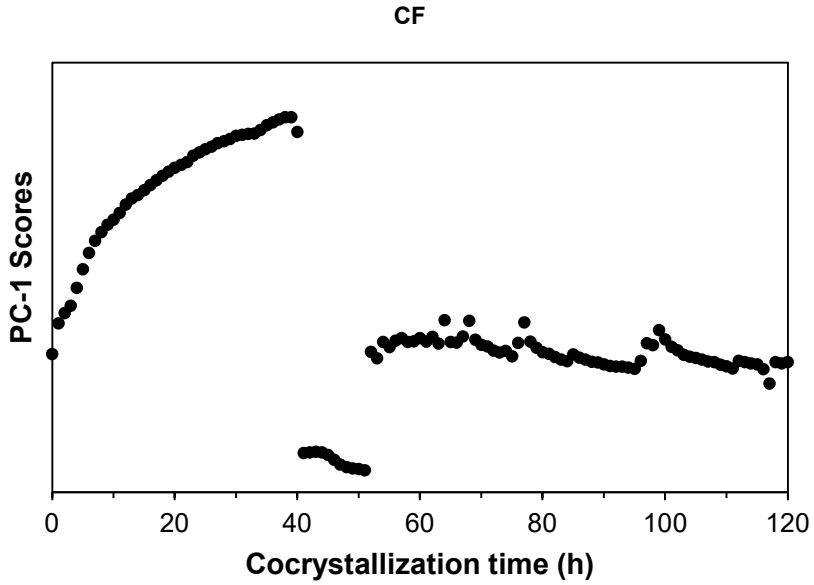

B

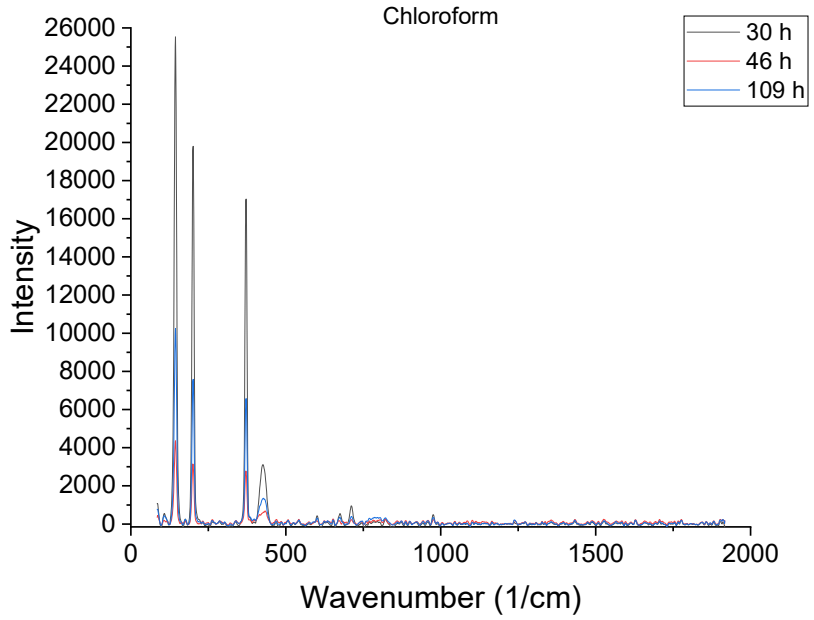

Figure 3.9. (A) Online multivariate Raman tracker of slurry co-crystallization from chloroform, at room temperature, and (B) Raman spectra acquired after 30 h, 46 h and 109 h.

A

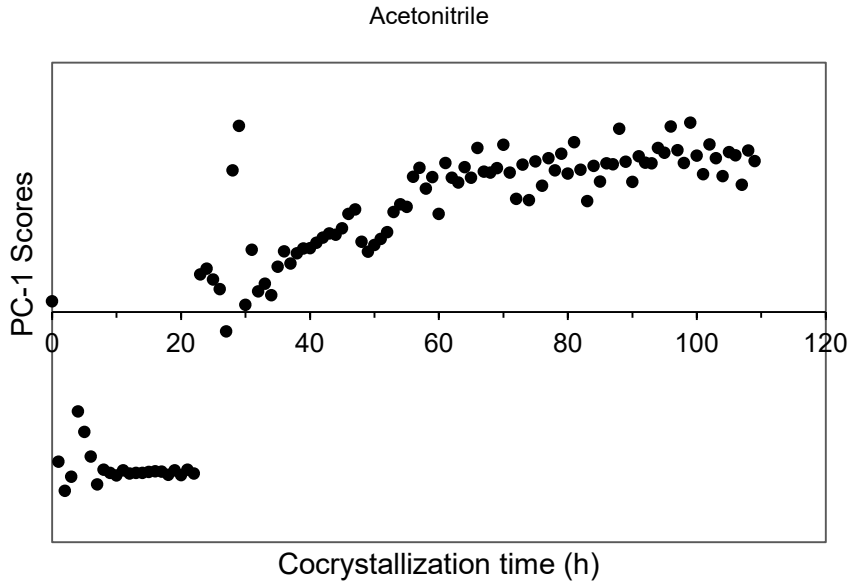

B

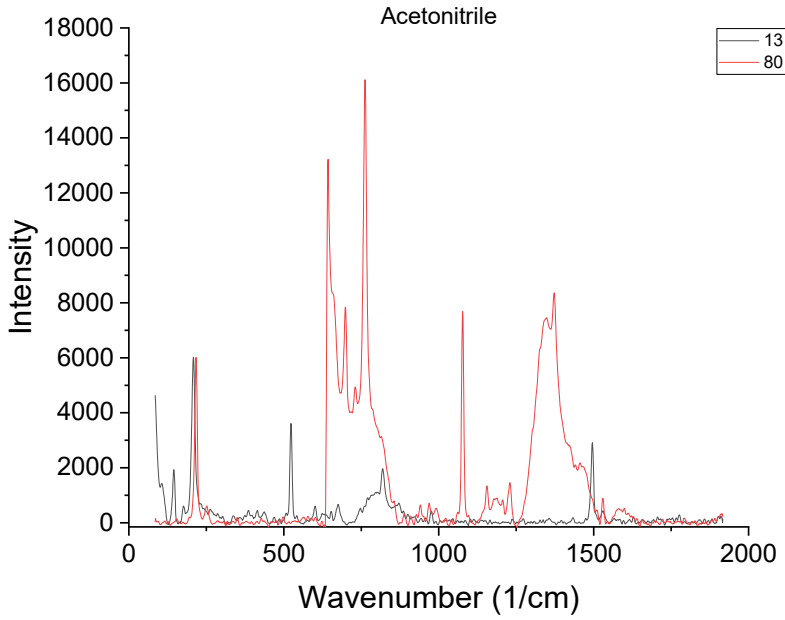

Figure 3.10. (A) Online multivariate Raman tracker of slurry co-crystallization from acetonitrile, at room temperature, and (B) Raman spectra acquired after 13 h and 80 h.

A

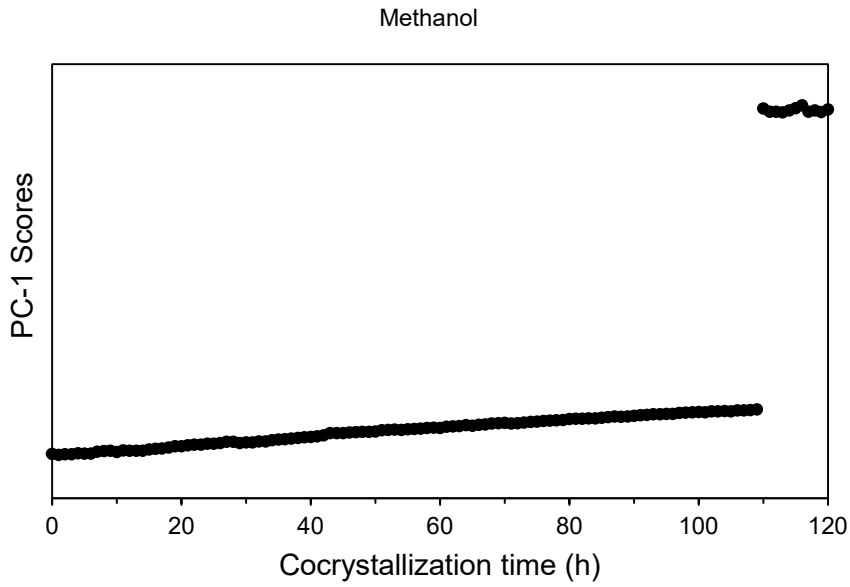

B

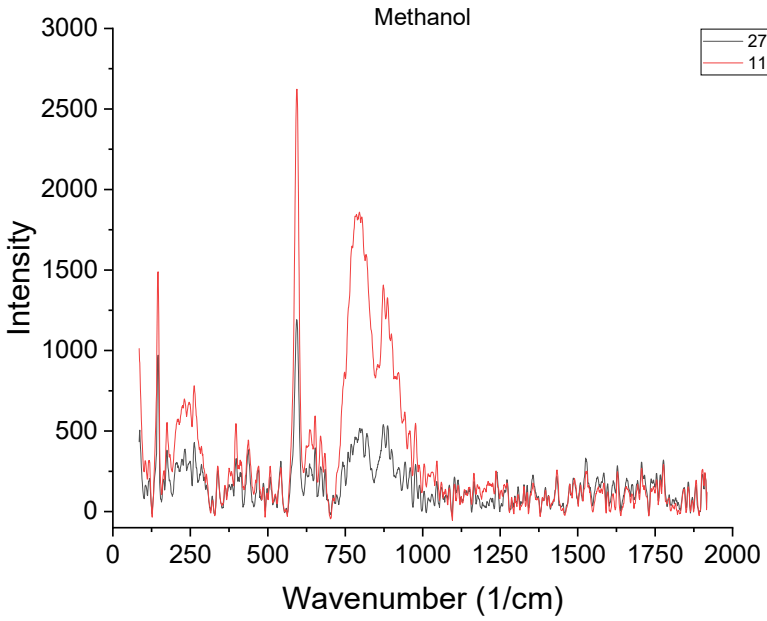

Figure 3.11. (A) Online multivariate Raman tracker of slurry co-crystallization from methanol, at room temperature, and (B) Raman spectra acquired after 27 h and 119 h.

3.4.4.1 Co-crystallization design space

Response surface models were developed to investigate solvent effect and find the optimal temperature (and agitation for evaporative co-crystallization) to obtain co-

crystals with high phase purity. A full-factorial DoE was performed for both semi-slurry (21 runs) and evaporation (42 run) co-crystallization processes (Table 3.6). Phase purity was calculated using data from the MCR model developed, Equation 2. Phase purity values determined for the semi-slurry were lower than those obtained for the evaporation co-crystallization for each corresponding solvent and temperature for a number of systems investigated (Figure 3.12).

Table 3.6. Design of Experiment of laboratory scale evaporation and slurry co-crystallizations. MeOH = methanol, Ace = acetone, DCM = dichloromethane, EtOAc = ethyl acetate, ACN = acetonitrile, iPro = 2-propanol, and EtOH = ethanol.

Slurry			**Evaporation**			
F-1	**F-2**	**Response**	**F-1**	**F-2**	**F-3**	**Response**
T (°C)	Solvent System	Phase purity (%)	T (°C)	Solvent System	Agitation (rpm)	Phase purity (%)
10	CF:Ace 1:1	67.30	10	DCM:Ace 1:1	65	85.83
40	Ace	73.65	10	DCM:Ace 1:1	0	94.83
25	EtOAc:Ace 4:1	73.29	25	EtOH	0	41.02
40	CF:Ace 1:1	70.58	25	Ace	0	95.01
10	DCM:Ace 1:1	68.36	25	DCM:Ace 1:1	65	99.83
25	MeOH	3.91	40	MeOH	0	77.89
25	EtOH	53.72	40	ACN	65	92.01
25	DCM:Ace 1:1	75.59	25	DCM:Ace 1:1	0	93.34
10	EtOAc:Ace 4:1	70.69	10	Ace	65	84.84
10	EtOH	68.28	40	EtOAc:Ace 4:1	65	93.60
10	MeOH	55.16	25	Ace	65	70.68
25	ACN	70.14	10	CF:Ace 1:1	65	86.35
40	ACN	70.36	25	MeOH	65	76.62
40	DCM:Ace 1:1	71.13	40	Ace	0	95.46
10	CAN	67.79	10	MeOH	0	5.23

40	EtOH	30.01	40	EtOH	0	58.08
25	Ace	77.16	10	EtOH	0	73.88
40	EtOAc:Ace 4:1	70.24	10	EtOAc:Ace 4:1	65	82.80
25	CF:Ace 1:1	78.41	25	CF:Ace 1:1	65	99.12
10	Ace	75.95	40	CF:Ace 1:1	0	72.47
40	MeOH	76.57	25	EtOAc:Ace 4:1	0	99.00
-	-	-	25	MeOH	0	56.26
-	-	-	40	DCM:Ace 1:1	65	93.39
-	-	-	40	Ace	65	95.40
-	-	-	10	CF:Ace 1:1	0	89.39
-	-	-	40	DCM:Ace 1:1	0	91.30
-	-	-	25	ACN	65	97.86
-	-	-	10	Ace	0	88.93
-	-	-	40	MeOH	65	95.31
-	-	-	40	EtOH	65	93.64
-	-	-	25	ACN	0	95.57
-	-	-	10	ACN	65	88.09
-	-	-	25	EtOAc:Ace 4:1	65	100.00
-	-	-	40	EtOAc:Ace 4:1	0	90.20
-	-	-	10	EtOAc:Ace 4:1	0	87.23
-	-	-	25	EtOH	65	68.09
-	-	-	10	EtOH	65	71.71
-	-	-	10	MeOH	65	33.74
-	-	-	40	CF:Ace 1:1	65	85.50
-	-	-	10	ACN	0	78.05
-	-	-	40	ACN	0	89.23
-	-	-	25	CF:Ace 1:1	0	94.78

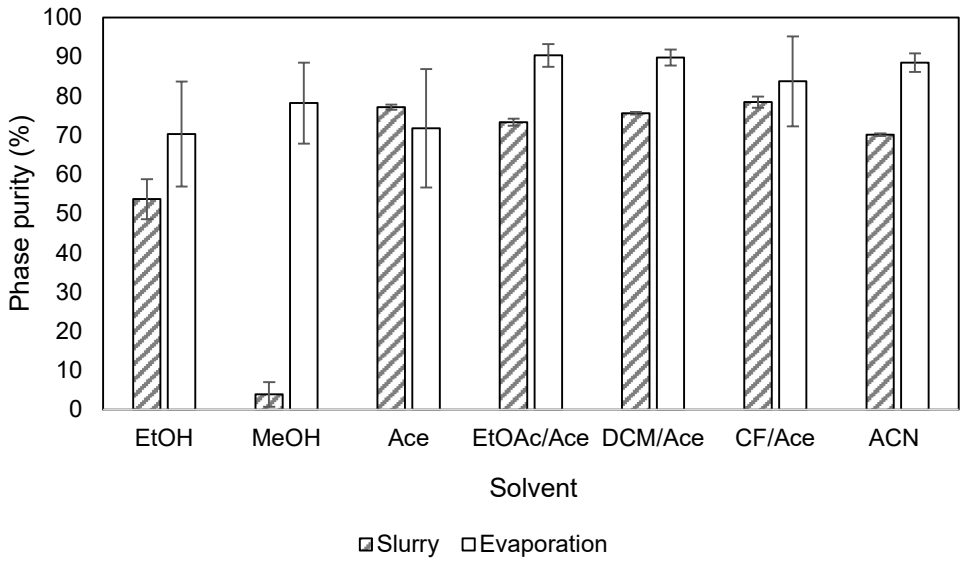

Figure 3.12. Comparison of co-crystal phase purity determined using MIR spectra and results of MCR model (Equation 2) for the system HTZ:NCT 1:1, at 25ºC. (n=5). EtOH = ethanol, MeOH = methanol, Ace = acetone, EtOAc = ethyl acetate, DCM = dichloromethane, and ACN = acetonitrile.

Overall, agitation optimized the evaporation co-crystallization process (Figure 3.13). The optimal conditions for evaporation co-crystallization observed were the following. The solvent systems ACN, CF:Ace 1:1, and DCM:Ace 1:1 produced the co-crystals with greatest phase purities at all temperatures investigated (Figure 3.13a). At 40 °C EtOAc:Ace 4:1, Ace and EtOH also produced co-crystal with high phase purity. Methanol and ethanol showed considerably lower co-crystal phase purity in comparison with the other solvent systems. There was a statistically significant association between the response variable and the factors (F-value of 9.88 and p-value less than 0.0001). Adjusted r^2, predicted r^2 and adeq. precision were found to be 0.7055, 0.5187 and 15.49, respectively, indicating that the model could be used to navigate the design space. The internally studentized residuals was normally distributed.

The DoE model of slurry co-crystallization also showed a statistically significant association between the response variable and the factors. (F-value of 5.30 and p-value of 0.025). Adjusted r^2, predicted r^2 and adeq. precision were found to be 0.7505, -5.467 and 10.10, respectively, indicating that the model could be used to navigate the design space. However, additional runs would be required if the model was to be used for predictions. The internally studentized residuals were normally distributed. The solvent systems Ace and DCM:Ace 1:1 produced co-crystals with greater phase purities (Figure 3.14). This was represented in the contour plot of the design space in which the relative purity obtained using those solvent systems fell within the same contour level for all temperatures. The solvent system CF:Ace 1:1 at the temperatures of 25 °C and 10 °C also produced co-crystals with great phase purities. Solvents EtOH and MeOH showed the lowest phase purity, similarly to evaporation co-crystallization.

A

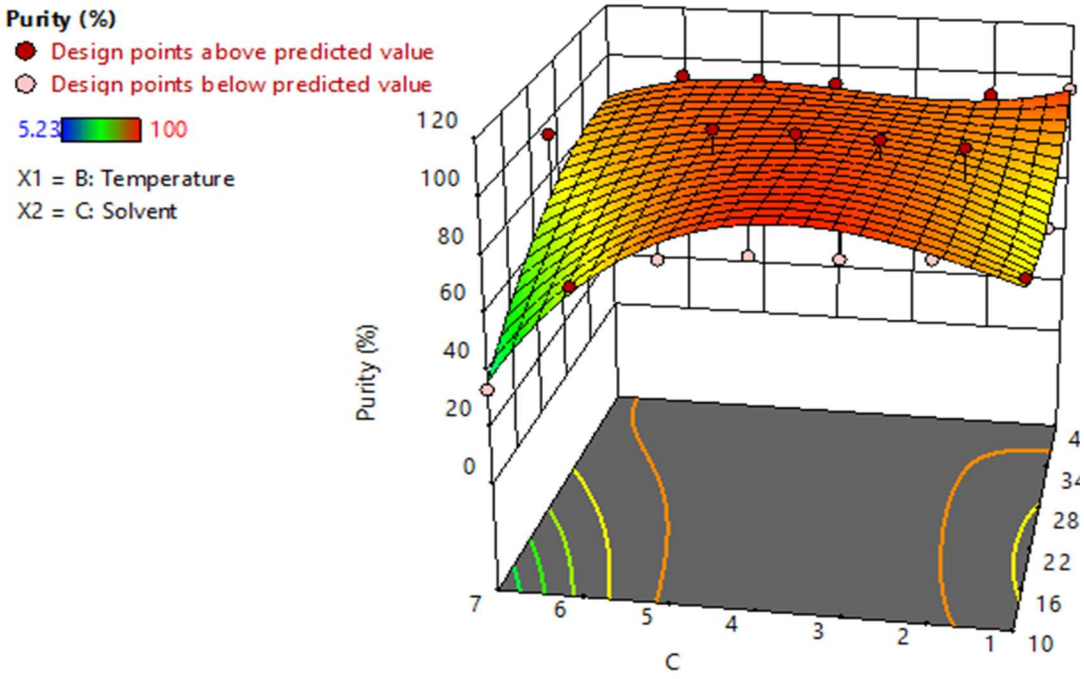

B

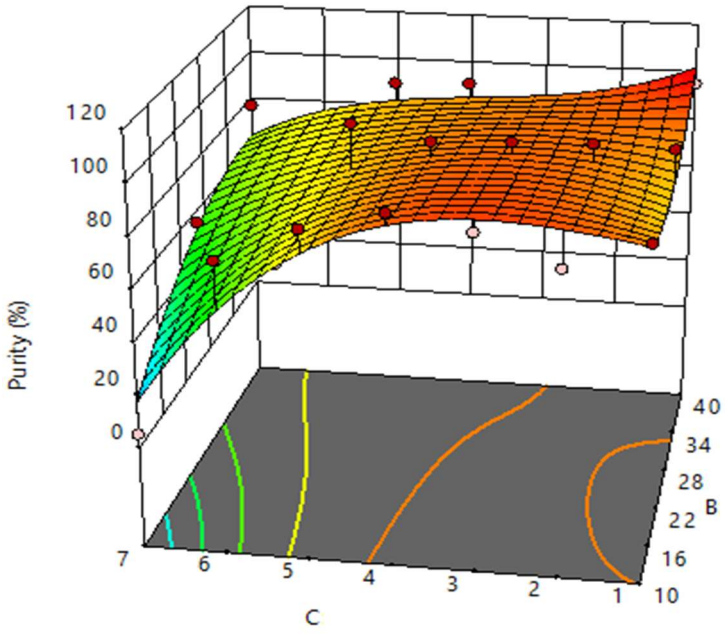

Figure 3.13. DoE contour plots of evaporation co-crystallization (A) with agitation of 65 rpm and (B) without agitation. Solvent indexes are 1 = Ace, 2 = ACN, 3 = CF:Ace 1:1, 4 = DCM:Ace 1:1, 5 = EtOAc:Ace 4:1, 6 = EtOH, 7 = MeOH. Temperature in °C.

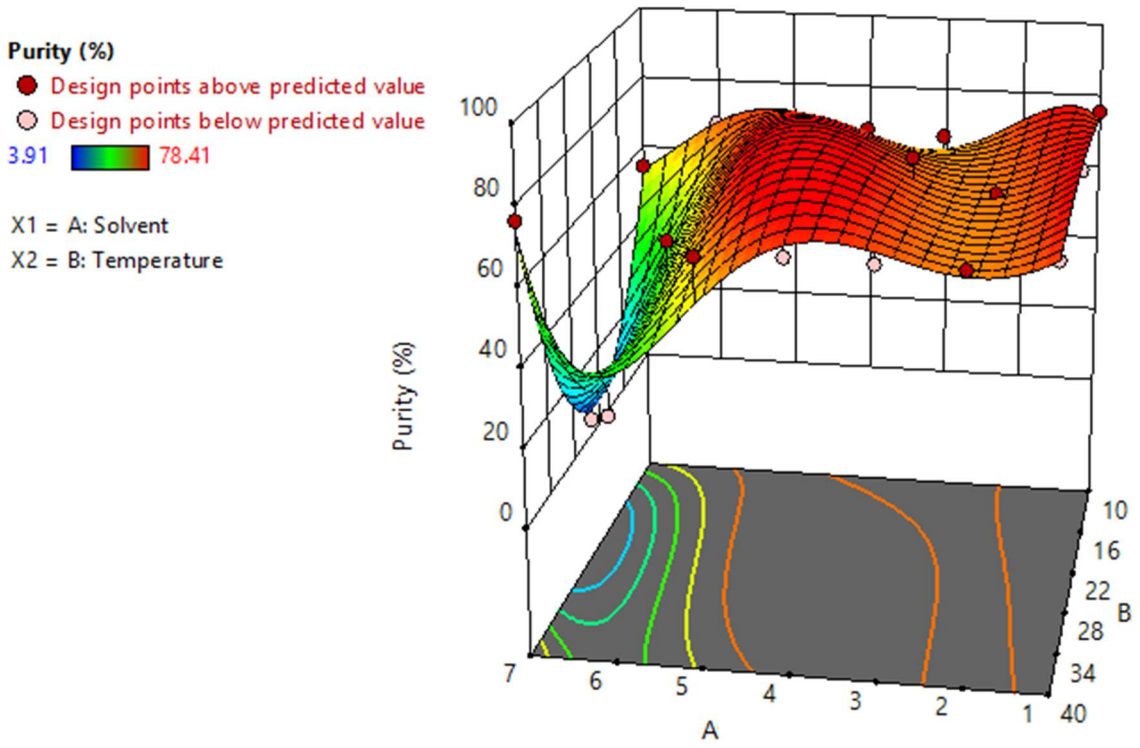

Figure 3.14. DoE contour plots of slurry co-crystallization. Solvent indexes are 1 = Ace, 2 = ACN, 3 = CF:Ace 1:1, 4 = DCM:Ace 1:1, 5 = EtOAc:Ace 4:1, 6 = EtOH, 7 = MeOH. Temperature in °C.

3.5 Discussion

This study addressed challenges of co-crystallization monitoring and co-crystal phase purity control. Quantum chemistry simulation was used for in-silico screening and selection of a coformer that was thermodynamically inclined to form a co-crystal with hydrochlorothiazide. All coformers screened had been previously investigated (Rodrigues et al., 2019, 2018b; Sanphui et al., 2015; Sanphui and Rajput, 2014). Interestingly, the relatively unfavourable mixing enthalpies/energies predicted in this study for the co-crystallisation of HTZ with malic and citric acids successful confirm the findings of a previous study that reported very low phase purity for products of such co-crystallizations (Rodrigues et al., 2018b). The co-crystal, HTZ-NCT ratio 1:1 was selected based on the quantum chemistry simulations was hydrochlorothiazide

that revealed high negative values of mixing enthalpy/energy computed for this system. The main goal of this study was the development of a model to predict co-crystal phase purity. Thus, the model co-crystal was also chosen based on the depth of characterization and the information available to confirm and validate the predictions.

A novel methodology was developed to quantify co-crystal phase purity using MIR in combination with MCR-ALS without a reference spectrum. Soares and Carneiro (2013, 2017) used Raman and MCR-ALS to investigate co-crystallization, however, initial estimates of both the pure substances and the co-crystal were used (Soares and Carneiro, 2017, 2013). In this study, the MCR-ALS model was performed without any initial estimate. The co-crystal spectra obtained from the model was later compared with reference substances: the co-crystal, and the physical mixture of drug and coformer, to confirm that the model was able to extract the co-crystal spectra without the initial estimates.

Another novel finding of the MCR model designed was the determination of the statistically optimal ratio of co-crystal formation. This includes the combined analysis of the percent variance captured by the two components of the MCR model and Pearson Correlation coefficient analysis (Table 3.4). This methodology was also confirmed by spectral analysis.

Comparison of MIR spectra of the reference co-crystals, HTZ, coformer and MCR loadings highlighted differences in regions related to co-crystal formation. Key differences were observed in the spectral regions related to O–H and N–H stretching.

HTZ co-crystals were reported to involve the primary and secondary sulfonamide groups from HTZ (Rodrigues et al., 2019; Silva et al., 2017).

HTZ:NCT co-crystals were reported to be formed due to hydrogen bonding between the NH of sulfonamide group of HTZ and the NCT carbonyl group (Rodrigues et al., 2019). Formation of new bands was observed in the region of OH stretch (peaks centered at 3440 and 3190 cm^{-1}), NH stretch of primary amine (3374 cm^{-1}), and C=O/C=C stretching (1654 cm^{-1}). Peaks in typical regions of S=O stretching were also observed, with new peaks forming at 1324, 1303, 1268, and 1076 cm^{-1}. Therefore, the results obtained in this study are in agreement with those previously reported in the literature.

In this study, the application of Raman combined with PCA was used as a non-contact and non-destructive PAT tool to quantify co-crystals formation and co-crystallization endpoint. MIR spectroscopy combined with MCR-ALS was shown to be a useful PAT tool to determine co-crystallization endpoint and quantify co-crystal phase purity (Mazivila et al., 2019). Substances that show weak MIR signal may have strong Raman signal (Larkin, 2017). Thus, Raman is a complementary technique to MIR, and the PAT tool developed in this study is complementary to the PAT tool developed by Mazivila et al. Fluorescence problems frequently encountered when Raman is used, are not observed when MIR is used (Rodrigues et al., 2019). The decision about which methodology should be used is dependent on the properties of the solvent and the substances used to produce the co-crystal. PCA of Raman spectra acquired online also showed whether the co-crystal formation happens via intermediate formation, as shown in Figure 3.7a in which co-crystals of NCT:HTZ 1:1 appeared to form an

intermediate when chloroform was used. Ishihara et al. (2019) showed that MIR and MCR were also able to investigate intermediate formation (Ishihara et al., 2019). Again, this shows that MIR and Raman spectroscopy can be used as complementary techniques to investigate co-crystallization process.

The final contribution of this study to the scientific development of co-crystallization processes was the comparative investigation between evaporation and slurry methodologies. Overall, evaporation co-crystallization produced co-crystals with greater phase purity than the slurry technique. This finding agrees with the study reported by previous studies that revealed that evaporation always shows greater yield if the drug and the coformer have similar solubility values (Rodrigues et al., 2018a; Rodrigues et al., 2020; Rodrigues et al., 2018b). The design of experiments also confirmed this finding. According to the results of the DoE model, DCM:Ace 1:1 was the only solvent system that produced co-crystal with the greatest purity in both slurry and evaporation co-crystallization, at all temperatures. Thus, co-crystals produced using DCM:Ace 1:1 could be used as a reference system for comparison of both techniques. In the evaporation co-crystallization with agitation the phase purities obtained using this system were 85.83, 99.83, and 93.39 % at 10, 25, and 40 °C, respectively. In the slurry co-crystallization the phase purities obtained at the same temperatures were considerably lower (i.e. 68.36, 75.59, and 71.13 % at 10, 25, and 40 °C, respectively). It is very difficult to discuss how the solvent affects co-crystallization outcome. There are several factors that can contribute to the co-crystal purity which is also dependent on the co-crystallization technique. For solvent evaporation co-crystallization, the choice of solvent is always dependent on the

solubility of each component in the solvent. Furthermore, the two components need to have a similar solubility in the solvent. In this way the phase diagram is symmetric, and it would be easier to obtain a pure co-crystal by solvent evaporation (Aitipamula et al., 2014; Sarraguça et al., 2016). Since normally, the co-former and API have different solubilities in a pre-determined solvent a mixture of solvents is usually used, as was in the case of this work in which the highest purity was obtained by a mixture of acetone and dichloromethane. Also, it is important that the solvent has a low vapor pressure to be able to evaporate at low temperatures. For slurry co-crystallization other physicochemical properties might be important such as polarity, dielectric constant, surface area, among others. An extensive and detailed analysis relating the physicochemical properties of the solvents and the purity of the cocrystals must be done to be able to define a systematic approach to solvent type co-crystallizations.

3.6 Conclusions

An MCR model was developed to determine co-crystal phase purity and identify the stoichiometric ratio for the formation of co-crystals. MCR-ALS was able to extract the spectrum of the co-crystal from a complex mixture i.e., non-reacted starting material mixed with co-crystals, even though a reference co-crystal spectrum was not provided, and determine the phase purity of co-crystallization products. Phase purities determined showed to be dependent on the solvent. The ratio of co-crystal formation determined by the MCR model proposed revealed that 1:1 was the optimal ratio, which is in accordance with the literature. A design space was determined by DoE using the % phase purity as response variable. The % phase purity obtained using

the proposed model coupled with MCR. The response surface models showed that in addition to the solvents, the process employed (evaporation versus slurry) also affects phase purity. In this study, co-crystals produced by evaporation co-crystallization with agitation of 65 rpm showed greatest phase purity.

Chapter 4 - Impact of percolation threshold and microcrystalline cellulose variability on tablet compression

Revised from publication in: *Powder Technology* (2019)

https://doi.org/10.1016/j.powtec.2019.05.027

4.1 Abstract

Percolation theory provides a statistical model which can be used to predict the behaviour of powder blends based on particle-particle interactions. The aim of this study was to investigate if percolation theory could be used to predict the drug loading concentration of pharmaceutical tablets, and the relative density of a blend, above which tablet tensile strength is reduced, resulting in the production of unsatisfactory products. The model blend studied contained ibuprofen as the API, which exhibits poor flow and compressibility, and microcrystalline cellulose (MCC) as the excipient, which exhibits good flowability and compressibility. Two MCC grades with differing physical properties were investigated, Vivapur® 102 (air streamed dried quality), and Emcocel® 90 (spray dried quality) to test the theory. Blends containing 2.5 to 40 % w/w of ibuprofen were compacted at a range of pressures and the values of the powder true density, compaction pressure, tablet envelope density, and tablet tensile strength were used to calculate the percolation thresholds mathematically. The drug loading threshold values predicted with the model (19.08% w/w and 17.76% w/w respectively for Vivapur® 102 and Emcocel® 90) were found to be in good agreement when compared to experimental data and the percolation threshold was visually confirmed using Raman imaging. The capability of multivariate analysis to predict the drug loading threshold was also tested. Principal component analysis was unable to identify the threshold. However, it provided an overview of the changes of the analysed properties as ibuprofen drug loading increased. It was also able to identify differences between blends containing Vivapur® or Emcocel®. In conclusion, percolation theory was able to predict the maximum acceptable drug

loading for this binary system of API and excipient. This methodology could be employed for other binary systems to predict maximum drug loading potential without the need for time consuming and expensive tablet production.

4.2 Introduction

Multi-component powder blends are critical components of numerous process trains across a wide variety of manufacturing sectors. Solid dosage forms manufactured from powder blends compose a large proportion of pharmaceutical production (Järvinen et al., 2013) Pharmaceutical powder blends are composed of a drug substance (active pharmaceutical ingredient) and inactive excipients to aid processing, stability and delivery (Leane et al., 2015). Drug load is an important factor to be considered during the design of these blends. The higher the drug load, the higher the probability of the drug's properties impacting the blend's manufacturability and finished dosage form properties. For instance, Wenzel et al. showed how the increase of drug load negatively affected granulation, compression, tablet disintegration and dissolution (Wenzel et al., 2017). In contrast to a gradual change in blend properties with increasing drug load, a threshold drug concentration was proposed, referred to as the percolation threshold (Leane et al., 2015). It is proposed that issues can be expected to occur in manufacturability and drug product quality above the percolation threshold concentration of drug (Leane et al., 2018, 2015). Within a QbD pharmaceutical approach, the percolation threshold model can aid identification of a threshold drug loading. The formulation should contain drug loadings below the percolation threshold to ensure critical quality attributes

compliance. Knowing the percolation threshold drug level can aid robust formulation development by maintaining the drug below this threshold.

Percolation is a geometrical-statistical theory that includes two model types: (*i*) lattice model, and (*ii*) continuum model. The lattice percolation model has been previously reported in the literature as appropriate to model tablet tensile strength for systems containing microcrystalline cellulose (Kozicki, 2007; Kuentz and Leuenberger, 2000, 1998; Leuenberger, 1999). In a lattice model, percolation threshold is described the random occupation of a lattice of one substance by particles of a second substance (Leuenberger, 1999). Consider initially a matrix of A being percolated by particles of B. As the concentration of B increases in the system, a threshold concentration will be reached, and a property phase transition will be noticed. Above this threshold the system is a matrix of B percolated by particles A. The property phase transition occurs because of the formation of clumps of particle B that are connected or close enough to each other in such a way that they are linked across the entire volume of the tablet, forming an infinite cluster i.e., a drug cluster that spans throughout the entire volume of the tablet. When this cluster is formed properties of the blend may undergo significant changes (Leuenberger, 1999). This theory can be extrapolated to the random distribution of a group of substances A in a lattice formed by a group of substances B (Leuenberger et al., 1992). In this case, the substances that form the group A need to have at least one similar property and at the same time this property must be dissimilar to the substances of group B. For example, in a tablet blend, drug substance and excipients that have poor flow could

be grouped together as A, while all the substances within the formulation that have good flow would belong to group B.

One of the critical quality attributes to consider during the development of a tablet blend for compaction is the tablet's tensile strength. Tensile strength is defined as the resistance of a material to undergo fracture under tension (Fell and Newton, 1970). It is considered a key physical property to ensure the quality of manufactured tablets. Tablets are required to have a minimum value of tensile strength to remain intact throughout downstream processing and handling. On the other hand, an increase in tensile strength can lead to an increase in the dissolution time (Bi et al., 1999). The application of the percolation threshold model to tablet tensile strength provides valuable information in relation to blend design. The main input of this model is the tablet relative density, which replaces ρ in Equation 1.19. Tablet relative density is a parameter that is related to a number of individual raw material characteristics, process parameters and many subsequent tablet physical properties. The inclusion of tablet relative density makes this model a highly practical theory.

Percolation thresholds have been estimated graphically in a number of previous studies; for binary blends of MCC and mannitol (Pérez Gago and Kleinebudde, 2017), for binary blends at different size ratios and for different grades of HPMC blended with hydrocortisone (Mohamed et al., 2015), and for complex blends of mefenamic acid and a range of excipients (Kimura et al., 2007). Kuentz and Leuenberger proposed a mathematical approach in which the percolation threshold of a blend of microcrystalline cellulose and paracetamol was modelled (Kuentz and Leuenberger, 2000). The authors recommended additional investigation to confirm their findings.

However, there are limited publications in which the percolation threshold is predicted mathematically in the field of pharmaceutical sciences. Busignies et al. (Busignies et al., 2007) showed that if the mathematical approach is selected, it is necessary to begin with modelling the percolation coefficient in order to be able to model the percolation threshold for each specific formulation, as the percolation coefficient did not seem to be universal.

The aim of this study was to define the percolation coefficient for a blend comprising MCC/ibuprofen based on a modified Heckel equation (Leuenberger, 1999). Having determined the percolation coefficient for the blend, Equation 1.19 was then employed to calculate the respective percolation thresholds. The blend considered contained a model drug, ibuprofen, and a commonly used excipient, MCC. These binary blend components were selected because ibuprofen exhibits poor flowability and compressibility and is prone to capping (Al-Karawi et al., 2018; Nokhodchi et al., 1995; Rasenack and Mü, 2002). MCC is a widely used excipient due to its good flowability, high dilution potential and compactibility (Thoorens et al., 2014). Therefore, the contrasting properties qualifies the combination of these substances as an appropriate case to apply the percolation model. Particle pore and particle shape can have significant impact on percolation threshold (Lin and Chen, 2018; Meyer et al., 2015; Nigro et al., 2013), therefore, two MCC grades with differing particle properties were investigated in this study: Vivapur® 102, an air streamed dried grade, and Emcocel® 90, a spray dried grade. Raman image analysis of compacted blends was employed to visually determine whether an infinite cluster of drug particles could be detected on the surface of tablets prepared above the

percolation threshold. Properties of the powder blends and the tablets manufactured were investigated using univariate and principal component analysis (PCA) analysis to determine properties which are diminished above the percolation threshold and investigate if PCA is able to identify the critical concentration related to the percolation threshold.

4.3 Materials and methods

4.3.1 Materials

Microcrystalline cellulose (Vivapur® 102, and Emcocel® 90) was supplied by JRS PHARMA Gmbh+Co. KG, Germany. Ibuprofen was obtained from Kemprotec Ltd., United Kingdom.

4.3.2 Methods

4.3.2.1 Powder characterization

4.3.2.1.1.1 Surface area

MCC samples were degassed for 3 h, at 120 ^{o}C and ibuprofen samples for 24 h, at 40 ^{o}C in a FlowPrep 060 sample degas system (Micromeritics, USA). The mass of each sample was between 0.4 - 0.6 g. Surface area was determined using a Gemini VI surface area and pore size analyser (Micromeritics, USA). The modelling equation applied was the Brunauer Emmett-Teller equation (BET) (Brunauer et al., 1938). Liquid nitrogen at - 196 ^{o}C kept isothermal conditions and N_2 was the absorbate gas utilized. The analysis was carried out in triplicate.

4.3.2.1.1.2 Laser diffraction particle sizing

Particle size distribution was measured using a particle Mastersizer 3000 size analyzer (Malvern Panalytical, UK). A dry powder method was employed. Laser obscuration was controlled to a maximum of 5 %, and the feeding was set to a rate of 20 % for MCC and 35 % for ibuprofen, both at 1.5 bar. The height of the feeder was set to 2.5 cm. Measurements were taken for a period of 10 seconds, in triplicate.

4.3.2.1.1.3 Thermogravimetric analysis

Microcrystalline cellulose moisture content was quantified using thermogravimetric analysis (TGA) (TA Q500 TGA, TA instruments, USA). N_2 was used as the controlled atmosphere. Samples between 5 - 7 mg were loaded on the platinum pan. A ramp operation module was set up following a heating rate of 10 ^oC/min up to 270 ^oC. The weight loss measured was assumed to be moisture loss as no other thermal events occur in MCC between 0°C and 120°C as confirmed by differential scanning calorimetry (DSC).

4.3.2.1.1.4 Morphology

MCC morphology was characterized using a Malvern Morphologi G3® particle characterization system (Malvern Instruments, Malvern, UK). This instrument allows characterization of the shape, form and size of particles. A sample volume of 7 mm^3 was automatically dry dispersed by the Sample Dispersion Unit (SDU) which injects compressed air for 20 ms at 1 bar through the sample, onto a glass plate. A settling time of 60 seconds was held between the air injection and presentation of the sample for analysis. Malvern Morphologi G3® recorded individual pictures of particles and

these images were acquired over 3 circular areas of the plate. The size parameters analysed were circle equivalent (CE) diameter, length and width, and the shape parameter analysed was aspect ratio. CE diameter is the corresponding diameter of a circular particle with the same area as the particle analysed. Aspect ratio is given by dividing width by length for each particle. Particles with an aspect ratio below 0.5 were classified as needle shaped.

4.3.2.1.1.5 Scanning electron microscopy (SEM)

Scanning electron microscopy (SEM) was used to obtain images of Vivapur® and Emcocel®. A JSM-5510 SEM, (Jeol, UK) was used with heated tungsten. The morphology and particle size of the samples were measured using an electron beam source. The voltage was constant at 3 kV. Samples were gold coated in SEM gold coater (Jeol, UK) prior to analysis to prevent charging of the samples by the SEM electron beam. A coating time of approximately 45 seconds was used to deposit a thin layer onto the samples.

4.3.2.2 Blend preparation

Binary blends of ibuprofen and Vivapur®, and ibuprofen and Emcocel®, were prepared at concentrations between 2.5 and 40 % w/w ibuprofen in MCC. A total of 300 g of each formulation was blended in Cube Mixer KB, ERWEKA (Universal Gear UG, Germany) at 30 rpm for a duration of 30 min.

4.3.2.3 Blend characterization

4.3.2.3.1.1 Bulk and tapped densities

Bulk and tapped densities were calculated as outlined in the European Pharmacopoeia (Ph Eur 9.0) (Council of Europe, 2019). A 100 ml cylinder was filled up to the mark with powder of a known mass, and the bulk density (ρ_{bulk}) was calculated by dividing the mass of the powder by the volume of the cylinder. The loaded cylinder was then placed in an SVM 122/222 tapped density tester, (Erweka GmbH.). The cylinder was tapped 500 and 750 times which compacted the powder by removing air from voids within the sample. The tapped density (ρ_{tapped}) was calculated by dividing the powder mass by the final volume that the powder occupied in the graduated cylinder.

4.3.2.3.1.2 True and relative densities

The true density (ρ_{true}) of materials was measured using a helium pycnometer Accupyc 1330 microprocessor-controlled gas pycnometer (Micromeritics, USA). The jar volume was 11.2 cm^3 and weight of the samples was 2 g. The results presented are the average of ten measurements. The relative density of powder blends ($\rho_{relative}$) was calculated by dividing ρ_{bulk} from Powder Flow Tester by ρ_{true}.

4.3.2.3.1.3 Flowability and compressibility

Flowability was determined by the calculation of the Hausner ratio (HR) (Equation 4.1) using the tapped and bulk densities determined (Council of Europe, 2019).

$$HR = \frac{\rho_{tapped}}{\rho_{bulk}} \qquad \text{(Equation 4.1)}$$

Hausner ratio measures the loose and dense packing conditions to which the powder is subjected (Council of Europe, 2019, Santomaso et al., 2003).

Powder flowability classification was also determined using an annular shear cell tester, Powder Flow Tester (PFT), Brookfield Engineering Laboratories, Inc., USA. This methodology is considered to be a more consistent and reliable method to determine powder flow compared to the Hausner ratio. The Hausner ratio can be variable depending on the procedure employed (Liu et al., 2008; Santomaso et al., 2003; Yu et al., 2012). A vane lid was used in order to perform a standard flow function test. The cell volume of 43 cm^3 was chosen and the mass to fill up the cell varied from 14 to 16 g across the different formulations. The major principal consolidation stresses were defined in a geometric progression that resulted in values of between 0.02 to 6.07 KPa for MCC and 0.02 and 2.98 KPa for ibuprofen. The maximum principal consolidation stresses were chosen based on earlier literature (Liu et al., 2008; Yu et al., 2012).

Compressibility was determined for each blend using the same set up as the flowability test, however the consolidation stresses were approximately between 0.02 and 25.5 KPa and a flat lid was used. The results were expressed as bulk density vs. major principal consolidation stresses (McGlinchey, 2005).

4.3.2.4 Direct compression

The formulations were directly compacted to form cylindrical and flat tablets with 8 mm diameter and weight of 270 ± 10 mg in a ten-station rotary tablet press (Riva™ Piccola, Argentina), at a speed of 20 rpm. The relative air humidity was 50 ± 5%. The compaction of each blend was performed under 14 different compaction pressures, between approximately 20 and 400 MPa. After compaction the tablets were stored for 48 hours under ambient conditions before further analysis.

4.3.2.5 Tablet characterization

Tablets's hardness, weight, thickness and diameter were measured using a semi-automatic tablet testing system, SmartTest 50 (Sotax, Switzerland) (N=20 per blend). Tablet envelope density, (ρ_{tablet}) was obtained by dividing tablet weight by tablet volume. Tablet relative density, ρ, was calculated by dividing the tablet envelope density by the true density obtained from the annular shear cell tester for the respective powder formulation, according to Equation 1.23.

Tablet porosity was determined using Equation 4.2. Tablet envelope density was determined dividing the mass by the volume of each tablet. The blend true density values were previously determined.

$$Porosity = 100 \times \left[1 - \left(\frac{tablet\ envelope\ density}{blend\ true\ density}\right)\right] \qquad \text{(Equation 4.2)}$$

4.3.2.6 Heckel analysis

The Heckel model was used to calculate the constant K according to Equation 1.18. Then the yield pressure (P_{yield}) for each blend was obtained from $P_{yield} = 1/(3 \cdot K)$.

4.3.2.7 Percolation coefficient and percolation threshold

Tablet tensile strength was determined for all blends produced at each compaction pressures using Equation 1.21. Percolation coefficient (T_f) was modelled using Equation 1.27. The percolation threshold, ρ_c(AB), as a critical solid fraction, was then determined by the linear correlation between tablets relative density (ρ) and $\sigma_T^{\frac{1}{T_f}}$, expressed by Equations 1.28 and 1.29, for each blend. Finally, the dilution capacity model of Equation 1.31 was applied in order to express the $\rho_C(A)$ in terms of mass fraction (Xc). Substances A and B were MCC and ibuprofen, respectively.

4.3.2.8 Raman spectroscopy

Raman imaging was carried out using a RA802 Pharmaceutical Analyser (Renishaw, UK) using a 785 nm line-focussed laser. First, reference spectra of air stream dried MCC, spray dried MCC, and ibuprofen were acquired. Then, tablets of the blends of ibuprofen and MCC were screened using the StreamLineTM fast imaging method that acquired around 76,000 spectra over the entire surface of each tablet, with a pixel size of 10 µm/20 µm and area of 8.3 mm x 8.3 mm. Those spectra were averaged to a single resulting spectrum. The total time of measurement for each individual tablet was 15 min. Images of the drug distribution on the surface of the tablet were generated by non-negative least squares (NNLS) component analysis.

4.3.2.9 Multivariate analysis

PCA was performed to investigate whether this technique could distinguish the behaviour of the blends below and above the percolation threshold, and, also to determine if there are differences between blends containing Vivapur® compared to those containing Emcocel®. Principal component analysis (PCA) was performed using Origin data analysis and graphing software (OriginLab, USA). The algorithm used was the singular value decomposition with full cross validation for all the blends and for the placebos of both grades of MCC. Three replicates of each blend were input into the model. The first was the mean value of each predictor, the second is the mean minus its standard deviation and the third is the mean plus its standard deviation. The optimal number of components was three, which explained 95.51% of the variance in the total data input. The results were represented graphically by bi-plots i.e., scores and loadings plotted in one single graphic. The scores represent the distance of each sample from the mean of all samples along each PC, therefore, blends (scores) located in close proximity are similar. The loading plot explains which variables are responsible for grouping the samples by similarity, if the grouping occurs.

4.4 Results

4.4.1 Powder characterization

The particulate and bulk properties of both MCC grades and ibuprofen are summarised in Table 4.1. Particle size distribution determined using laser diffraction particle size analysis showed that Vivapur® had a slightly greater volume of particles

with a larger particle size in comparison to Emcocel® (Figure 4.1a) and hence a larger D_{50} value (Table 4.1). A second particle size analysis method, the Morphologi G3® which determines particle size distribution and shape using statistical image analysis, clearly showed that the Vivapur® sample contained a greater percentage of particles with a larger circle equivalent (CE) diameter in comparison to Emcocel® (Figure 4.1b).

Table 4.1. Particulate and bulk powder properties of Vivapur®, Emcocel®, and ibuprofen. Average values are shown ± standard deviation.

Property	Emcocel®	Vivapur®	Ibuprofen
D10 (µm) (n=5)	30.0 ± 0.25	31.1 ± 0.30	16.5 ± 0.08
D50 (µm) (n=5)	111.6 ± 0.73	118.0 ± 1.60	54.9 ± 0.21
D90 (µm) (n=5)	236.8 ± 1.55	240.0 ± 2.17	129.0 ± 1.09
Surface area (m^2/g) (n=3)	1.32 ± 0.01	1.37 ± 0.01	0.22 ± 0.02
True density (g/cm^3) (n=10)	1.58 ± 0.00	1.57± 0.00	1.12 ± 0.00
Bulk density (g/cm^3) (n=3)	0.33 ± 0.00	0.31 ± 0.00	0.36 ± 0.01
Relative density	0.21	0.20	0.32
Tapped density (g/cm^3) (n=3)	0.43 ± 0.01	0.40 ± 0.00	0.57± 0.01
Hausner Ratio	1.32 (easy flowing)	1.32 (easy flowing)	1.58 (cohesive)
Flow function coefficient (n=3)	7.0 ± 0.91 (easy flowing)	6.9 ± 0.00 (easy flowing)	3.9 ± 0.11 (cohesive)

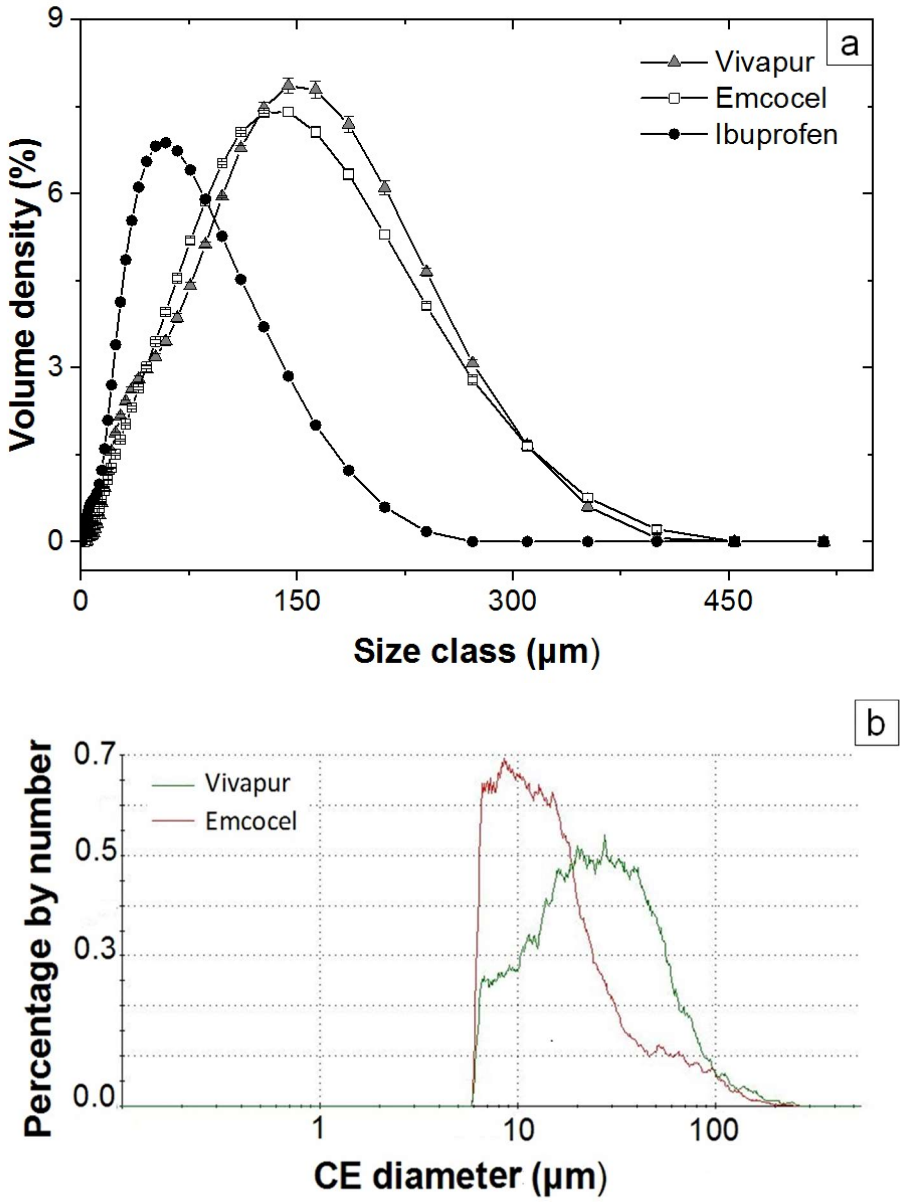

Figure 4.1. Particle size distribution of Emcocel® and Vivapur® samples measured by (a) Malvern Mastersizer 3000 and (b) Morphologi G3.

Despite containing larger particles, as shown by laser diffraction particle sizing and CE, Vivapur® sample was also determined to have a significantly higher surface area in comparison to Emcocel®. An inverse relationship between particle size and surface area was not observed as MCC has a highly porous structure, as observed in the SEM images (Figure 4.2). According to (Thoorens et al., 2014) approximately 90-95% of its surface is internal, therefore there is no relationship between particle size and

surface area. A pronounced difference in the morphology between the two grades of MCC was also observed when the aspect ratio was analysed by the Morphologi G3®. The percentage of needle shaped particles of Vivapur® sample was 51%, while for Emcocel® sample this value was 34%. The model drug, ibuprofen, showed dissimilar properties to microcrystalline cellulose samples, exhibiting a smaller particle size distribution and surface area (Table 4.1, Figure 4.1a).

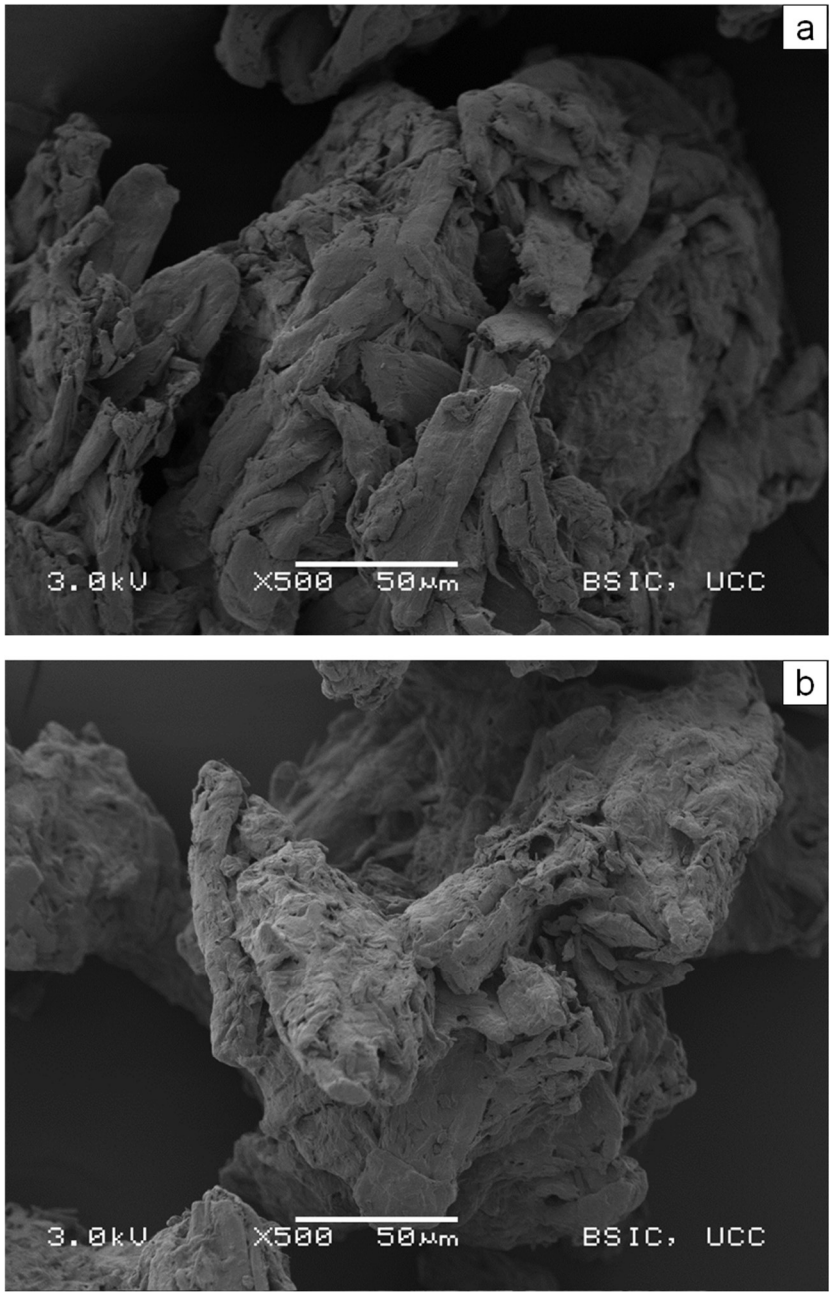

Figure 4.2. SEM images of (a) Vivapur® and (b) Emcocel®.

The true, bulk, tapped and relative densities of both MCC samples were similar (Table 4.1). Figure 4.3a shows that both MCC samples displayed similar powder compressibility with increase in consolidating stress. In comparison to MCC, the relative density and compressibility of ibuprofen was greater. Compressibility as a function of tapped and bulk density confirmed the findings. Both MCC grades exhibited good flowability, as expressed by Hausner ratio and flow function coefficient (Table 4.1). Ibuprofen was classified as cohesive when expressed by Hausner ratio and by flow function coefficient (Carr, 1965; Thomas and Schubert, 1979). Ibuprofen/MCC blends were characterized in terms of density, flow and compressibility properties (Table 4.2, Figure 4.3b, 4.3c). It was observed that an increase in drug content resulted in increased bulk and relative density and poorer flow properties, as indicated by the blend Hausner ratio and powder flowability classification.

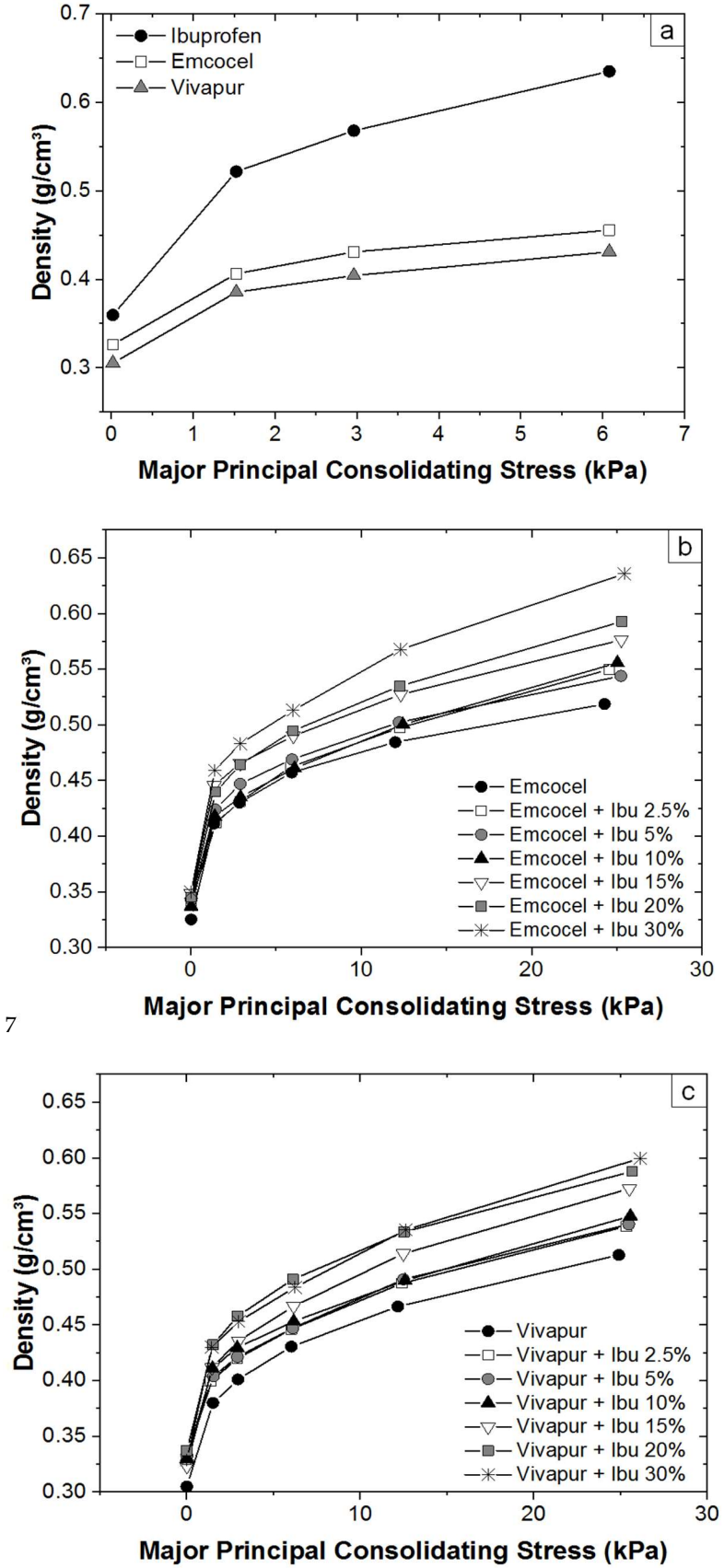

7

Figure 4.3. Plot of bulk density of (a) ibuprofen, Emcocel® and Vivapur®, blends of (b) Emcocel®, and blends of (c) Vivapur ® under increasing consolidating stresses.

4.4.2 Blend behaviour during tableting

Ibuprofen/MCC blends with ibuprofen content between 0 % and 30 % w/w were compacted and tensile strength calculated with respect to compaction pressure. Formulations containing 40% w/w ibuprofen/MCC could not be tabletted due to poor flow from the hopper and incomplete filling of dies. Tabletability profiles (Figure 4.4) showed that both microcrystalline cellulose grades formed tablets with high tensile strength, even at low compaction pressures. As ibuprofen concentration was increased, a drop in tablet tensile strength was observed.

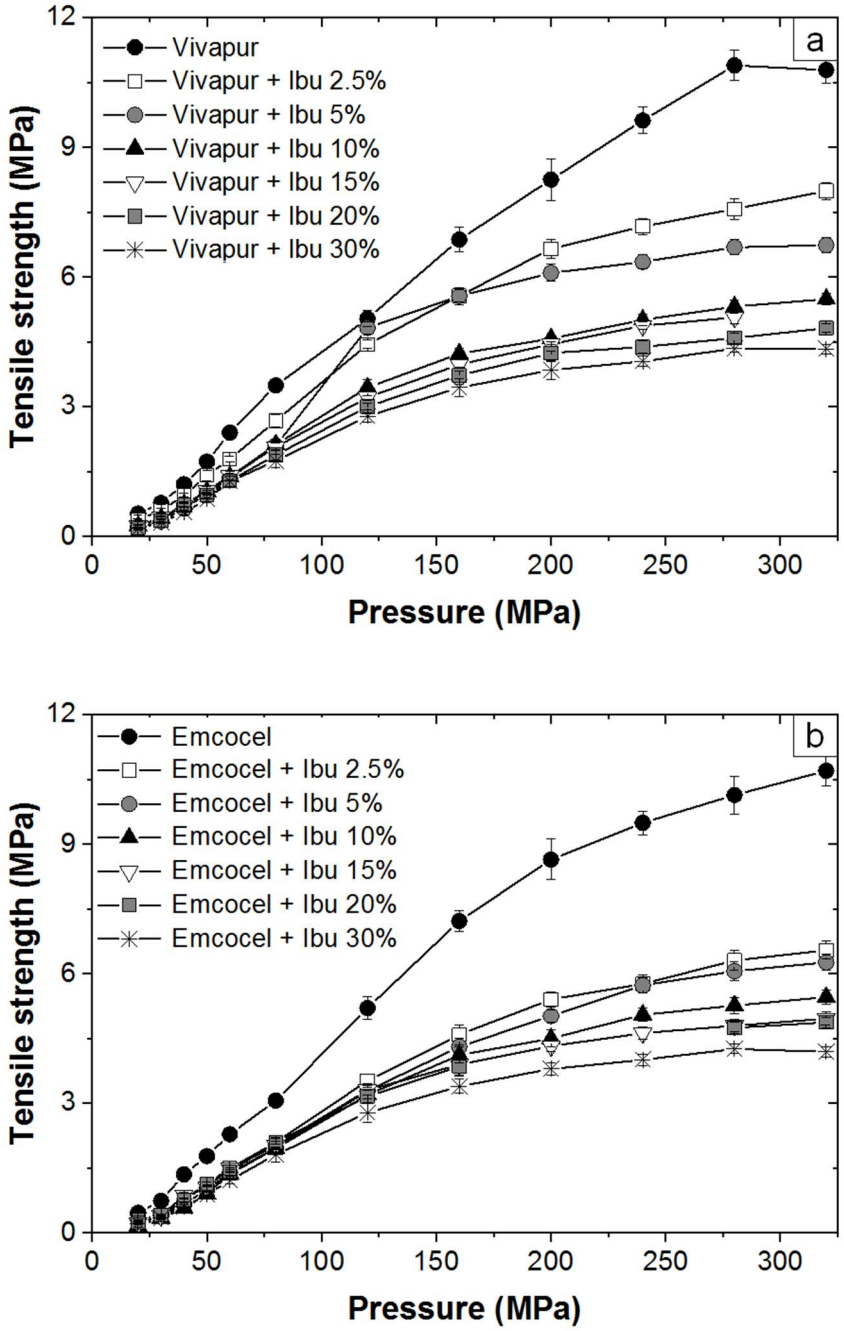

Figure 4.4. Tabletability profiles of ibuprofen/MCC blends (a) Vivapur® and (b) Emcocel®. N=20, y-error bars indicate standard deviation.

Tablet weight variability, expressed as % relative standard deviation (%RSD), increased for blends with 20 % w/w ibuprofen and above (Figure 4.5). Increase in weight variability was attributed to a deterioration in blend flow and this behaviour is in agreement with blend flow behaviour measured for these blends (Table 4.2).

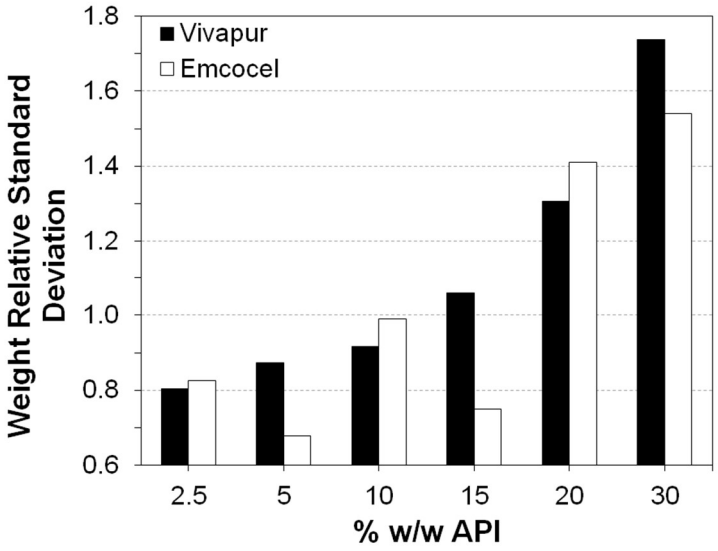

Figure 4.5. Tablet weight variation expressed as percent relative standard deviation (%RSD) (n=280 individual tablet weights).

Table 4.2. Blend density, compressibility, and flow properties.

Emcocel®						
Ibuprofen (% w/w)	Bulk density (g/cm^3)	Tapped density (g/cm^3)	True density (g/cm^3)	Relative density (g/cm^3)	Hausner Ratio	Flow character
2.5	0.34	0.43	1.52	0.22	1.26	Easy flowing
5	0.34	0.45	1.51	0.23	1.30	Easy flowing
10	0.34	0.44	1.49	0.23	1.28	Easy flowing
15	0.35	0.46	1.47	0.24	1.32	Easy flowing
20	0.35	0.47	1.45	0.24	1.36	Cohesive
30	0.35	0.49	1.38	0.25	1.39	Cohesive
Vivapur®						
Ibuprofen (% w/w)	Bulk density (g/cm^3)	Tapped density (g/cm^3)	True density (g/cm^3)	Relative density (g/cm^3)	Hausner Ratio	Flow character
2.5	0.33	0.42	1.53	0.22	1.27	Easy flowing
5	0.33	0.43	1.52	0.22	1.30	Easy flowing
10	0.33	0.43	1.48	0.22	1.30	Easy flowing
15	0.32	0.44	1.47	0.22	1.34	Easy flowing
20	0.34	0.46	1.45	0.23	1.36	Cohesive
30	0.33	0.46	1.40	0.24	1.40	Cohesive

4.4.3 Percolation threshold modelling

Compaction pressures between 20 MPa to 60 MPa were selected to model percolation as the rearrangement of the particles inside the die, the phenomenon of interest, occurs at lower pressures. The modified Heckel model proposed by (Kuentz and Leuenberger, 1999) was applied for each ibuprofen/MCC blend and the respective percolation coefficient calculated (Table 4.3). No significant difference was observed between the percolation coefficients determined for blends prepared from Vivapur® and Emcocel® (t-value = 0.78, p-value of 0.449, p-value > 0.05). Therefore, the global mean of the individual percolation coefficients was calculated (T_f =3.5 ± 0.2) and used to determine the percolation threshold.

Table 4.3. Percolation coefficient (T_f) values calculated for each Ibuprofen/MCC blend. r refers to Pearson's correlation coefficient.

Ibuprofen	**Vivapur®**		**Emcocel®**	
(% w/w)	T_f	r	T_f	r
0%	2.96	0.997	3.23	0.996
2.5%	3.23	0.996	3.29	0.979
5%	3.57	0.994	3.81	0.995
10%	3.52	0.996	3.80	0.996
15%	3.51	0.996	3.67	0.998
20%	3.62	0.997	3.66	0.995
30%	3.70	0.997	3.41	0.998

The linear correlation of Equation 1.28 is shown in Figure 4.6. The percolation threshold, ρc (AB), was determined for each blend according to Equations 1.28 and

1.29, using the empirical coefficient of 3.5 (Figure 4.7, Table 4.4). The minimum relative density required to produce tablets with significant strength, $\rho_C(B)$, and solid fraction $\rho_C(A)$ related to the dilution capacity of substance A (MCC) were calculated by fitting the mass fraction of MCC.

Table 4.4. Critical solid fraction, ρc (ab), for each blend with increase in Ibuprofen concentration. r refers to Pearson's correlation coefficient.

MCC	**Emcocel®**		**Vivapur®**	
mass fraction	ρc (AB)	r	ρc (AB)	r
1.000	0.156	1.000	0.169	1.000
0.975	0.208	1.000	0.224	1.000
0.950	0.211	1.000	0.233	1.000
0.900	0.234	1.000	0.270	1.000
0.850	0.247	1.000	0.292	1.000
0.800	0.271	1.000	0.276	0.999
0.700	0.318	1.000	0.351	1.000

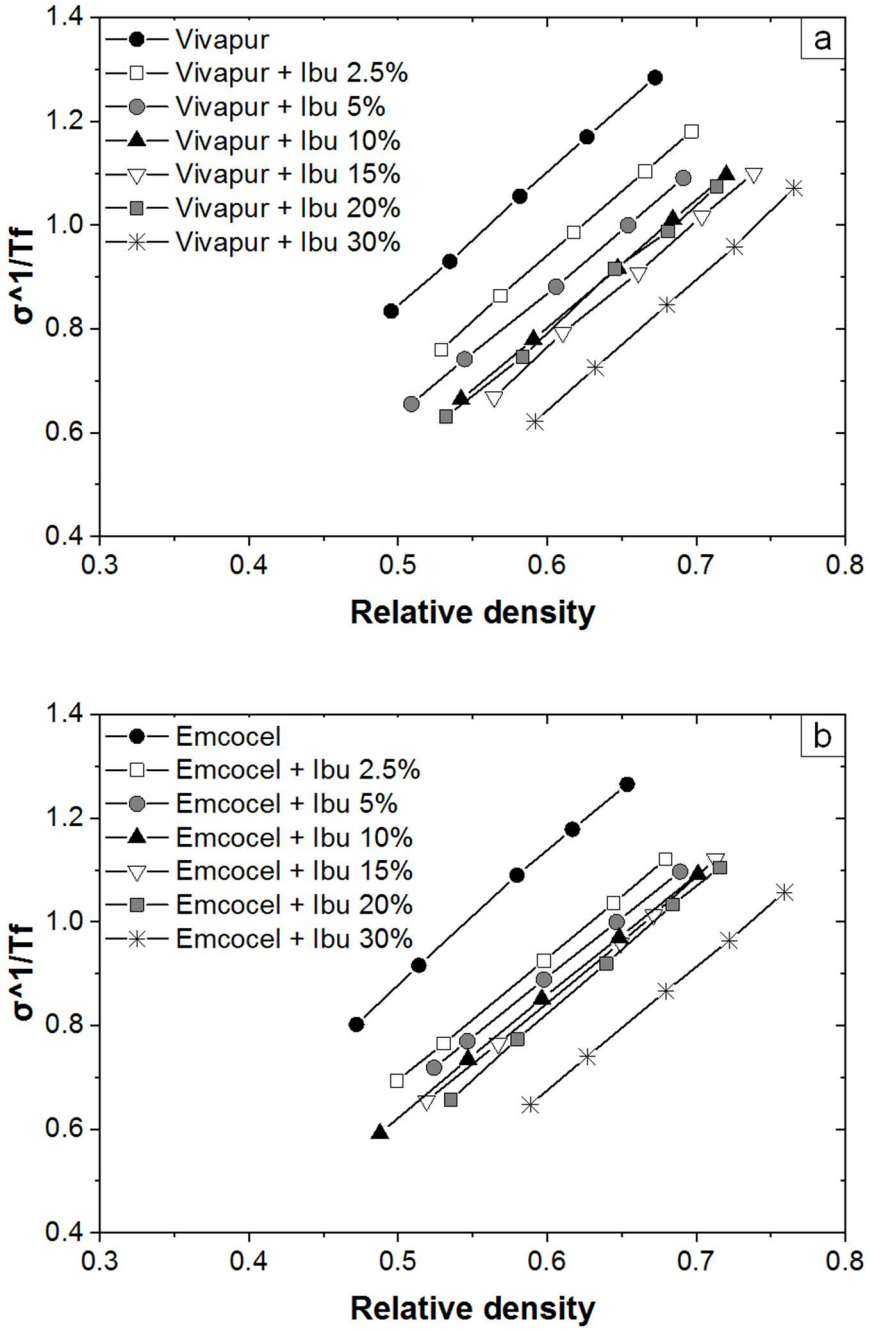

Figure 4.6. Linear correlation between tablets relative density (ρ) and ${\sigma_T}^{T_f}$, as represented by Equation 1.27.

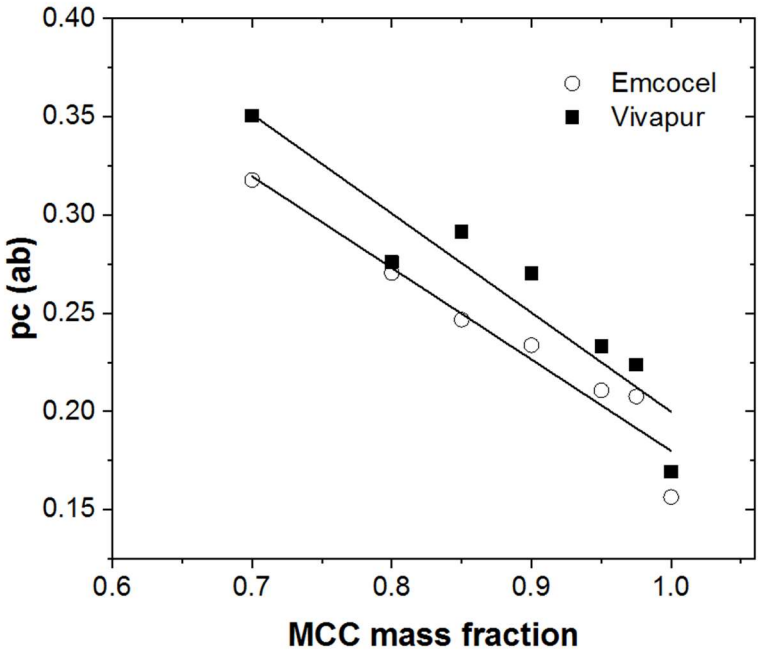

Figure 4.7. Relationship between blends percolation threshold, pc (AB), and microcrystalline cellulose mass fraction, as represented by Equation 1.30.

Table 4.5 lists the value of $\rho_C(B)$ expressed by the threshold relative density where there is a change in tensile strength behaviour. The values of $\rho_C(B)$ were 0.646 and 0.704 for blends of Emcocel® and of Vivapur®, respectively. Plots of tensile strength vs. relative density of all blends were investigated and confirmed the existence of the change in tablet strength behaviour at the predicted relative density of approx. 0.70. This behaviour is shown for selected blends in Figure 4.8.

Table 4.5. Comparison between theoretical (Kuentz and Leuenberger, 1998) and empirical percolation and mass fraction parameters modelled. r refers to Pearson's correlation coefficient.

	Emcocel®		**Vivapur®**	
Percolation coefficient	3.5 (empirical)	2.7 (theoretical)	3.5 (empirical)	2.7 (theoretical)
pc(A)	0.180	0.267	0.200	0.288
pc(B)	0.646	0.698	0.704	0.736
r	-0.970	-0.970	-0.938	-0.934
% critical mass fraction	17.76	23.54	19.08	24.68

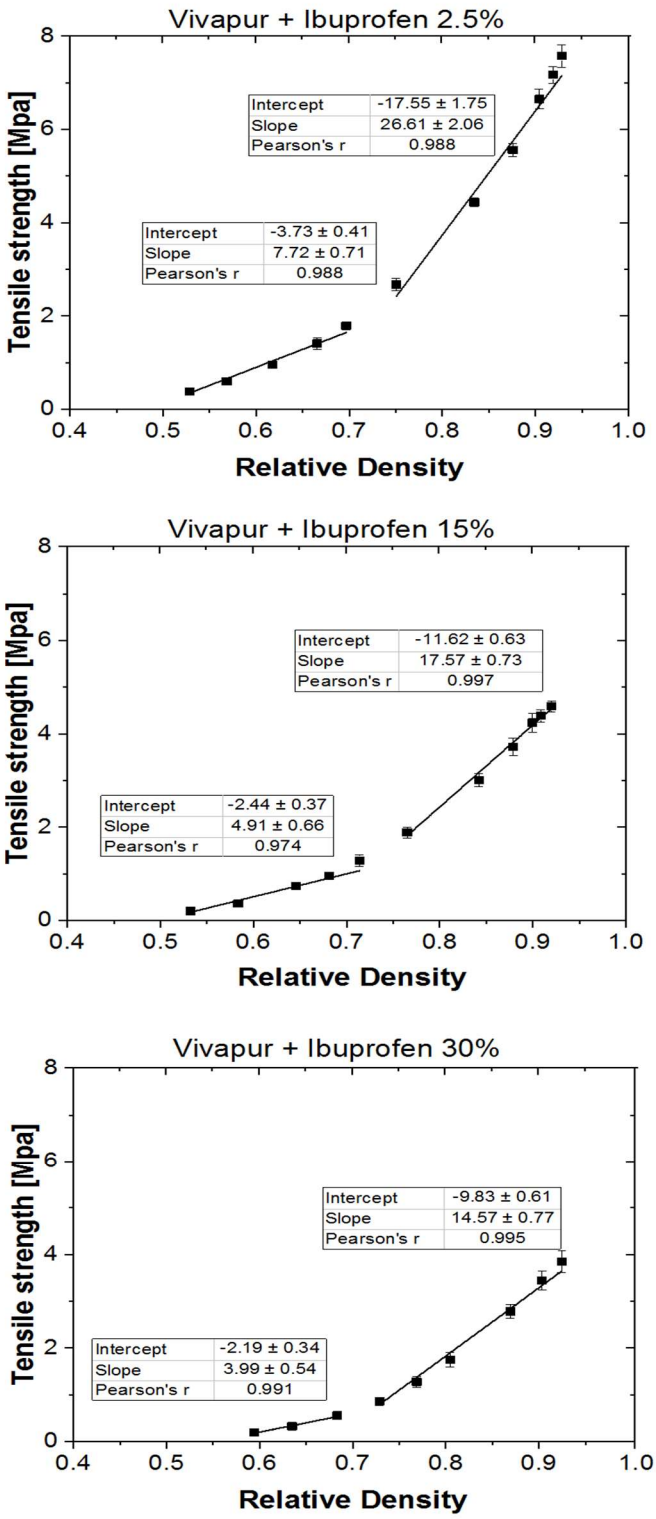

Figure 4.8. Tensile strength of Vivapur®/ibuprofen blends at different relative densities. A change in tensile strength behaviour was predicted to occur in the point of intersection of two linear fits, for each blend.

Finally, the critical mass fraction (Xc) was calculated from $\rho_C(A)$ using Equation 1.31. The Xc values obtained for Emcocel® and Vivapur® were 17.76 % w/w and 19.08 % w/w ibuprofen, respectively. The percolation thresholds and the critical mass fractions were also calculated by applying a theoretical value of percolation coefficient previously published ($T_f = 2.7$) (Guyon et al., 1987) to the Equation 1.27. This theoretical percolation coefficient was proposed for binary mixtures in which one of the substances compacts well and the second is poorly compactable, which would apply to the ibuprofen/MCC blends. A comparison of percolation threshold values obtained using the empirical value and theoretical value is reported in Table 4.5.

4.4.4 Properties behaviour above and below the thresholds

Raman imaging showed how ibuprofen and MCC particles were distributed at the surface of the tablets (Figure 4.9). At drug concentrations below 15 % w/w drug the drug was distributed within a MC matrix. Significant sized clusters were observed at the concentration of 15 % w/w. However, they do not form a complete pathway able to link the entire surface of the tablet. At 20 % w/w a phase transition was noticed. As predicted by the percolation threshold model, there was an infinite cluster of ibuprofen particles at the surface at drug concentrations of 20 % w/w ibuprofen. The properties of the blend are majority ruled by material that forms an infinite cluster i.e., by the ibuprofen above the threshold and by MCC below the threshold.

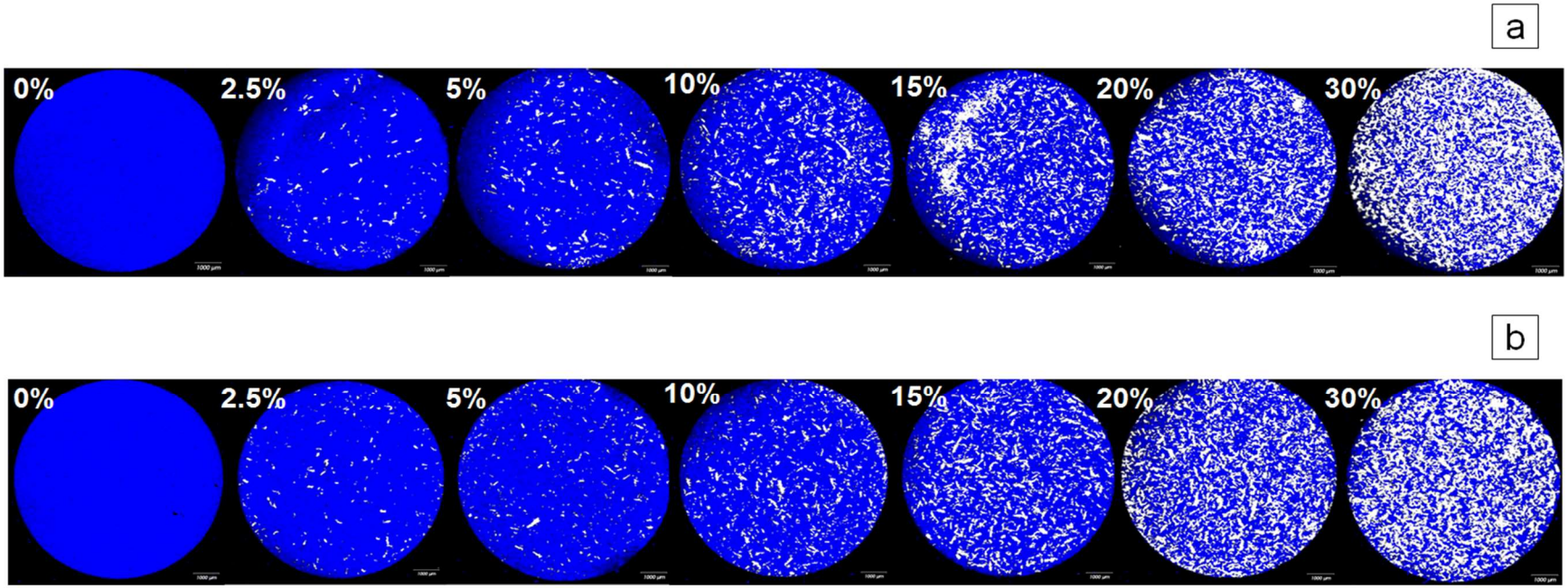

Figure 4.9. Raman imaging of (a) Emcocel® and ibuprofen and (b) Vivapur® and ibuprofen blends. The areas in blue correspond to the excipient particles while the areas in white to API particles. The percentage express the % w/w of ibuprofen in the blend with MCC.

PCA summarised the experimental data collected during the development of the model, classified the samples into different groups, and identified the variables responsible for the variance between the samples. Initially the data was grouped into three groups (*i*) Microcrystalline cellulose, which comprises the placebo samples, (*ii*) Blends Above Threshold (concentrations of > 20 % w/w API), and (*iii*) Blends Below Threshold (concentrations of < 20 % w/w API). In Figure 4.10a, scores of blends above the percolation threshold showed negative correlation to tensile strength (TS) loadings for all the pressures, therefore, above the threshold lower strength tablets were observed. In contrast, Hausner ratio (HR) and compressibility (ΔBD) showed a positive correlation to blends above the threshold, which means high compressibility and poor flowability. These relationships in compressibility and flowability highlighted by PCA, was also noted by univariate analysis of data (Table 4.2). Low porosity (Po) at different compaction pressures and true density (TRD) showed to be highly correlated with Blends Above Threshold, which highlights that tensile strength was not improved with the reduction of porosity for the blends studied. The confidence interval of the groups Blends Below Threshold and Blends Above Threshold overlapped. This showed that PCA was not able to precisely predict a threshold drug concentration. Placebo samples showed a clear clustering represented by the group Microcrystalline cellulose. The separation of the placebo from the blends was explained mainly by the higher tensile strength and lower values of tapped (TAD), bulk (BD) and relative (RD) densities.

Figure 4.10b shows the second data grouping, which provides an overview of the differences between blends prepared with Vivapur® and blends prepared with

Emcocel®. PC-3 differentiated these blends, to some degree (Figure 4.10b). There is an overlap between the groups for a selection of samples with < 10% ibuprofen loading and interestingly blends with different grades of MCC separate from one another at higher drug loadings. This is surprising and may highlight that despite both MCC grades exhibiting similar properties, at high drug loadings their interaction with the drug differs in the blend resulting in small differences in density parameters. Overall, Emcocel® blends had slightly higher porosity and tensile strength. They also showed slightly higher tapped, relative and bulk densities, and were less compressible than those containing Vivapur®.

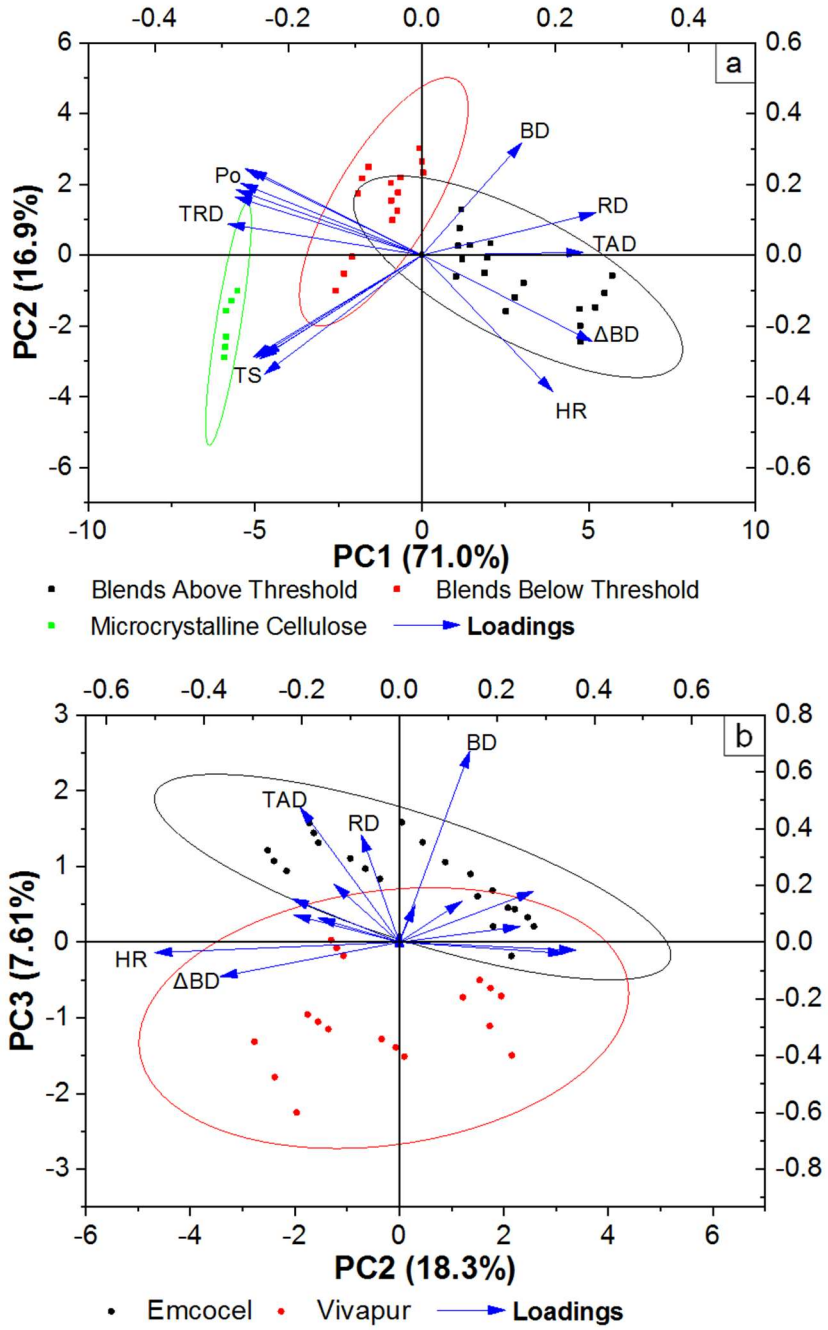

Figure 4.10. Principle component Bi-plot (scores and loadings) for (a) PC-1 vs. PC-2 and (b) PC-2 vs. PC-3, eigenvalues of 11.36, 2.71, and 1.17 for PC-1, PC-2, and PC-3, respectively. The ellipses around each group represents a 95% confidence interval. The squares represent the scores while the arrows represent the loadings.

4.5 Discussion

The percolation coefficient value determined in this study ($T_f = 3.5$) was higher than the theoretical coefficient ($T_f = 2.7$) published by (Guyon et al., 1987). According to (Busignies et al., 2007), the percolation coefficient is dependent on the excipient and does not present a universal character. Thus, a difference between theoretical and empirical percolation coefficients was expected to occur. Other empirical strength percolation coefficients available in the literature are $T_f = 3.2$ for paracetamol and MCC (Avicel PH101) (Kuentz and Leuenberger, 2000), $T_f = 2.1$ for Lactose, $T_f = 3.8$ microcrystalline cellulose, and magnesium stearate (Busignies et al., 2007), $T_f = 4.6$ for lactose powder, and $T_f = 6.6$ for lactose granules (Leuenberger and Ineichen, 1997), and , T_f= 3.89 for colloidal silica (Ehrburger and Lahaye, 1989). The percolation threshold coefficient has not been published for ibuprofen/MCC blends. Moreover, it was observed that other coefficients reported in the literature follow the same trend of being slightly greater than the theoretical coefficient.

In this study the percolation coefficient was modelled from compaction pressure and tensile strength, which can be easily measured. Also, the coefficient calculated could be generalised for both grades of MCC, as there was no statistically significant difference between the values calculated. This shows that the coefficient model is robust, and the resulting value did not vary for blends of the same substances, even though there may exist morphological differences (particle size and shape).

The percolation threshold determined for the binary blends with Vivapur® 102 and Emcocel® 90 differed marginally, with values of 0.1884 and 0.1718, respectively. Percolation theory explains that the threshold is a range of values close to the

modelled percolation threshold, but it is not possible to determine how close (Kuentz and Leuenberger, 2000). Therefore, the slight difference in p_c between different MCC grades may be negligible. The critical mass fraction calculated using the theoretical coefficient resulted in higher values, 23.54 % w/w and 24.68 % w/w for blends of Emcocel® and of Vivapur®, respectively. However, the flow behavior and Raman imaging showed experimentally that the threshold happens between 15 % and 20 % w/w ibuprofen. The Raman technique used gave information on the drug distribution on the tablet surface. In future studies it would be useful to consider techniques such as 3D tomographic technologies e.g., X-ray Computational Tomography or a 3D Raman model to confirm whether the infinite cluster observed on the surface extended throughout the structure. Overall, ideally, the coefficient should be calculated for each powder blend, rather than considered as a theoretical universal value.

Blends below the critical mass fraction (≤ 15 % w/w) showed good powder flowability, which is characteristic of microcrystalline cellulose. On the other hand, blends above the critical mass fraction (≥ 20 % w/w) presented cohesive character, as the ibuprofen powder. Raman images were used to investigate ibuprofen domains in the tablets and showed for the first time ever, the visualization of the phase transition predicted for tablets using the percolation threshold model. For the blends analysed, this phase transition was observed between the mass concentrations of 15-20 % w/w, because an infinite cluster consisting of ibuprofen domains connected to each other was observed at the concentration of 20 % w/w.

When the critical concentration has been estimated graphically (Kimura et al., 2007; Mohamed et al., 2015; Pérez Gago and Kleinebudde, 2017), it was a retrospective methodology and had to be modelled for data from more complex analysis e.g., dissolution. This more complex analysis would also include failure systems (above the threshold) that would need to be carried out unnecessarily. Due to advances in data processing software packages since the earlier paper (Kuentz and Leuenberger, 2000) it is no longer challenging to model the percolation threshold mathematically. The advantage of modelling the percolation threshold mathematically is that this is a predictive tool. Flowability behaviour and tablet tensile strength could be predicted in this study based on a simple model that was only dependent on compaction pressure, tensile strength, and relative density. The other numerous characterization techniques used in this study had the aim to prove the values modelled and investigate differences between the two different grades of MCC; they are not necessary for the percolation threshold model. Therefore, the percolation threshold model shown in this study represents a simplified mathematical predictive tool that can easily be applied for different formulations.

Principal Component Analysis was not able to identify a clear threshold level with increasing drug loading. However, PCA was able to summarize all the data collected and aided in clarifying differences between the blends according to the drug loading, and differences between the blends containing Vivapur® and the blends containing Emcocel®. Low porosity strongly and negatively correlated to blends with high drug loading which confirms that the porous regions present in the MCC placebo matrix were occupied by particles of ibuprofen as drug was introduced. The explained

variance of PC-3 (7.61 %) showed that the PCA model only captured a small difference between Vivapur® and Emcocel® blends. The most expressive differences between these two groups along PC-3 were bulk, tapped, and relative densities, which are related to the morphological differences between both grades of MCC, captured in the SEM and Morphologi G3® analysis.

4.6 Conclusions

In this study a percolation coefficient for an ibuprofen/MCC combination was successfully modelled and the value obtained ($T_f = 3.5$) was consistent with earlier reported values for similar drug/excipient combinations. Dilution capacities of 19.08 % w/w and 17.76 % w/w ibuprofen were calculated for both Vivapur® and Emcocel® blends, respectively. A change in blend behaviour above the threshold value was confirmed by experimental flow data. Also, Raman imaging confirmed the presence of infinite clusters of drug particles on the tablet surface above the threshold value. The minor differences in physical properties between MCC grades did not result in significantly different dilution capacities. PCA of the data was not able to identify a clear threshold level with increasing drug loading. The modelling approach used in this study can be applied to early formulation development studies to identify optimal drug loading for robust pharmaceutical blend processing.

Chapter 5 - Application of percolation threshold to disintegration and dissolution of ibuprofen tablets with different microcrystalline cellulose grades

Revised from publication in: *International Journal of Pharmaceutics* (2020)

https://doi.org/10.1016/j.ijpharm.2020.119838

5.1 Abstract

The study presented was conducted to determine whether a percolation threshold value, determined in Chater 4 for ibuprofen/ microcrystalline cellulose (MCC) blends using percolation theory and compression data (Queiroz et al., 2019), could also be observed during tablet disintegration and dissolution. The influence of MCC grade (air stream dried versus spray dried) on tablet disintegration and dissolution was also investigated. Complementary to conventional disintegration and dissolution testing, Raman imaging determined drug distribution within tablets, and in-line particle video microscopy (PVM) and focused-beam reflectance measurement (FBRM) monitored tablet disintegration. Tablets were prepared containing 0 to 30% w/w ibuprofen. Raman imaging confirmed the percolation threshold by quantifying the number and equivalent circular diameters of ibuprofen domains on tablet surfaces. Across the percolation threshold a step change in dissolution behaviour occurred, and tablets containing air stream dried MCC showed slower disintegration rates compared to tablets containing spray dried MCC. Dissolution measurements confirmed experimentally a percolation threshold in agreement with that determined using percolation theory and compression data. An increase in drug domains, due to cluster formation, and less efficient tablet disintegration contributed to slower ibuprofen dissolution above the percolation threshold. Slower dissolution was measured for tablets containing air stream dried compared to spray dried MCC.

5.2 Introduction

Disintegration and dissolution behaviours are critical quality attributes assessed to evaluate drug release performance (Dressman and Krämer, 2005; Huang et al., 2011; Nickerson et al., 2018). Disintegration is often the rate determining step for drug release, particularly for poorly water soluble drugs (Caramella et al., 1988). Disintegration is the mechanical fragmentation of the compressed tablet into small granules or agglomerates. Disintegration is initiated by liquid penetration in the porous of the compact. Swelling is one of the most accepted disintegration mechanisms, which is characterized by an enlargement of the particles that builds up pressure to fragment the tablet matrix (Markl and Zeitler, 2017). The bonding mechanism during compression and the bonding surface area have a direct impact on tablet disintegration. Swelling depends on an optimal tablet porosity, such that the liquid can enter the tablet matrix, however, the void spaces are too large to suppress the swelling action of disintegrants (Desai et al., 2016).

The application of modelling approaches to enhance product knowledge has been motivated by quality guidelines as an alternative to iterative testing approaches during formulation development (International Council for Harmonisation, 2012, 2008, 2005a, 2005b; Kimura et al., 2013). The percolation threshold model has been used to explain how particle-particle interactions of drug and diluents alters dissolution performance of formulations containing different drug loadings (Bonny and Leuenberger, 1993, 1991, Kimura et al., 2007, 2013; Stillhart et al., 2017; Wenzel et al., 2017).

Previous studies determined the percolation threshold value from disintegration and dissolution experimental data (Kimura et al., 2007; Stillhart et al., 2017; Wenzel et al., 2017). These studies experimentally determined critical loadings at which disintegration times undergo a step change. These were then assumed to be the percolation thresholds. However, Kimura, Betz and Leuenberger, 2007 recommended further studies to investigate if the change in disintegration behaviour was linked to the formation of the infinite cluster described by the percolation threshold theory (Kimura et al., 2007). Since these earlier studies, technological advancements have provided novel techniques to study drug distribution in tablets and tablet disintegration behaviour. These techniques can be key to providing data to support the percolation threshold concepts and the findings of previous studies.

Spectral imaging techniques have been used to provide in-depth information related to drug distribution in pharmaceutical tablets. These techniques can be used to investigate the cluster formation predicted by the percolation theory. Fourier transform infrared spectroscopy (ATR-FTIR), X-ray diffraction (XRD), and Raman spectroscopy are the main techniques employed (Chan et al., 2005; Kazarian and Ewing, 2013; Miller and Havrilla, 2005; Zhang et al., 2005). Among those, advancements in Raman instruments has enabled the technique to rapidly map drug distribution in tablets. Raman imaging instruments have been designed to capture rich spectroscopic data which can be translated to provide high-resolution chemical information for tablets (as low as 1 µm per pixel) and require short acquisition times (approx. 15 min for a tablet of 13 mm diameter) (Ali et al., 2013).

Focused Beam Reflectance Method (FBRM) and in-line Particle Video Microscopy (PVM) are innovative techniques that can give real-time in-situ information regarding disintegration and dissolution performance of tablets. FBRM has been used to monitor the rate and the degree of change in the number of particles and particle structures in a process (Barrett et al., 2011; Gregory, 2009; Simon et al., 2019; Zhong et al., 2020). Measurement of the solid particles using FBRM is performed without the need for sampling and performing off-line analysis. The system gives particle count, dimension and shape information in real time by monitoring changes in the system as they occur (Barrett and Glennon, 1999). PVM provides real-time images of the system allowing the user to visually track changes in the solids over time (Barrett and Glennon, 2002). Alternatively, automatic algorithms of image analysis can be coupled to it. The imaging window measures an area of approximately 800 µm by 1100 µm. PVM also records a Relative Backscatter Index (RBI) trend which can be used to track changes in the shape and size of solid particles as well as changes in the solids concentration (Werner et al., 2017). RBI is comparable to turbidity monitoring. Increased RBI indicates a larger amount of solids (Hartwig and Hass, 2018). As tablet disintegration progresses the number of particles in the slurry increase as larger particles fragment. Therefore, as disintegration proceeds, more particles are captured in the image and the RBI increases.

FBRM and PVM techniques are commonly used in crystallization studies (mass transfer from solution to solid phase) (Barrett et al., 2011; Hartwig and Hass, 2018; Jiang et al., 2014; Liu et al., 2011; Mitchell et al., 2011; Simon et al., 2019; Simone et al., 2015). FBRM has also been utilized in previous studies for investigating tablet

disintegration and dissolution (Coutant et al., 2010; Han et al., 2009; Menning, 2016; Metzler et al., 2017). PVM has the potential to monitor tablet disintegration and dissolution because changes in particle size and shape in suspension are key features observed during tablet disintegration and dissolution.

The aim of this study was to investigate if a step change in disintegration and dissolution behaviour was observed for tablets produced with drug loadings below and above a predetermined percolation threshold. The percolation threshold of these systems was determined in an earlier study using the physical principles of blending and compaction (Queiroz et al., 2019). The model system investigated was tablets produced from binary blends of microcrystalline cellulose (MCC) and ibuprofen (IBU) at a range of ibuprofen mass loadings. Tablets were prepared with two different MCC grades; one spray dried and one air stream dried. The percolation threshold values determined were 19.08% w/w and 17.76% w/w IBU for blends with air stream dried MCC and spray dried MCC, respectively (Queiroz et al., 2019). A secondary study aim was to determine if the grade of MCC altered any changes in disintegration and dissolution behaviour observed.

In the context of the previous and the present study, percolation threshold is a geometric phase transition in which the concentration of ibuprofen particles is high enough to form a cluster that spans throughout the entire volume of the tablet. When this ibuprofen particle cluster is formed, it is anticipated that a step change in properties of the blend will occur. For example, a reduction in flow, compaction and dissolution would be anticipated with ibuprofen particle cluster formation, as ibuprofen has poor flowability and compressibility properties compared to MCC (Al-

Karawi et al., 2018; Liu et al., 2008), and is considerably more hydrophobic (Kawabata et al., 2011).

In addition to traditional pharmacopeial disintegration and dissolution techniques, process analytical technologies (FBRM and PVM) were employed to better understand tablet disintegration behaviour, and hence its influence on drug dissolution. Building on the application of Raman imaging to qualitatively identify clusters of ibuprofen particles (Queiroz et al., 2019), the present study demonstrated how Raman spectroscopy can be used to quantitatively determine the size and the number of ibuprofen clusters formed on tablets surfaces and hence confirm the percolation threshold determined from compaction data. The MCC grades studied, have similar specifications; average particle size of 130 µm determined by laser diffraction, and similar bulk density (0.28–0.33 g/mL for the air stream dried and 0.25–0.37 g/mL for the spray dried). Queiroz et al. confirmed similarities in particle size distribution between grades by dry powder, laser diffraction analysis. Particle analysis employing an image analysis technique, identified morphological differences between MCC grades: the air stream dried grade contained a greater number of particles with needle shaped geometry, while the spray dried grade contained a greater number of spherical-shaped particles (Queiroz et al., 2019).

5.3 Materials

Emcocel®90 (spray dried) and Vivapur®102 (air stream dried) were supplied by JRS Pharma (Weissenborn, Germany) and ibuprofen by Kemprotec (Cumbria, UK). The two MCC products studied were medium size standard grades with theoretical bulk density of 0.28 - 0.33 g/mL for the air stream dried and 0.25 – 0.37 g/mL for the spray

dried MCC. A range of particulate and bulk powder properties of the batches of ibuprofen, air stream dried MCC and spray dried MCC used in this study had been previously determined in Chapter 4 (Table 4.1). Other materials used such as buffer components and HPLC mobile phase were all supplied by Sigma Aldrich, Ireland.

5.4 Methods

5.4.1 Tablet manufacture and characterization

Binary blends of MCC and IBU were prepared containing a range of IBU concentrations: 2.5, 5, 7.5, 10, 12.5, 15, 20, and 30 % w/w. Each blend, total weight 300 g, was prepared using a cube mixer KB 15 (Erweka, Heusenstamm, Germany) at 30 rpm for a duration of 30 min. Tablets were prepared according to section 4.2.2.4. However, the tablet hardness was controlled to 120 ± 10 N, tablet weight variation to 270 ± 10 mg, the room air humidity to 50 ± 5 % and temperature to 19 ± 2 °C. The tablets were characterized according to the methods described in section 4.2.2.5.

5.4.2 Raman imaging analysis of tablet surface

Tablets had theirs Raman imaging acquired and then cut in horizontal and vertical layers. Raman imaging analysis of those segments were also performed. Drug and excipient distributions on external surfaces and surfaces of internal sections of tablets were investigated by Raman imaging analysis using a RA802 Pharmaceutical analyser (Renishaw, New Mills, UK) as described in section 4.2.2.8. Domains of each substance were determined based on the reference spectra acquired for the pure substances. Domains of each substance in the generated images were analysed using Particle Analysis in Renishaw's WiRE software. This software resolves the image

domains and determines particle metrics. The numbers of domains of ibuprofen on the entire surface of each tablet and their average equivalent circle diameters were determined.

Raman imaging also gives an averaged spectrum of the surface of the tablet. The spectra of the tablets were used to build a PCA. Unscrambler X (Camo Analytics, Oslo, Norway) was used to perform the PCA with full cross validation, using the algorithm Singular Value Decomposition (SVN).

5.4.3 Disintegration analysis

In vitro disintegration time was determined in water at 37 °C ± 2 °C, using a tablet disintegration tester ZT42 (Erweka, Edison, USA) which complies with Ph. Eur. 2.9.1 (Disintegration of tablets and capsules) (Council of Europe, 2019). Each tablet was placed inside of one basket which were continuously and automatically agitated vertically in the disintegration medium. The disintegration process was observed until the tablets disintegrated into small enough particles that could escape the basket so that no substantial material remained in the basket. Analysis was performed in triplicate.

5.4.4 FBRM and PVM analysis

FBRM (FBRM G600) and PVM (PVM V19) (Mettler Toledo, Leicester, England) were used to monitor tablet disintegration using a Mettler Toledo Easymax^{TM} 102 system. The disintegration medium was phosphate buffer (pH 7.2). The system used consisted of 100 mL glass vessels with automated internal temperature and agitation control. System specific PTFE (polytetrafluoroethylene) lids allowed for integration

of the FBRM and PVM probes. A visual check of the system was possible through an inspection window at the front of the system.

The working volume of the system was 50 mL. Experiments were performed at 37 °C and the agitation rate was 250 rpm using an upward pumping, pitch blade impeller for 30 minutes after the tablet was added to the vessel. The powder or tablet was added to the glass vessel under agitation. PVM and FBRM monitoring was performed throughout the duration of the experiment; FBRM data was recorded every 2 seconds and two PVM images were recorded every second.

5.4.5 Dissolution studies

The dissolution studies were carried out using a DT 600 dissolution tester of Ph. Eur. 2.9.3 (paddle) (Erweka, Edison, USA). A volume of 500 mL of phosphate buffer pH 7.2 equilibrated at 37 ˚C was used as the dissolution medium and the paddle rotation was kept at 50 rpm. Solubility of ibuprofen in the given conditions is 3.74 mg/ml (Dabbagh and Taghipour, 2007). The experiment was conducted using sink conditions; the theoretical concentration of Ibuprofen in the dissolution medium following complete dissolution of 30 % w/w ibuprofen tablets was 0.16 mg/ml. Following addition of the tablet sample to the dissolution medium, samples of 0.5 ml volume were withdrawn at 1, 5, 15, 30, 60 and 120, 180, and 240 min intervals in order to determine the dissolution profiles. An additional sample was taken at the 24 h time point to determine the total amount of drug in each tablet tested. At the 24 h time point the tablet had completely disintegrated and complete IBU dissolution was assumed.

All samples were filtered using 0.45 µm filter and 0.5 mL of fresh, pre-warmed medium was immediately added to the system in order to correct the volume to the sample volume withdrawn. Samples were analysed by HPLC. The % cumulative amount IBU released was calculated and plotted against time.

HPLC analysis was performed using an Agilent 1200 series HPLC system with an UV/Vis detector (Agilent Technologies, Santa Clara, USA). A reversed-phase column (Gemini C-18, 250 × 4 mm x 5 µm, Phenomenex Ltd. UK), mobile phase of acetonitrile and water (60:40, pH adjusted to 2.5) at a flow rate of 1.5 ml/min and injection volume of 20 µL were employed. The wavelength for Ibuprofen detection was set at 215 nm and retention time was 7 min.

5.5 Results

5.5.1 Tablet Characterisation

The average content of ibuprofen was determined for all tablets analysed and compared to the theoretical content (Table 5.1). Greatest variance between actual and theoretical content was measured for the 30 % w/w ibuprofen loading. Drug content uniformity was also determined with the percentage relative standard deviation less than 7 % for all drug loading. Tablet porosity was also determined (Table 5.1) as it can influence tablet disintegration and dissolution (Ibrahim, 1985; Yassin et al., 2015). Porosity of tablets decreased as ibuprofen content increased. The porosity of tablets containing spray dried MCC was slightly greater than tablets containing the air stream dried MCC at all drug loadings except for 15%.

Table 5.1. Tablet ibuprofen theoretical and average actual content ± % relative standard deviation (n=5), blend true density and tablet porosity. * Values obtained from Table 4.2.

Theoretical drug concentration (% w/w)	Theoretical drug content (mg)	**Air stream dried MCC**					**Spray dried MCC**				
		Actual drug content (mg)			Porosity (%)	True density* (g/cm^3)	Actual drug content (mg)			Porosity (%)	True density* (g/cm^3)
2.5 %	6.75	6.63	±	2.60 %	30.3	1.53	6.82	±	1.57 %	32.3	1.52
5 %	13.50	13.40	±	2.21 %	30.9	1.52	13.17	±	2.79 %	31.1	1.51
10 %	27.00	27.33	±	2.81 %	28.5	1.48	27.06	±	1.38 %	29.7	1.49
15 %	40.50	41.68	±	1.78 %	28.6	1.47	41.94	±	5.02 %	28.5	1.47
20 %	54.00	54.13	±	4.26 %	26.1	1.45	55.04	±	2.01 %	28.4	1.45
30 %	81.00	78.33	±	6.77 %	23.1	1.40	85.34	±	2.00 %	24.10	1.38

5.5.2 Raman imaging analysis of tablet surface

Raman spectroscopy did not show differences between the characteristic bands of the MCC tablets (air stream dried and spray dried MCC only), indicating similar chemical identity of microcrystalline cellulose between grades. In respect to the ibuprofen loading, spectral peaks related to ibuprofen increased in intensity when ibuprofen loading was increased (Figure 5.1).

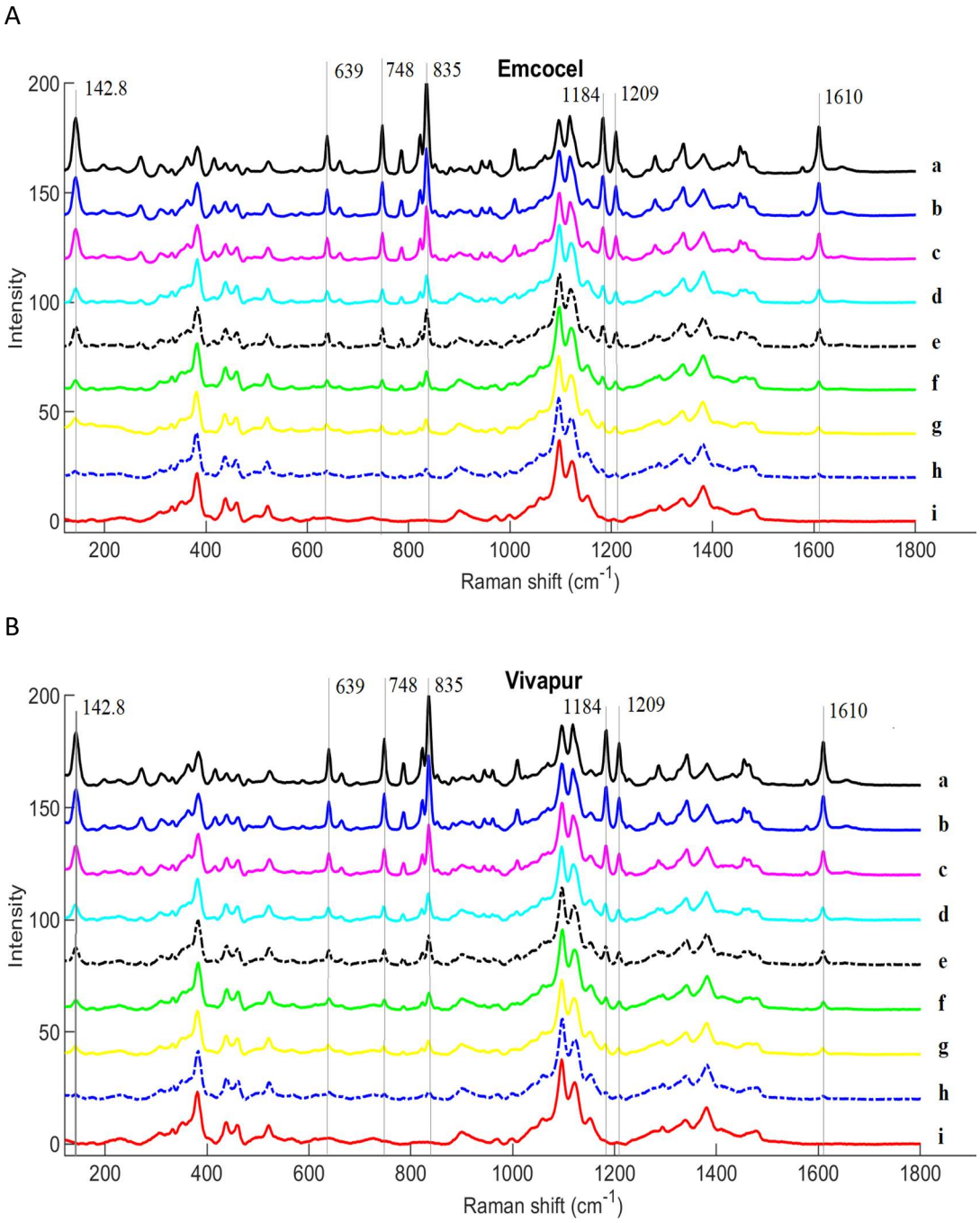

Figure 5.1. Average Raman spectra of the surface of (A) Spray dried MCC (Emcocel®) and (B) Air stream dried MCC (Vivapur®) tablets containing a range of ibuprofen loadings: (a) 30 %, (b) 20 %, (c) 15 %, (d) 12.5 %, (e) 10 %, (f) 7.5 %, (g) 5 %, (h) 2.5 %, and (i) 0 % ibuprofen w/w. Vertical lines indicate characteristic peaks of ibuprofen.

Raman images for tablets of all drug loadings were shown in Figure 4.9. In this study the number of ibuprofen domains on surfaces of each tablet was determined from these Raman images, as described in section 3.2. The number of ibuprofen domains

decreases for the tablets with drug loading above 15 % w/w (Table 5.2), despite an increase in the overall intensity peaks related to ibuprofen (Figure 5.1). Above the percolation threshold the domains of ibuprofen start to connect to the neighbouring ibuprofen domains. Thus, one single domain with larger area is counted, instead of numerous smaller neighbouring domains. In the case of the compacted tablets, it results in a change in the drug distribution from dispersion of drug particles in a matrix of MCC (large number of small drug domains) to distribution of MCC in a matrix of drug (smaller number of larger drug domains). The resulting larger domains were characterized by continuously increased equivalent circular diameter of ibuprofen domains with a more pronounced increase between the concentrations of 15% and 20% w/w ibuprofen (Table 5.2). These results build on the results in the earlier study which qualitatively confirmed the percolation threshold values determined by visual appearance, which can be subjective. In this study the quantitative data obtained related to the number and size of ibuprofen domains provides a less subjective confirmation of the percolation threshold value.

Table 5.2. The number of ibuprofen domains (N) and the equivalent circular diameter (ECD) of ibuprofen domains on the surface of Air stream dried MCC and Spray dried MCC tablets containing a range of ibuprofen loadings (2.5 to 30% w/w ibuprofen). The number of domains and the equivalent circular diameter values were determined from images generated using Raman image analysis.

% w/w Ibuprofen	**Air stream dried MCC**		**Spray dried MCC tablets**	
	N	ECD of ibuprofen domains (µm)	N	ECD of ibuprofen domains (µm)
2.5 %	158	69.2	130	62.0
5 %	264	70.4	218	59.6
7.5%	264	76.7	343	74.4
10 %	462	79.5	475	71.8
12.5%	377	74.3	469	77.1
15 %	513	90.5	483	88.6
20 %	377	103.5	376	103.4
30 %	112	153.7	72	138.9

PCA of Raman spectra of the surface of tablets showed that the first principal component (PC-1) captured the effect of drug loading i.e., what blend behaviours change as the drug loading increases, while the second principal component (PC-2) captured variability within the samples due to both MCC grade and due to ibuprofen drug loading. The scores plot showed samples that are similar or different from each other i.e., samples geometrically located at distance are dissimilar to each other while neighbouring samples are similar (Figure 5.2a). PC-1 and PC-2 explained 88% and 7% of the variance captured by the model, respectively. Raman shifts of 93, 142.8, 639, 748, 835, 1184, 1209, and 1610 cm^{-1} were the variables that mostly contributed to discriminating the samples along the first component of the model

(PC-1) (Figure 5.2b). Those bands are characteristic of ibuprofen (Sütő et al., 2016) and they were not observed in the spectra of the tablets containing pure MCC (Figure 5.1). As stated previously, these peak heights increased with the increase in drug loading. The PCA model showed that tablets containing air stream dried MCC differed from tablets containing spray dried MCC along PC-2. Loadings of PC-2 contained peaks assigned to both ibuprofen and MCC. PC-2 also showed a general upwards shifting of the baseline with reduction in Raman shift. Both chemical and physical attributes of the tablets may explain this variability in Raman spectra. Differences in tablet porosity was observed with increase in drug loading and between MCC grades (Table 5.1). Raman spectra can show stronger intensities for more compacted (less porous) samples due to an increased number of scattering molecules that will produce a Raman signal (Gómez et al., 2019). The upwards shift may also be due to Raman fluorescence, which is a material-dependent phenomenon; fluorescence is phenomena intrinsic to MCC. Microcrystalline cellulose is known to be fluorescent mainly due to the presence of lignin (Castellan et al., 2007). Variance related to ibuprofen peaks (e.g., at the shifts 835 and 1610 cm^{-1}) and the main characteristic Raman bands assigned to cellulose (e.g., at 1096 cm^{-1} and within the region 275-550 cm^{-1}) (Wiley and Atalla, 1987) are also present in the loadings of PC-2. The region of 275-550 cm^{-1} is known to hold crystallinity information of cellulosic materials (Agarwal et al., 2010). Thus, the separation of the samples along PC-2 may be an indication that the differences between the spray dried and the air stream dried MCC grades included crystallinity, lignin content, and compact density. The spectral comparison between the air stream and the spray dried samples is available in Figure 5.3.

A

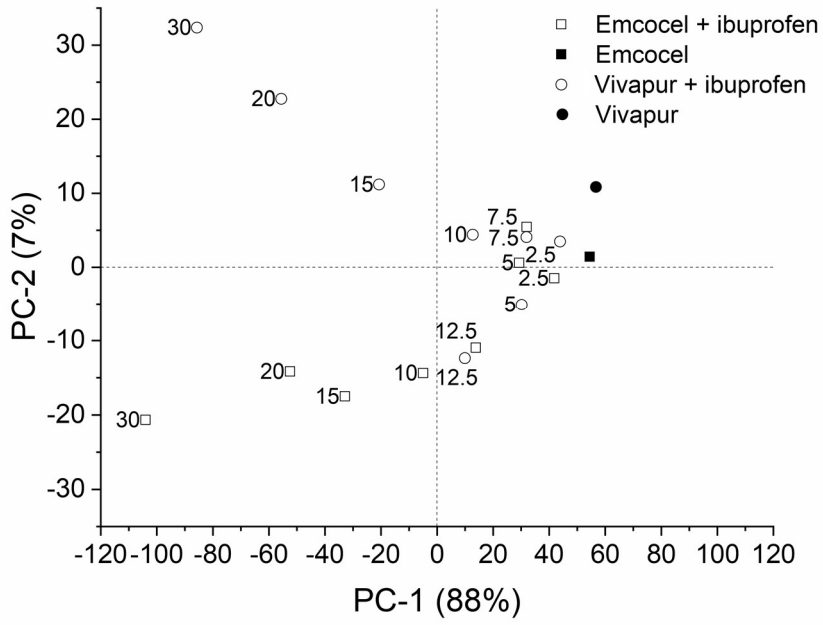

B

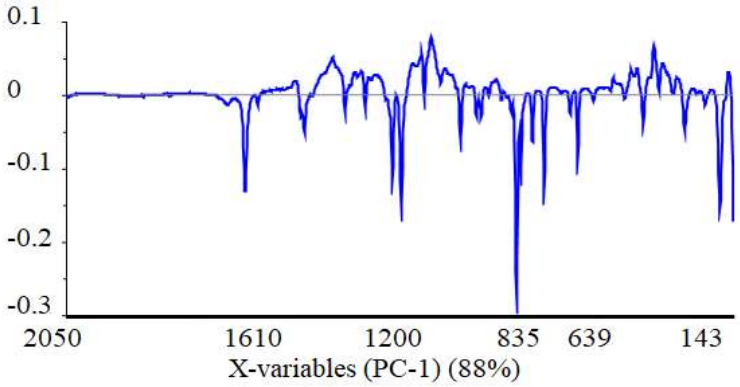

C

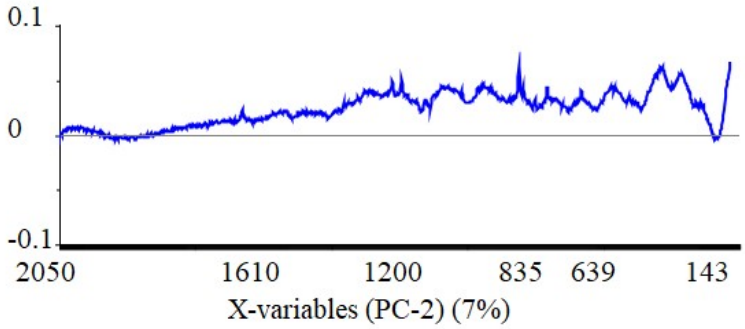

Figure 5.2 (A) Scores plot and (B and C) loading plots of the principal component analysis of Raman spectra acquired from Spray dried MCC (Emcocel®) and Air stream dried MCC (Vivapur®) tablets and tablets containing a range of ibuprofen loadings (2.5 % to 30 % w/w ibuprofen). PC-1 and PC-2 are the first and the second principal components, respectively.

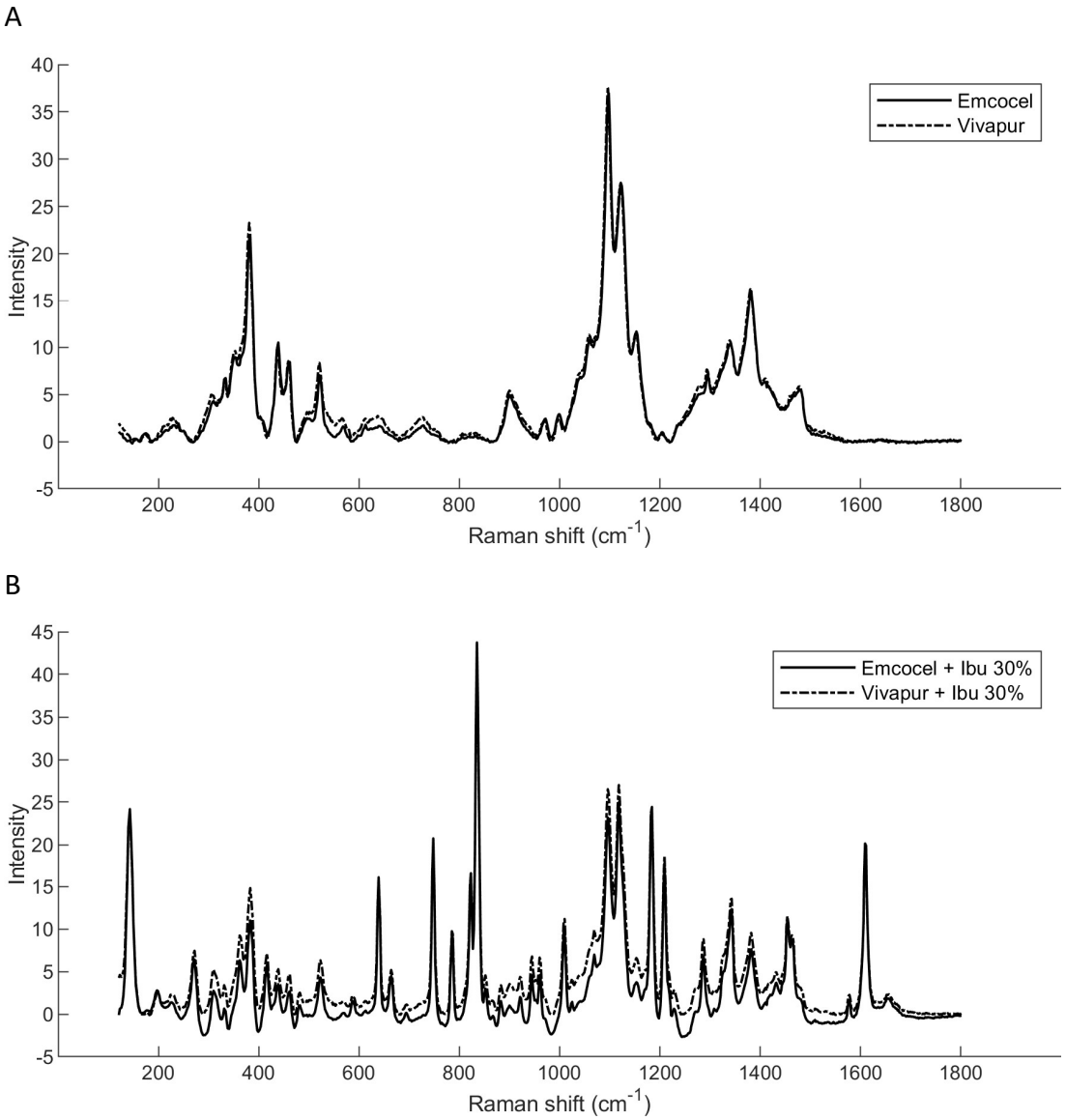

Figure 5.3.Raman spectra of compacts (A) of spray dried microcrystalline cellulose (Emcocel®), and air stream dried microcrystalline cellulose (Vivapur®), and (B) of tablets containing 30 %w/w ibuprofen/microcrystalline cellulose.

5.5.3 Disintegration and dissolution studies

Tablet disintegration using Ph. Eur. 2.9.1 disintegration apparatus showed that all tablets had completely disintegrated in less than 5 min. Differences between tablets containing different drug loadings or MCC grades could not be accurately determined by the Ph. Eur. 2.9.1 apparatus. The tablets investigated contain a high percentage in

mass of MCC, which is highly hygroscopic and a noted disintegrant (Rowe et al., 2009). Thus, disintegration happened fast independently of the MCC grade.

The results of the Ph. Eur. 2.9.3 dissolution study showed that increased ibuprofen concentration had a negative impact on the dissolution behaviour of Ibuprofen/MCC tablets (Figure 5.4). The effect of ibuprofen loading on drug dissolution was evident for ibuprofen concentrations above the percolation threshold, 20 and 30% w/w of ibuprofen; time to achieve 100% ibuprofen release increased significantly (Figure 5.5). Tablets containing the air stream dried MCC required statistically significantly longer durations to achieve 100% ibuprofen release for all drug loadings, in comparison to tablets containing the spray dried MCC. Tablets containing 30% w/w IBU and air stream dried MCC did not reach 100% release in 240 min. Complete release was confirmed after 24h. It is also interesting to note that an increase in time to reach 100% cumulative ibuprofen release was observed between 2.5 and 5% drug loading (air stream dried MCC) and 2.5 and 7.5% drug loading (spray dried MCC) (Figure 5.5). This change in dissolution behaviour was not related to a percolation threshold of ibuprofen in the MCC matrix but may have resulted due to other factors such as differences in porosity and particulate bonding disintegration behaviour (Desai et al., 2016) and hence dissolution.

A

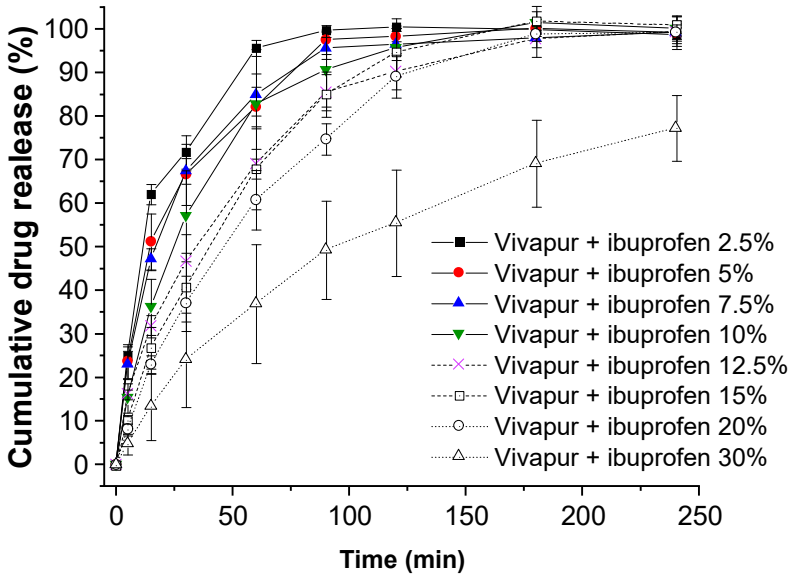

B

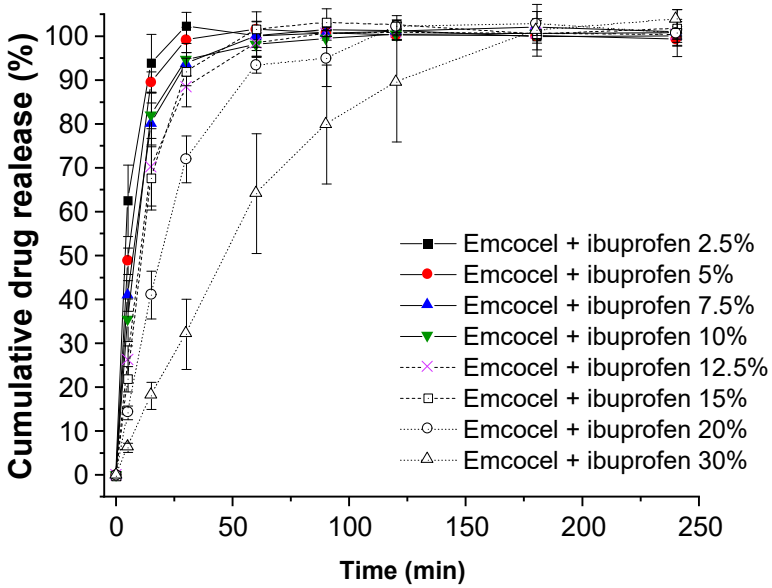

Figure 5.4 Dissolution profiles of tablets containing (A) Air stream dried MCC (Vivapur®) and (B) Spray dried MCC (Emcocel®) and different ibuprofen w/w loadings (2.5 to 30% w/w). Dissolution was performed in phosphate buffer pH 7.2 at 37ºC. Average values shown with y-error bars indicating standard deviation, n= 5.

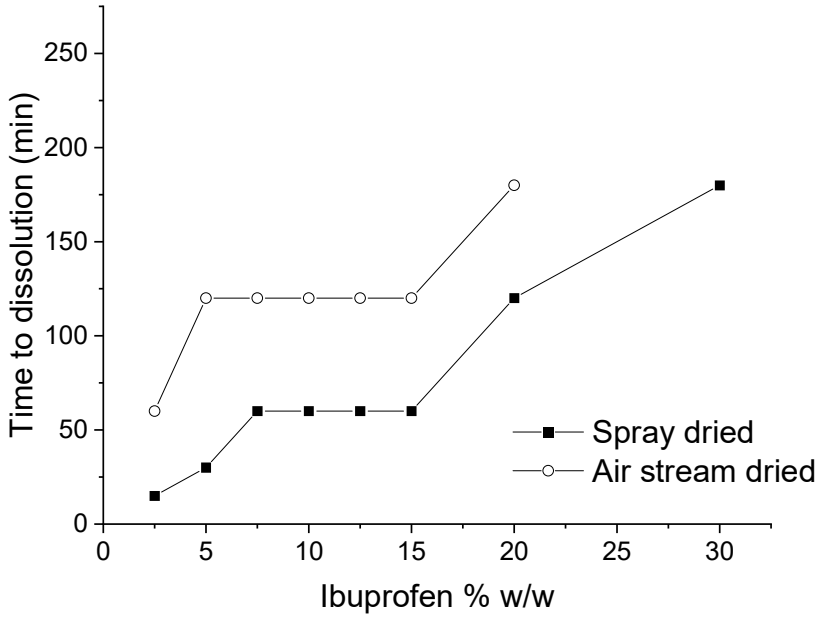

Figure 5.5 Time to reach 100% ibuprofen release during dissolution of tablets containing Spray dried and Air stream dried MCC and different ibuprofen w/w loadings (2.5 to 30% w/w). Tablets containing air stream dried MCC and 30% w/w of ibuprofen did not reach 100% release in 240 min. However, the complete release was confirmed after 24h. Dissolution was performed in phosphate buffer pH 7.2 at 37^{o}C. Average values shown with y-error bars indicating standard deviation, n= 5.

5.5.4 FBRM monitoring

FBRM was used as a PAT tool to determine if tablet disintegration played a role in the differences observed between dissolution of tablets containing air stream dried and spray dried MCC grades with increasing drug loading. Two aspects were investigated: the differences among tablets below and above the percolation threshold and the differences between both MCC grades. This analysis was complementary to the pharmacopoeial disintegration test which was not able to capture differences regarding these two aspects. As mentioned previously, FBRM gives particle count, dimension information in real-time (Barrett and Glennon, 1999). It was hoped that the ibuprofen clusters observed in the tablets by Raman imaging could be observed in the disintegration medium and potentially explain the differences in dissolution

observed between tablets containing spray dried and air stream dried MCC grades at different drug loadings.

Initially, disintegration monitored by FBRM was performed using spray dried and air stream dried MCC tablets without ibuprofen to determine differences in disintegration due to MCC grade. Both tablets displayed very similar behaviour with a sharp increase in particle counts upon addition of the tablet to the phosphate buffer pH 7.2. Figure 5.6 shows that the counts vs time profile for the two MCC grades were very similar, indicating that the tablets disintegrated at the same rate.

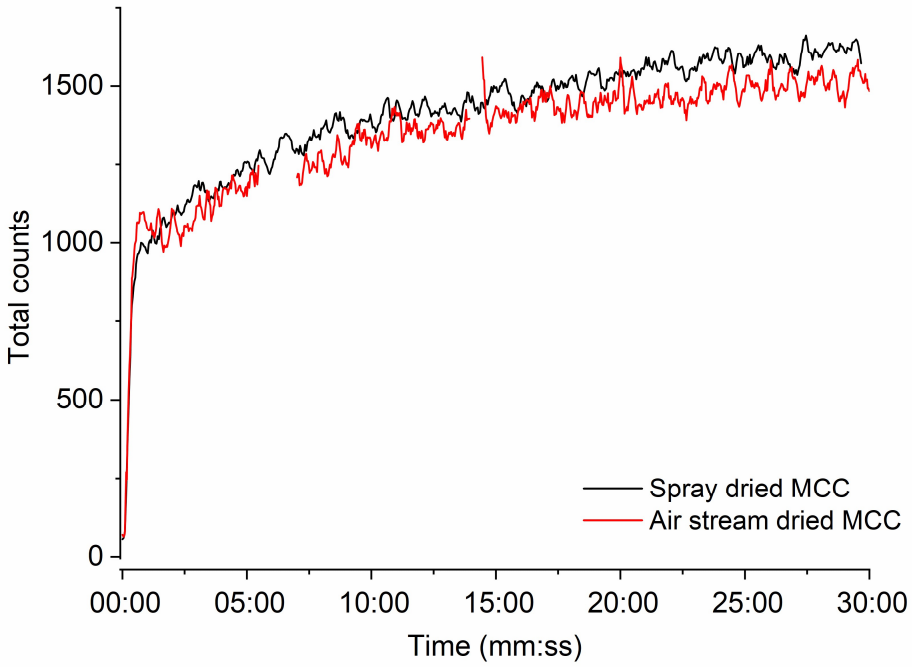

Figure 5.6. Focused Beam Reflectance Measurement (FBRM) counts 1-1000 µm versus time for tablets containing air stream dried and spray dried MCC in phosphate buffer pH 7.2, and temperature of 37 °C.

Figure 5.7 shows the FBRM total counts vs time for ibuprofen tablets added to the disintegration medium for the first 30 minutes. All tablets show a rapid increase in counts for the first 5 minutes approximately, indicating that, as with the tablets of air stream dried and spray dried MCC without ibuprofen, tablet disintegration began

immediately upon addition of the tablet to the medium for all ibuprofen loadings. A similar profile is seen for each tablet of spray dried MCC regardless of ibuprofen loading. The counts increased sharply in the first 30 seconds after addition to the medium and then continued to increase at a slower rate for the following minutes. Overall, air stream dried MCC tablets showed a less consistent total counts versus time profile for different drug loadings in comparison to spray dried MCC tablets. When the different ibuprofen loadings were compared, the loadings of 20 % and 30 % w/w ibuprofen showed reduced total counts profiles compared to lower drug loadings. The total counts profiles for tablets containing air stream dried MCC was also lower in comparison to tablets containing spray dried MCC, for all ibuprofen loadings (Figure 5.8). These differences were more pronounced above the percolation threshold > 15% ibuprofen.

A

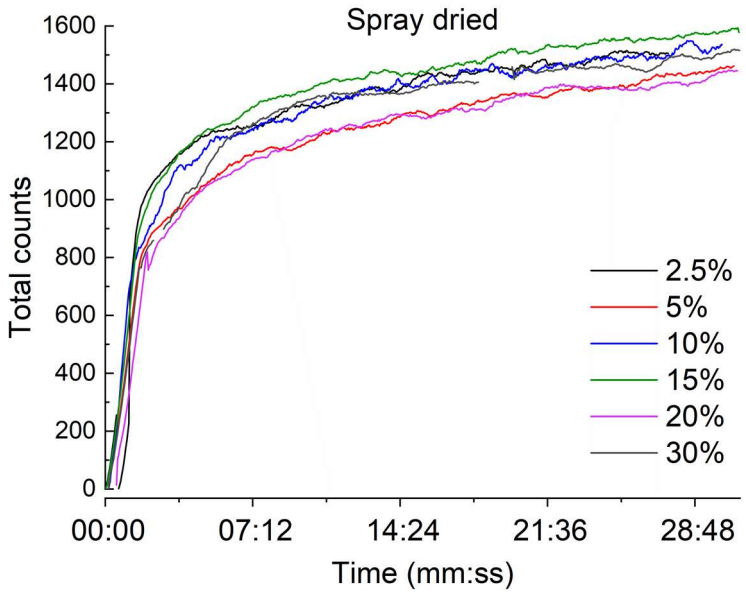

B

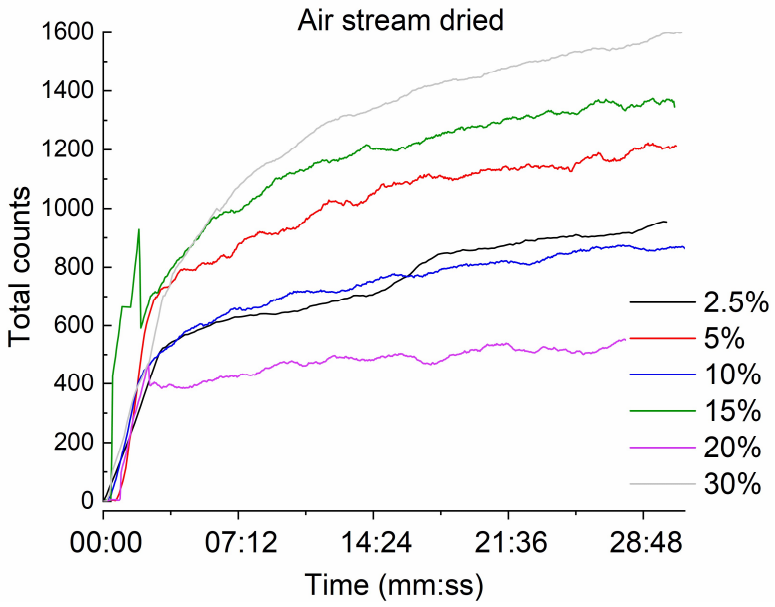

Figure 5.7. Focused Beam Reflectance Measurement (FBRM) total particle counts (counts 1-1000 µm) versus time for tablet containing (A) Spray dried MCC and (C) Air stream dried MCC and different ibuprofen w/w loadings (2.5 to 30% w/w) in phosphate buffer pH 7.2 and temperature of 37 °C.

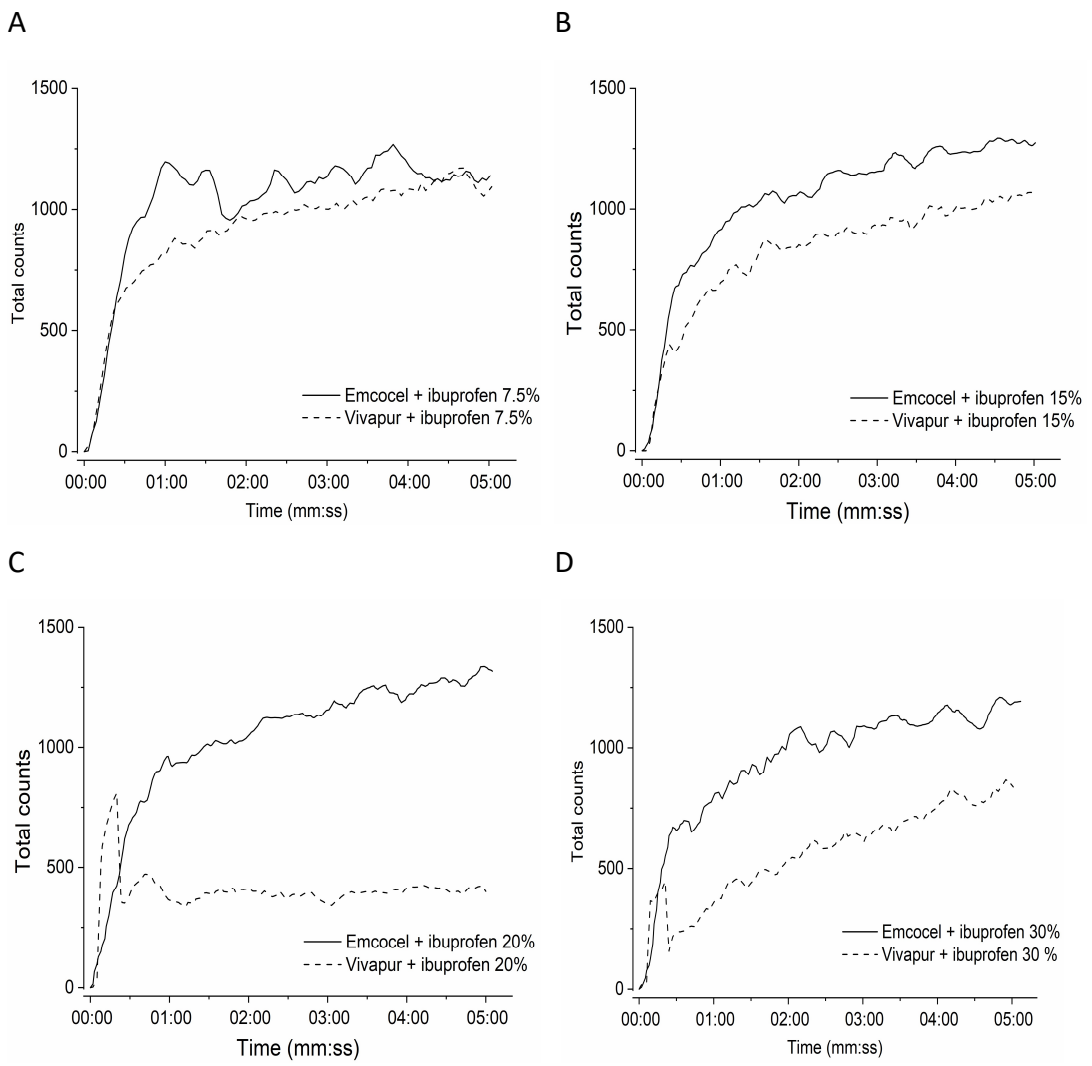

Figure 5.8. Focused Beam Reflectance Measurement (FBRM) total counts over time for Air stream dried MCC (Vivapur®) and Spray dried MCC (Emcocel®) tablets containing ibuprofen (A) 7.5 %, (B) 15 %, (C) 20 %, and (D) 30% w/w in phosphate buffer pH 7.2 and temperature of 37 °C.

Due to the variability in the total number of counts for each tablet a relative increase in FBRM counts was measured for each tablet to enable comparison between tablets behaviour during the disintegration process. Figure 5.9 shows the time required to reach 50, 60, 70, 80, 90% total counts. All tablets were tracked for 30 minutes. Thus, 100% was considered the total counts at 30 min for each tablet. After 30 minutes the disintegration process for all tablets was considered complete. The overall trend

showed a longer time for tablets containing air stream dried MCC compared to spray dried MCC, indicating a slower disintegration rate.

A

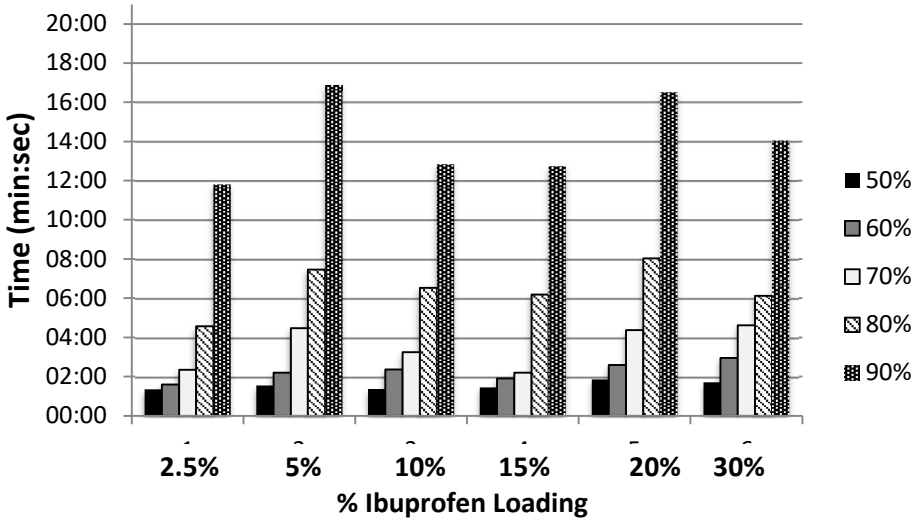

B

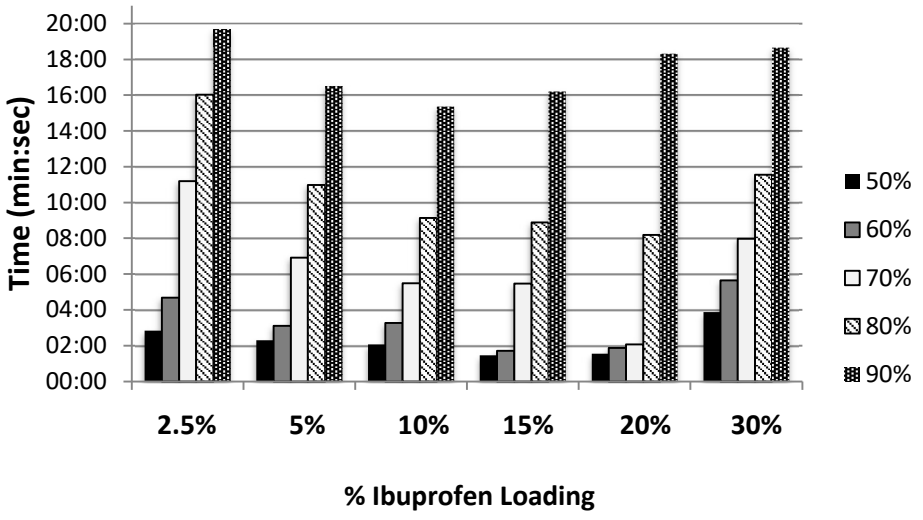

Figure 5.9. Time to reach percentage of total counts measured by FBRM for tablets during disintegration containing (A) Spray dried MCC and (B) Air stream dried MCC and different ibuprofen w/w loadings (2.5 to 30% w/w) in phosphate buffer pH 7.2 at 37^{o}C. Percentages expressed relative to total counts at 30 mins considered 100%.

An indication of particle size distribution during disintegration was obtained from the FBRM chord length distributions and square weighted chord length distributions (SQWT). Representative tablets with 12.5, 15 % w/w, and 30 % w/w ibuprofen loadings after 5 minutes of dissolution are shown in Figure 5.10. These distributions are automatically generated for the user by the iC FBRM software. The CLD is comparable to a particle size distribution. It is the number of chord lengths recorded in the measurement scan time vs the chord length. The SQWCLD is useful for visual comparison of systems by emphasising differences in the coarse counts (100 – 1000 µm). This is achieved by applying a channel (size intervals or bins) specific weight w_i to counts n_i. The weighted channels y_i are obtained via:

$$y_i = w_i . n_i \qquad \text{(Equation 5.1)}$$

The weights w_i are obtained from the channel midpoints M_i via:

$$w_i = \frac{M_i^{\gamma}}{\sum_{j=1}^{N} M_j^{\gamma}} \cdot N \qquad \text{(Equation 5.2)}$$

Where γ is 2 for the square weight, N is the number of channels, which was 90 in this study, i = 1, 2, …, N and j =1, 2, …, N.

A

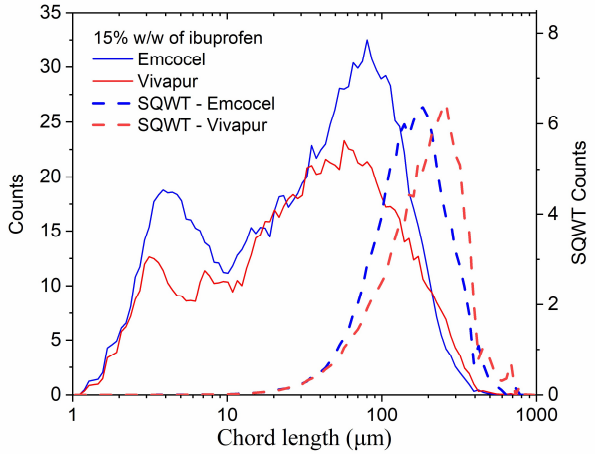

B

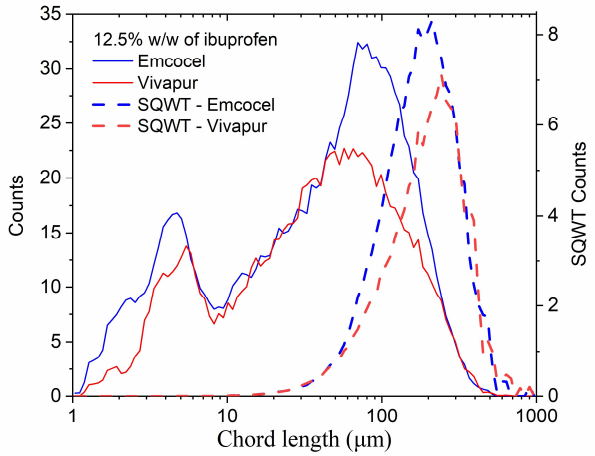

C

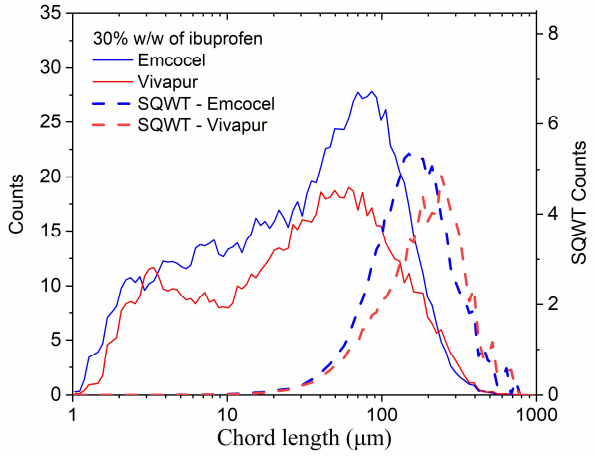

Figure 5.10. Focused Beam Reflectance Measurement (FBRM) chord length distributions and square weighted chord length distributions for Emcocel® (spray dried MCC) and Vivapur® (air stream dried MCC) tablets with ibuprofen loading (A) 12.5 %, (B) 15%, and (C) 30 % w/w, 5 minutes after addition to the disintegration medium, phosphate buffer pH 7.2 and temperature of 37 °C.

Coarse counts account for a much larger proportion of the mass of material compared with fine counts (1-10 µm). While the CLDs for both systems have a similar shape profile, the increased number of total counts and shorter chord length counts was evident for the spray dried compared to the air stream dried MCC. Fine counts may be related to disaggregation of MCC particles during disintegration. MCC is composed of cellulose fibrils agglomerated into larger particles (Queiroz et al., 2019.). Therefore, particle disaggregation during disintegration can result in smaller particle sizes observed in the buffer compared to the particle size distribution reported for dry MCC particles (Table 4.1). When the square weighted CLDs are compared there is a distinct shift to the right for air stream dried, highlighting the increased particle size present 5 minutes after the tablet addition to the buffer. An increase in fine counts (1-10 µm) in the CDL present in the spray dried MCC system suggested that tablets of the spray dried MCC disintegrated more effectively than tablets of the air stream dried MCC at a 30 % w/w ibuprofen loading. For loading below the percolation threshold, a similar trend was seen although the shift to the right for air stream dried in the square weighted CLD is less pronounced. This is exemplified by 12.5 % w/w ibuprofen tablets in Figure 5.10.

The plots of chord length distributions at different time points during disintegration for all tablets were generated and selected profiles shown in Figure 5.11. The increase in counts over time happens similarly across all chord lengths for a same tablet i.e., the distribution did not show a shape change at different time points. Interestingly, the increase in count is clearly more significant up to 5 min. After 5 minutes, the change chord length distributions were comparatively small.

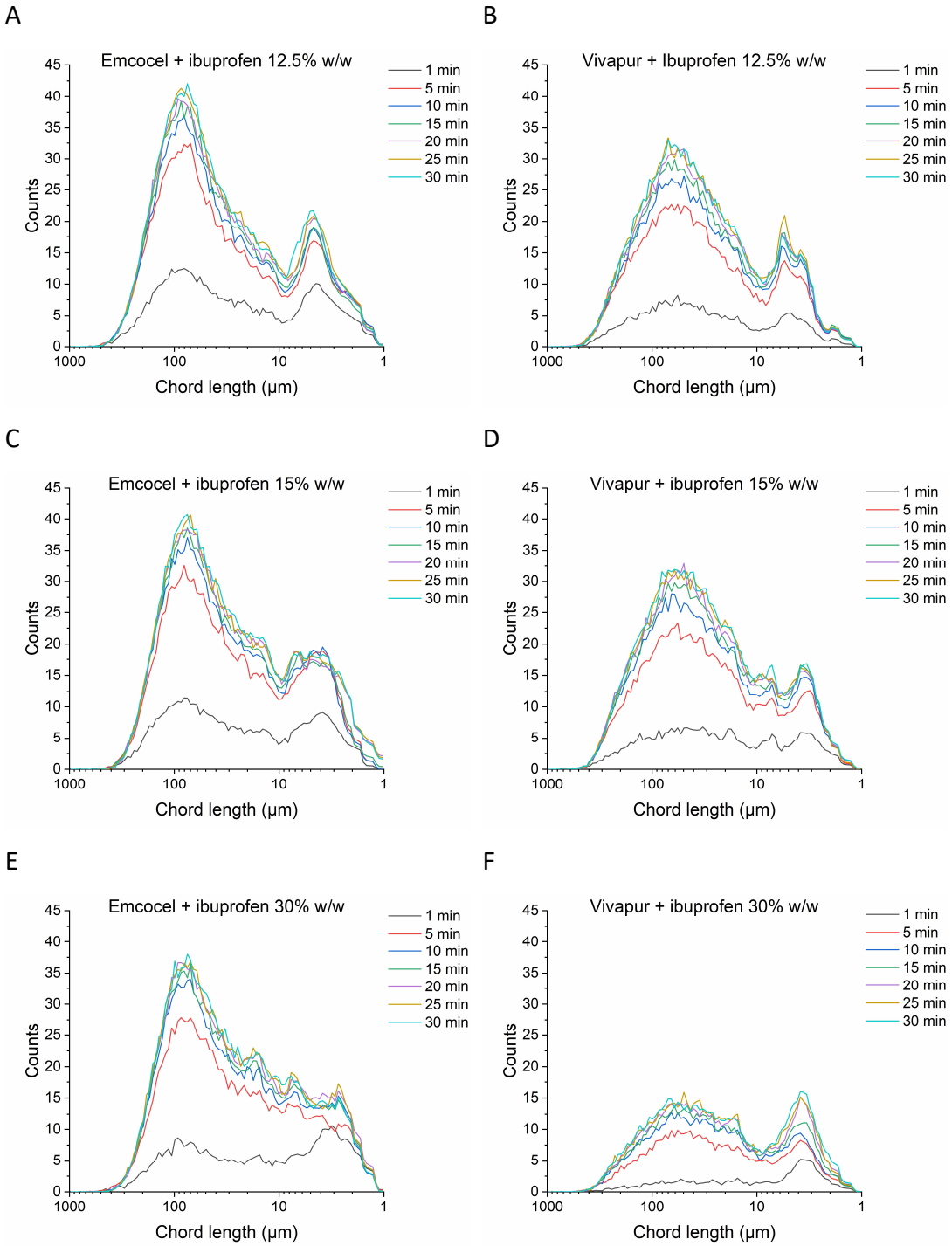

Figure 5.11. Focused Beam Reflectance Measurement (FBRM) chord length distributions for tablets with ibuprofen loadings of 12.5 %, 15%, and 30 % w/w and (A, C, and D) Spray dried MCC (Emcocel®) and (B, D, and F) and Air stream dried MCC (Vivapur®), respectively, at different times after addition to the disintegration medium, phosphate buffer pH 7.2 and temperature of 37 °C.

Based on the results shown in Figure 5.11, the greatest degree of disintegration occurred in the first 5 minutes, the cumulative drug release at 5 min was plotted

against drug loading to investigate the differences in drug release below and above the threshold during tablet disintegration (Figure 5.12). Similar graphical approaches have been previously used to determine the percolation threshold from disintegration and dissolution (Kimura et al., 2007; Wenzel et al., 2017). Cumulative ibuprofen release decreased sharply from 2.5 to 15% w/w of ibuprofen loading. However, at drug loadings above the reported percolation threshold (20% w/w and 30% w/w ibuprofen) the reduction in drug release with increase in drug loading was decreased. Tablets containing the air stream dried MCC showed significantly lower drug release for all drug loadings in comparison to tablets containing the spray dried MCC. These findings confirmed a step change in drug dissolution behaviour at drug concentrations above and below the predicted percolation threshold following tablet disintegration.

A

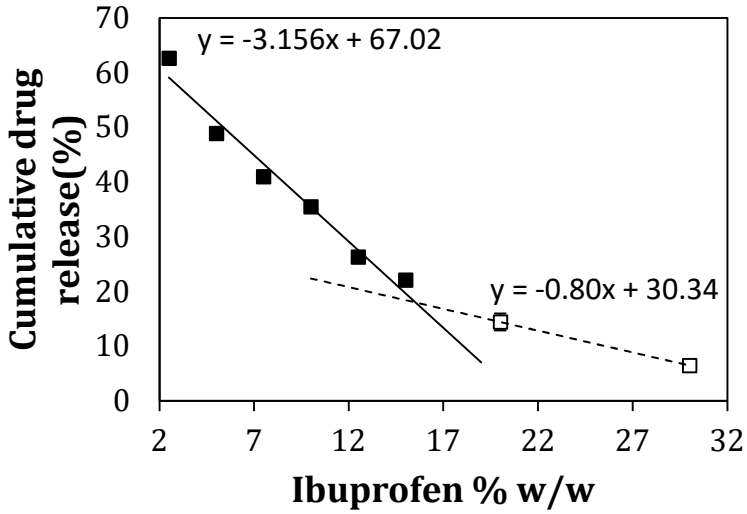

B

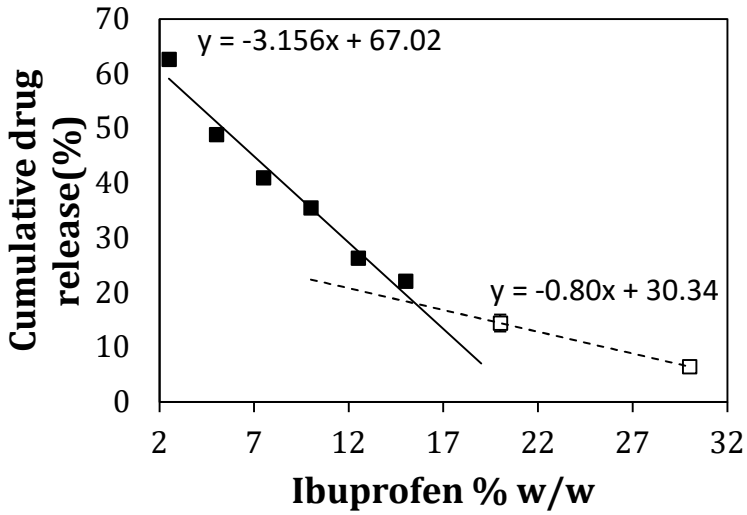

Figure 5.12. Estimation of percolation threshold based on the dissolution cumulative release of ibuprofen from the tablets containing (A) Air stream dried MCC and (B) Spray dried MCC, at 5 min of dissolution. The time of 5 minutes was chosen to represent the differences in behaviour during disintegration.

5.5.5 PVM analysis

PVM analysis was performed to provide real-time images of particles in dissolution medium during tablet disintegration. Besides the images, PVM relative backscatter index was used as a quantitative measure of disintegration. Initially, images were

collected using the PVM probe for ibuprofen powder and both MCC only tablets in a buffer. The ibuprofen particles had a distinct rod-shaped habit (Figure 5.13a). Dispersed ibuprofen powder was present as both discrete particles and aggregates. The ibuprofen particles appeared to be between 100 and 300 µm in length and 30 and 50 µm in width. When compared with the particle size for the dry powder from laser diffraction (Table 4.1), where the D50 was 55 µm, it appears that larger ibuprofen particles in the PVM images may be aggregated. PVM images of the disintegrated spray dried MCC tablet (Figure 5.13b) indicated that fine material was present along with uniform distinct particles having a rough surface. Images of disintegrated air stream dried MCC tablets (Figure 5.13c) are similar to spray dried MCC. These images would support the presence of fine particles observed during FBRM analysis, Figures 5.10 and 5.11. These appeared to be rod shaped particles present which are similar in appearance to the ibuprofen particles.

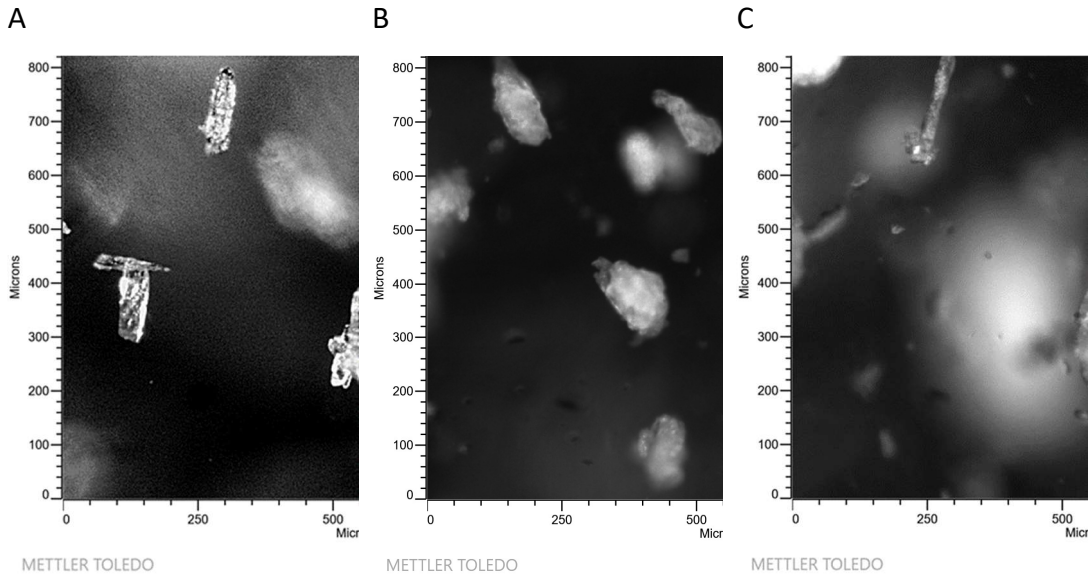

Figure 5.13. PVM images of (A) ibuprofen powder, and (B) Spray dried MCC (Emcocel®) and (C) Air stream dried MCC (Vivapur®) particles following tablet disintegration in phosphate buffer pH7.2 and temperature of 37 °C.

Side by side comparison of PVM images of disintegrated tablets containing spray dried and air stream dried MCC with equivalent ibuprofen loading showed that it is difficult to distinguish definite differences between the two systems. One difference noted was that air stream dried tablets showed more elongated particles (Figure 5.14). There are rod shaped particles present in the air stream dried suspension (Figure 5.13), hence it was not possible to distinguish whether this rod-shaped material following the 15% w/w ibuprofen tablet disintegration is ibuprofen or MCC.

Relative Backscatter Index (RBI) measured by PVM is the relationship between the incident and the detected light. As disintegration progresses the number of particles in the media increases due to fragmentation of larger particles to smaller particles and RBI increases. The change in the PVM RBI versus time during disintegration does indicate differences for tablets containing 20% and 30% ibuprofen loading tablets compared to tablets containing lower ibuprofen loadings (Figure 5.15). For ibuprofen loadings below the percolation threshold the RBI for both spray dried and air stream dried MCC tablets was similar. The air stream dried MCC tablets with a 20 and 30% w/w ibuprofen had a significantly lower final RBI during disintegration compared to air stream dried MCC (Figure 5.15d).

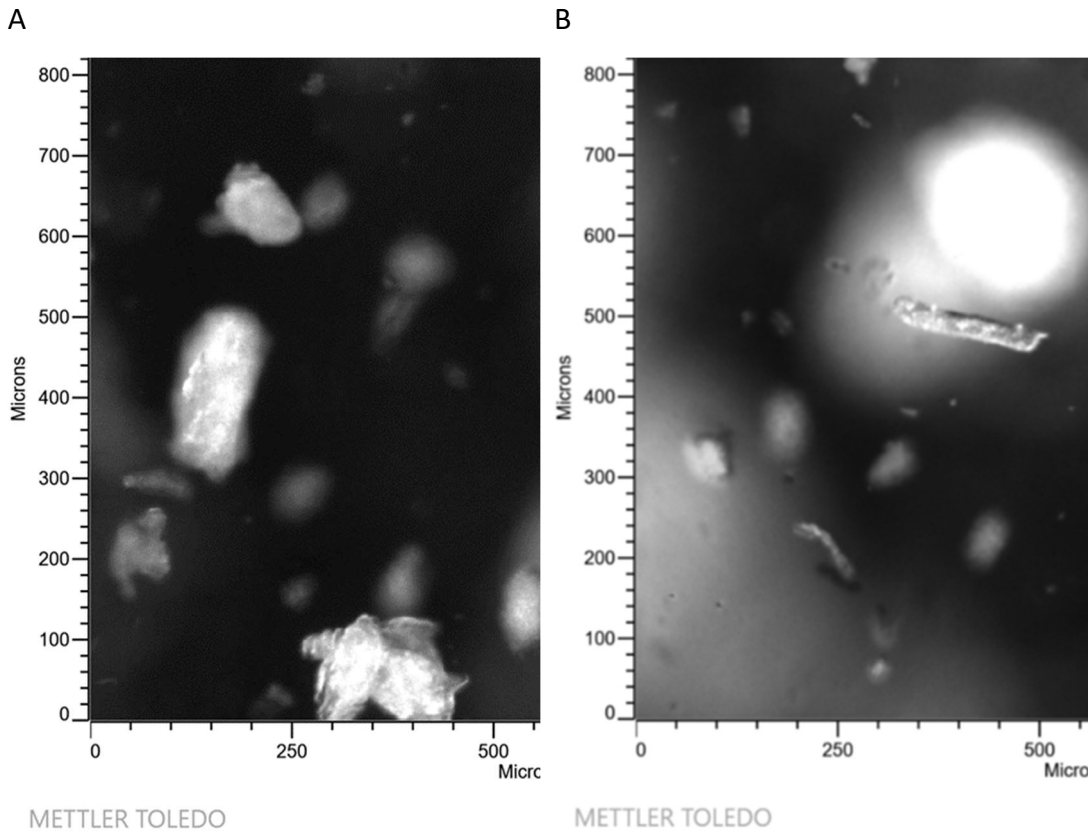

Figure 5.14. Representative PVM images of particles following disintegration of (A) Spray dried MCC and (B) Air stream dried MCC tablets with a 15 % w/w ibuprofen loading in phosphate buffer pH7.2 and temperature of 37 °C.

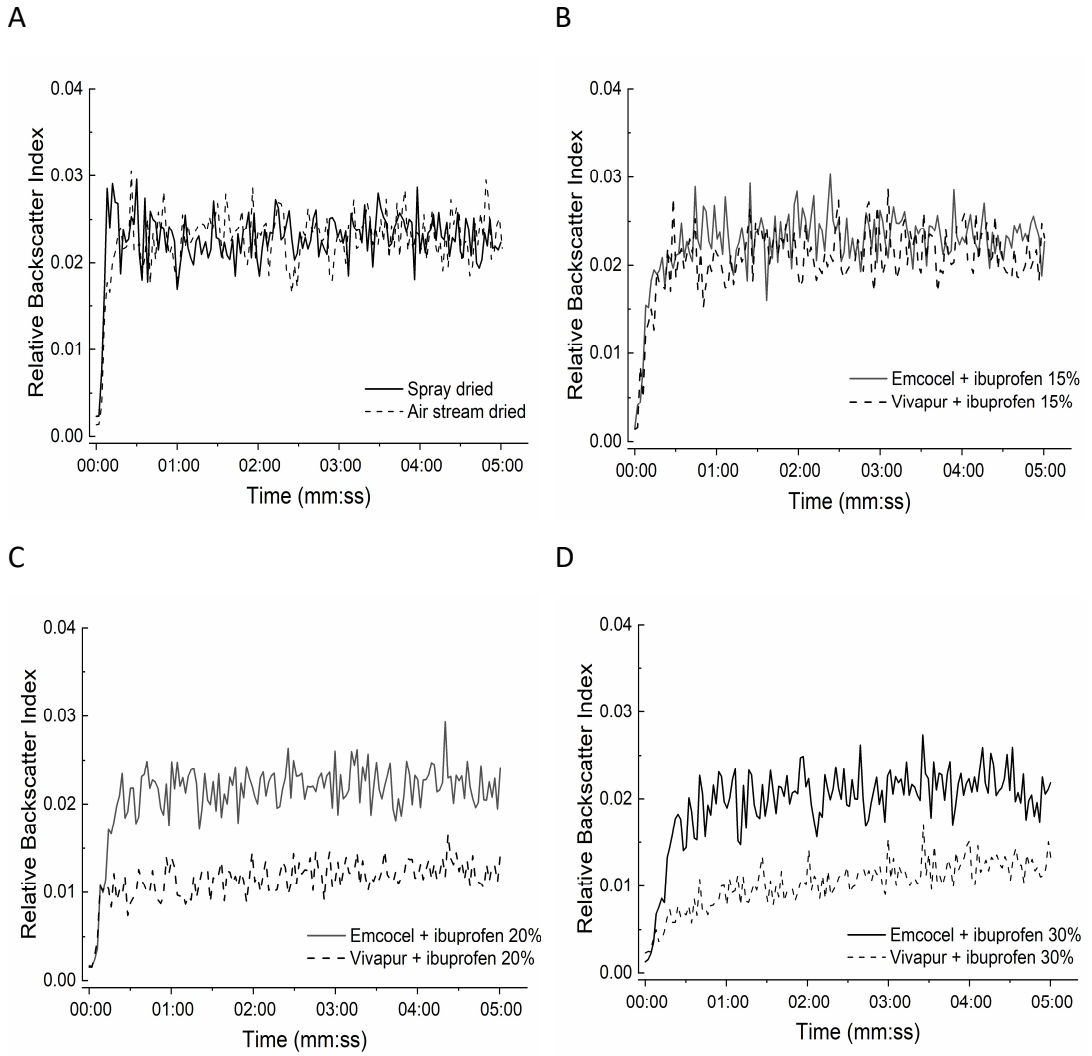

Figure 5.15. Relative Backscatter Index (RBI) vs time following disintegration of Spry dried MCC (Emcocel®) and Air stream dried MCC (Vivapur®) tablets (A) 0% w/w, (B) 15% w/w, (C) 20% w/w and (D) 30% w/w ibuprofen in phosphate buffer pH7.2 and temperature of 37 °C.

5.6 Discussion

The research presented was conducted to determine whether a percolation threshold value, previously determined for ibuprofen/MCC blends using percolation theory and compression data (Queiroz et al., 2019) could also be observed during tablet disintegration and dissolution data. Previous studies determined a percolation threshold value experimentally from disintegration and dissolution data (Kimura et al., 2007; Stillhart et al., 2017; Wenzel et al., 2017). For ibuprofen/ MCC blends, the

existence of a percolation threshold was predicted mathematically and confirmed experimentally from blend properties and a compaction behaviour perspective (Queiroz et al., 2019). In the present study, disintegration and dissolution experiments were carried out to confirm experimentally whether the percolation threshold, previously predicted for ibuprofen/ MCC blends, causes a step change in tablet disintegration and dissolution behaviour.

Dissolution testing confirmed the presence of the percolation threshold in the region previously reported. A change in behaviour above the percolation threshold was observed during dissolution; % drug released at 5 min during the tablet disintegration process (Figure 5.12), and in relation to the time to achieve complete dissolution (Figure 5.5). Blends above the percolation threshold showed slower dissolution profiles. Kimura, Betz and Leuenberger, 2007 also revealed a decreased disintegration performance above the critical loading of a poorly water-soluble drug. In the case of tablets containing MCC and ibuprofen, it was hypothesised that the connected MCC particles would form the water-conducting clusters promoting disintegration. Above the threshold predicted a continuous cluster of ibuprofen particles is formed. Relative to MCC, ibuprofen is poorly water soluble, and the formation of continuous ibuprofen clusters would decrease disintegration. Thus, the explanation for the reduction in dissolution above the percolation threshold can be attributed to the combined effect of decreased drug surface area to mass due to the presence of continuous clusters evidenced by Raman imaging and a change in the disintegration process.

In this study, Raman imaging and image domain analysis were combined to confirm percolation threshold in pharmaceutical tablets. The methodology developed

confirmed the percolation threshold previously predicted for the binary blend investigated (Queiroz et al., 2019) by an increasing number of drug clusters up to the percolation threshold and reduction above due to the formation of continuous clusters. For the drug loading above 15%, the number of ibuprofen domains dramatically decreased, and their equivalent circle diameter increased which confirms the cluster formation and would contribute to a slower rate of ibuprofen dissolution due to a reduced surface area to mass ratio.

The influence of the presence of continuous ibuprofen clusters on tablet disintegration was difficult to establish by pharmacopoeial disintegration testing. However, the use of FBRM and PVM to interrogate the tablet disintegration process with respect to drug loading demonstrated a change in behaviour above the percolation threshold, particularly for tablets containing air stream dried MCC (Figures 5.8 and 5.15). In this study, the dissolution of the disintegrated particles could not be monitored by FBRM nor PVM due to similarity in morphology of the disaggregated MCC particles and ibuprofen particles (Figure 5.14) and the insoluble nature of MCC in the disintegration medium. However, it may be possible to monitor drug dissolution for formulations with high drug loadings and soluble excipients, such as lactose, using PVM and FBRM techniques.

The secondary objective of this study was to investigate the influence of MCC grade on disintegration and dissolution behaviour relative to the percolation threshold. Despite the MCC grades having similar bulk properties, the interaction of each grade with the model drug ibuprofen resulted in differing dissolution behaviour. In all cases, the tablets containing the air stream dried grade showed slower disintegration and dissolution rates. Air stream dried MCC tablets showed a reduction in disintegration

rate above the percolation threshold value while spray dried MCC did not (Figure 5.7 and 5.15). Air stream dried MCC tablets displayed slower dissolution rates (Figure 5.5) across all drug loading.

The mechanistic explanation for the differences in disintegration and dissolution behaviour observed between MCC grades investigated is unclear. Raman image analysis showed similar distribution and size of ibuprofen clusters for both tablets containing both MCC grades (Table 5.2). However, tablet porosity differed between MCC grades, with tablets produced from the air stream dried MCC grade being slightly less porous (Table 5.1). Tablet porosity is a function of drug loading and for blends of poorly compressible drugs with MCC porosity is reduced above the percolation threshold value. Porosity is also a dependent on the grade of MCC (Queiroz et al., 2019). MCC samples with less dense crystalline regions were reported to swell more as they are more accessible for the water molecules, and the cohesive forces between the chain segments are weaker, in comparison to the crystalline domains (Desai et al., 2016; Schott, 1992). Therefore, differences in MCC crystallinity could also contribute to differences in tablet disintegration behaviour. Further studies are required to determine the exact mechanisms causing the reduced dissolution rates for tablets containing air stream dried MCC compared to the spray dried grade.

It was challenging to discriminate between the effects of tablet porosity and percolation threshold in relation to tablet disintegration. The compaction parameters and bonding mechanism of particles during compaction directly impact tablet porosity, the ingress of the disintegration medium, MCC swelling and hence tablet disintegration (Yassin et al., 2015). Despite confounding variation observed in

tablet porosity in this study, a clear step change in dissolution behaviour was observed for tablets with drug loadings above the percolation threshold.

5.7 Conclusions

Dissolution data showed that a percolation threshold value previously determined for ibuprofen/MCC binary blends, from compaction data, translated to tablet dissolution data. Slower ibuprofen dissolution behaviour was observed for tablets above the predetermined percolation threshold. This confirmed the presence of the percolation threshold and its relevance to dissolution studies. In addition, slower dissolution was observed for all tablets containing an air stream dried MCC grade, compared to a spray dried MCC grade. FBRM and PVM showed less efficient disintegration above the percolation threshold for tablets containing air stream dried MCC. The results experimentally demonstrate that both larger drug domains, quantified by Raman imaging, and a less efficient tablet disintegration measured by FBRM and PVM (in the case of air stream dried MCC) contributed to slower ibuprofen dissolution profiles above the percolation threshold.

Chapter 6 - General Discussion

6.1 General Discussion

The technological advances of the 4th industrial revolution have brought opportunities for process development and knowledge growth in the pharmaceutical sector. One important innovation is the adoption of continuous manufacturing. Technologies that can support the understanding, design, operation, and control of continuous processes must be developed in order to progress towards Pharma 4.0 and implement advanced quality approaches.

The overall aim of this thesis was to increase understanding of pharmaceutical materials attributes and processes performance by (*i*) characterization of CMAs, API/excipient interactions, and CQAs, and (*ii*) the development of descriptive and predictive models and PAT tools applied to tableting and co-crystallization process development and monitoring.

The focus of this thesis was to address challenges around direct compression, which is the preferential process for continuous tableting manufacturing. Three main stages of the process were investigated; raw material characterization and variability were investigated in Chapters 2, 4, and 5, crystal engineering process development and process characterization was investigated in Chapter 3, and process characterization and analysis of the impact of constituent raw material attributes on process performance was investigated in Chapters 4 and 5 (Figure 6.1).

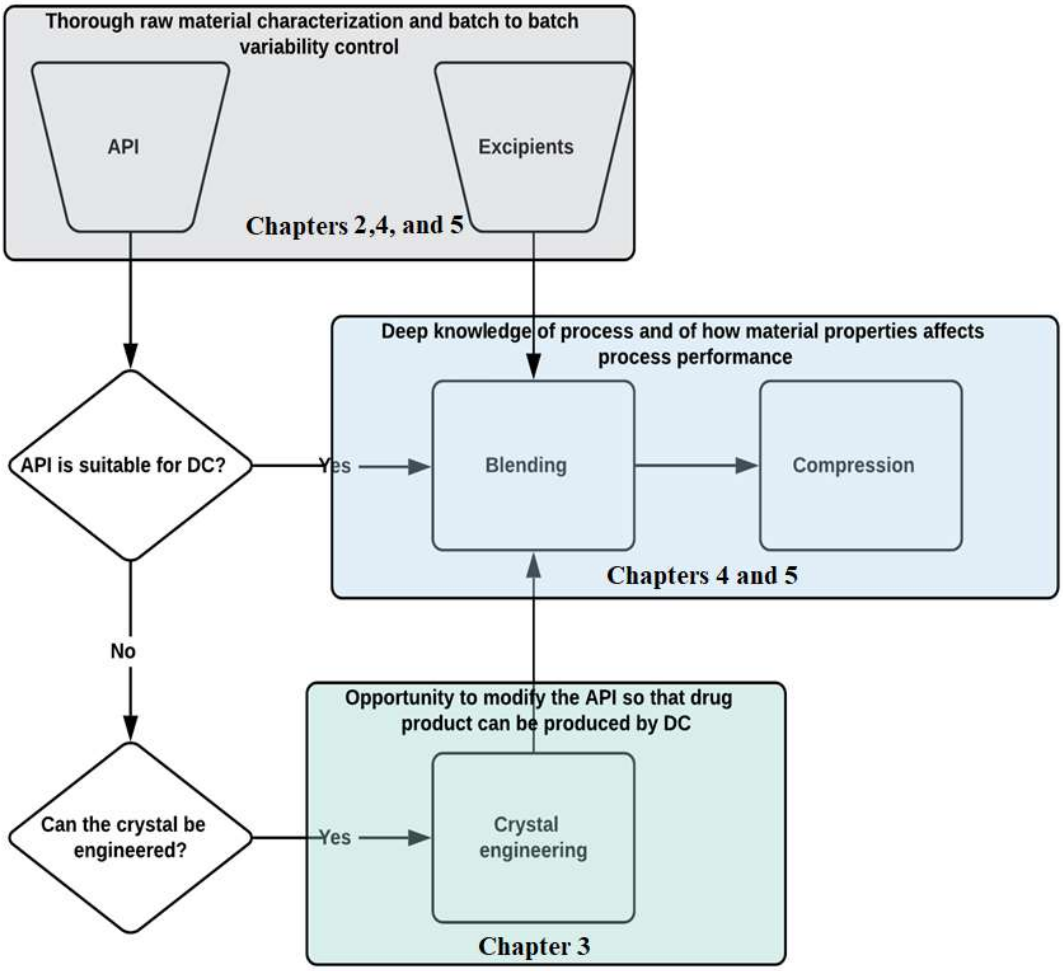

Figure 6.1. Tablet direct compression (DC) scheme.

6.2 Knowledge related to Microcrystalline Cellulose variability

Microcrystalline cellulose is important excipient used in most solid dosage formulations. However, it is necessary to improve knowledge about MCC CMAs in order to control the effects of MCC CMA on process and product performance (Foster et al., 2018; Rowe et al., 1994; Shi et al., 2011; Trache et al., 2016). Several MCC attributes were investigated in this thesis (Table 6.1).

Table 6.1. Microcrystalline cellulose attributes investigated in this thesis.

Material attribute	Model	Chapter
Crystallinity by Raman	PLS, univariate model	2
Moisture sorption by DVS	GAB equation	2
Moisture sorption by TGA LOD	-	4
Surface area	BET	4
Laser diffraction particle size	-	4
Morphology and particle size by morphology G3	-	4
Morphology and particle size by SEM	-	4
Bulk, tap, true and relative densities	-	4
Flowability	Hausner ratio	4
Flowability by Powder Flow Tester (PFT)	-	4
Compressibility, tabletatibility and Compactability	Compaction triangle	4
Yield pressure	Heckel equation	4
Capacity of dilution of ibuprofen	Percolation threshold theory	4
Disintegration	-	5
Disintegration and dissolution of ibuprofen	-	5

Knowledge related to MCC batch-to-batch, supplier to supplier and grade to grade variability was obtained by investigating MCC moisture sorption and crystallinity variability in Chapter 2. Raman spectroscopy was used with a univariate model that is a function between the ratio of the peaks at 380 and 1096 cm^{-1}, and with partial least squares regression model, to provide a PAT tool to determine the MCC

crystallinity index. The PAT tool designed was packaged into a free online calculator, MCCrystal. This work is a further development of the work developed by Agarwal et al. (Agarwal, 2019; Agarwal et al., 2018, 2010). The contributions of this thesis to the previous work were the application of the models to 30 commercial grades of MCC, which proved the efficiency of those models to commercial grades, and the development of an online, free access, PAT tool that can be used by other academics and industry personnel.

A range of MCC crystallinity was noted between samples. While variability in moisture sorption behaviour was also noted between samples, a PAT tool to predict MCC moisture sorption based on crystallinity of MCC could not be designed. A correlation between moisture sorption and crystallinity index was investigated. However, it was not possible to build a model with predictive power. It was found that for the set of 30 MCC commercial batches investigated, moisture sorption was not solely dependent on the crystallinity index of the sample. Mihranyan et al. suggested that moisture sorption in MCC may be also dependent on other structural attributes such as pore volume and surface area (Mihranyan et al., 2004).

Excipient variability has been highlighted by many authors as a critical part of the design and control strategies of new drug products (Badawy et al., 2016; Kushner IV, 2013; Kushner et al., 2011; Narang, 2015; Zarmpi et al., 2020). In Chapters 4 and 5, the impact of excipient variability on tablet CQAs was highlighted by investigating two different MCC grades. One grade was air stream dried and the second spray dried. Grades had similar average particle size distribution determined by laser diffraction, but different morphology determined by image analysis. Tablets were

prepared from binary blends of MCC with ibuprofen. The use of PAT tools to determine tablets CQAs was proposed and compared to traditional methodologies. The PAT tools used, PVM and FBRM, are widely used to track in-process particle changes (Barrett et al., 2011; Gregory, 2009; Simon et al., 2019; Zhong et al., 2020). However, they have not been used to monitor disintegration and dissolution behaviours. Both traditional testing and tests assisted by PAT tools showed that the morphological differences due to grade-to-grade variability resulted in significant differences in tablet dissolution. The PAT tools, PVM and FBRM, provided more sensitive information regarding tablet disintegration compared to the traditional disintegration test. The study highlights the applicability of those PAT tools to identify differences in the disintegration of immediate release tablets. Furthermore, disintegration is a limiting step to dissolution. Therefore, in Chapter 5, the disintegration differences observed using the PAT tools indicated that dissolution differences could be expected. Indeed, significant dissolution differences were confirmed by traditional dissolution testing with HPLC analysis of the % cumulative drug release.

The impact of MCC grade variability on formulation processability during tableting was also investigated in Chapter 4. This contrasts with Chapter 5 where the effect of MCC grade variability on tablet CQAs (hardness, disintegration, and dissolution) was evident. The air stream dried MCC grade showed considerably lower tablet dissolution rates in comparison to the air stream dried MCC. The differences observed were attributed to the minor differences in tablet solid fraction or porosity,

which directly affects the rate at which water enters through the tablet matrix and hence disintegration (Yassin et al., 2015).

6.3 Knowledge related to physical drug-excipient interactions

The interaction between drug and excipient was investigated in Chapters 3 and 4. In Chapter 4 drug-excipient interactions at a particle level in a blend containing ibuprofen and MCC were investigated using Percolation Threshold modelling and Raman imaging. The Raman imaging instrument used a short time for analysis i.e., approximately 15 minutes for each tablet with a diameter of 10 mm. The use of this instrument provides a fast and detailed analysis of tablets. Raman imaging, used here as an analytical technique, provided important formulation information, such as the measurement of drug distribution, and indirectly percolation threshold. Moreover, it is not necessary to perform any further analysis, the instrument generates all the information necessary for those applications during analysis. Other authors have investigated the percolation threshold of MCC (Kozicki, 2007; Kuentz and Leuenberger, 2000, 1998; Leuenberger, 1999). However, in this thesis, the critical exponent of the percolation power law was determined for the first time for the binary blend of MCC and ibuprofen. An accurate prediction of the threshold from compaction data was obtained using the percolation power law only because the coefficient has been determined as the initial step. The effects of the particle-particle interactions between ibuprofen and MCC on tablet CQAs disintegration and dissolution were investigated in Chapter 5. A step change in dissolution behaviour was noted across the percolation threshold determined.

In Chapter 3, drug-excipient interactions at a molecular level were investigated. API, hydrochlorthiazide, and several coformers were investigated *in silico* using quantum chemistry and thermodynamics simulations, and experimentally with a range of spectroscopic techniques, DSC and PXRD. The type of simulation used was proven to have good predictive power for cocrystal screening using excess/mixing enthalpy of supercooled API-coformer blends (Loschen and Klamt, 2015). The coformers screened had been previously investigated experimentally (Rodrigues et al., 2019, 2018b; Sanphui et al., 2015; Sanphui and Rajput, 2014). The simulations performed in this thesis agreed with the experimental results obtained by these authors.

6.4 Development of descriptive and predictive models and PAT tools

Descriptive models are models used for process understanding. PAT-based models were designed to support analytical procedures and for process monitoring in Chapters 2, 3, and 5 (Table 6.2). Other types of models were applied to support process design: percolation threshold was used for tablet binary formulation design in Chapter 4, DoE was used for co-crystallization design in Chapter 3, COSMO-RS theory was used in Chapter 3 to screen for suitable coformers in early-stage co-crystallization design, and the Heckel model was used to generate knowledge on blend processability in Chapter 4. The models were classified as mechanistic, hybrid or empirical (Table 6.3).

Table 6.2. Process analytical technology instruments and models used in the different case studies of this thesis.

Application	PAT instrument	Model	Chapter
Determine critical drug loading in tablet formulation	Raman	PCA	5
Determine cocrystal optimal ratio	MIR	MCR	3
Determine co-crystal phase purity	MIR	MCR	3
Determine slurry co-crystallization end time	Raman	PCA	3
Determine co-crystallization mechanism	Raman	PCA	3
Determine tablet CQAs (disintegration profile)	FBRM and PVM	-	5
Determine MCC CMA (crystallinity)	Raman	PCA and PLS	2

Table 6.3. Classification of the models used in this thesis within the groups mechanistic, hybrid, or empirical.

Mechanistic	Hybrid	Empirical
COSMO-RS theory	Heckel	PLS
Simulation of theoretical PXRD	Percolation threshold theory	PCA
380-method		MCR
		DOE
		GAB equation

The models investigated in this thesis provided significant knowledge about materials and processes studied when used individually or in combination. In Chapter 3, for example, COSMO-RS theory was used for early-stage process design aiming to select appropriate coformers and solvents. Next, MCR was used to determine relative phase purity. Subsequently, a DOE model used the relative phase purity from the MCR model as response variable to define optimal process parameters (temperature

and agitation for each solvent). Finally, PCA was also performed in the same study to define a process parameter (slurry co-crystallization end time).

The impact of choice of PAT probe was also investigated in this thesis. In Chapter 2, the results showed that Raman instruments with larger laser diameter provided a more representative information of the overall structure of the batch, averaging out localised variability. Smaller laser diameters could predict crystallinity from Raman spectra if a larger number of spectra are averaged. However, Raman instruments with larger laser diameter require less replicates, which greatly reduces time for analysis. In contrast, in Chapters 4 and 5 a Raman instrument with higher resolution, RA802 Pharmaceutical Analyser, was used to map ibuprofen distribution and quantitatively and qualitatively determine drug percolation threshold in a binary ibuprofen/MCC tablet. The imaging method involved the acquisition of around 76,000 spectra over the entire surface of each tablet, with a pixel size of 10 µm/20 µm.

The main benefits of PAT-based methods used in this thesis were:

- All techniques used are non-destructive, and they do not interfere on process transformations when they are used in situ.
- The analysers can be used in situ to generate information on process transformation during the entire duration of the process e.g., Raman and PCA used in Chapter 3 to determine co-crystallization end point.
- PAT based methods provided information that may not be captured by traditional techniques e.g., in Chapter 5 PVM and FBRM showed

disintegration nuances to which traditional tablet disintegration techniques were not sensitive.

On the other hand, PAT models are data driven. This means that the model is built from experimental data and a design space is defined. Thus, the model cannot be applied for processes that are outside that design space, for example, for a different instrument. In this study, in Chapter 2 the constant values for the univariate linear model previously published for this technique (Agarwal et al., 2018) were specific to the instrument used and had to be redetermined in this study. Thus, a celebration of the model to the new design space had to be performed.

A direct comparison between a univariate and a multivariate model was investigated in Chapter 2. The advantage of using the univariate model (380-method) is that it is simple enough to perform the linear regressions required to calibrate the model to the Raman instrument used and to calculate the crystallinity by the ratio of the peaks. However, milling the sample and Raman spectra deconvolution are required which makes the workflow tedious. On the other hand, by performing a PLS regression model deconvolution is discarded. Thus, milling a sample for calibration or for each batch analysed is not necessary. PLS regression models are rather simpler to be performed and have a much shorter time to analysis in comparison with the multi-steps 380-method. Although, PLS regressions entails the usage of a multivariate analysis software or development of a code in a programming language such as Python or R.

6.5 Strengths and Limitations of the thesis

6.5.1 Strengths

- The effects of critical material attributes on the critical quality attributes were investigated in depth through a case study including intensive material, formulation, and product characterisation. Detailed scientific knowledge was developed on the relationship between MCC grade, percolation threshold of blends and tablet dissolution behaviour, and the effect of MCC variability on tablet disintegration and dissolution.
- PAT tools were compared against traditional analytical techniques for a wide range of applications.
- A wide range of modelling approaches were investigated. These included mechanistic, hybrid models and empirical models.
- Rapid methods to determine a range of behaviours related to pharmaceutical dosage form manufacture and performance have been developed

6.5.2 Limitations

- Blends of ibuprofen and microcrystalline cellulose were used to investigate whether percolation threshold can predict the critical drug loading concentration and relative density of pharmaceutical tablets. However, commercial tablet formulations are composed of more complex blends with several ingredients. Thus, it would be valuable to apply the knowledge developed in this study to commercial tablet formulations.

- All models were developed for offline and retrospective usage, although online monitorization of processes with feedback control would have had a higher impact for industrial applications.
- A wide range of PATs, models and unit operations were investigated prohibiting more in-depth investigation of each subject area.

6.6 Recommendations for future work

Based on the findings of this thesis the following work is suggested:

- Further investigate the relationship between MCC CMAs e.g., crystallinity and moisture sorption.
- Investigate how CPPs can be controlled based on the knowledge of the variability of MCC CMA. For example, how wet massing in a wet granulation tableting process can be controlled based on MCC crystallinity.
- Investigate the application of percolation threshold model to multicomponent oral dosage form formulations.
- Use particle modelling tools such as Monte Carlo simulation to estimate percolation threshold for complex formulations.
- Investigate the application of Raman as a PAT tool to monitor tablet disintegration and dissolution.

6.7 Conclusions

Extensive knowledge about tablet direct compression was produced: traditional techniques for determination of raw material and products characterization were critically investigated and alternative technologies were proposed when suitable, and percolation threshold model was used to predict formulation behaviour during tableting in pilot scale, disintegration, and dissolution.

Different PAT tools were successfully designed: Raman with PLS to determine microcrystalline cellulose crystallinity index; MIR with MCR to determine optimal ratio of co-crystal formation and co-crystal phase purity; Raman with PCA to determine co-crystallization endpoint and in-process changes; Raman and PCA to identify differences between tablets produced with different grades of MCC; and PVM and FBRM provided information on tablet disintegration that traditional testing was not able to capture.

Mechanistic and hybrid models were developed to support process design: percolation threshold theory was used to determine a critical threshold above which disintegration and dissolution showed a significant decrease; DOE was used to determine the optimal conditions to obtain the high purity co-crystals; and quantum chemistry models were used as an in silico coformer screening, which reduced time and cost of performing experimental screenings.

Bibliography

Abbas, O., Dardenne, P., Baeten, V., 2012. Near-infrared, mid-infrared, and Raman spectroscopy, in: Chemical Analysis of Food: Techniques and Applications - Google Books. Academic Press, pp. 59–91.

Abramov, Y.A., Loschen, C., Klamt, A., 2012. Rational coformer or solvent selection for pharmaceutical cocrystallization or desolvation. J. Pharm. Sci. 101, 3687–3697. https://doi.org/10.1002/jps.23227

Agarwal, U.P., 2019. Analysis of cellulose and lignocellulose materials by raman spectroscopy: A review of the current status. Molecules. https://doi.org/10.3390/molecules24091659

Agarwal, U.P., Ralph, S.A., Reiner, R.S., Baez, C., 2018. New cellulose crystallinity estimation method that differentiates between organized and crystalline phases. Carbohydr. Polym. 190, 262–270. https://doi.org/10.1016/j.carbpol.2018.03.003

Agarwal, U.P., Reiner, R.S., Ralph, S.A., 2010. Cellulose I crystallinity determination using FT-Raman spectroscopy: Univariate and multivariate methods. Cellulose 17, 721–733. https://doi.org/10.1007/s10570-010-9420-z

Agrawal, A.M., Manek, R. V., Kolling, W.M., Neau, S.H., 2004. Water distribution studies within microcrystalline cellulose and chitosan using differential scanning calorimetry and dynamic vapor sorption analysis. J. Pharm. Sci. 93, 1766–1779. https://doi.org/10.1002/jps.20085

Aher, S., Dhumal, R., Mahadik, K., Paradkar, A., York, P., 2010. Ultrasound assisted cocrystallization from solution (USSC) containing a non-congruently soluble cocrystal component pair: Caffeine/maleic acid. Eur. J. Pharm. Sci. 41, 597–602. https://doi.org/10.1016/j.ejps.2010.08.012

Al-Karawi, C., Cech, T., Bang, F., Leopold, C.S., 2018. Investigation of the tableting behavior of Ibuprofen DC 85 W. Drug Dev. Ind. Pharm. 44, 1262–1272. https://doi.org/10.1080/03639045.2018.1442846

Ali, S.M., Bonnier, F., Lambkin, H., Flynn, K., McDonagh, V., Healy, C., Lee, T.C., Lyng, F.M., Byrne, H.J., 2013. A comparison of Raman, FTIR and ATR-FTIR micro spectroscopy for imaging human skin tissue sections. Anal. Methods 5, 2281–2291. https://doi.org/10.1039/c3ay40185e

Allesø, M., Velaga, S., Alhalaweh, A., Cornett, C., Rasmussen, M.A., Van Den Berg, F., De Diego, H.L., Rantanen, J., 2008. Near-infrared spectroscopy for cocrystal screening. A comparative study with Raman spectroscopy. Anal. Chem. 80, 7755–7764. https://doi.org/10.1021/ac8011329

Alshahateet, S.F., 2010. Synthesis and supramolecularity of hydrogen-bonded cocrystals of pharmaceutical model rac-ibuprofen with pyridine derivatives. Mol. Cryst. Liq. Cryst. 533, 152–161. https://doi.org/10.1080/15421406.2010.526557

Amidon, G.E., Houghton, M.E., 1995. The Effect of Moisture on the Mechanical and Powder Flow Properties of Microcrystalline Cellulose. Pharm. Res. 12, 923–929. https://doi.org/10.1023/A:1016233725612

Anderson, J.D., Degroote, J., Degrez, G., Dick, E., Grundmann, R., Vierendeels, J., 1995. Computational Fluid Dynamics, 3rd Editio. ed. Springer.

Awa, K., Shinzawa, H., Ozaki, Y., 2015. The Effect of Microcrystalline Cellulose Crystallinity on the Hydrophilic Property of Tablets and the Hydrolysis of Acetylsalicylic Acid as Active Pharmaceutical Ingredient Inside Tablets. AAPS PharmSciTech 16, 865–870. https://doi.org/10.1208/s12249-014-0276-7

Badawy, S.I.F., Narang, A.S., Lamarche, K.R., Subramanian, G.A., Varia, S.A., Lin, J., Stevens, T., Shah, P.A., 2016. Integrated Application of Quality-by-Design Principles to Drug Product Development: A Case Study of Brivanib Alaninate Film-Coated Tablets. J. Pharm. Sci. 105, 168–181. https://doi.org/10.1016/j.xphs.2015.11.023

Badman, C., Trout, B.L., 2014. Achieving Continuous Manufacturing. Continuous Symposium Continuous Manufacturing White Papers. J. Pharm. Sci. 104, 779–780.

Bakeev, K.A., 2010. Process Analytical Technology – Spectroscopic Tools and Implementation Strategies. John Wiley & Sons. https://doi.org/10.1002/9780470689592

Barmpalexis, P., Karagianni, A., Nikolakakis, I., Kachrimanis, K., 2018. Artificial neural networks (ANNs) and partial least squares (PLS) regression in the quantitative analysis of cocrystal formulations by Raman and ATR-FTIR spectroscopy. J. Pharm. Biomed. Anal. 158, 214–224. https://doi.org/10.1016/j.jpba.2018.06.004

Barrett, M., Hao, H., Maher, A., Hodnett, K., Glennon, B., Croker, D., 2011. In Situ Monitoring of Supersaturation and Polymorphic Form of Piracetam during Batch Cooling Crystallization. Org. Process Res. Dev. 15, 681–687. https://doi.org/10.1021/op2000628

Barrett, P., Glennon, B., 2002. Characterizing the Metastable Zone Width and Solubility Curve Using Lasentec FBRM and PVM. Chem. Eng. Res. Des. 80, 799–805. https://doi.org/https://doi.org/10.1205/026387602320776876

Barrett, P., Glennon, B., 1999. In-line FBRM Monitoring of Particle Size in Dilute Agitated Suspensions. Part. Part. Syst. Charact. 16, 207–211. https://doi.org/10.1002/(SICI)1521-4117(199910)16:5<207::AID-PPSC207>3.0.CO;2-U

Basavoju, S., Boström, D., Velaga, S.P., 2006. Pharmaceutical cocrystal and salts of norfloxacin. Cryst. Growth Des. 6, 2699–2708. https://doi.org/10.1021/cg060327x

Baxendale, I.R., Braatz, R.D., Hodnett, B.K., Jensen, K.F., Johnson, M.D., Sharratt, P., Sherlock, J.P., Florence, A.J., 2015. Achieving Continuous Manufacturing: Technologies and Approaches for Synthesis, Workup, and Isolation of Drug Substance May 20–21, 2014 Continuous Manufacturing Symposium, in: Journal of Pharmaceutical Sciences. Elsevier B.V., pp. 781–791. https://doi.org/10.1002/jps.24252

Becke, A.D., 1988. Density-functional exchange-energy approximation with correct

asymptotic behavior. Phys. Rev. A 38, 3098–3100. https://doi.org/10.1103/PhysRevA.38.3098

Benesty, J., Chen, J., Huang, Y., Cohen, I., 2009. Pearson Correlation Coefficient, in: Cohen, I., Huang, Y., Chen, J., Benesty, J. (Eds.), Noise Reduction in Speech Processing 2. Springer Berlin Heidelberg. https://doi.org/10.1007/978-3-642-00296-0_5

Betz, G., Junker-Bürgin, P., Leuenberger, H., 2003. Batch and continuous processing in the production of pharmaceutical granules, in: Pharmaceutical Development and Technology. Taylor & Francis, pp. 289–297. https://doi.org/10.1081/PDT-120022157

Bi, Y.X., Sunada, H., Yonezawa, Y., Danjo, K., 1999. Evaluation of rapidly disintegrating tablets prepared by a direct compression method. Drug Dev. Ind. Pharm. 25, 571–581. https://doi.org/10.1081/DDC-100102211

Bian, L., Zhao, H., Hao, H., Yin, Q., Wu, S., Gong, J., Dong, W., 2013. Novel glutaric acid cocrystal formation via cogrinding and solution crystallization. Chem. Eng. Technol. 36, 1292–1299. https://doi.org/10.1002/ceat.201200720

Blahovec, J., Yanniotis, S., 2008. Gab generalized equation for sorption phenomena. Food Bioprocess Technol. 1, 82–90. https://doi.org/10.1007/s11947-007-0012-3

Bocklitz, T., Walter, A., Hartmann, K., Rösch, P., Popp, J., 2011. How to pre-process Raman spectra for reliable and stable models? Anal. Chim. Acta 704, 47–56. https://doi.org/10.1016/j.aca.2011.06.043

Bolhuis, G.K., Chowhan, Z.T., 1996. Materials for direct compaction. Drugs Pharm. Sci. 71, 419–500.

Bonny, J.D., Leuenberger, H., 1993. Matrix type controlled release systems II. Percolation effects in non-swellable matrices. Pharm. Acta Helv. 68, 25–33. https://doi.org/10.1016/0031-6865(93)90005-Q

Bonny, J.D., Leuenberger, H., 1991. Matrix type controlled release systems: I. Effect of percolation on drug dissolution kinetics. Pharm. Acta Helv. 66, 160–164.

Booth, D.E., 2005. Chemometrics: From Basics to Wavelet Transform. Technometrics 47, 240–240. https://doi.org/10.1198/tech.2005.s267

Borchers, H.W., 2019. pracma: Practical Numerical Math Functions.

Brunauer, S., Emmett, P.H., Teller, E., 1938. Adsorption of Gases in Multimolecular Layers. J. Am. Chem. Soc. 60, 309–319. https://doi.org/10.1021/ja01269a023

Burke, C.J., Zylberberg, C., 2019. Sources of Variability in Manufacturing of Cell Therapeutics. Regen. Eng. Transl. Med. 5, 332–340. https://doi.org/10.1007/s40883-019-00130-5

Busignies, V., Leclerc, B., Porion, P., Evesque, P., Couarraze, G., Tchoreloff, P., 2007. Application of percolation model to the tensile strength and the reduced modulus of elasticity of three compacted pharmaceutical excipients. Eur. J. Pharm. Biopharm. 67, 507–514. https://doi.org/10.1016/j.ejpb.2007.02.005

CAMO Analytics, 2011. The Unscrambler Appendices: Method References.

Caramella, C., Colombo, P., Conte, U., Ferrari, F., Gazzaniga, A., LaManna, A., Peppas, N.A., 1988. A physical analysis of the phenomenon of tablet disintegration. Int. J. Pharm. 44, 177–186. https://doi.org/10.1016/0378-5173(88)90114-7

Carr, R., 1965. Evaluating flow properties of solids. Chem. Eng. 72, 163–168. https://doi.org/10.5897/AJFS2015.1279

Castellan, A., Ruggiero, R., Frollini, E., Ramos, L.A., Chirat, C., 2007. Studies on fluorescence of cellulosics. Holzforschung 61, 504–508. https://doi.org/10.1515/HF.2007.090

Chan, K.L.A., Elkhider, N., Kazarian, S.G., 2005. Spectroscopic imaging of compacted pharmaceutical tablets. Chem. Eng. Res. Des. 83, 1303–1310. https://doi.org/10.1205/cherd.05088

Chang, W., Borges Ribeiro, B., 2018. Shinydashboard: create dashboards with'Shiny'.

Chang, W., Cheng, J., Allaire, J., Xie, Y., McPherson, J., 2019. shiny: Web Application Framework for R.

Chatterjee, S., Moore, C.M. V, Nasr, M.M., 2017. An Overview of the Role of Mathematical Models in Implementation of Quality by Design Paradigm for Drug Development and Manufacture, in: Comprehensive Quality by Design for Pharmaceutical Product Development and Manufacture. pp. 9–24. https://doi.org/10.1002/9781119356189.ch2

Chi, Z., Wang, M., Yang, L., Li, X., Cong, X., Liu, S., Cai, B., 2013. Fourier transform near-infrared spectroscopy used for purity determination of rhein-l-arginine cocrystal (argirein). Anal. Sci. 29, 661–664. https://doi.org/10.2116/analsci.29.661

Childs, S.L., Hardcastle, K.I., 2007. Cocrystals of piroxicam with carboxylic acids. Cryst. Growth Des. 7, 1291–1304. https://doi.org/10.1021/cg060742p

Council of Europe, 2019. European Pharmacopoeia (Ph. Eur.).

Coutant, C., Skibic, M., Doddridge, G., Kemp, C., Sperry, D., 2010. In Vitro Monitoring of Dissolution of an Immediate Release Tablet by Focused Beam Reflectance Measurement. Mol. Pharm. 7. https://doi.org/10.1021/mp1001476

Crowley, M.E., Crean, A.M., 2015. Quality by design in an evolving manufacturing sector. Eur. J. Parenter. Pharm. Sci. 20, 63–69.

Da Xu, L., Xu, E.L., Li, L., 2018. Industry 4.0: state of the art and future trends. Int. J. Prod. Res. 56, 2941–2962. https://doi.org/10.1080/00207543.2018.1444806

Dabbagh, M.A., Taghipour, B., 2007. Investigation of Solid Dispersion Technique in Improvement of Physicochemical Characteristics of Ibuprofen Powder. Iran. J. Pharm. Sci. 3, 69–76.

Darby, M.L., Nikolaou, M., 2012. MPC: Current practice and challenges. Control Eng. Pract. 20, 328–342. https://doi.org/10.1016/j.conengprac.2011.12.004

Datta, S., Grant, D.J.W., 2004. Crystal structures of drugs: Advances in determination, prediction and engineering. Nat. Rev. Drug Discov. 3, 42–57.

https://doi.org/10.1038/nrd1280

De Beer, T., Burggraeve, A., Fonteyne, M., Saerens, L., Remon, J.P., Vervaet, C., 2011. Near infrared and Raman spectroscopy for the in-process monitoring of pharmaceutical production processes. Int. J. Pharm. 417, 32–47. https://doi.org/10.1016/j.ijpharm.2010.12.012

De Jong, S., 1993. SIMPLS: An alternative approach to partial least squares regression. Chemom. Intell. Lab. Syst. 18, 251–263. https://doi.org/10.1016/0169-7439(93)85002-X

De Juan, A., Jaumot, J., Tauler, R., 2014. Multivariate Curve Resolution (MCR). Solving the mixture analysis problem. Anal. Methods 6, 4964–4976. https://doi.org/10.1039/c4ay00571f

De Juan, A., Tauler, R., 2006. Multivariate Curve Resolution (MCR) from 2000: Progress in concepts and applications. Crit. Rev. Anal. Chem. https://doi.org/10.1080/10408340600970005

De Matas, M., De Beer, T., Folestad, S., Ketolainen, J., Lindén, H., Lopes, J.A., Oostra, W., Weimer, M., Öhrngren, P., Rantanen, J., 2016. Strategic framework for education and training in Quality by Design (QbD) and process analytical technology (PAT). Eur. J. Pharm. Sci. 90, 2–7. https://doi.org/10.1016/j.ejps.2016.04.024

Desai, P.M., Liew, C.V., Heng, P.W.S., 2016. Review of Disintegrants and the Disintegration Phenomena. J. Pharm. Sci. 105, 2545–2555. https://doi.org/10.1016/j.xphs.2015.12.019

Djuris, J., Djuric, Z., 2017. Modeling in the quality by design environment: Regulatory requirements and recommendations for design space and control strategy appointment. Int. J. Pharm. 533, 346–356. https://doi.org/10.1016/j.ijpharm.2017.05.070

Dressman, J., Krämer, J., 2005. Pharmaceutical dissolution testing, Pharmaceutical Dissolution Testing. Taylor & Francis. https://doi.org/10.1016/0168-3659(94)90064-7

Du, S., Wang, Y., Wu, S., Yu, B., Shi, P., Bian, L., Zhang, D., Hou, J., Wang, J., Gong, J., 2017. Two novel cocrystals of lamotrigine with isomeric bipyridines and in situ monitoring of the cocrystallization. Eur. J. Pharm. Sci. 110, 19–25. https://doi.org/10.1016/j.ejps.2017.06.001

Eddelbuettel, D., Sanderson, C., 2014. RcppArmadillo: Accelerating R with high-performance C++ linear algebra. Comput. Stat. Data Anal. 71, 1054–1063. https://doi.org/10.1016/j.csda.2013.02.005

Ehrburger, F., Lahaye, J., 1989. Behaviour of colloidal silicas during uniaxial compaction. J. Phys. 50, 1349–1359. https://doi.org/10.1051/jphys:0198900500110134900

El-Sakhawy, M., Hassan, M.L., 2007. Physical and mechanical properties of microcrystalline cellulose prepared from agricultural residues. Carbohydr. Polym. 67, 1–10. https://doi.org/10.1016/j.carbpol.2006.04.009

Emami, S., Siahi-Shadbad, M., Adibkia, K., Barzegar-Jalali, M., 2018. Recent advances in improving oral drug bioavailability by cocrystals. BioImpacts 8, 305–320. https://doi.org/10.15171/bi.2018.33

Engisch, W.E., Muzzio, F.J., 2014. Loss-in-Weight Feeding Trials Case Study: Pharmaceutical Formulation. J. Pharm. Innov. 10, 56–75. https://doi.org/10.1007/s12247-014-9206-1

Erxleben, A., 2016. Application of vibrational spectroscopy to study solid-state transformations of pharmaceuticals. Curr. Pharm. Des. 22, 4883-4911(29).

Esbensen, K.H., Swarbrick, B., 2019. Multivariate Data Analysis in Practice 6th Edition Multivariate Data Analysis, 6th Editio. ed. Camo Analytics.

European Medicines Agency, 2015. Reflection paper on the use of cocrystals of active substances in medicinal products.

European Medicines Agency, n.d. Quality by design [WWW Document]. URL https://www.ema.europa.eu/en/human-regulatory/research-development/quality-design (accessed 4.2.20).

FDA, 2015. Size, Shape and Other Physical Attributes of Generic Tablets and Capsules, Guidance for Industry.

FDA, 2012. Quality by Design for ANDAs : An Example for Immediate-Release Dosage Forms 1–107.

Fell, J.T., Newton, J.M., 1970. Determination of tablet strength by the diametral-compression test. J. Pharm. Sci. 59, 688–691. https://doi.org/10.1002/jps.2600590523

Foster, E.J., Moon, R.J., Agarwal, U.P., Bortner, M.J., Bras, J., Camarero-Espinosa, S., Chan, K.J., Clift, M.J.D., Cranston, E.D., Eichhorn, S.J., Fox, D.M., Hamad, W.Y., Heux, L., Jean, B., Korey, M., Nieh, W., Ong, K.J., Reid, M.S., Renneckar, S., Roberts, R., Shatkin, J.A., Simonsen, J., Stinson-Bagby, K., Wanasekara, N., Youngblood, J., 2018. Current characterization methods for cellulose nanomaterials. Chem. Soc. Rev. 47, 2609–2679. https://doi.org/10.1039/c6cs00895j

Fuertes, I., Miranda, A., Millán, M., Caraballo, I., 2006. Estimation of the percolation thresholds in acyclovir hydrophilic matrix tablets. Eur. J. Pharm. Biopharm. 64, 336–342. https://doi.org/10.1016/j.ejpb.2006.05.009

Gagniere, E., Puel, F., Mangin, D., Valour, J.P., Rivoire, A., Galvan, J.M., Monnier, O., Klein, J.P., 2012. In Situ Monitoring of Cocrystallization Processes - Complementary Use of Sensing Technologies. Chem. Eng. Technol. 35, 1039–1044. https://doi.org/10.1002/ceat.201100711

Gautam, R., Vanga, S., Ariese, F., Umapathy, S., 2015. Review of multidimensional data processing approaches for Raman and infrared spectroscopy. EPJ Tech. Instrum. 2, 1–38. https://doi.org/10.1140/epjti/s40485-015-0018-6

Gibis, M., Schuh, V., Weiss, J., 2015. Effects of carboxymethyl cellulose (CMC) and microcrystalline cellulose (MCC) as fat replacers on the microstructure and sensory characteristics of fried beef patties. Food Hydrocoll. 45, 236–246.

https://doi.org/10.1016/j.foodhyd.2014.11.021

Gohel, M.C., Jogani, P.D., 2005. A review of co-processed directly compressible excipients. J. Pharm. Pharm. Sci. 8, 76–93.

Gómez, D.A., Coello, J., Maspoch, S., 2019. The influence of particle size on the intensity and reproducibility of Raman spectra of compacted samples. Vib. Spectrosc. 100, 48–56. https://doi.org/10.1016/j.vibspec.2018.10.011

Gonçalves-Araújo, T., Rajabi-Siahboomi, A.R., Caraballo, I., 2008. Application of percolation theory in the study of an extended release Verapamil hydrochloride formulation. Int. J. Pharm. 361, 112–117. https://doi.org/10.1016/j.ijpharm.2008.05.022

Goud, N.R., Gangavaram, S., Suresh, K., Pal, S., Manjunatha, S.G., Nambiar, S., Nangia, A., 2012. Novel furosemide cocrystals and selection of high solubility drug forms. J. Pharm. Sci. 101, 664–680. https://doi.org/10.1002/jps.22805

Gregory, J., 2009. Monitoring particle aggregation processes. Adv. Colloid Interface Sci. 147–148, 109–123. https://doi.org/10.1016/j.cis.2008.09.003

Gubbi, J., Buyya, R., Marusic, S., Palaniswami, M., 2013. Internet of Things (IoT): A vision, architectural elements, and future directions. Futur. Gener. Comput. Syst. 29, 1645–1660. https://doi.org/10.1016/j.future.2013.01.010

Guyon, E., Roux, S., Bergman, D., 1987. Critical behaviour of electric failure thresholds in percolation. J. Phys. 48, 903–904. https://doi.org/10.1051/jphys:01987004806090300

Han, J.-H., Ferro, L., Vaidya, A., George, S., Pandey, A., Smith, B., 2009. Real-time Study of Disintegration and Dissolution in Solid Oral Dosage Forms with Focused Beam Reflectance Measurement (FBRM) Technology, in: AAPS Annual Meeting and Exposition Los Angeles, CA.

Hartwig, A., Hass, R., 2018. Monitoring Lactose Crystallization at Industrially Relevant Concentrations by Photon Density Wave Spectroscopy. Chem. Eng. Technol. 41, 1139–1146. https://doi.org/10.1002/ceat.201700685

Hausner, D.B., 2018. Enabling Continuous Direct Compression Pharma Manufacturing, in: IPSE Continuous Manufacturing Workshop.

Huang, J., Goolcharran, C., Ghosh, K., 2011. A Quality by Design approach to investigate tablet dissolution shift upon accelerated stability by multivariate methods. Eur. J. Pharm. Biopharm. 78, 141–150. https://doi.org/10.1016/j.ejpb.2010.12.012

Hwang, K.M., Cho, C.H., Tung, N.T., Kim, J.Y., Rhee, Y.S., Park, E.S., 2017. Release kinetics of highly porous floating tablets containing cilostazol. Eur. J. Pharm. Biopharm. 115, 39–51. https://doi.org/10.1016/j.ejpb.2017.01.027

Ibrahim, H.G., 1985. Observations on the dissolution behavior of a tablet formulation: Effect of compression forces. J. Pharm. Sci. 74, 575–577. https://doi.org/10.1002/jps.2600740519

Ilkka, J., Paronen, P., 1993. Prediction of the compression behaviour of powder

mixtures by the Heckel equation. Int. J. Pharm. 94, 181–187. https://doi.org/10.1016/0378-5173(93)90022-8

Inoue, M., Hisada, H., Koide, T., Carriere, J., Heyler, R., Fukami, T., 2017. Real-Time Formation Monitoring of Cocrystals with Different Stoichiometries Using Probe-Type Low-Frequency Raman Spectroscopy. Ind. Eng. Chem. Res. 56, 12693–12697. https://doi.org/10.1021/acs.iecr.7b03141

International Council for Harmonisation, 2019. ICH M9 Biopharmaceutics classification system-based biowaivers.

International Council for Harmonisation, 2018. ICH Q13 Continuous Manufacturing of Drug Substances and Drug Products.

International Council for Harmonisation, 2014. ICH Q12 Technical and regulatory considerations for pharmaceutical product lifecycle management.

International Council for Harmonisation, 2012. ICH Q 11 Development and manufacture of drug substances (chemical entities and biotechnological/biological entities).

International Council for Harmonisation, 2008. ICH Q10 Pharmaceutical quality system.

International Council for Harmonisation, 2005a. ICH Q8 (R2) Pharmaceutical development.

International Council for Harmonisation, 2005b. ICH Q9 Quality risk management.

International Council for Harmonisation, 1999. ICH Q6A - Q6B Specifications.

Ishihara, S., Hattori, Y., Otsuka, M., 2019. MCR-ALS analysis of IR spectroscopy and XRD for the investigation of ibuprofen - nicotinamide cocrystal formation. Spectrochim. Acta - Part A Mol. Biomol. Spectrosc. 221, 117142. https://doi.org/10.1016/j.saa.2019.117142

Islam, M.T., Scoutaris, N., Maniruzzaman, M., Moradiya, H.G., Halsey, S.A., Bradley, M.S.A., Chowdhry, B.Z., Snowden, M.J., Douroumis, D., 2015. Implementation of transmission NIR as a PAT tool for monitoring drug transformation during HME processing. Eur. J. Pharm. Biopharm. 96, 106–116. https://doi.org/10.1016/j.ejpb.2015.06.021

Järvinen, M.A., Paaso, J., Paavola, M., Leiviskä, K., Juuti, M., Muzzio, F., Järvinen, K., 2013. Continuous direct tablet compression: Effects of impeller rotation rate, total feed rate and drug content on the tablet properties and drug release. Drug Dev. Ind. Pharm. 39, 1802–1808. https://doi.org/10.3109/03639045.2012.738681

Jiang, M., Zhu, X., Molaro, M.C., Rasche, M.L., Zhang, H., Chadwick, K., Raimondo, D.M., Kim, K.-K.K., Zhou, L., Zhu, Z., Wong, M.H., O'Grady, D., Hebrault, D., Tedesco, J., Braatz, R.D., 2014. Modification of Crystal Shape through Deep Temperature Cycling. Ind. Eng. Chem. Res. 53, 5325–5336. https://doi.org/10.1021/ie400859d

Joliffe, I., Morgan, B., 1992. Principal component analysis and exploratory factor

analysis. Stat. Methods Med. Res. 1, 69–95. https://doi.org/10.1177/096228029200100105

Jolliffe, I.T., 1982. A Note on the Use of Principal Components in Regression. Appl. Stat. 31, 300. https://doi.org/10.2307/2348005

Juran, J., 1992. Juran on quality by design: the new steps for planning quality into goods and services., Simon and Schuster. Simon and Schuster.

Kazarian, S.G., Ewing, A. V., 2013. Applications of Fourier transform infrared spectroscopic imaging to tablet dissolution and drug release. Expert Opin. Drug Deliv. https://doi.org/10.1517/17425247.2013.801452

Kelly, A.L., Gough, T., Dhumal, R.S., Halsey, S.A., Paradkar, A., 2012. Monitoring ibuprofen-nicotinamide cocrystal formation during solvent free continuous cocrystallization (SFCC) using near infrared spectroscopy as a PAT tool. Int. J. Pharm. 426, 15–20. https://doi.org/10.1016/j.ijpharm.2011.12.033

Ketterhagen, W.R., Am Ende, M.T., Hancock, B.C., 2009. Process modeling in the pharmaceutical industry using the discrete element method. J. Pharm. Sci. 98, 442–470. https://doi.org/10.1002/jps.21466

Kimura, G., Betz, G., Leuenberger, H., 2007. Influence of Loading Volume of Mefenamic Acid on Granules and Tablet Characteristics Using a Compaction Simulator. Pharm. Dev. Technol. 12, 627–635. https://doi.org/10.1080/10837450701634037

Kimura, G., Puchkov, M., Leuenberger, H., 2013. An attempt to calculate in silico disintegration time of tablets containing mefenamic acid, a low water-soluble drug. J. Pharm. Sci. 102, 2166–2178. https://doi.org/10.1002/jps.23541

Kojima, T., Tsutsumi, S., Yamamoto, K., Ikeda, Y., Moriwaki, T., 2010. High-throughput cocrystal slurry screening by use of in situ Raman microscopy and multi-well plate. Int. J. Pharm. 399, 52–59. https://doi.org/10.1016/j.ijpharm.2010.07.055

Kourti, T., Lepore, J., Liesum, L., Nasr, M., Chatterjee, S., Moore, C.M.V., Korakianiti, E., 2014. Scientific and regulatory considerations for implementing mathematical models in the quality by design (QbD) framework (part 2). Pharm. Eng. 34.

Kozicki, J., 2007. Application of discrete models to describe the fracture process in brittle materials. Gdansk Univ. Technol.

Kuentz, M., Leuenberger, H., 2000. A new theoretical approach to tablet strength of a binary mixture consisting of a well and a poorly compactable substance. Eur. J. Pharm. Biopharm. 49, 151–159. https://doi.org/10.1016/S0939-6411(99)00078-8

Kuentz, M., Leuenberger, H., 1999. Pressure susceptibility of polymer tablets as a critical property: A modified Heckel equation. J. Pharm. Sci. 88, 174–179. https://doi.org/10.1021/js980369a

Kuentz, M., Leuenberger, H., 1998. Modified Young's modulus of microcrystalline cellulose tablets and the directed continuum percolation model. Pharm. Dev. Technol. 3, 13–19. https://doi.org/10.3109/10837459809028475

Kuentz, M., Leuenberger, H., Kolb, M., 1999. Fracture in disordered media and tensile strength of microcrystalline cellulose tablets at low relative densities. Int. J. Pharm. 182, 243–255. https://doi.org/10.1016/S0378-5173(99)00081-2

Kushner IV, J., 2013. Utilizing quantitative certificate of analysis data to assess the amount of excipient lot-to-lot variability sampled during drug product development. Pharm. Dev. Technol. 18, 333–342. https://doi.org/10.3109/10837450.2011.604784

Kushner, J., Langdon, B.A., Hiller, J.I., Carlson, G.T., 2011. Examining the impact of excipient material property variation on drug product quality attributes: A quality-by-design study for a roller compacted, immediate release tablet. J. Pharm. Sci. 100, 2222–2239. https://doi.org/10.1002/jps.22455

Landín, M., Martínez-Pacheco, R., Gómez-Amoza, J.L., Souto, C., Concheiro, A., Rowe, R.C., 1993. Effect of batch variation and source of pulp on the properties of microcrystalline cellulose. Int. J. Pharm. 91, 133–141. https://doi.org/10.1016/0378-5173(93)90332-A

LaPlant, F., Zhang, X., 2005. Quantitation of polymorphs in drug product by Raman spectroscopy. Am. Pharm. Rev.

Larkin, P., 2017. Infrared and Raman spectroscopy: principles and spectral interpretation.

Lasi, H., Fettke, P., Kemper, H.G., Feld, T., Hoffmann, M., 2014. Industry 4.0. Bus. Inf. Syst. Eng. 6, 239–242. https://doi.org/10.1007/s12599-014-0334-4

Lawson, C., Hanson, R., 1995. Solving least squares problems. Society for industrial and applied mathematics, illustrate. ed. SIAM, 1995.

Lawton, W.H., Sylvestre, E.A., 1971. Self modeling curve resolution. Technometrics 13, 617–633. https://doi.org/10.1080/00401706.1971.10488823

Leane, M., Pitt, K., Reynolds, G., Anwar, J., Charlton, S., Crean, A., Creekmore, R., Davies, C., DeBeer, T., De-Matas, M., Djemai, A., Douroumis, D., Gaisford, S., Gamble, J., Stone, E.H., Kavanagh, A., Khimyak, Y., Kleinebudde, P., Moreton, C., Paudel, A., Storey, R., Toschkoff, G., Vyas, K., 2015. A proposal for a drug product Manufacturing Classification System (MCS) for oral solid dosage forms. Pharm. Dev. Technol. 20, 12–21. https://doi.org/10.3109/10837450.2014.954728

Leane, M., Pitt, K., Reynolds, G.K., Dawson, N., Ziegler, I., Szepes, A., Crean, A.M., Dall Agnol, R., 2018. Manufacturing classification system in the real world: factors influencing manufacturing process choices for filed commercial oral solid dosage formulations, case studies from industry and considerations for continuous processing. Pharm. Dev. Technol. 23, 964–977. https://doi.org/10.1080/10837450.2018.1534863

Lee, J., Bagheri, B., Kao, H.A., 2015. A Cyber-Physical Systems architecture for Industry 4.0-based manufacturing systems. Manuf. Lett. 3, 18–23. https://doi.org/10.1016/j.mfglet.2014.12.001

Lee, K.S., Kim, K.J., Ulrich, J., 2014. In situ monitoring of cocrystallization of salicylic acid-4,4'- dipyridyl in solution using raman spectroscopy. Cryst. Growth Des. 14,

2893–2899. https://doi.org/10.1021/cg5001864

Lee, S.L., O'Connor, T.F., Yang, X., Cruz, C.N., Chatterjee, S., Madurawe, R.D., Moore, C.M.V., Yu, L.X., Woodcock, J., 2015. Modernizing Pharmaceutical Manufacturing: from Batch to Continuous Production. J. Pharm. Innov. 10, 191–199. https://doi.org/10.1007/s12247-015-9215-8

Leu, R., Leuenberger, H., 1993. The application of percolation theory to the compaction of pharmaceutical powders. Int. J. Pharm. 90, 213–219. https://doi.org/10.1016/0378-5173(93)90193-J

Leuenberger, H., 1999. Application of percolation theory in powder technology. Adv. Powder Technol. https://doi.org/10.1163/156855299X00190

Leuenberger, H., Ineichen, L., 1997. Percolation theory and physics of compression. Eur. J. Pharm. Biopharm. 44, 269–272. https://doi.org/10.1016/S0939-6411(97)00130-6

Leuenberger, H., Leu, R., 1992. Formation of a tablet: A site and bond percolation phenomenon. J. Pharm. Sci. 81, 976–982. https://doi.org/10.1002/jps.2600811004

Leuenberger, H., Leu, R., Bonny, J.D., 1992. Application of percolation theory and fractal geometry to tablet compaction. Drug Dev. Ind. Pharm. 18, 723–766. https://doi.org/10.3109/03639049209058559

Lin, J., Chen, H., 2018. Effect of particle morphologies on the percolation of particulate porous media: A study of superballs. Powder Technol. 335, 388–400. https://doi.org/10.1016/j.powtec.2018.05.015

Liu, L.X., Marziano, I., Bentham, A.C., Litster, J.D., E.T.White, Howes, T., 2008. Effect of particle properties on the flowability of ibuprofen powders. Int. J. Pharm. 362, 109–117. https://doi.org/10.1016/j.ijpharm.2008.06.023

Liu, X., Sun, D., Wang, F., Wu, Y., Chen, Y., Wang, L., 2011. Monitoring of antisolvent crystallization of sodium scutellarein by combined FBRM–PVM–NIR. J. Pharm. Sci. 100, 2452–2459. https://doi.org/10.1002/jps.22439

Loschen, C., Klamt, A., 2015. Solubility prediction, solvate and cocrystal screening as tools for rational crystal engineering. J. Pharm. Pharmacol. 67, 803–811. https://doi.org/10.1111/jphp.12376

Lukin, S., Stolar, T., Tireli, M., Blanco, M.V., Babić, D., Friščić, T., Užarević, K., Halasz, I., 2017. Tandem In Situ Monitoring for Quantitative Assessment of Mechanochemical Reactions Involving Structurally Unknown Phases. Chem. - A Eur. J. 23, 13941–13949. https://doi.org/10.1002/chem.201702489

Mangal, H., Kleinebudde, P., 2018. Is the adjustment of the impeller speed a reliable attempt to influence granule size in continuous dry granulation? Adv. Powder Technol. 29, 1339–1347. https://doi.org/10.1016/j.apt.2018.02.029

Manne, R., 1995. On the resolution problem in hyphenated chromatography. Chemom. Intell. Lab. Syst. 27, 89–94. https://doi.org/10.1016/0169-7439(95)80009-X

Manzano, T., Langer, G., 2018. Getting Ready for Pharma 4.0. Data integrity in cloud and big data applications. Tech. Inf. Syst. 72–79.

Markl, D., Wahl, P.R., Menezes, J.C., Koller, D.M., Kavsek, B., Francois, K., Roblegg, E., Khinast, J.G., 2013. Supervisory control system for monitoring a pharmaceutical hot melt extrusion process. AAPS PharmSciTech 14, 1034–1044. https://doi.org/10.1208/s12249-013-9992-7

Markl, D., Zeitler, J.A., 2017. A Review of Disintegration Mechanisms and Measurement Techniques. Pharm. Res. 34, 890–917. https://doi.org/10.1007/s11095-017-2129-z

Martens, H., 1979. Factor analysis of chemical mixtures. Non-negative Factor Solutions for Spectra of Cereal Amino Acids1 1 Presented at the International Conference on Computers and Optimization in Analytical Chemistry, Amsterdam, April 1978. Anal. Chim. Acta 112, 423–442. https://doi.org/10.1016/S0003-2670(01)85040-6

Mascia, S., Heider, P.L., Zhang, H., Lakerveld, R., Benyahia, B., Barton, P.I., Braatz, R.D., Cooney, C.L., Evans, J.M.B., Jamison, T.F., Jensen, K.F., Myerson, A.S., Trout, B.L., 2013. End-to-end continuous manufacturing of pharmaceuticals: Integrated synthesis, purification, and final dosage formation. Angew. Chemie - Int. Ed. 52, 12359–12363. https://doi.org/10.1002/anie.201305429

Mattonai, M., Pawcenis, D., del Seppia, S., Łojewska, J., Ribechini, E., 2018. Effect of ball-milling on crystallinity index, degree of polymerization and thermal stability of cellulose. Bioresour. Technol. 270, 270–277. https://doi.org/10.1016/j.biortech.2018.09.029

Mazivila, S.J., Castro, R.A.E., Leitão, J.M.M., Esteves da Silva, J.C.G., 2019. At-line green synthesis monitoring of new pharmaceutical co-crystals lamivudine:theophylline polymorph I and II, quantification of polymorph I among its APIs using FT-IR spectroscopy and MCR-ALS. J. Pharm. Biomed. Anal. 169, 235–244. https://doi.org/10.1016/j.jpba.2019.03.014

Mazivila, S.J., Olivieri, A.C., 2018. Chemometrics coupled to vibrational spectroscopy and spectroscopic imaging for the analysis of solid-phase pharmaceutical products: A brief review on non-destructive analytical methods. Trends Anal. Chem. 108, 74–87. https://doi.org/10.1016/j.trac.2018.08.013

McGlinchey, D. (Ed.), 2005. Characterisation of Bulk Solids. Blackwell Publishing.

Mei, W., Yu, G., 2018. basicTrendline: Add Trendline and Confidence Interval of Basic Regression Models to Plot.

Meireles, J.E., Schweiger, A.K., Cavender-Bares, J., 2018. spectrolab: Class and Methods for Hyperspectral Data.

Mendieta, J., Díaz-Cruz, M.S., Esteban, M., Tauler, R., 1998. Multivariate curve resolution: A possible tool in the detection of intermediate structures in protein folding. Biophys. J. 74, 2876–2888. https://doi.org/10.1016/S0006-3495(98)77994-9

Menning, M., 2016. Towards a Fundamental Understanding of Particle Kinetics

through Dynamic Characterization of Pharmaceutical Solid Dosage Forms. University College Dublin.

Metzler, C., Bullard, J.W., Waldo, M., McCarty, K., Do, M., 2017. Using a Focused Beam Reflectance Measurement (FBRM) Probe to Characterize Tablet Disintegration Behavior As a Function of Drug Product Processing Conditions, in: AIChE Annual Meeting, Minneapolis. p. 720(a).

Mevik, B.-H., Wehrens, R., 2015. Introduction to the pls Package. Help Sect. "pls" Packag. RStudio Softw. 1–23.

Meyer, H., Van Der Schoot, P., Schilling, T., 2015. Percolation in suspensions of polydisperse hard rods: Quasi universality and finite-size effects. J. Chem. Phys. 143, 044901. https://doi.org/10.1063/1.4926946

Mihranyan, A., Llagostera, A.P., Karmhag, R., Strømme, M., Ek, R., 2004. Moisture sorption by cellulose powders of varying crystallinity. Int. J. Pharm. 269, 433–442. https://doi.org/10.1016/j.ijpharm.2003.09.030

Miller, T.C., Havrilla, G.J., 2005. Elemental imaging for pharmaceutical tablet formulation analysis by micro X-ray fluorescence. Powder Diffr. 20, 153–157. https://doi.org/10.1154/1.1913720

Mitchell, N.A., Frawley, P.J., Ó'Ciardhá, C.T., 2011. Nucleation kinetics of paracetamol–ethanol solutions from induction time experiments using Lasentec FBRM®. J. Cryst. Growth 321, 91–99. https://doi.org/https://doi.org/10.1016/j.jcrysgro.2011.02.027

Mittapalli, S., Chaitanya Mannava, M.K., Sahoo, R., Nangia, A., 2019. Cocrystals, Salts, and Supramolecular Gels of Nonsteroidal Anti-Inflammatory Drug Niflumic Acid. Cryst. Growth Des. 19, 219–230. https://doi.org/10.1021/acs.cgd.8b01298

Mockus, L., Peterson, J.J., Lainez, J.M., Reklaitis, G. V., 2015. Batch-to-Batch Variation: A Key Component for Modeling Chemical Manufacturing Processes. Org. Process Res. Dev. 19, 908–914. https://doi.org/10.1021/op500244f

Mohamed, F.A.A., Roberts, M., Seton, L., Ford, J.L., Levina, M., Rajabi-Siahboomi, A.R., 2015. The effect of HPMC particle size on the drug release rate and the percolation threshold in extended-release mini-tablets. Drug Dev. Ind. Pharm. 41, 70–78. https://doi.org/10.3109/03639045.2013.845843

Narang, A.S., 2015. Addressing excipient variability in formulation design and drug development, in: Excipient Applications in Formulation Design and Drug Delivery. Springer International Publishing, pp. 541–567. https://doi.org/10.1007/978-3-319-20206-8_18

Nasr, M.M., Krumme, M., Matsuda, Y., Trout, B.L., Badman, C., Mascia, S., Cooney, C.L., Jensen, K.D., Florence, A., Johnston, C., Konstantinov, K., Lee, S.L., 2017. Regulatory Perspectives on Continuous Pharmaceutical Manufacturing: Moving From Theory to Practice: September 26-27, 2016, International Symposium on the Continuous Manufacturing of Pharmaceuticals. J. Pharm. Sci. 106, 3199–3206. https://doi.org/10.1016/j.xphs.2017.06.015

Ng, K.S., 2013. A Simple Explanation of Partial least squares 1–10.

https://doi.org/10.1.1.352.4447

Nickerson, B., Kong, A., Gerst, P., Kao, S., 2018. Correlation of dissolution and disintegration results for an immediate-release tablet. J. Pharm. Biomed. Anal. 150, 333–340. https://doi.org/10.1016/j.jpba.2017.12.017

Nigro, B., Grimaldi, C., Ryser, P., Chatterjee, A.P., Van Der Schoot, P., 2013. Quasiuniversal connectedness percolation of polydisperse rod systems. Phys. Rev. Lett. 110, 015701. https://doi.org/10.1103/PhysRevLett.110.015701

Nokhodchi, A., 2005. An overview of the effect of moisture on compaction and compression. Pharm. Technol. 6, 46–66.

Nokhodchi, A., Rubinstein, M.H., Larhrib, H., Guyot, J.C., 1995. The effect of moisture on the properties of ibuprofen tablets. Int. J. Pharm. 118, 191–197. https://doi.org/10.1016/0378-5173(94)00354-8

Ntschi, L.J., Bolboac, S.-D., 2006. Pearson versus Spearman, Kendall's Tau Correlation Analysis on Structure-Activity Relationships of Biologic Active Compounds. Leonardo J. Sci. 5, 179–200.

Nunes de Barros, F., Bhaskar, A., Singh, R., 2017. A Validated Model for Design and Evaluation of Control Architectures for a Continuous Tablet Compaction Process. Processes 5, 76. https://doi.org/10.3390/pr5040076

O'Regan, C., 2018. Study of acid hydrolysis based synthesis of microcrystalline cellulose. University College Cork.

Otaki, T., Tanabe, Y., Kojima, T., Miura, M., Ikeda, Y., Koide, T., Fukami, T., 2018. In situ monitoring of cocrystals in formulation development using low-frequency Raman spectroscopy. Int. J. Pharm. 542, 56–65. https://doi.org/10.1016/j.ijpharm.2018.03.008

Paduszyński, K., 2017. An overview of the performance of the COSMO-RS approach in predicting the activity coefficients of molecular solutes in ionic liquids and derived properties at infinite dilution. Phys. Chem. Chem. Phys. 19, 11835–11850. https://doi.org/10.1039/c7cp00226b

Page, T., Dubina, H., Fillipi, G., Guidat, R., Patnaik, S., Poechlauer, P., Shering, P., Guinn, M., Mcdonnell, P., Johnston, C., 2015. Equipment and analytical companies meeting continuous challenges May 20-21, 2014 continuous manufacturing symposium. J. Pharm. Sci. https://doi.org/10.1002/jps.24282

Patel, S., Kaushal, A.M., Bansal, A.K., 2006. Compression physics in the formulation development of tablets. Crit. Rev. Ther. Drug Carrier Syst. 23, 1–65. https://doi.org/10.1615/critrevtherdrugcarriersyst.v23.i1.10

Pearson, K., 1901. LIII. On lines and planes of closest fit to systems of points in space . London, Edinburgh, Dublin Philos. Mag. J. Sci. 2, 559–572. https://doi.org/10.1080/14786440109462720

Pérez Gago, A., Kleinebudde, P., 2017. MCC–mannitol mixtures after roll compaction/dry granulation: percolation thresholds for ribbon microhardness and granule size distribution. Pharm. Dev. Technol. 22, 764–774. https://doi.org/10.3109/10837450.2016.1163388

Pomerantsev, A.L., Rodionova, O.Y., 2012. Process analytical technology: A critical view of the chemometricians. J. Chemom. https://doi.org/10.1002/cem.2445

Potter, C.J., 2009. PQLI application of science- and risk-based approaches (ICH Q8, Q9, and Q10) to existing products. J. Pharm. Innov. 4, 4–23. https://doi.org/10.1007/s12247-009-9051-9

Powell, K.A., Bartolini, G., Wittering, K.E., Saleemi, A.N., Wilson, C.C., Rielly, C.D., Nagy, Z.K., 2015. Toward Continuous Crystallization of Urea-Barbituric Acid: A Polymorphic Co-Crystal System. Cryst. Growth Des. 15, 4821–4836. https://doi.org/10.1021/acs.cgd.5b00599

Powell, K.A., Croker, D.M., Rielly, C.D., Nagy, Z.K., 2016. PAT-based design of agrochemical co-crystallization processes: A case-study for the selective crystallization of 1:1 and 3:2 co-crystals of p-toluenesulfonamide/triphenylphosphine oxide. Chem. Eng. Sci. 152, 95–108. https://doi.org/10.1016/j.ces.2016.06.005

Pozo Valenzuela, C., Rodriguez-Llamazares, S., 2016. spftir: Pre-Processing and Analysis of Mid-Infrared Spectral Region.

Qiao, N., Li, M., Schlindwein, W., Malek, N., Davies, A., Trappitt, G., 2011. Pharmaceutical cocrystals: An overview. Int. J. Pharm. https://doi.org/10.1016/j.ijpharm.2011.07.037

Queiroz, A.L.P., Faisal, W., Devine, K., Garvie-Cook, H., Vucen, S., Crean, A.M., 2019. The application of percolation threshold theory to predict compaction behaviour of pharmaceutical powder blends. Powder Technol. 354, 188–198. https://doi.org/10.1016/j.powtec.2019.05.027

R Core Team, 2019. R: A language and environment for statistical computing. https://doi.org/10.1016/j.dendro.2008.01.002

Rantanen, J., Khinast, J., 2015. The Future of Pharmaceutical Manufacturing Sciences. J. Pharm. Sci. 104, 3612–3638. https://doi.org/10.1002/jps.24594

Rasenack, N., Mü, B.W., 2002. Crystal habit and tableting behavior. Int. J. Pharm. 244, 45–57.

Rathbone, M.J., Hadgraft, J., Roberts, M.S. (Eds.), 2003. Modified-Release Drug Delivery Technology. Marcel Dekker, Inc. https://doi.org/10.1016/j.ejpb.2003.10.011

Rathore, A.S., Winkle, H., 2009. Quality by design for biopharmaceuticals. Nat. Biotechnol. https://doi.org/10.1038/nbt0109-26

Reddy, J.N., 1989. An Introduction to the Finite Element Method. J. Press. Vessel Technol. 111, 348–349. https://doi.org/10.1115/1.3265687

Reich, G., 2005. Near-infrared spectroscopy and imaging: Basic principles and pharmaceutical applications. Adv. Drug Deliv. Rev. 57, 1109–1143. https://doi.org/10.1016/j.addr.2005.01.020

Remenar, J.F., Morissette, S.L., Peterson, M.L., Moulton, B., MacPhee, J.M., Guzmán, H.R., Almarsson, Ö., 2003. Crystal engineering of novel cocrystals of a triazole

drug with 1,4-dicarboxylic acids. J. Am. Chem. Soc. 125, 8456–8457. https://doi.org/10.1021/ja035776p

Rencher, A.C., 2003. Methods of multivariate analysis. J. Wiley.

Rodrigues, M., 2019. High-throughput screening of hydrochlorothiazide cocrystals by vibrational spectroscopy. Universidade do Porto.

Rodrigues, M., Baptista, B., Lopes, J.A., Sarraguça, M.C., 2018a. Pharmaceutical cocrystallization techniques. Advances and challenges. Int. J. Pharm. https://doi.org/10.1016/j.ijpharm.2018.06.024

Rodrigues, M., Lopes, J., Guedes, A., Sarraguça, J., Sarraguça, M., 2019. Considerations on high-throughput cocrystals screening by ultrasound assisted cocrystallization and vibrational spectroscopy. Spectrochim. Acta - Part A Mol. Biomol. Spectrosc. 229. https://doi.org/10.1016/j.saa.2019.117876

Rodrigues, M., Lopes, J., Sarraguça, M., 2018b. Vibrational spectroscopy for cocrystals screening. A comparative study. Molecules 23, 3263. https://doi.org/10.3390/molecules23123263

Rogers, L., Jensen, K.F., 2019. Continuous manufacturing-the Green Chemistry promise? Green Chem. 21, 3481–3498. https://doi.org/10.1039/c9gc00773c

Ross, S.A., Lamprou, D.A., Douroumis, D., 2016. Engineering and manufacturing of pharmaceutical co-crystals: A review of solvent-free manufacturing technologies. Chem. Commun. https://doi.org/10.1039/c6cc01289b

Rowe, R.C., McKillop, A.G., Bray, D., 1994. The effect of batch and source variation on the crystallinity of microcrystalline cellulose. Int. J. Pharm. 101, 169–172. https://doi.org/10.1016/0378-5173(94)90087-6

Rowe, R.C., Sheskey, P.J., Quinn, M.E., 2009. Handbook Of Pharmaceutical Exipients, Pharmaceutical Press. Pharmaceutical Press.

RStudio Team, 2019. RStudio: Integrated Development Environment for R.

Sanphui, P., Devi, V.K., Clara, D., Malviya, N., Ganguly, S., Desiraju, G.R., 2015. Cocrystals of hydrochlorothiazide: Solubility and diffusion/permeability enhancements through drug-coformer interactions. Mol. Pharm. 12, 1615–1622. https://doi.org/10.1021/acs.molpharmaceut.5b00020

Sanphui, P., Rajput, L., 2014. Tuning solubility and stability of hydrochloro-thiazide co-crystals. Acta Crystallogr. Sect. B Struct. Sci. Cryst. Eng. Mater. 70, 81–90. https://doi.org/10.1107/S2052520613026917

Santomaso, A., Lazzaro, P., Canu, P., 2003. Powder flowability and density ratios: The impact of granules packing. Chem. Eng. Sci. 58, 2857–2874. https://doi.org/10.1016/S0009-2509(03)00137-4

Sarraguça, M.C., Lopes, J.A., 2009. Quality control of pharmaceuticals with NIR: From lab to process line. Vib. Spectrosc. 49, 204–210. https://doi.org/10.1016/j.vibspec.2008.07.013

Sarraguça, M.C., Paisana, M., Pinto, J., Lopes, J.A., 2016. Real-time monitoring of cocrystallization processes by solvent evaporation: A near infrared study. Eur. J.

Pharm. Sci. 90, 76–84. https://doi.org/10.1016/j.ejps.2015.12.025

Sarraguça, M.C., Ribeiro, P.R.S., Santos, A.O., Silva, M.C.D., Lopes, J.A., 2014. A PAT approach for the on-line monitoring of pharmaceutical co-crystals formation with near infrared spectroscopy. Int. J. Pharm. 471, 478–484. https://doi.org/10.1016/j.ijpharm.2014.06.003

Sarraguça, M.C., Ribeiro, P.R.S., Santos, A.O.D., Lopes, J.A., 2015. Batch Statistical Process Monitoring Approach to a Cocrystallization Process. J. Pharm. Sci. 104, 4099–4108. https://doi.org/10.1002/jps.24623

Schäfer, A., Huber, C., Ahlrichs, R., 1994. Fully optimized contracted Gaussian basis sets of triple zeta valence quality for atoms Li to Kr. J. Chem. Phys. 100, 5829–5835. https://doi.org/10.1063/1.467146

Schenzel, K., Fischer, S., Brendler, E., 2005. New method for determining the degree of cellulose I crystallinity by means of FT Raman spectroscopy. Cellulose 12, 223–231. https://doi.org/10.1007/s10570-004-3885-6

Schott, H., 1992. Swelling kinetics of polymers. J. Macromol. Sci. Part B 31, 1–9. https://doi.org/10.1080/00222349208215453

Schultheiss, N., Bethune, S., Henck, J.O., 2010. Nutraceutical cocrystals: Utilizing pterostilbene as a cocrystal former. CrystEngComm 12, 2436–2442. https://doi.org/10.1039/c002045a

Segal, L., Creely, J.J., Martin, A.E., Conrad, C.M., 1959. An Empirical Method for Estimating the Degree of Crystallinity of Native Cellulose Using the X-Ray Diffractometer. Text. Res. J. 29, 786–794. https://doi.org/10.1177/004051755902901003

Shan, N., Perry, M.L., Weyna, D.R., Zaworotko, M.J., 2014. Impact of pharmaceutical cocrystals: The effects on drug pharmacokinetics. Expert Opin. Drug Metab. Toxicol. https://doi.org/10.1517/17425255.2014.942281

Sharma, M., Sharma, V., Majumdar, D.K., 2014. Influence of Tableting on Enzymatic Activity of Papain along with Determination of Its Percolation Threshold with Microcrystalline Cellulose. Int. Sch. Res. Not. 2014, 1–8. https://doi.org/10.1155/2014/140891

Sheng, F., Chow, P.S., Yu, Z.Q., Tan, R.B.H., 2016. Online Classification of Mixed Co-Crystal and Solute Suspensions using Raman Spectroscopy. Org. Process Res. Dev. 20, 1068–1074. https://doi.org/10.1021/acs.oprd.6b00123

Shi, L., Feng, Y., Sun, C.C., 2011. Initial moisture content in raw material can profoundly influence high shear wet granulation process. Int. J. Pharm. 416, 43–48. https://doi.org/10.1016/j.ijpharm.2011.05.080

Silva, A.F.T.T., Sarraguça, M.C., Ribeiro, P.R., Santos, A.O., De Beer, T., Lopes, J.A., 2017. Statistical process control of cocrystallization processes: A comparison between OPLS and PLS. Int. J. Pharm. 520, 29–38. https://doi.org/10.1016/j.ijpharm.2017.01.052

Silva Filho, S.F., Pereira, A.C., Sarraguça, J.M.G., Sarraguça, M.C., Lopes, J., Façanha Filho, P. de F., dos Santos, A.O., da Silva Ribeiro, P.R., 2018. Synthesis of a

Glibenclamide Cocrystal: Full Spectroscopic and Thermal Characterization. J. Pharm. Sci. 107, 1597–1604. https://doi.org/10.1016/j.xphs.2018.01.029

Simon, M., Wood, B., Ferguson, S., Glennon, B., Jones, R.C., 2019. Diastereomeric salt crystallization of chiral molecules via sequential coupled-Batch operation. AIChE J. 65, 604–616. https://doi.org/10.1002/aic.16466

Simone, E., Sal, A., Nagy, Z., 2015. In Situ Monitoring of Polymorphic Transformations Using a Composite Sensor Array of Raman, NIR, and ATR-UV/vis Spectroscopy, FBRM, and PVM for an Intelligent Decision Support System. Org. Process Res. Dev. 19, 167–177. https://doi.org/10.1021/op5000122

Sin, G., Gernaey, K. V., Lantz, A.E., 2009. Good modeling practice for PAT applications: Propagation of input uncertainty and sensitivity analysis, in: Biotechnology Progress. American Chemical Society (ACS), pp. 1043–1053. https://doi.org/10.1002/btpr.166

Sinha, A.R., Tomar, M., Sinha, R., Singh, A.K., 2018. Typical Physical Attributes Of Microcrystalline Cellulose Dried By Spray, Spin Flash And Bulk Drier And Their Resultant Effects On Tablet Properties. Artic. Int. J. Pharm. Sci. Res. 9, 1545–1554. https://doi.org/10.13040/IJPSR.0975-8232.9(4).1545-54

Sinnecker, S., Rajendran, A., Klamt, A., Diedenhofen, M., Neese, F., 2006. Calculation of solvent shifts on electronic g-tensors with the conductor-like screening model (COSMO) and its self-consistent generalization to real solvents (direct COSMO-RS). J. Phys. Chem. A 110, 2235–2245. https://doi.org/10.1021/jp056016z

Soares, F.L.F., Carneiro, R.L., 2017. In-line monitoring of cocrystallization process and quantification of carbamazepine-nicotinamide cocrystal using Raman spectroscopy and chemometric tools. Spectrochim. Acta - Part A Mol. Biomol. Spectrosc. 180, 1–8. https://doi.org/10.1016/j.saa.2017.02.045

Soares, F.L.F., Carneiro, R.L., 2013. Green synthesis of ibuprofen-nicotinamide cocrystals and in-line evaluation by Raman spectroscopy. Cryst. Growth Des. 13, 1510–1517. https://doi.org/10.1021/cg3017112

Sommeregger, W., Sissolak, B., Kandra, K., von Stosch, M., Mayer, M., Striedner, G., 2017. Quality by control: Towards model predictive control of mammalian cell culture bioprocesses. Biotechnol. J. https://doi.org/10.1002/biot.201600546

Spes, J., Levin, W., 2018. Big Data, Pharma 4.0 and Legacy Products [WWW Document]. https://doi.org/10.1029/2009GL041262

Stauffer, F., Vanhoorne, V., Pilcer, G., Chavez, P.F., Rome, S., Schubert, M.A., Aerts, L., De Beer, T., 2018. Raw material variability of an active pharmaceutical ingredient and its relevance for processability in secondary continuous pharmaceutical manufacturing. Eur. J. Pharm. Biopharm. 127, 92–103. https://doi.org/10.1016/j.ejpb.2018.02.017

Stauffer, F., Vanhoorne, V., Pilcer, G., Chavez, P.F., Vervaet, C., De Beer, T., 2019. Managing API raw material variability in a continuous manufacturing line – Prediction of process robustness. Int. J. Pharm. 569, 118525. https://doi.org/10.1016/j.ijpharm.2019.118525

Steinwandter, V., Borchert, D., Herwig, C., 2019. Data science tools and applications on the way to Pharma 4.0. Drug Discov. Today. https://doi.org/10.1016/j.drudis.2019.06.005

Stevens, A., Ramirez-Lopez, L., 2013. An introduction to the prospectr package.

Stillhart, C., Parrott, N.J., Lindenberg, M., Chalus, P., Bentley, D., Szepes, A., 2017. Characterising Drug Release from Immediate-Release Formulations of a Poorly Soluble Compound, Basmisanil, Through Absorption Modelling and Dissolution Testing. AAPS J. 19, 827–836. https://doi.org/10.1208/s12248-017-0060-1

Su, Q., Ganesh, S., Moreno, M., Bommireddy, Y., Gonzalez, M., Reklaitis, G. V., Nagy, Z.K., 2019. A perspective on Quality-by-Control (QbC) in pharmaceutical continuous manufacturing. Comput. Chem. Eng. 125, 216–231. https://doi.org/10.1016/j.compchemeng.2019.03.001

Su, Q., Moreno, M., Giridhar, A., Reklaitis, G. V., Nagy, Z.K., 2017. A Systematic Framework for Process Control Design and Risk Analysis in Continuous Pharmaceutical Solid-Dosage Manufacturing. J. Pharm. Innov. 12, 327–346. https://doi.org/10.1007/s12247-017-9297-6

Sun, C.C., 2013. Cocrystallization for successful drug delivery. Expert Opin. Drug Deliv. https://doi.org/10.1517/17425247.2013.747508

Sun, C.C., 2008. Mechanism of moisture induced variations in true density and compaction properties of microcrystalline cellulose. Int. J. Pharm. 346, 93–101. https://doi.org/10.1016/j.ijpharm.2007.06.017

Sun, W.J., Aburub, A., Sun, C.C., 2017. Particle Engineering for Enabling a Formulation Platform Suitable for Manufacturing Low-Dose Tablets by Direct Compression. J. Pharm. Sci. 106, 1772–1777. https://doi.org/10.1016/j.xphs.2017.03.005

Sütő, B., Berkó, S., Kozma, G., Kukovecz, Á., Budai-Szucs, M., Erös, G., Kemény, L., Sztojkov-Ivanov, A., Gáspár, R., Csányi, E., 2016. Development of ibuprofen-loaded nanostructured lipid carrier-based gels: Characterization and investigation of in vitro and in vivo penetration through the skin. Int. J. Nanomedicine 11, 1201–1212. https://doi.org/10.2147/IJN.S99198

Suzuki, T., Nakagami, H., 1999. Effect of crystallinity of microcrystalline cellulose on the compactability and dissolution of tablets. Eur. J. Pharm. Biopharm. 47, 225–230. https://doi.org/10.1016/S0939-6411(98)00102-7

Szilágyi, B., Borsos, Á., Pal, K., Nagy, Z.K., 2019. Experimental implementation of a Quality-by-Control (QbC) framework using a mechanistic PBM-based nonlinear model predictive control involving chord length distribution measurement for the batch cooling crystallization of L-ascorbic acid. Chem. Eng. Sci. 195, 335–346. https://doi.org/10.1016/j.ces.2018.09.032

Takeuchi, H., Nagira, S., Yamamoto, H., Kawashima, Y., 2004. Die wall pressure measurement for evaluation of compactionproperty of pharmaceutical materials. Int. J. Pharm. 274, 131–138.

Tanaka, R., Hattori, Y., Ashizawa, K., Otsuka, M., 2019. Kinetics Study of Cocrystal Formation Between Indomethacin and Saccharin Using High-Shear Granulation

With In Situ Raman Spectroscopy. J. Pharm. Sci. 108, 3201–3208. https://doi.org/10.1016/j.xphs.2019.06.019

Tauler, R., 1995. Multivariate curve resolution applied to second order data. Chemom. Intell. Lab. Syst. 30, 133–146. https://doi.org/10.1016/0169-7439(95)00047-X

Tauler, R., Walczak, B., Brown, S., 2009. Comprehensive Chemometrics: Chemical and Biochemical Data Analysis. Elsevier.

Teng, Y., Qiu, Z., Wen, H., 2009. Systematical approach of formulation and process development using roller compaction. Eur. J. Pharm. Biopharm. https://doi.org/10.1016/j.ejpb.2009.04.008

Terinte, N., Ibbett, R., Schuster, K.C., 2011. Overview on Native Cellulose and Microcrystalline Cellulose I Structure Studied By X-Ray Diffraction (Waxd): Comparison Between Measurement Techniques. Lenzinger Berichte 89, 118–131. https://doi.org/10.1163/156856198X00740

Thomas, J., Schubert, H., 1979. Particle Characterization. Partec.

Thoorens, G., Krier, F., Leclercq, B., Carlin, B., Evrard, B., 2014. Microcrystalline cellulose, a direct compression binder in a quality by design environment - A review. Int. J. Pharm. 473, 64–72. https://doi.org/10.1016/j.ijpharm.2014.06.055

Thoorens, G., Krier, F., Rozet, E., Carlin, B., Evrard, B., 2015. Understanding the impact of microcrystalline cellulose physicochemical properties on tabletability. Int. J. Pharm. 490, 47–54. https://doi.org/10.1016/j.ijpharm.2015.05.026

Timmermann, E.O., 2003. Multilayer sorption parameters: BET or GAB values? Colloids Surfaces A Physicochem. Eng. Asp. 220, 235–260. https://doi.org/10.1016/S0927-7757(03)00059-1

Trache, D., Hussin, M.H., Hui Chuin, C.T., Sabar, S., Fazita, M.R.N., Taiwo, O.F.A., Hassan, T.M., Haafiz, M.K.M., 2016. Microcrystalline cellulose: Isolation, characterization and bio-composites application—A review. Int. J. Biol. Macromol. https://doi.org/10.1016/j.ijbiomac.2016.09.056

Trask, A. V, Samuel Motherwell, W.D., Jones, W., 2005. Pharmaceutical cocrystallization: Engineering a remedy for caffeine hydration. Cryst. Growth Des. 5, 1013–1021. https://doi.org/10.1021/cg0496540

US FDA, 2004. Center for Drug Evaluation and Research, Guidance for Industry: PAT - A Framework for Innovative Pharmaceutical Manufacturing and Quality Assurance.

Van Eerdenbrugh, B., Taylor, L.S., 2011. Application of mid-IR spectroscopy for the characterization of pharmaceutical systems. Int. J. Pharm. 417, 3–16. https://doi.org/10.1016/j.ijpharm.2010.12.011

Vasconcelos, T., Sarmento, B., Costa, P., 2007. Solid dispersions as strategy to improve oral bioavailability of poor water soluble drugs. Drug Discov. Today 12, 1068–1075. https://doi.org/10.1016/j.drudis.2007.09.005

Vishweshwar, P., McMahon, J.A., Bis, J.A., Zaworotko, M.J., 2006. Pharmaceutical co-crystals. J. Pharm. Sci. https://doi.org/10.1002/jps.20578

Vonbehren, D., Lynch, M.G., Miranda, A.C., 2010. Cosmetic composition containing microcrystalline cellulose. United States Pat.

Wenzel, T., Stillhart, C., Kleinebudde, P., Szepes, A., 2017. Influence of drug load on dissolution behavior of tablets containing a poorly water-soluble drug: estimation of the percolation threshold. Drug Dev. Ind. Pharm. 43, 1265–1275. https://doi.org/10.1080/03639045.2017.1313856

Werner, P., Münzberg, M., Hass, R., Reich, O., 2017. Process analytical approaches for the coil-to-globule transition of poly(N-isopropylacrylamide) in a concentrated aqueous suspension. Anal. Bioanal. Chem. 409, 807–819. https://doi.org/10.1007/s00216-016-0050-7

Wickham, H., 2016. ggplot2: Elegant Graphics for Data Analysis. Springer-Verlag New York.

Wiley, J.H., Atalla, R.H., 1987. Band assignments in the raman spectra of celluloses. Carbohydr. Res. 160, 113–129. https://doi.org/10.1016/0008-6215(87)80306-3

Woodcock, J., 2004. The concept of pharmaceutical quality. Am. Pharm. Rev. 7, 10–15.

Wu, C.Y., Benet, L.Z., 2005. Predicting drug disposition via application of BCS: Transport/absorption/ elimination interplay and development of a biopharmaceutics drug disposition classification system. Pharm. Res. 22, 11–23. https://doi.org/10.1007/s11095-004-9004-4

Yang, W., Ping, P., Wang, L.-L., Bo-Yuan Chen, T., Chun-Yin Yuen, A., Zhu, S.-E., Wang, N.-N., Hu, Y.-L., Yang, P.-P., Sun, C., Zhang, C.-Y., Lu, H.-D., Chan, Q.N., Yeoh, G.-H., 2018. Fabrication of Fully Bio-Based Aerogels via Microcrystalline Cellulose and Hydroxyapatite Nanorods with Highly Effective Flame-Retardant Properties. ACS Appl. Nano Mater. 1, 1921–1931. https://doi.org/10.1021/acsanm.8b00312

Yassin, S., Goodwin, D.J., Anderson, A., Sibik, J., Wilson, D.I., Gladden, L.F., Zeitler, J.A., 2015. The Disintegration Process in Microcrystalline Cellulose Based Tablets, Part 1: Influence of Temperature, Porosity and Superdisintegrants. J. Pharm. Sci. 104, 3440–3450. https://doi.org/10.1002/jps.24544

Yu, L.X., 2008. Pharmaceutical quality by design: Product and process development, understanding, and control. Pharm. Res. 25, 781–791. https://doi.org/10.1007/s11095-007-9511-1

Yu, L.X., Amidon, G., Khan, M.A., Hoag, S.W., Polli, J., Raju, G.K., Woodcock, J., 2014. Understanding pharmaceutical quality by design. AAPS J. 16, 771–783. https://doi.org/10.1208/s12248-014-9598-3

Yu, S., Gururajan, B., Reynolds, G., Roberts, R., Adams, M.J., Wu, C.Y., 2012. A comparative study of roll compaction of free-flowing and cohesive pharmaceutical powders. Int. J. Pharm. 428, 39–47. https://doi.org/10.1016/j.ijpharm.2012.02.033

Zarmpi, P., Flanagan, T., Meehan, E., Mann, J., Østergaard, J., Fotaki, N., 2020. Biopharmaceutical implications of excipient variability on drug dissolution from immediate release products. Eur. J. Pharm. Biopharm. 154, 195–209. https://doi.org/10.1016/j.ejpb.2020.07.014

Zhang, L., Henson, M.J., Sekulic, S.S., 2005. Multivariate data analysis for Raman imaging of a model pharmaceutical tablet. Anal. Chim. Acta 545, 262–278. https://doi.org/10.1016/j.aca.2005.04.080

Zhao, L., Raval, V., Briggs, N.E.B., Bhardwaj, R.M., McGlone, T., Oswald, I.D.H., Florence, A.J., 2014. From discovery to scale-up: α-lipoic acid: Nicotinamide co-crystals in a continuous oscillatory baffled crystalliser. CrystEngComm 16, 5769–5780. https://doi.org/10.1039/c4ce00154k

Zhong, L., Gao, L., Li, L., Zang, H., 2020. Trends-process analytical technology in solid oral dosage manufacturing. Eur. J. Pharm. Biopharm. 153, 187–199. https://doi.org/10.1016/j.ejpb.2020.06.008